An Investigation of Reduced Size Planar Fed Microstrip Patch Antennas

Michael Elsdon

A thesis in partial fulfilment of the requirements of the University of Northumbria for the degree of Doctor of Philosophy

April 2005

School of Engineering and Technology,

Northumbria University

Abstract

The primary goal of this research work is to investigate the use of slot loading in reduced size planar fed microstrip patch antennas and develop new antenna structures based on this technique.

At present, little theoretical investigation or design methodology exists to support the design of compact structures and research in this field is largely empirical. Moreover, little work exists on the use of planar fed designs. This necessitates a primary requirement to firstly address this knowledge gap. To facilitate this, a mathematical modelling technique that can be applied to such structures is developed. This is based upon the segmentation and Green's function approach. Using this model, the performance of slot loaded structures in terms of circuit characteristics including resonant frequency, input impedance, and Q factor is determined. Using this knowledge, a design procedure is established and subsequently used to provide a framework for the design of novel slot loaded antennas for specific applications.

Several new slot loaded patch antenna configurations are designed that produce size reduction whilst allowing the use of a planar feed. The validity of the designs are confirmed through the use of commercial full-wave modelling software package Ensemble. Three linear polarised antennas are presented which are shown to achieve size reduction of 12, 40 and 55% respectively. Several compact circular polarised antenna structures are successfully implemented producing size reduction of up to 43%. A novel design for a reduced size antenna with a dual frequency response is also presented with a tuneable frequency ratio of between 1.03 ~ 2.0. Prototypes of the aforementioned antennas are fabricated and tested, and practical results are shown.

TABLE OF CONTENTS

LIST OF FIGURES

LIST OF TABLES

Acknowledgements

First and foremost I would like to express my gratitude to my supervisors, Professor A.J. Sambell, Prof. R.A. Cryan and Dr. D. Smith for the continued support throughout the course of this research.

I would like to thank Dr. S.C. Gao for his advice and fruitful discussions.

I would also like to thank the technical support received from members of the School of Engineering and Technology at Northumbria University

I am indebted to my family for their constant support and encouragement.

Finally, I would like to dedicate this thesis to the memory of my late mother Mrs. H. Elsdon who passed away during the course of this research.

GLOSSARY OF ACRONYMS

AR ..... Axial Ratio

ARBW ..... Axial Ratio Bandwidth

BW ..... Bandwidth

Co-pol ..... co-polarisation

CP ..... Circular Polarisation

FBW ..... Fractional Bandwidth

FTB ..... Front- to- back

GHz ..... Gigahertz

GPS ..... Global Positioning System

LHCP ..... Left-hand Circular Polarisation

LP ..... Linear Polaristion

MEMS ..... Micromachined Electromagnetic System

MHz ..... Megahertz

MPA ..... Microstrip Patch Antenna

Q ..... Quality

RHCP ..... Right-hand Circular Polarisation

SAR ..... Synthetic Aperture Radar

TM ..... Transverse Magnetic

VSWR ..... Voltage Standing Wave Ratio

x-pol ..... cross-polarisation

GLOSSARY OF SYMBOLS

α ..... attenuation constant

α_{cg} ..... attenuation constant due to ground plane loss

α_{cs} ..... attenuation constant due to conductor loss

α_d ..... attenuation constant due to dielectric loss

α_g ..... total attenuation constant

β_g ..... phase constant

β_z ..... phase shift in z direction

γ ..... propagation constant

δ ..... loss tangent of patch antenna

ε ..... permittivity

ε_0 ..... permittivity of free space (= 1)

ε_r ..... relative permittivity of dielectric

ε_{eff} ..... effective permittivity of dielectric

ϕ ..... eigenfunctions of patch antenna

η_0 ..... impedance of free space (= 120π)

θ ..... phase angle of radiated components

λ_0 ..... free-space wavelength

μ ..... permeability of dielectric

μ_0 ..... permeability of free space (= $4\pi \times 10^{-7}$)

μ_r ..... relative permeability of dielectric

σ_c ..... metal conductivity (= 5.7×10^7)

ω ..... angular frequency

Δf ..... antenna bandwidth

ΔL ..... line extension due to fringing fields

Γ_1, Γ_2 ..... matrices describing connection topology

A_{mn} ..... amplitude of TM_{mn} modes

a, b ..... patch dimensions

a_p ..... radius of shorting pins

B ..... capacitance due to fringing fields

c ..... speed of light (= 3×10^8 m/s)

C_p ..... patch antenna boundary

d ..... separation between shorting pin and probe feed

dl ..... perturbation length for nearly square CP patch

D_p ..... region inside patch antenna

D ..... antenna directivity

e ..... antenna radiation efficiency

E_1 ..... amplitude of Electric field in x direction

E_2 ..... amplitude of Electric field in y direction

E_x ..... total Electric field in x direction

E_y ..... total Electric field in y direction

E_z ..... total Electric field in z direction

f_r ..... antenna resonant frequency

G_n ..... antenna gain

G ..... Green's functions

G_r ..... radiation conductance

h ..... substrate height

I_c ..... current at c port

I_j ..... current at j port

I_p ..... current at p port

J_z ..... z-directed current source

J_s ..... current source at point s

k_0 ..... wavenumber of fundamental mode in dielectric

$k_{m,n}$ ..... wavenumber of TM_{mn} modes in dielectric

L ..... patch length

L_e ..... effective patch length

m,n ..... integers relating to mode numbers

Q_c ..... Q factor due to conduction loss

Q_d ..... Q factor due to dielectric loss

Q_r ..... Q factor due to radiation loss

Q_{sw} ..... Q factor due to surface wave loss

Q_t ..... total Q factor

th ..... metal thickness

tanδ ..... dielectric loss tangent

$V(x,y)$ ..... voltage at point (x,y)

V_c ..... voltage at c port

V_p ..... voltage at p port

V_i ..... voltage at i port

W ..... patch width

W_e ..... effective patch width

W_c ..... width of port C

W_i ..... width of port i

W_j ..... width of port j

W_p ..... width of port P

(x_0, y_0) ..... position of current source within patch

Y_0 ..... antenna admittance

Z_{cc} ..... interaction between C ports

Z_{cp} ..... interaction between C and P ports

Z_{ii} ..... interaction between i ports

Z_{ij} ..... interaction between i and j ports

Z_{ji} ..... interaction between j and i ports

Z_{jj} ..... interaction between j ports

Z_{pc} ..... interaction between P and C ports

Z_{pp} ..... interaction between P ports

Z_{in} ..... antenna input impedance

Z_m ..... impedance of antenna matching network

Z_0 ..... characteristic impedance of patch antenna

CHAPTER 1

INTRODUCTION

1.1 Introduction

Microstrip antennas are a relatively new concept. Although radiation from a stripline was considered by Lewin [1], the idea was largely dormant until the 1970s, and did not become practically realisable until the early 1980s. The basic microstrip patch antenna configuration is a metallic patch printed on a thin, grounded dielectric substrate, and is excited with either a coaxial or coplanar microstrip feed. The microstrip antenna can thus be made conformal which implies a number of key advantages over their counterparts, including:

- Potentially low cost and ease of manufacture using printed circuit technology
- Lightweight and thin profile
- Easy integration with associated microwave circuitry and arrays.

Conversely, they also suffer from the following major disadvantages:

- The radiating elements have a restricted bandwidth arising from the intrinsic high-Q resonator action of the thin substrate
- Several effects, including dielectric losses, generation of surface waves at the dielectric-air interface, and losses in the co-planar feed lines, may lead to low overall efficiency
- It is difficult to obtain high polarisation purity
- Low gain dictated by patch size and substrate
- Relatively strict manufacturing tolerances

Microstrip antennas are a relatively new concept, but there are a number of active ongoing research work, including:

- Bandwidth extension techniques [2-16]
- Control of radiation patterns [17-30]
- Methods of reducing losses and increasing radiation efficiency [31-33]

- Improving feeder systems [17-26, 34-37]
- Size reduction techniques [38 - 64].

Future system demands will be a dominant factor in the development of microstrip antennas. The microstrip antenna is now an established form of antenna that has found use in a wide range of communication equipment including radar, satellites and GPS.

As a result of new technology, whilst the circuitry associated with such equipment has reduced considerably, the same cannot be said of the antennas themselves. The main reason for this is due to the fact that antenna size is determined by the fundamental laws of physics. The antenna size with respect to the wavelength will have a preponderant influence on the radiation characteristics [38]. Thus any reduction in size will be at the expense of other antenna parameters such as gain, bandwidth and efficiency [39-44]. However, given that the cost of commercial application is highly dependant on its overall size, any reduction in antenna size would be greatly beneficial.

As any proposed antennas are designed for eventual use in commercial applications, using planar fed structures will provide ease of integration with associated microwave circuitry. The concept of reducing the board space occupied by the antenna is not simply limited to reducing the size of a single frequency patch antenna. For certain applications, such as global positioning systems (GPS) and synthetic aperture radar (SAR), a dual frequency response is often required. At present, little theoretical investigation or design methodology exists to support the design of compact structures and research in this field is largely empirical. This thesis is therefore focussed on the analysis and investigation of planar fed reduced size patch antennas. This investigation will then provide the basis to design new reduced size patch antennas that are planar fed and overcome limitations identified

with previously reported structures. With this in mind, the following specific aims must be met:

- Investigate different techniques for achieving compact operation of patch antennas and identify the most suitable for the design of planar structures.
- Develop an analytical model that can be applied to determine the performance of the chosen compact patch antenna design.
- Undertake analysis of design parameters and their effect on patch performance in terms of circuit characteristics and identify trade-offs of such designs.
- Propose a design methodology to provide a framework for the design of slot loaded antennas for specific applications.
- Propose new slot loaded patch antenna configurations that overcome some of the trade-offs associated with existing structures. These include the design of single frequency linear and circular polarised antennas, together with design of a patch antenna with a dual frequency response.

1.2 Thesis Organisation

Following this introductory chapter, analysis of a standard rectangular patch antenna is presented in Chapter 2. Miniaturising an antenna will affect its radiation characteristics [1,38-46], and influence its bandwidth, gain, efficiency and polarisation purity. Moreover, it is not always easy to feed a small antenna efficiently [47]. The focus of this chapter is therefore to provide an understanding of the most important patch antenna characteristics in relation to miniaturisation techniques, including: TM_{mn} ode field distribution; input impedance; radiation characteristics; and generation of circular polarisation.

Chapter 3 presents a detailed review of present methods of reducing the size of patch antennas. The concept of reducing the board space occupied by the antenna is not simply limited to reducing the size of a single frequency patch antenna. For certain applications, such as global positioning systems (GPS) and synthetic aperture radar (SAR), a dual frequency response is often required. A number of techniques of modifying the frequency response of a regular patch antenna have been suggested.

The most significant techniques include; edge-shorted patch [45-52], folded patch [53,54] , meandered ground plane [55], slot loaded ground plane [56,57], meandered patch [58,59], and slot loaded patch antenna [60-64]. With appropriate selection of the correct technique it is possible to produce reduced size, dual frequency or wideband patch antennas. It is determined that the most promising method of reducing the size of the patch antenna is the slot loading technique. It is also identified that using this approach, it should be possible to produce compact patch antenna with both linear and circular polarisation, together with dual frequency and wideband antennas. Chapter 3 also highlights that a lack of detailed analysis of such structures exists, with the majority of work being empirical.

Subsequent chapters within this thesis involve the design and analysis of slot loaded antennas similar to those illustrated in figure 1.1.

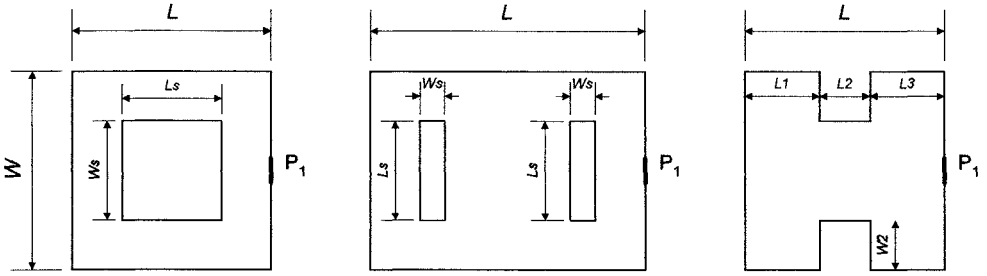

Figure 1.1: Slot loaded patch antenna structures

To facilitate this, the focus of Chapter 4 is to develop a modelling technique that can be applied to such structures. The modelling approach will be used to determine the performance of the antennas in terms of circuit characteristics including resonant frequency, input impedance, and Q factor. A number of possible modelling approaches are outlined including transmission line, cavity model, co-planar multi-port network, segmentation and full-wave modelling. The most applicable technique is the segmental approach used in conjunction with multiport network modelling. This approach offers flexibility in modelling patch antennas with complicated structures.

The focus of Chapter 5 is to fully investigate the use of slot loading and its effect on patch performance in terms of circuit characteristics. In the design of linear polarised patch antennas, a number of criteria in terms of circuit and far-field characteristics must be met. Considering the circuit characteristics, these include resonant frequency, input impedance, Q factor and VSWR BW. The relationship between these parameters is well established for conventional patch antennas. However, the same is not true of slot loaded patch designs. To address this, a rigorous analysis of the effect of slot loading on patch performance is detailed. From this, the relationship between slot parameters and resonant frequency, input impedance, feed position and Q factor is determined. Using this knowledge, a design procedure is established and used to design a new planar fed patch structure which is optimized for both size reduction and input impedance.

The focus of Chapter 6 is to develop planar fed reduced size CP patch antennas. Traditional methods of producing single-fed CP patch antennas include truncated corners, nearly square patch, and the cutting of a diagonal slot in the centre of a square patch [65]. To produce compact CP operation slot loading technique has been mainly applied to patch antennas with truncated corners [66-69] or square patch with unequal length slots [70] or tuning stubs [71]. At present, due to the strict manufacturing tolerances and narrow axial ratio bandwidth, little work exists on the use of slot loaded nearly square CP patch antennas. Moreover, the majority of compact slot loaded CP designs are excited using a probe or aperture feed, with little work existing on the use of a microstrip feed. The reason for this is attributed to the relationship between slot loading and input impedance. To overcome these problems, two novel planar fed reduced size structures with different types of slot loading are proposed, which are shown to achieve significant size reduction.

The reduced size patch antennas proposed in Chapters 5 and 6 achieve size reduction by modifying the impedance response of the fundamental mode (s).

Although these designs are planar fed, as with conventional patch antennas they still require the use of an impedance matching network. In Chapter 7, the problem of impedance matching has been removed completely by the development of novel antenna structures with an input impedance of 50 Ω. Such designs operate by creating an additional $TM_{0\delta}$ mode, which has a different frequency and impedance response from the fundamental modes. This allows the use of a direct planar feed and hence further reduces the overall element size. It is demonstrated that this structure can be successfully applied to produce compact linear polarised patch antennas with a single or dual frequency response.

Chapter 8 concludes this thesis, summarising the main contributions and suggesting some future research directions.

Within this thesis, the phrases patch antennas and microstrip antennas are the same expression and are used interchangeably.

1.3 Contributions and Published Work

The main contributions of this research work are summarised below:-

- A rigorous investigation of slot loaded patch antennas, through the application of segmentation model, to determine the relationship between slot parameters and patch performance in terms of circuit characteristics and highlighting associated trade-offs. The results of this study provides a design methodology for future antenna configurations. (Chapter 5)
- The following new antenna configurations have been proposed, designed and implemented:
    - Reduced size inset fed linear polarised planar fed patch antennas based upon modification of TM_{01} mode. (Chapter 5)
    - Reduced size circular polarised planar fed patch antennas based upon modification of the TM_{01} and TM_{10} modes. (Chapter 6)
    - Reduced size linear polarised direct feed based upon creation of additional $TM_{0\delta}$ mode. (Chapter 7)

- Planar fed dual frequency patch antenna based on modification of TM_{01} and creation of additional $TM_{0\delta}$ mode. (Chapter 7)

The research reported in this thesis has led to the following publications:

[1] M. Elsdon, A. Sambell and S. Gao, "Inset Microstrip-line Fed Dual Frequency Microstrip Patch Antenna," 12th International Conference on Antennas & Propagation, Exeter, England, **491**, (1), p28-30, 31st March – 3rd April 2003

[2] M. Elsdon, A. Sambell and S. Gao, "Novel Compact Harmonic-Suppressed Planar-Fed Microstrip Antenna, 5th European Personal Mobile Communications Conference, Glasgow, Scotland, **492**, p1-4 , 22nd – 25th April 2003

[3] M. Elsdon, A. Sambell, S. Gao and Y. Qin, "Compact Circular Polarised Patch Antenna with Relaxed Manufacturing Tolerance and Improved Axial Ratio Bandwidth," IEE Electronic Letters, **39**(18), p1296-1298 , 4th September 2003

[4] M. Elsdon, A. Sambell, S. Gao and Y. Qin, "Planar Fed Compact Circular Polarised Microstrip Antenna with Triangular Slot Loading," Microwave and Optical Technology Letters, **41**(3), p226-228, 5th May 2004

[5] Y. Qin, S. Gao, A. Sambell, E. Korolkewicz and M. Elsdon, "Broadband Patch Antenna with Ring Slot Coupling," IEE Electronic Letters, **40**(1), p5-6, 8th January 2004

CHAPTER 2

PATCH ANTENNA OPERATION

2.1 Introduction

Several techniques can be used to reduce the size of a patch antenna. These include the use of: slot loading; shorting pin loading; folded patch; high permittivity substrate; and other miscellaneous techniques. The majority of such techniques operate by modifying the field distribution of the patch antenna. Miniaturising an antenna will affect its radiation characteristics [39-43,72-75] and influence its bandwidth, gain, efficiency and polarisation purity. Moreover, it is not always easy to feed a small antenna efficiently [38].

The focus of this chapter is therefore to provide an understanding of the most important patch antenna characteristics in relation to miniaturisation techniques, including: TM_{mn} mode field distribution; input impedance; radiation characteristics; and generation of circular polarisation.

Reducing the size of a patch antenna may also change the structure of the patch antenna, and can thus present problems in modelling. Consequently, a review of different modelling techniques is also presented in order to ascertain which provides the most appropriate approach for modelling such patch structures.

2.2 Rectangular Patch Antenna Operation

2.2.1 Basic characteristics, design and performance

With reference to figure 2.1, the rectangular microstrip patch antenna consists of a thin metallic strip (patch) placed at a distance h above a ground plane, separated by

a dielectric substrate with permittivity ε_r. There are numerous substrates that can be used for the design of microstrip antennas, with typical dielectric constants in the range of $2.2 \leq \varepsilon_r \leq 12$. Using a thick substrate produces increased bandwidth, but reduced efficiency. A similar relationship exists between dielectric constant, bandwidth and efficiency. This trend is illustrated later in this chapter in figure 2.2. A compromise is therefore needed.

For antenna design, the most desirable substrates are thick with a low dielectric constant, as they provide improved efficiency, larger bandwidth and loosely bound fields for radiation into space, but at the expense of larger element size [76]. Conversely, for microwave circuitry thin substrates with higher dielectric constants are desirable as they require tighter bound fields to minimize radiation, and lead to smaller element size. As microstrip antennas are often integrated with associated circuitry, a compromise is needed between antenna performance and circuit design.

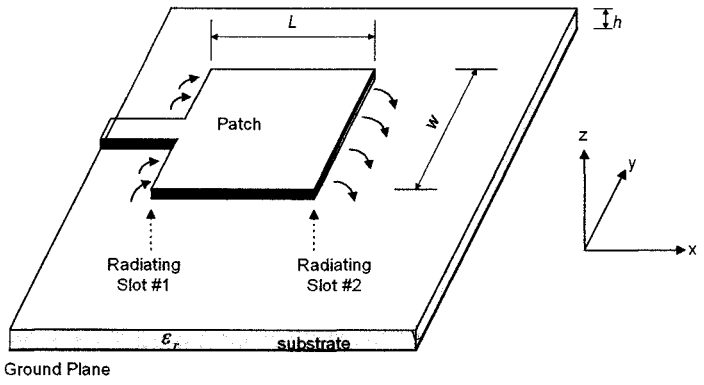

(a) top view

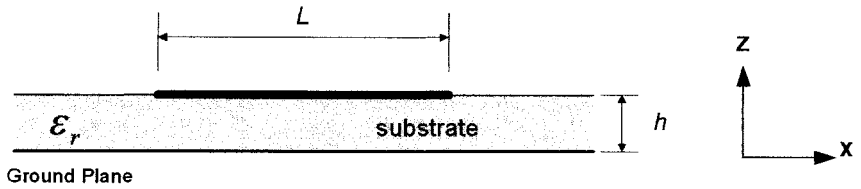

(b) side view

Figure 2.1: Microstrip antenna structure

The most common configurations that can be used to excite microstrip antennas include microstrip line, coaxial probe, aperture coupling and proximity coupling [31,35,76-81]. The microstrip line feed is easy to fabricate, simple to match with either an inset feed or quarter-wave matching and simple to model. However, as the substrate thickness increases spurious feed radiation increases, thus limiting the bandwidth and efficiency. The coaxial-line feed is also easy to fabricate and match, and has low spurious radiation. However, it has narrow bandwidth, is more difficult to model and moreover is non-planar. Both the microstrip line and coaxial probe feed possess inherent asymmetries which generate higher order modes that can produce cross-polarised radiation [82]. To overcome some of these problems, aperture and proximity coupling feeds can be used.

Aperture coupling consists of two substrates separated by a ground plane. The lower substrate has a microstrip feed on the bottom side. The energy from this line is coupled to a patch on the upper substrate through a slot in the ground plane. This design is more difficult to manufacture, however it has low spurious radiation. One of the most significant advantages of this arrangement is that it allows independent optimisation of the feed and antenna substrate.

The proximity coupling feed [83,84] uses a two-layer substrate with a microstrip line on the lower substrate, terminating in an open stub below the patch which is printed on the upper substrate. This technique also allows independent optimisation of the feed and antenna substrate, however fabrication is more difficult because of the requirement for accurate alignment of substrates [76]. A significant disadvantage of both aperture coupling and proximity coupling is that they are both non-planar and hence increase antenna size and complexity.

The main design parameters of patch antennas together with their relevant computational formulas are now briefly defined.

2.2.1.1 Standard patch design

The rectangular microstrip patch antenna is characterised by length L and width W, as shown in figure 2.1. The resonant frequency of a rectangular patch antenna is defined as the frequency where the input impedance is purely resistive and is given by [82]:

$$f_r = \frac{1}{2\pi\sqrt{\varepsilon_r \mu_r}}\sqrt{\left(\frac{m\pi}{L}\right)^2 + \left(\frac{n\pi}{W}\right)^2} \tag{2.1}$$

where ε_r and μ_r are is the permitivitty and permeability of the substrate and m and n are the related TM_{mn} mode numbers within the cavity.

Equation (2.1) is based on the assumption of a perfect magnetic wall along the perimeter of the patch. To account for the fringing fields around the patch edges, an outward extension, Δl, term is included and is given by [85]:

$$\frac{\Delta L}{h} = 0.412\frac{\left(\varepsilon_{eff} + 0.3\right)\left(\frac{W}{h} + 0.264\right)}{\left(\varepsilon_{eff} - 0.258\right)\left(\frac{W}{h} + 0.8\right)}\ , \tag{2.2}$$

where ε_{eff} is the effective permittivity of the substrate and is given by [91]:

$$\varepsilon_{eff} = \frac{\varepsilon_r + 1}{2} + \frac{\varepsilon_r - 1}{2}\left(1 + 12\frac{t}{W}\right)^{-1/2}\ ,\ . \tag{2.3}$$

The effective length and width of a rectangular patch antenna are given by [86]:

$$L_e = L + 2\Delta L\ , \tag{2.4}$$

$$W_e = W + \frac{t}{\pi}\left(1 + \ln\left(\frac{2h}{t}\right)\right), \tag{2.5}$$

where L and W are the length and width of the microstip antenna and t is the thickness of the metal.

2.2.1.2 Q Factor, bandwidth and efficiency

The Q factor, Bandwidth and Efficiency are antenna figures of merit, all of which are interrelated. Thus, there is no complete freedom to independently optimise each one.

Q Factor:

The Q factor represents the antenna loss factors and is given by [82]:

$$\frac{1}{Q_t}=\frac{1}{Q_r}+\frac{1}{Q_c}+\frac{1}{Q_d}+\frac{1}{Q_{sw}}, \tag{2.6}$$

where Q_t represents total Q factor of the patch antenna, Q_r is Q factor due to radiation losses, Q_c is due to conduction losses and Q_d is due to dielectric losses. For thin substrates, the losses due to surfaces wave Q_{sw} are very small and can be neglected [87], thus:

$$Q_t=\left(\frac{1}{Q_d}+\frac{1}{Q_c}+\frac{1}{Q_r}\right)^{-1} \tag{2.7}$$

Approximate formulas for the individual Q factors are given by [87,88]:

$$Q_d=\frac{1}{\tan\delta}\quad, \tag{2.8}$$

where $\tan\delta$ is the loss tangent of the dielectric

$$Q_c=h\sqrt{\mu_0\mu f_r\sigma_c}\,, \tag{2.9}$$

where σ_c is the conductivity of the metal

$$Q_r=\frac{\pi}{4G_rZ_0}, \tag{2.10}$$

where G_r is the radiation conductance and Z_0 is the characteristic impedance of the patch. Expressions for the radiation conductance have been given by [89]:

$$G_r = \frac{W_e^{\,2}}{90\lambda_0^{\,2}}, \qquad W_e \prec 0.35\lambda_0$$

$$G_r = \frac{W_e}{120\lambda_0} - \frac{1}{60\pi^2}, \qquad 0.35\lambda_0 \le W_e \le 2\lambda_0$$

$$G_r = \frac{W_e^{\,2}}{120\lambda_0}, \qquad 2\lambda_0 \prec W_e \tag{2.11}$$

where W_e is the effective width given in given in (2.5).

The expression for the characteristic impedance Z_0 is given in [91]:

$$Z_0 = \frac{120\pi}{\sqrt{\varepsilon_{eff}}\left[\frac{W_e}{h} + 1.393 + 0.67\ln\left(\frac{W_e}{h} + 1.44\right)\right]} \qquad \frac{W}{h} \ge 1 \tag{2.12}$$

In an efficient antenna design the radiation loss is the dominant loss of the structure.

Bandwidth:

The fractional bandwidth of the patch is inversely proportional to the total Q-factor of the antenna and can be defined by [82]:

$$FBW = \frac{\Delta f}{f_r} = \frac{1}{Q_t}, \tag{2.13}$$

where Δf is the bandwidth.

In practical terms a more useful definition of the fractional bandwidth is the frequency range where the *VSWR* at the input terminals of the antenna is equal or less than a desired maximum value, assuming that the *VSWR* is unity at the desired frequency. A modified form of (2.13) which takes into account impedance matching is given by [90]:

$$\frac{\Delta f}{f_r} = \frac{VSWR - 1}{Q_t\sqrt{VSWR}}. \tag{2.14}$$

In general the fractional bandwidth is proportional to the patch volume [82], which can be expressed as:

$$BW \sim volume = area * height = length * width * height \qquad (2.15)$$

Efficiency:

The radiation efficiency of an antenna is defined as the ratio of power radiated to the input power. It can also be expressed in terms of Q factors, which for a microstrip antenna is given by [82]:

$$e = \frac{Q_t}{Q_{rad}}, \qquad (2.16)$$

From (2.14, 2.16), typical variations of efficiency as a function of substrate height for a microstrip antenna, with two different substrates, are shown in figure 2.2 [76].

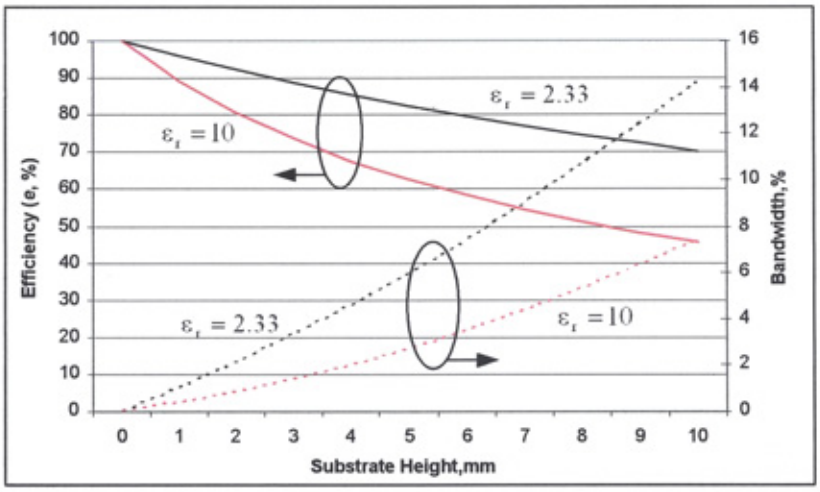

Figure 2.2: Efficiency and bandwidth versus substrate height at constant resonant frequency for square microstrip patch antenna

The above graph illustrates that for a conventional patch antenna, a trade-off exists between bandwidth and efficiency with increased substrate height. This is mainly attributed to the fact that increased generation of surface waves in thicker substrates. The optimum operating point is dependant on the application.

2.2.1.3 Gain and directivity

The directive gain of an antenna is given by [77]:

$$G_n = eD, \tag{2.17}$$

where e is given is (2.16) and D is directivity and is given by [77]:

$$D \approx \frac{4(k_0 W)^2}{\pi \eta_0 G_r}, \tag{2.18}$$

where η_0 is the impedance of free-space and k_0 is the wavenumber in the dielectric and is given by [82]:

$$k_0 = \omega\sqrt{\mu_0 \varepsilon_r}, \tag{2.19}$$

The above formulae (2.18) illustrates that directivity is not sensitive to substrate thickness and resonant frequency. Equation (2.18) demonstrates that gain increases with patch width and resonant frequency.

2.2.1.4 Input impedance

Within this thesis a microstrip feed will be used as it provides a planar structure and also reduces patch size and complexity. To excite the patch antenna efficiently it is necessary to achieve impedance matching between the feed structure and patch antenna. One method of achieving this is through the use of a quarter wave matching circuit to match the patch input impedance to the 50 Ω source impedance. The first stage is to determine the input impedance at the patch periphery. For a simple rectangular patch, this can be derived using the transmission line model. This technique represents the rectangular patch antenna by two slots [90], separated by a low impedance transmission line of length L, as shown in figure 2.3. The width of each slot is assumed to be equal to the substrate thickness h. Consequently, the slots can be represented by a parallel admittance, with conductance G_r, and susceptance B.

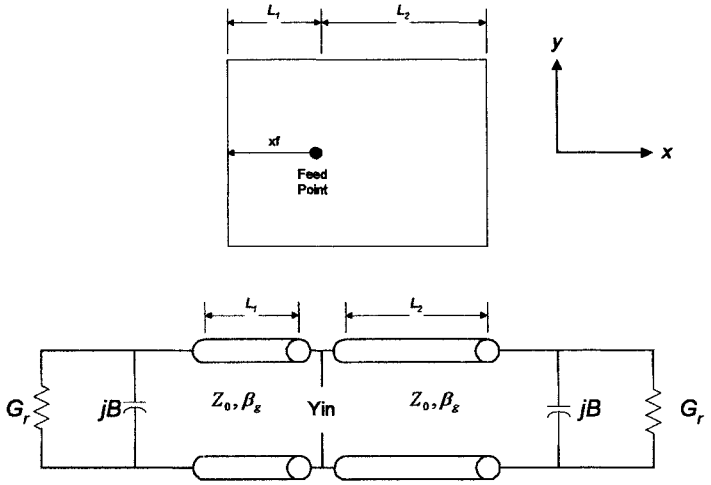

Figure 2.3: Transmission line model of rectangular patch

The conductive component G_r, is defined in equation (2.11) and relates to the radiation loss. The capacitive component B, relates to the fringing fields of the patch antenna respectively, and can be approximated by [89]:

$$B = \frac{k_0 \Delta L}{Z_0} \sqrt{\varepsilon_{eff}}, \tag{2.20}$$

Z_0 and β_g are the characteristic impedance and phase constant of the fundamental mode of the patch antenna, and can be approximated by [90]:

$$Z_0 = \frac{1}{Y_0} \approx \frac{\eta_0}{\sqrt{\varepsilon r}} \left(\frac{h}{W} \right), \tag{2.21}$$

$$\beta_g = k_0 \sqrt{\varepsilon_{eff}}, \tag{2.22}$$

where η_0 and k_0 are the wave impedance and wavenumber in free space, and h is the substrate thickness, and ε_{eff} is given by (2.3), and Y_0 is the antenna admittance.

The input impedance at an arbitrary point along the x axis can be calculated using [82]:

$$Y_{in} = Y_0\left[\frac{(G_r + jB) + Y_0 \tanh(\gamma L_1)}{(G_r + jB)\tanh(\gamma L_1) + Y_0}\right] + Y_0\left[\frac{(G_r + jB) + Y_0 \tanh(\gamma L_2)}{(G_r + jB)\tanh(\gamma L_2) + Y_0}\right], \tag{2.23}$$

where γ is the propagation constant and is given by:

$$\gamma = \alpha_g + j\beta_g, \tag{2.24}$$

α_g is the attenuation constant, used to account for losses in the microstrip line and is given by:

$$\alpha_g = \alpha_d + \alpha_{cs} + \alpha_{cg}, \tag{2.25}$$

α_d represents the dielectric losses, α_{cs} represents losses in the strip conductor and α_{cg} represents losses associated with the ground plane.

Typical values of input impedance for a standard rectangular patch antennas are in the region of 150-400 Ω.

At the design frequency, the antenna input impedance is purely real. The input impedance at the patch periphery can therefore be determined by rearranging (2.23) to give:

$$Z_{in} = \frac{1}{2G_r} \tag{2.26}$$

The value of the matching circuit is then given by:

$$Z_m = \sqrt{Z_{in} Z_L}. \tag{2.27}$$

where Z_m is the impedance of the matching circuit and Z_L represents the impedance at the patch edge.

The width of the matching circuit, Z_m, is dependant on the substrate parameters and decreases with increasing impedance. A stage is reached where it is no longer possible to use a traditional quarter wave transformer due to the finite width of the matching circuit, thus placing a constraint on the patch input impedance. Due to the

manufacturing process, the narrowest width line that can be produced is approximately 0.35 mm. To determine the impedance of a line of this width Atwaters equations (2.28-2.31) [91] are used.

$$Z_{OL} = \frac{60}{\left(\varepsilon_{eff(0)}\right)^{0.5}} \ln\left(8\frac{h}{W_e} + 0.25\frac{W_e}{h}\right), \qquad (W_e/h \le 1)$$

$$Z_{OL} = \frac{120\pi/\left(\varepsilon_{eff(0)}\right)^{0.5}}{\frac{W_{eff}}{h} + 1.393 + 0.667\ln\left(W_e/h + 1.444\right)}, \qquad (W_e/h \ge 1) \tag{2.28}$$

where $\varepsilon_{eff(0)}$ is the low frequency dielectric constant and is given by:

$$\varepsilon_{eff(0)} = \frac{\varepsilon_r + 1}{2} + \frac{\varepsilon_r - 1}{2}\left[\left(1 + 12\frac{h}{W_e}\right)^{-0.5} + 0.04\left(1 - \frac{W_e}{h}\right)^2\right], \qquad (W_e/h \le 1)$$

$$\varepsilon_{eff(0)} = \frac{\varepsilon_r + 1}{2} + \frac{\varepsilon_r - 1}{2}\left(1 + 12\frac{h}{W_e}\right)^{-0.5}, \qquad (W_e/h \ge 1) \tag{2.29}$$

Assuming RTduroid substrate is used with permittivity 2.33 and thickness 1.57 mm, this translates to an transmission line impedance of 158 Ω. Assuming the antenna is to be impedance matched to 50Ω, equation (2.27) can be rearranged to find the maximum antenna input impedance:

$$Z_L = \frac{Z_m^{\,2}}{Z_{in}} = \frac{158^2}{50}, \tag{2.30}$$

For the chosen substrate, this translates to a maximum antenna input impedance of approximately 500 Ω.

2.2.1.5 Input impedance variation with feed position

An alternate method of achieving input impedance matching is through the use of an inset feed. Therefore, the variation of input impedance of a patch antenna with

feed position in the x direction needs to be examined. In this instance, only the TM_{01} mode will be considered, for the TM_{10} mode, similar results are achieved with feed position along the y direction.

Using (2.23), a normalised plot of input impedance versus feed position is shown in figure 2.4.

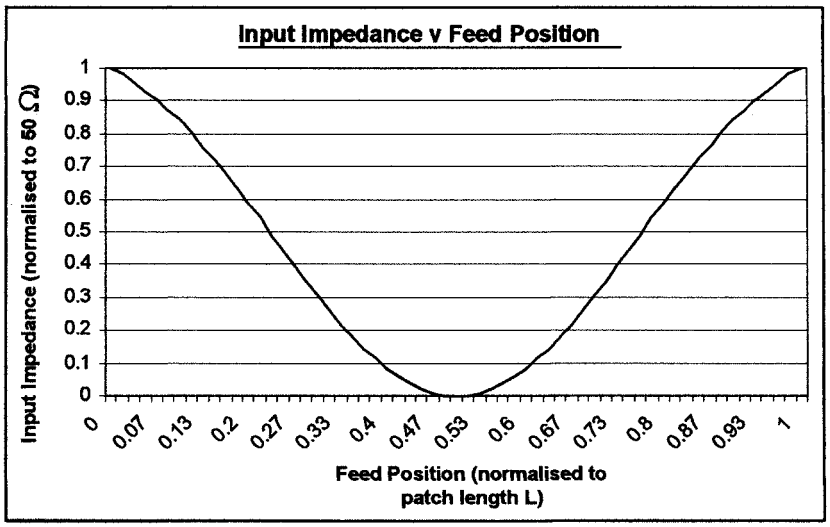

Figure 2.4: Normalised plot of input impedance versus feed position

The above results demonstrate, that the maximum value of input impedance occurs at the patch periphery, whilst the minimum occurs at the patch centre.

2.2.1.6 Typical patch performance parameters

In order to provide a 'benchmark' for subsequent patch designs within this thesis, a traditional patch antenna, shown in figure 2.5, was analysed using Ensemble.

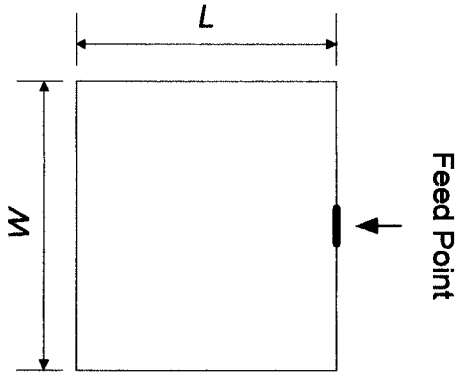

$\varepsilon_r = 2.33$, $h = 1.57$mm, $L = W = 30$mm

Figure 2.5: Typical planar fed square patch antenna

The patch designs developed in this thesis are to be fabricated on RTDuroid 5870 with permittivity of 2.33 and thickness of 1.57 mm. The corresponding performance is shown in table 2.1

Resonant Frequency (GHz)	Input Impedance (Ω)	Q	FBW (%)	Gain (dB)	Efficiency (%)
3.17	330	61	1.7	6	87.9

Table 2.1: Typical square patch performance

Table 2.1 illustrates that for a resonant frequency of 3.17 GHz, an input impedance of 330 Ω, Q factor of 61 and fractional bandwidth of 1.7%. In subsequent chapters, the introduction of slot loading into the patch antenna is expected to have a significant effect on these parameters.

2.2.2 Field Configurations of TM_{mn} modes

The aim of this thesis is to investigate and design new methods of reducing the size of a patch antenna. Typical methods of achieving this involves the use of slot or shorting pin loading. Such techniques operate by modifying the voltage and current distributions of the resonant TM_{mn} modes of a patch antenna. To understand such antennas, the voltage and current distributions of these modes are illustrated in this section.

To determine the field configurations inside the patch antenna, the cavity model has been employed [82]. The cavity model treats the region between the patch and ground plane as a cavity, bounded by electric walls above and below, and a magnetic wall along the perimeter of the patch. In order to account for the fringing fields the patch boundary is extended outwards.

For conventional patch antennas, the substrate height h, is small compared to the wavelength in order to prevent the generation of surface waves. It can therefore be assumed that the field variations in the z direction can be neglected.

The fields within the patch are described by the following two-dimensional wave equation [82]:

$$\frac{\partial^2 E_z}{\partial x^2}+\frac{\partial^2 E_z}{\partial y^2}+k_{m,n}{}^2 E_Z=0, \tag{2.31}$$

subject to the following boundary condition along the side walls

$$\frac{\partial E_Z}{\partial x}=0, \qquad \frac{\partial E_Z}{\partial y}=0, \tag{2.32}$$

where k is the wavenumber in the dielectric and is given by:

$$k_{m,n}{}^2=\left(\frac{m\pi}{a}\right)^2+\left(\frac{n\pi}{b}\right)^2, \tag{2.33}$$

where a and b are the patch length L and width W, and m and n are integers which represent the mode numbers within the cavity.

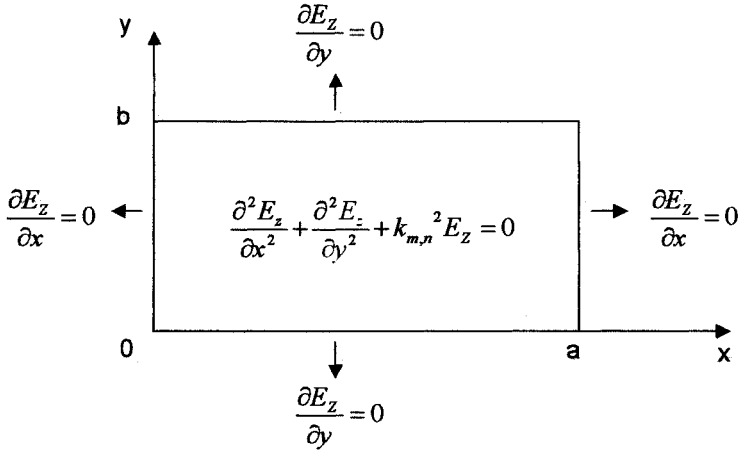

Figure 2.6: Boundary value problem

Solution of the associated fields is a boundary value problem and is illustrated in figure 2.6, to which the associated eigenfunctions are given by:

$$\phi_{m,n}(x,y)=k_{m,n}\cos\left(\frac{m\pi x}{a}\right)\cos\left(\frac{n\pi y}{b}\right), \qquad m,n=0,1,2\ldots \tag{2.34}$$

From (2.34), diagrams of TM_{0n} mode voltage and current distribution along the radiating patch edges for the first three modes are shown in figures 2.7.

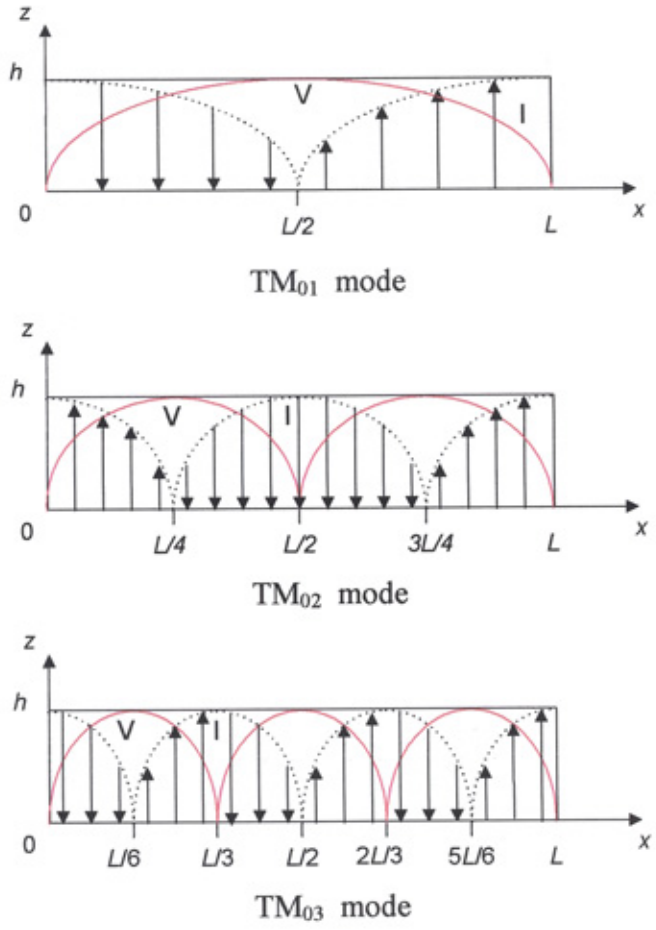

TM_{01} mode

TM_{02} mode

TM_{03} mode

Figure 2.7: Field configurations of TM_{mn} modes

For the TM_{0n} modes, the voltage and current show a sinusoidal distribution in the x direction. The TM_{01} mode has a single null voltage point and hence current maximum exists along the patch centre, at $y = L/2$. Conversely, two voltage maxima and current minima exists at both patch edges, at $y = 0$ and $y = L$. The TM_{02} mode has two null voltage points and thus current maxima at $y = L/4$ and $y = 3L/4$. Conversely, three voltage maxima and current minima exist at $y = 0, y = L/2$ and $y = L$. The TM_{03} mode has three null voltage points and thus current maxima at $y = L/6, y = L/2$ and $y = 5L/6$. Conversely, four voltage maxima and current minima exist at $y = 0, y = L/3, y = 2L/3$ and $y = L$.

Following a similar derivation the voltage and current of the TM_{m0} modes show an equivalent distribution in the y direction.

2.2.3 Radiation patterns of TM_{mn} modes

Whilst it is possible to operate a patch antenna at different frequencies corresponding to the various resonant TM_{mn} modes, for practical applications the radiation patterns and polarisation planes should ideally be identical in each frequency band. The first three modes with the same polarisation are the TM_{01}, TM_{02} and TM_{03} modes. The radiation patterns of these modes, determined through the use of full-wave modelling using full-wave analysis through the use of Ensemble [92], are shown in figures 2.8-2.10.

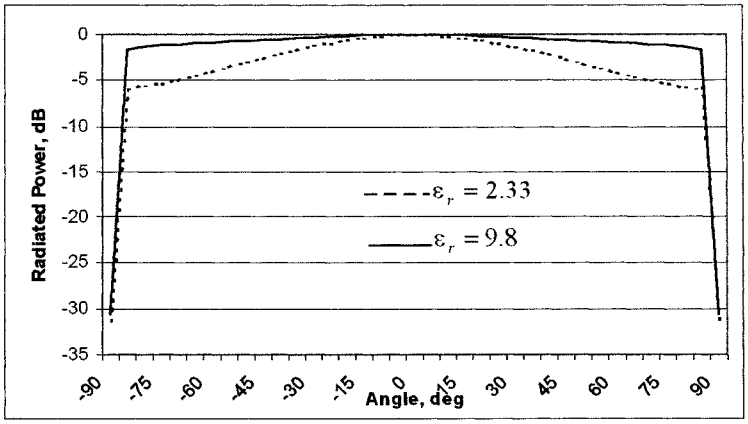

Figure 2.8: E-plane radiation pattern of TM_{01} mode

Conventional rectangular patch antennas operate using the fundamental TM_{01} and / or TM_{10} resonant modes as they provide good broadside radiation, as demonstrated in figure 2.8. It can be seen that using a lower dielectric constant provides a more directional radiation pattern.

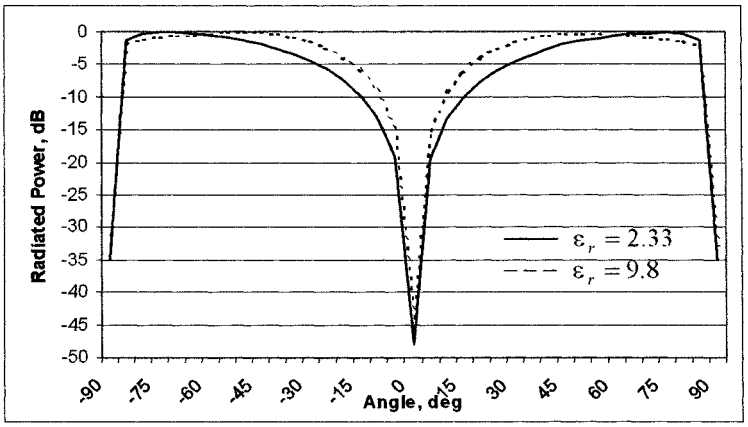

Figure 2.9: E-plane radiation pattern of TM_{02} mode

The radiation pattern of the TM_{02} mode, shown in figure 2.9, has a broadside null and is thus unsuitable for practical applications.

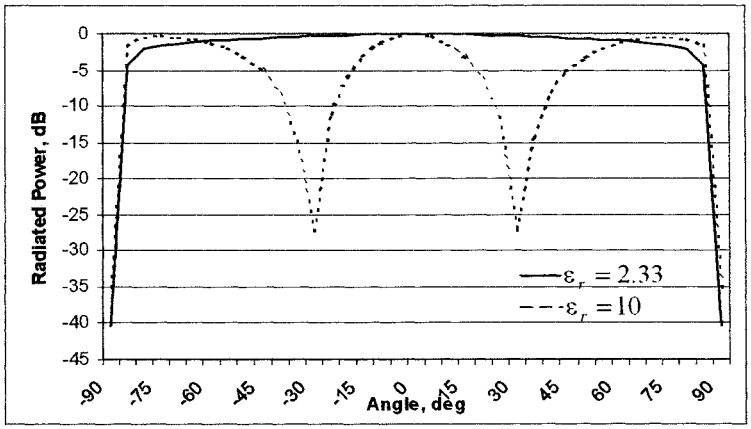

Figure 2.10: E-plane radiation pattern of TM_{03} mode

The TM_{03} (and TM_{30}) modes have also received attention. As with the TM_{01} (and TM_{30} modes) these modes also have broadside radiation. The patterns do not appear to be sensitive to patch dimensions, however they do change appreciably with substrate permittivity ε_r. It can be seen that using a low permittivity substrate, figure 2.10(a), the TM_{03} mode has two broadside nulls. Conversely, due to its reduced efficiency, using a higher permittivity substrate, as in figure 2.10(b), broadside radiation is achieved.

2.2.4 Polarisation

Polarisation of a radiated wave is defined [82] as "that property of an electromagnetic wave describing the time varying direction and relative magnitude of the electric-field vector". Polarisation may be classified as linear, circular, or elliptical, which are illustrated in figure 2.11.

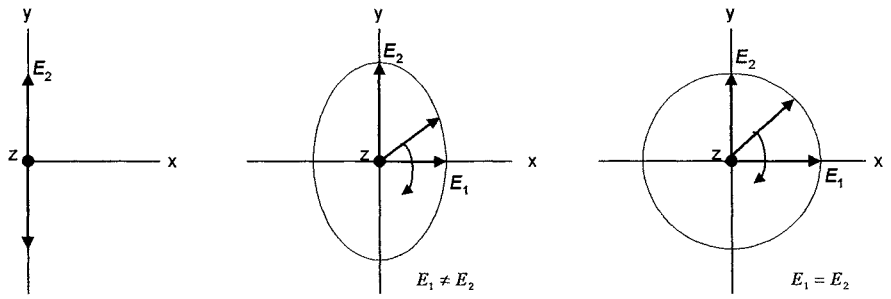

(a) Linear polarisation (b) Elliptical polarisation c) Circular polarisation

Figure 2.11: States of wave polarisation

Figure 2.6(a) shows a plane wave travelling in a positive z-direction with the electric field orientated in the y-direction at all times. This type of wave is said to be linear polarised in the y-direction. In terms of time and position, the electric field of this wave is given by:

$$E_y = E_2 \sin(\omega t - \beta_z), \tag{2.35}$$

where β_z is the phase shift varying with distance in the z-direction.

In general, the electric field has a component in both the x and y-directions, as shown in figure 2.6(b) and (c), and are termed elliptical and circular polarised waves respectively. These type of waves can be resolved into linear polarised components in the x and y-directions [43].

$$E_x = E_1 \sin(\omega t - \beta_z) \tag{2.36}$$

$$E_y = E_2 \sin(\omega t - \beta_z + \delta), \tag{2.37}$$

where E_1 and E_2 are the amplitudes of the fields in the x and y directions respectively, and δ represents the time-phase difference between E_1 and E_2.

If $E_1 \neq E_2$, the wave is said to be elliptically polarised. To achieve circular polarisation, the magnitude of both E_1 and E_2 should be equal and the phase difference δ, between them ±90°. Left Hand Circular Polarisation (LHCP) is achieved when δ = +90°, whilst Right Hand Circular Polarisation (RHCP) occurs when δ = -90°.In order to achieve perfect circular polarisation, the travelling wave must consist of two orthogonally linear polarised components of equal amplitude. In practice, the magnitude of the two orthogonal modes E_1 and E_2 are not always equal and the phase difference is not exactly 90°. The phase error introduces a tilt angle (ι) [93] hence producing elliptical polarisation.

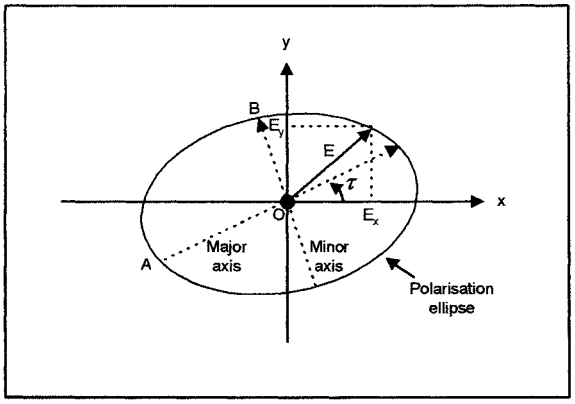

Figure 2.12: Polarisation ellipse

With reference to figure 2.12, the Axial Ratio is defined as:

$$AR = \frac{Major\_axis}{Minor\_axis} = \frac{OA}{OB}, \qquad 1 \leq AR \leq \infty \qquad (2.38)$$

which represents the ratio of the maximum to minimum signal strength of the electric field vector.

In terms of magnitude and phase difference of the radiated field components, the Axial Ratio is given by [94]:

$$AR = 10\log\frac{E_x^{\,2} + E_y^{\,2} + \left[E_x^{\,4} + E_y^{\,4} + 2E_x^{\,2}E_y^{\,2}\cos(2\theta)\right]^{0.5}}{E_x^{\,2} + E_y^{\,2} - \left[E_x^{\,4} + E_y^{\,4} + 2E_x^{\,2}E_y^{\,2}\cos(2\theta)\right]^{0.5}}, \qquad (2.39)$$

where, E_x and E_y are the magnitude of the radiated field components, and θ is the phase difference between the radiated field components.

For efficient antenna design, the accepted axial ratio is below 3 dB. In practical applications, a measure of the axial ratio bandwidth is required. This is a measure of frequencies over which the axial ratio is below the accepted value of 3 dB.

2.2.5 Generation of circular polarisation

Using circular polarisation provides benefits in communication systems, such as aircraft and road-tolling systems, when multipath situations occur as a result of reflections. When a right-hand circular polarised signal strikes a symmetric surface the resultant reflected wave is left-hand circular polarised. An antenna that is designed to transmit and receive right hand-circular signal will reject left hand circular signals. Circular polarisation is also less sensitive to antenna orientation. There are various types of circular polarised microstrip antennas which are widely used in many communication systems, and can be accomplished using single or dual feeds. In both single fed CP patches, the TM_{01} mode produces an electric field which is linear polarised in the y direction and the TM_{10} mode produces a linear polarised electric field in the x direction.

2.2.5.1 Dual-fed circular polarised patch antennas

For a square patch element, the easiest way to excite circular polarisation is to feed the antenna at two adjacent sides to excite two orthogonal TM_{01} and TM_{10} modes. The two fundamental configurations of dual-fed circular polarised antennas are shown in figure 2.13.

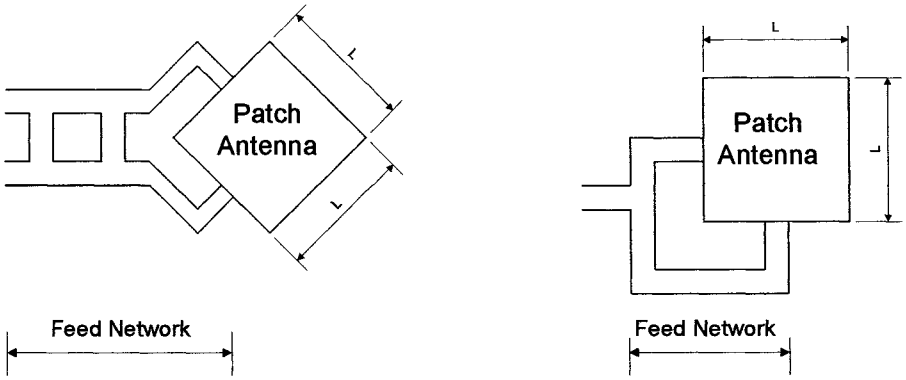

(a) Hybrid coupler (b) Offset feed

Figure 2.13: Dual fed CP patch arrangements

The patches are fed with two inputs of equal amplitude and 90° out of phase by using an external polariser. Figure 2.13(a) incorporates a 3dB hybrid coupler to produce the required inputs. Each input terminal of the hybrid gives an opposite sense of circular polarisation; using the upper input produces LHCP, whilst the lower input results in RHCP. This arrangement is advantageous as the input VSWR is broadband due to the broadband nature of the 3dB hybrid.Figure 2.8(b) illustrates a patch excited by an offset feed. This arrangement uses two feed lines with lengths l and $l + \lambda/4$ respectively to produce the required 90° phase difference. The major disadvantage of this configuration is the narrow bandwidth, since the frequency dependency of an offset line is greater than that of the 3 dB hybrid.

2.2.5.2 Single feed circular polarised patch antennas

To overcome the complexities associated with dual-feed arrangements and reduce antenna size, circular polarisation can be achieved with a single feed. The operational principle is based on the fact that the generated mode can be separated into two orthogonal modes (#1 and #2) by introducing a perturbation segment [80]. This increases the frequency of one mode, with its orthogonal mode decreasing in frequency by the same amount. Since the two modes have slightly different frequencies, the patch can be designed so that the frequency of one mode leads by

+45° and that of the second mode lags by -45°, thus achieving the required 90° phase difference [88]. The associated amplitude and phase diagrams are shown in figure 2.14.

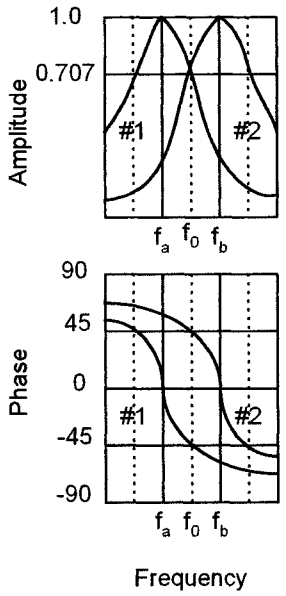

Figure 2.14: Amplitude and phase diagrams for single-fed CP patch

Two fundamental configurations of single-feed circular polarised antennas are shown in figures 2.15.

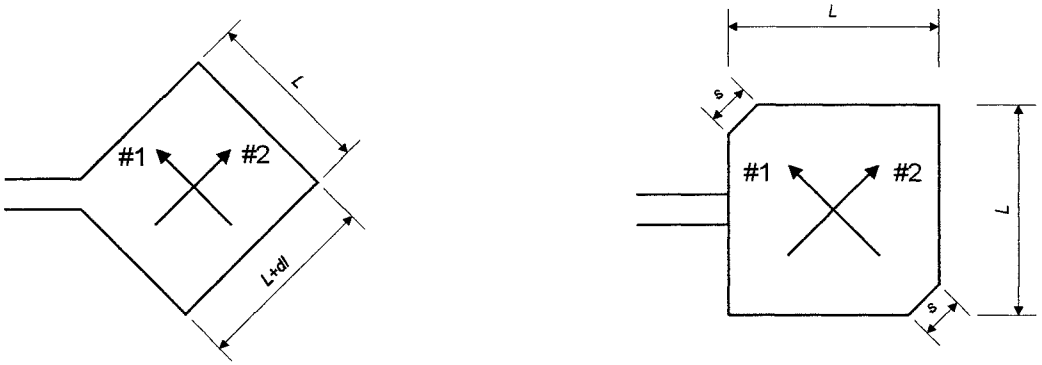

(a) Nearly square (b) Truncated corners

Figure 2.15: Single feed CP patch arrangements

A Nearly Square CP Patch is shown in figure 2.15(a). In this design, the dimensions of *dl* are small thus keeping both sides almost equal in length such that there is significant overlap between the TM_{01} and TM_{10} modes. Another method of

achieving circular polarisation is to trim the ends of two appropriate corners of a square patch, as shown in figure 2.15(b). By setting the perturbation segment, *s*, at an appropriate position, two orthogonally polarised TM_{01} and TM_{10} modes can also be excited.

2.3 Patch Antenna Modelling Techniques

The focus of this thesis centres around an investigation of slot loaded patch antennas. Thus, the focus of this section is to examine different modelling techniques to ascertain the most appropriate approach for the analysis of such structures. To determine the electromagnetic fields within a microstrip, Maxwell's equations must be solved and the appropriate boundary conditions also satisfied. For microstrip antennas, the problem becomes complex because the structure presents in homogeneities of three different types:

- The electromagnetic fields of the waves extend over several propagation media; air and dielectric, or air and several dielectrics.
- The air-to-dielectric interface is partly covered with metal, so different boundary conditions apply at different parts of the structure.
- The transverse dimensions of the substrate are finite because both the dielectric substrate and ground plane have to end at a certain distance from the circuit.

This triple inhomogeneity involves a rigorous analysis.

Full-wave analysis [97, 98] involves the solution of Maxwell's equations for the electric current distributions on the conducting elements. Once this has been determined, all other parameters of interest can be derived. The currents produce electromagnetic fields which must satisfy Maxwell's equations which relate the fields, current sources and charges. Using this approach, space wave radiation, surface wave modes, dielectric losses, conductor losses and coupling to external elements can be included in the analysis. Although this technique provides the most accurate

solution for impedance and radiation characteristics [80], it requires considerable computational resources and yields little physical insight. Full wave analysis is employed in this thesis to determine the far field characteristics of the above antenna, through the application of a commercially available software, Ansoft Ensemble [92].

To overcome the complexities associated with full-wave analysis, a number of approximate methods have been developed that maintain simplicity at the expense of accuracy or versatility. These include transmission line, cavity and coplanar multi-port network models that operate using the general assumption that substrates are electrically thin.

The transmission line model and cavity model have been applied within this chapter to determine the input impedance and field distributions within a rectangular patch. Neither of these models in their present form could be applied directly to model a patch antenna with embedded slot loading. Although the transmission line model is simple to use, it suffers from numerous disadvantages, for example the fringing factor must be empirically determined and field variations along the radiating edges are ignored. Moreover, it is based on the assumption that the patch antenna can be regarded as a wide microstrip transmission line. The presence of slot loading changes the structure of the patch, which suggests that this assumption is no longer appropriate. Another disadvantage of this modelling technique is that the Q factor is also empirically determined. The presence of slot loading is expected to have a significant effect on this parameter, which reinforces the suggestion that the transmission line model is not the most effective approach.

The cavity model overcomes some of the disadvantages of the transmission line model. Using this approach, the patch is viewed as a thin TM_z mode cavity with magnetic walls [97 – 105]. The field between the patch and the ground plane is

expanded in terms of a series of resonant modes or eigenfunctions along with the eigenvalues or resonant frequencies associated with each mode. This results in a much more accurate formulation for antenna parameters such as resonant frequency and input impedance [78]. However, the cavity model is only applicable for patch antennas having geometries for which the corresponding wave equation can be solved by separation of variables, i.e. rectangular, circular, triangular. Again, the modified patch shape due to the presence of slot loading suggests the need for a different approach.

The multiport network model approach [105] may be considered as an extension, or generalisation of the cavity model [106] to antennas of composite geometries. Coplanar analysis is based upon relating the voltage at a point on the patch perimeter to the normal current density at another point on the perimeter by means of the Green's functions of the patch geometry. This approach is only applicable to patch shapes for which Green's functions are available such as; square, rectangular, triangular, circular or annular.

For many practical applications where Green's functions are not available, it is often possible to reconstruct the given structure by combining regular shapes for which Greens function are available. Coplanar analysis is then used to establish multiport perimeter connections between the segments, as illustrated in figure 2.21.

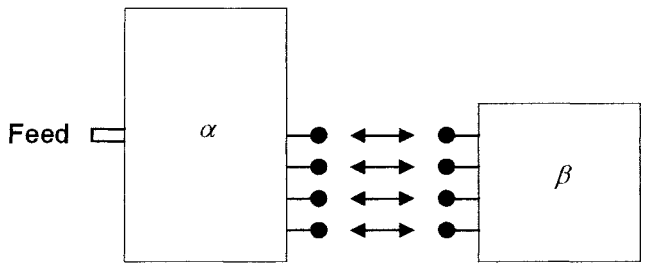

Figure 2.16: Illustration of multiport segment interconnection

A multiport network matrix circuit analysis [107] can then be used to determine the circuit characteristics of the composite antenna structure. Synthesis of the segments is then achieved through the use of either segmentation or desegmentation technique.

In order to analyse slot loaded patch configurations for circuit characteristics such as input impedance, Q factor and bandwidth, it was found that the coplanar multiport network model is the most applicable. This approach offers flexibility in modelling patch antennas with complicated structures. The multiport network model has the advantage of being capable of handling fairly arbitrary patch shapes and multiport elements [76]. It can also be used to model microstrip feeds, parasitic elements and mutual coupling in arrays. It provides efficient modelling in terms of programming simplicity, computational resources and accuracy, thus making it suitable for use in conjunction with optimisation routines.

2.4 Summary

In this chapter the antenna design parameters for a traditional patch antenna, together with typical performance characteristics have been defined. Miniaturising a patch antenna affects it radiation [39-43, 72-75] and influence its bandwidth, gain, efficiency, polarisation purity and input impedance. Specific attention has been made to the most important performance characteristics for reduced size patch antennas. These include: TM_{mn} mode distribution; input impedance; radiation characteristics; and generation of circular polarisation. A review of different modelling techniques, including transmission line, cavity, co-planar network, segmentation / desegmentation and full-wave modelling. It has been argued that the most appropriate method for slot loaded reduced size patch structure is the segmentation / desegmentation approach.

CHAPTER 3

COMPACT PATCH ANTENNA OPERATION

3.1 Introduction

In recent years significant progress has been made in the design of compact patch antennas. A number of techniques have been reported to reduce the size of a microstrip antenna at a fixed operating frequency, including: the use of high permittivity substrate; shorted patch antennas; folded patch; slot loaded patch; slot loaded ground plane; and various 'miscellaneous' techniques. The focus of this chapter is to provide a review of such techniques to ascertain the most appropriate technique to achieve the ultimate aim of producing planar fed reduced size patch antennas. Aside from reducing the element size, some of these techniques outlined above have also been employed to produce patch antennas with a dual frequency response. These designs operate using a similar principle of operation through TM_{mn} mode modification. Hence a review of such designs are incorporated within this discussion.

It is predicted that the deployment of such techniques will have an adverse effect on patch performance. Subsequently, there are a number potential trade-offs to be considered, such as input impedance, bandwidth, gain, cross-polarisation, which will also be addressed within this chapter.

Following this brief introduction, section 3.2 will give a brief overview of present methods of patch antenna size reduction. Section 3.3 will focus on shorted patch technique, while section 3.4 will focus on slot loaded ground plane. Another method of achieving size reduction can be achieved by inserting slots in the patch rather

than the ground plane. The importance of this technique to this thesis demands that a more thorough investigation be conducted, which is given in section 3.5. In section 3.6, the choice of a suitable method for application to reduced size planar fed patch antenna design is discussed. Section 3.7 will summarise the major outcomes of this chapter.

3.2 Size Reduction Techniques

(i) Use of high permittivity substrate

Conventional microstrip antennas are half-wave resonators that operate at the fundamental TM_{01} and / or TM_{10} modes. In such structures, the resonant frequency is related to both the patch length and permittivity and was given in (2.1) as:

$$f_r = \frac{1}{2\pi\sqrt{\varepsilon_r \mu_r}} \sqrt{\left(\frac{m\pi}{L}\right)^2 + \left(\frac{n\pi}{W}\right)^2}, \tag{3.1}$$

Examination of the (3.1) suggests that one obvious way of reducing the patch size is to use regular patch shapes on high permittivity substrates. However, this has an adverse effect on both cost and patch performance. Pozar [76] described an important trend that suggests the Q factor increases with increasing permittivity, thus reducing the antenna bandwidth. A higher permittivity is also often equivalent to higher dielectric losses [109]. Moreover these substrates are often ceramic based and require specialist machining equipment, which dramatically increases the cost of the antenna.

(ii) Shorted patch

The use of a edge-shorted patch is a well known technique for achieving reduced size operation of a patch antenna. By using this approach the antenna operates as a quarter-wavelength structure and can therefore be used to reduce the antennas

physical length by half at a fixed operating frequency [110]. The use of a partial shorting wall or pin has been shown to further reduce the resonant frequency [44,45] and hence antenna size. However, this technique has an adverse affect on the bandwidth, cross-polarisation and E-plane radiation patterns.

(iii) Folded patch

This method of reducing the size of a patch antenna, which involves the use of an inverted U-shaped patch has been suggested by Chair et al [52] and Wong et al [111]. Using this approach, the excited current path of the TM_{mn} mode / (s) is lengthened, thus reducing the antenna resonant frequency for a fixed projection area. Extensions of this technique include a folded patch [53], double-folded patch [53], and a planar inverted-L patch antenna [112,113]. Such designs are often incorporated with air substrate designs for applications where compact patch antennas with increased bandwidth are required. A major disadvantage of these designs is their non-planar structure, with size reduction being achieved at the expense of increased projection area and a more complex manufacturing process.

(iv) Slot loaded patch

An alternate method of meandering the surface current path can be achieved through the use of embedded slots in the patch antenna. The slot loaded patch has a meandering effect on the excited current path of the TM_{mn} mode / (s), thus accounting for a reduction in operating frequency, and hence size reduction[44,58,62,64,114].

(v) Slot loaded ground plane

A similar meandering effect on the excited current path can also be achieved by embedding slots in the ground plane. It has been experimentally observed [56] that similar effects on resonant frequency, and hence size reduction to those with the

design using a slot loaded patch can be obtained. However, one of the major disadvantages of slot loaded ground planes is the creation of back radiation [57].

(vi) Miscellaneous techniques

There are a number of 'miscellaneous' techniques that can be used to reduce the size of a microstrip antenna. These include the use of fractal antenna [115], lumped element loading [111,116], the use of use of electromagnetic bandgap material [117], and the use of shorted coplanar feedline [118].

The research described in this thesis relates to the use of compact patch antennas that do not compromise its planar structure. Consequently, the most suitable approaches are the use of shorted patch, slot loaded patch, or slot loaded ground plane.

3.3 Shorted Patch

The use of a edge-shorted patch, as shown in figure 3.1(a), is a well known technique for achieving reduced size operation of a patch antenna. This approach makes the antenna operate as a quarter-wavelength structure and can therefore reduce the antenna's physical length by half at a fixed operating frequency. Size reduction can also be achieved using a partial shorting plate (see figure 3.1(b)), or a shorting pin (see figure 3.1 (c)).

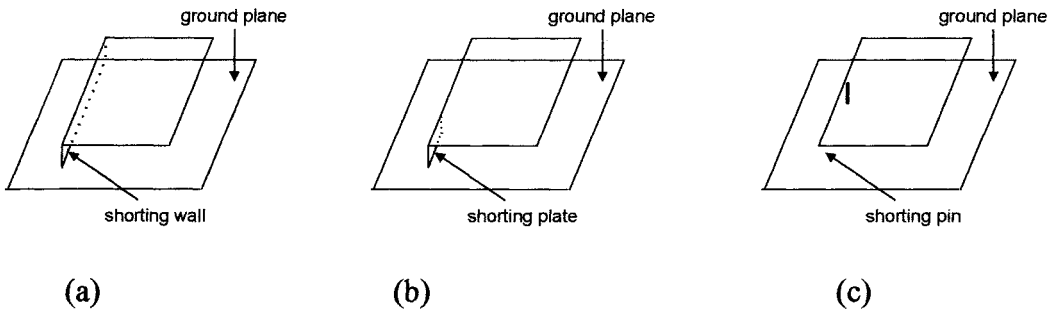

Figure 3.1: Geometries of a rectangular patch with (a) a shorting wall, (b) a partial shorting plate, and (c) a shorting pin

To understand the basic principle of operation of the shorting pin loading technique, it is worth considering the case of a standard rectangular patch operating n the fundamental TM_{01} mode. The resonant frequency of this structure is given in [108]:

$$f_0 \approx \frac{c}{2L\sqrt{\varepsilon_r}} \quad , \tag{3.2}$$

If a shorting wall is placed along the centre of the patch edge ($x = L, y = W/2$) and the feed position is chosen on the x axis, the first resonant frequency occurs at $0.5f_{01}$. In this case the structure is operating as a quarter-wavelength antenna. The effect of multiple shorting pins on the resonant frequency of a patch antenna has been reported by Sanad [119]. It is demonstrated that this structure can be analysed by modelling the shorting pins as short pieces of a transmission line of length h. Hence a series inductance L and a shunt capacitance C is added to the microstrip antenna. The values of L and C can be approximated by [119]:

$$L = \frac{t\mu}{\pi}\cosh^{-1}\left(\frac{d}{2a_p}\right) \quad , \qquad C = \frac{t\pi\mu}{\cosh^{-1}\left(\frac{d}{2a_p}\right)} \quad , \tag{3.3}$$

where a_p is the radius of the pins, and d is the separation between them.

From this it can be seen that increasing ($d/2a_p$) increases L and decreases C. If the inductive reactance of the shorting posts increases the frequency decreases. If multiple shorting pins are used, the distance between them is small. As the number of shorting pins reduces, the distance between increases. Following this analogy, this suggests that greater size reduction can be achieved using a single shorting pin as opposed to a shorting wall [119]. This has been applied by Wong [110] who demonstrated that when a single shorting pin is placed at the centre of the patch

edge ($x = L, y = W/2$) and the feed position is chosen on the x axis, the first resonant frequency occurs at $0.38f_{01}$ [110].

Size reduction achieved using shorting pin loaded technique is mainly due to the shifting of the null-voltage point at the patch centre to the patch edge, thus making the shorted patches resonate at a much lower frequency. Maximum size reduction is achieved when the shorting pin is placed at the centre of the patch edge, and decreases as the shorting pin moves towards the patch centre ($x = L/2, y = W/2$). To confirm this, a rectangular patch with single shorting-pin loading and fed with a microstrip feed, as shown in figure 3.2, was constructed. Analysis of the configuration using Ensemble [92] determined the effect of shorting pin position on the first resonant frequency, with results are shown in figure 3.3.

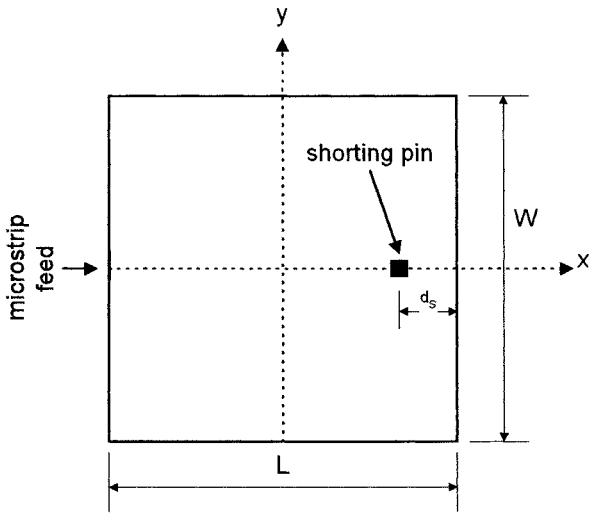

Figure 3.2: Shorting pin loaded rectangular patch

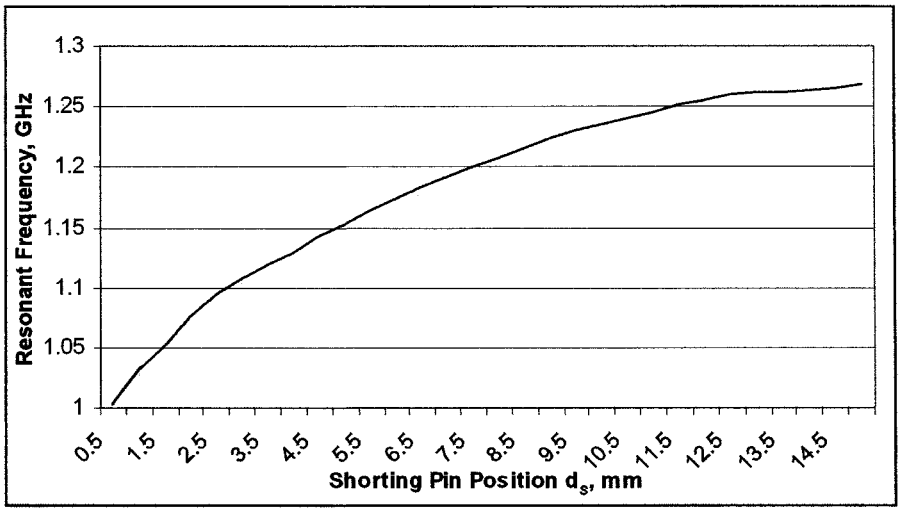

$\varepsilon_r = 2.33$, $h = 1.57$ mm, $L = W = 30$ mm

(b)

Figure 3.3: Effect of single shorting pin position on 1st resonant frequency

The technique of shorting pin loading has been applied to a number of patch configurations including rectangular [120], circular [46,49,121] and triangular [48,49] geometries, as shown in figure 3.4, to produce reduced size operation of a microstrip patch antenna. The technique has also been applied to an H-shaped structure [51]. In all cases, the antenna is excited using a probe feed.

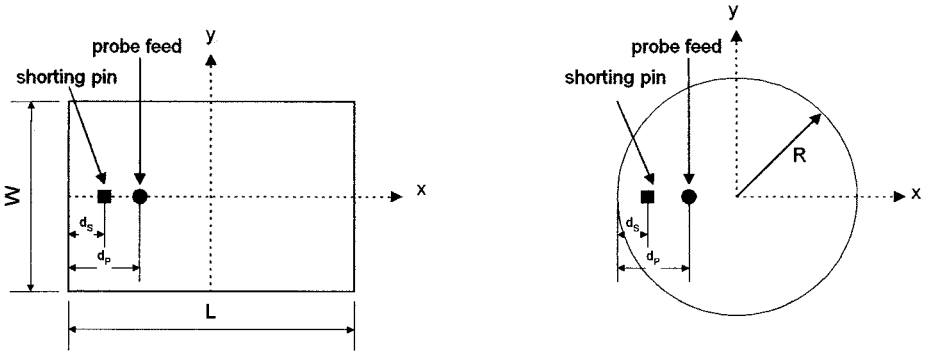

(a) (b)

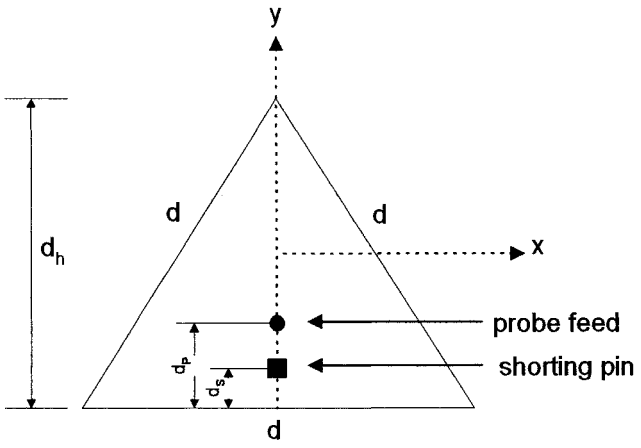

(c)

Figure 3.4: Geometries of shorting pin loaded (a) rectangular, (b) circular, and (c) triangular patch antennas

The use of shorting pin loading has also been used by Wong et al [122] to produce dual frequency operation of a rectangular patch antenna, with both frequencies having the same polarisation sense. The patch is excited using a probe feed at an appropriate position along the centre-line ($y = W/2$). The configuration is illustrated in figure 3.5.

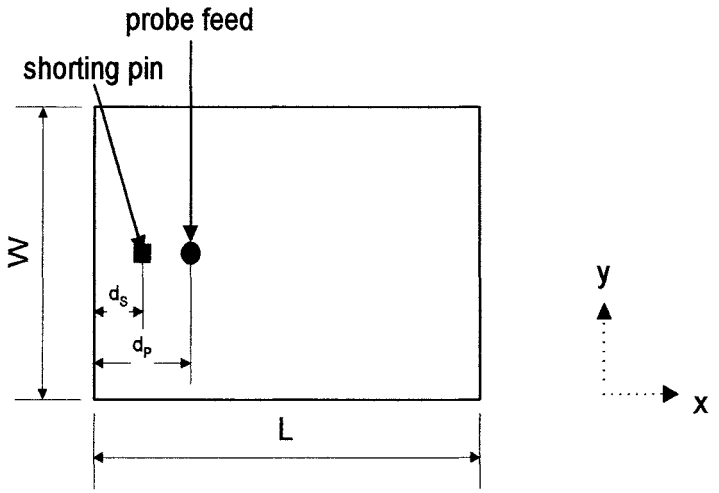

$L = 37.3$ mm, $W = 24.87$ mm, $\varepsilon_r = 4.4$, $h = 1.6$ mm

Figure 3.5: Geometry of compact single-feed dual-frequency rectangular microstrip antenna

In this paper, Wong et al [122] reports the effect of shorting pin position on the first (f_1) and second (f_2) resonant frequencies. When the shorting pin is placed almost at the patch edge ($x = 0, y = W/2$), the first two resonant frequencies occur at ~722 MHz and ~2330 MHz respectively, thus achieving a frequency ratio (FR) of 3.2. As the shorting pin is moved towards the patch centre, f_1 increases and f_2 decreases. With the shorting pin placed at the patch centre ($x = L/2, y = W/2$) f_1 and f_2 occur at ~950 MHz and ~1900 MHz respectively, thus achieving a frequency ratio of 2.0. A similar technique has also been applied to circular [123], triangular [124] and bow-tie [125] patch geometries.

Despite the significant advantages in terms of size reduction, there are a number of disadvantages both in terms of circuit and far-field characteristics. Considering the circuit characteristics, one trade off involves the patch excitation. Although incorporating a single shorting pin effectively reduces the patch size, Sanad [119] reports that the input impedance at resonance becomes significantly larger. Research has shown very small conductors for both the coaxial feed and the shorting pin must be used and located in close proximity [46] to reduce the input impedance at resonance close to 50 Ω. The small diameter of these components, typically less than $0.01\lambda_g$ [126] (where λ_g is the guided wavelength) are difficult to realise practically. These two factors suggest strict manufacturing tolerances. From this it would also appear difficult to excite the patch efficiently using a planar feed.

Another trade-off regards the narrow bandwidth. Waterhouse [45] reports that for a circular patch with single shorting-pin loading a 10 dB return loss bandwidth of 1.2% is achieved. This compares with a value of 1.8% for a conventional circular microstrip patch with the same resonant frequency and substrate. The difference is attributed to the bandwidth's relationship to the electrical volume of the antenna.

Considering the effect of shorting pin loading on the far-field characteristics of the antenna, the patch configuration shown in figure 3.2, was simulated using Ensemble [92]. In this instance the shorting pin was placed at a distance ds =1mm from the patch edge, producing a resonant frequency f_1 of 1.032 GHz. The E and H-plane radiation patterns are shown in figures 3.6 and 3.7 respectively.

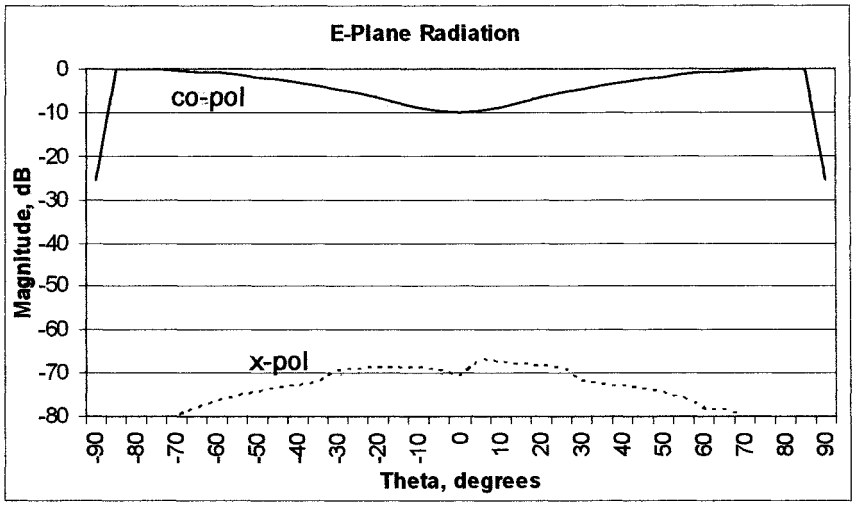

Figure 3.6: E-plane radiation pattern of shorted patch

The results show that there is a decrease in the E-plane gain at broadside. Waterhouse [127] reports that the extent of the decrease in magnitude is dependant on the relative position of the shorting pin and probe feed with respect to the patch centre. However, it can also be seen that the E-plane cross-polarisation levels remained largely unaffected, with the level remaining at less than -70 dB.

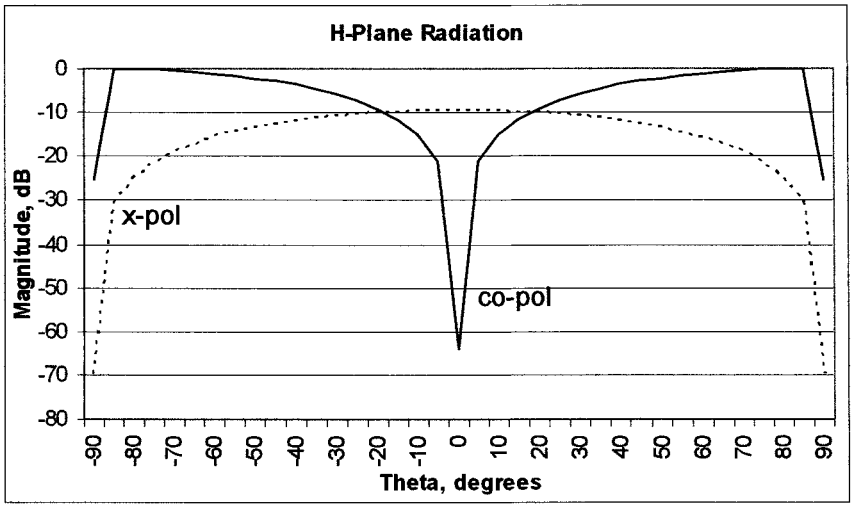

Figure 3.7: H-plane radiation pattern of shorted patch

A fundamental problem of the shorted patch is the excitation of other TM_{mn} modes as a result of the discontinuity on the patch conductor. This results in high level of cross-polarised fields generated in the H-plane, as shown by figure 3.7. A theoretical comparison of the cross-polarisation levels for a shorted patch and a conventional circular patch was performed by Waterhouse [127]. It is reported that the H-plane cross polarisation levels for the shorted patch are approximately 14 dB greater than for the conventional circular patch.

3.4 Slot Loaded Ground Plane

The use of a slot loaded ground plane provides an alternate method of modifying the frequency response of a conventional patch antenna. This has the effect of lengthening the excited surface current path of the fundamental modes, thus reducing its resonant frequency and accounting for size reduction. To produce compact operation of a single frequency microstrip antenna with linear polarisation, Kuo et al [56] have proposed a conventional rectangular patch shape with a meandered ground plane, as shown in figure 3.8.

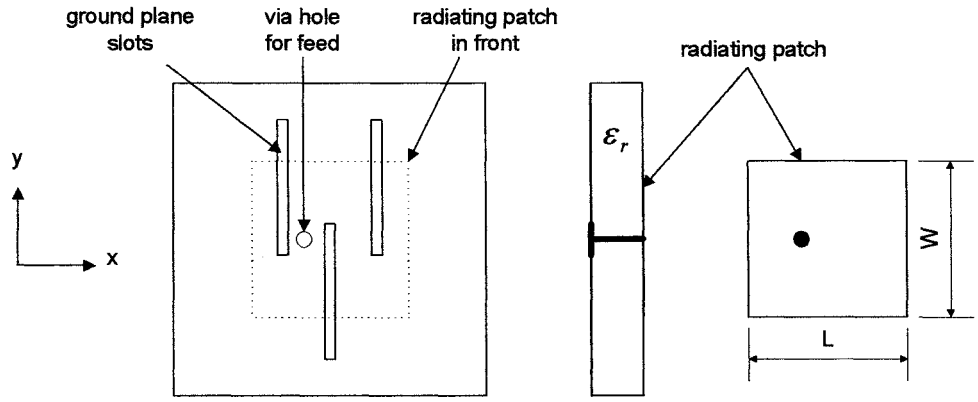

Figure 3.8: Compact microstrip antenna with meandered ground plane

It is reported that a frequency reduction from 2387 MHz, for a conventional rectangular patch, to 1587 MHz for the proposed design is achieved, which equates to a patch size area reduction of 56%. Previous research indicates that an increased bandwidth, as high as 3.7%, is achieved using the proposed design [56]. This compares to a bandwidth of 2% for a conventional rectangular patch fabricated on the same FR4 substrate. This is attributed to the meandering effect of the ground plane which effectively lowers the quality factor of the antenna. It is also reported that using this approach increases the radiation efficiency of the antenna [57]. However, a significant proportion of this is back radiation and therefore should not be included in radiation efficiency calculation.

A similar approach has also been suggested by Chiou et al [57], which incorporates a single pair of narrow slots in the ground plane, thus producing a symmetrical structure, as shown in figure 3.9.

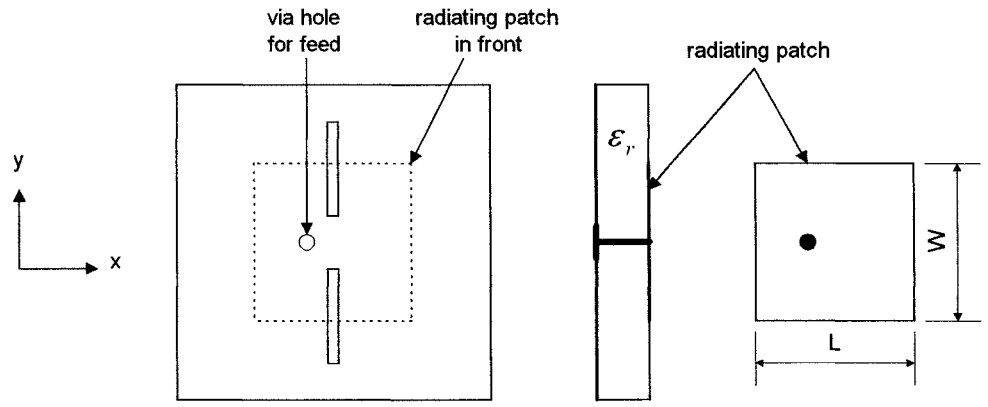

Figure 3.9: Compact microstrip antenna with single pair of ground plane slots

An extension of this technique, which incorporates two pairs of narrow slots in the ground plane, as shown in figure 3.10, to produce reduced size dual or circular polarisation operation has also been reported [57].

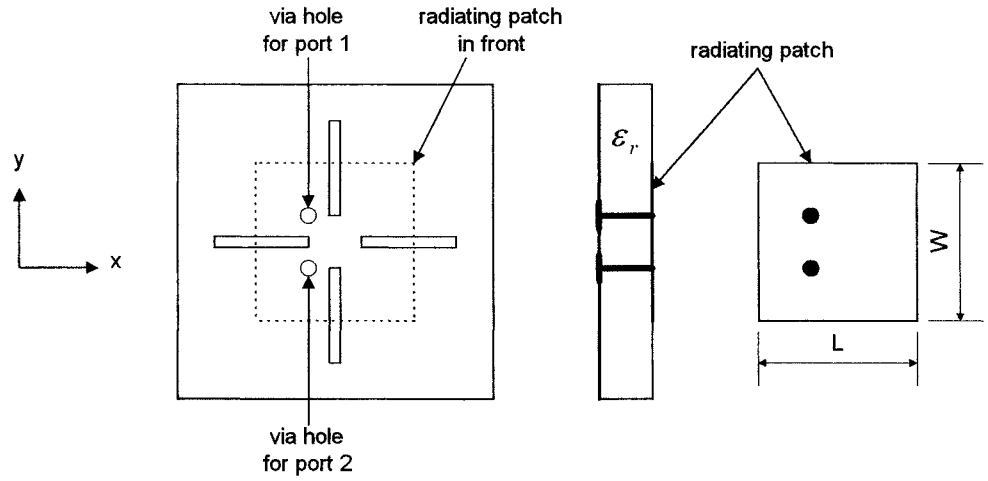

Figure 3.10: Compact microstrip antenna with two pairs of ground plane slots

Compact dual polarised operation of this design is achieved by using two pairs of equal length slots and exciting with two probe feeds along the diagonals of the patch. Compact circular polarisation operation is achieved by using two pairs of

unequal length slots and using a single feed along one of the patch diagonals to excite two near-degenerate orthogonal modes.

One of the major disadvantages of slot loaded ground planes is the creation of back radiation. This is due to the presence of slots in the ground plane, and the decreased ground-plane size in wavelength. Prior investigation indicates that the front to back (FTB) ratio decreases with increasing slot size. When maximum size reduction is achieved the FTB ratio decreases from 9.3 dB, for a conventional design, to 2.0dB for the proposed design. To confirm this, the patch configuration shown in figure 3.11 was simulated using Ensemble, with results shown in figure 3.12(a). For comparison, figure 3.12(b) demonstrates the radiation pattern of a conventional rectangular patch.

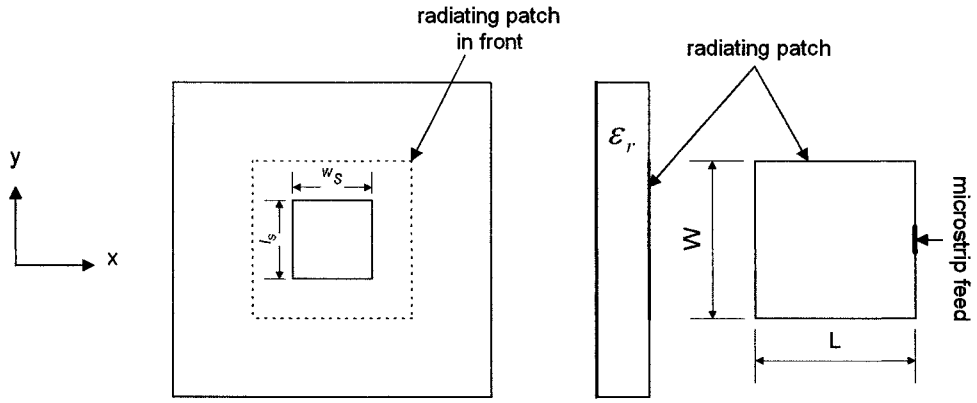

$\varepsilon_r = 2.33$, $h = 1.57$ mm, $L = W = 30$ mm, $l_S = 10$ mm, $w_S = 10$ mm

Figure 3.11: Rectangular patch antenna with slot loaded ground plane

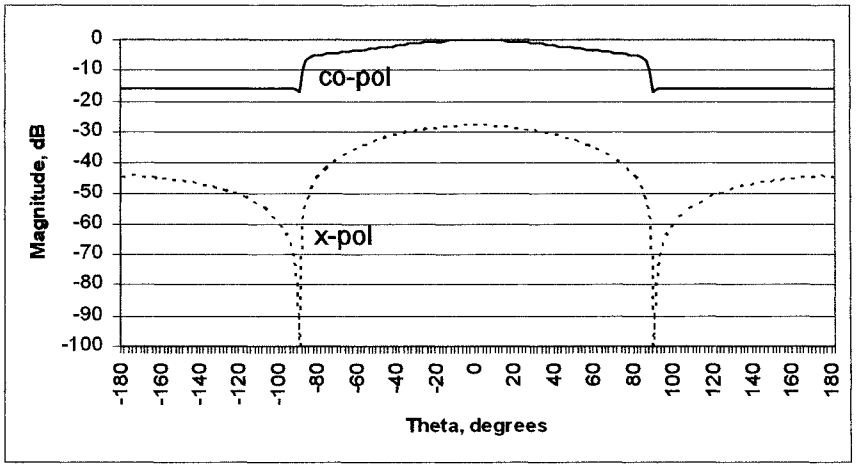

(a)

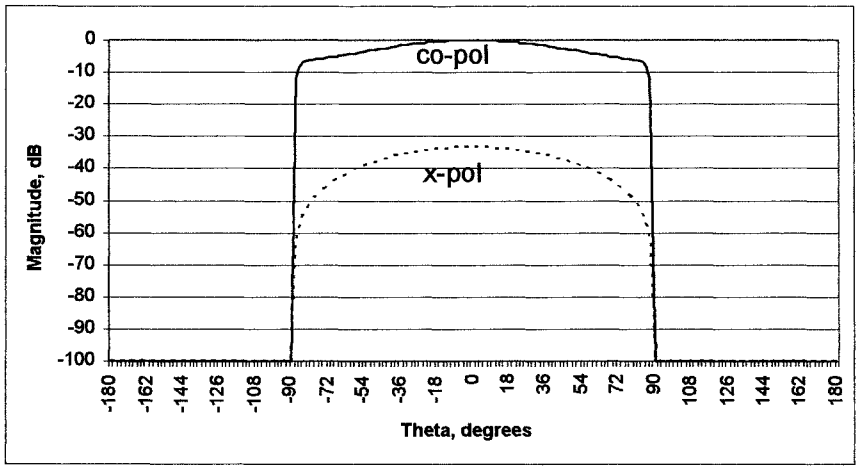

(b)

Figure 3.12: E-plane radiation pattern of (a) patch with slot loaded ground plane and (b) conventional patch antenna

The results confirm the prediction that large levels of back radiation exist as a result of the slot loaded ground plane.

3.5 Slot Loaded Patch

The technique of inserting slots within regular patch shapes has also been shown to change the operation of a standard patch antenna. The insertion of slots results in perturbation of different TM_{mn} modes. The modes which are affected and to what

extent is dependant on the slot shape and dimensions, together with its position. The insertion of slots in certain positions can also result in the creation of additional modes. By perturbing the correct mode / s, it is possible to produce compact linear and circular polarised antennas, dual frequency antennas and wideband antennas.

3.5.1 Modification of fundamental TM_{mn} modes

In recent years, a number of authors have proposed designs for compact antennas with both linear and circular polarised operation for single frequency operation. Several designs have also been suggested for compact dual frequency patch antennas with the two frequencies being orthogonally polarised. Such designs rely on modifying the current paths of the fundamental TM_{01} and TM_{10} modes by embedding slots within a standard rectangular patch. In this section, an overview of the most significant designs are outlined.

3.5.1.1 Single square slot

The technique of square slot loading within a square or rectangular patch has been employed by a number of authors to reduce the size of a patch antenna. Inserting a single square slot in the centre of a square patch increases the surface current path of the fundamental TM_{01} and TM_{10} modes, and thus accounts for a lower operating frequency [128]. As described in Chapter 2, the slot has maximum effect on the fundamental mode when it is placed in the centre of the patch where the current is at a maximum.The technique of embedding a square slot loading inside a square patch to perturb the TM_{01} modes current path, as shown in figure 3.13, has been employed by Palanisbury et al [51] to produce a compact linear polarised patch with size reduction of 17.5%.

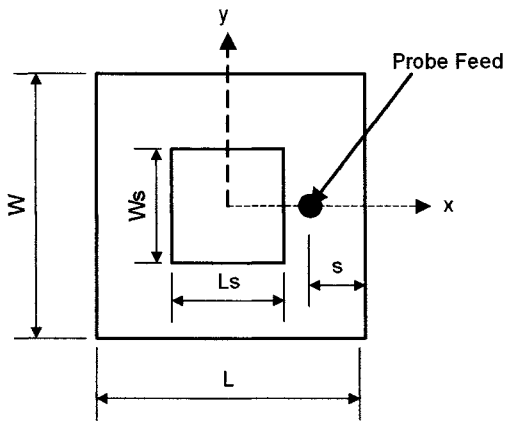

Figure 3.13: Patch with single square slot

The same technique has been applied to a square patch with truncated corners by Chen et al [128] to produce compact CP operation. In this instance both the TM_{01} and TM_{10} modes were lengthened to produce a patch with a centre frequency lowered by 10%, which corresponds to a patch size reduction of 19%. This technique has also been used by Chen [66] in a rectangular patch to produce a reduced size dual frequency patch, with the two frequencies being orthogonally polarised. The first two dominant frequencies, relating to the TM_{01} and TM_{10} modes, were reduced by 9%, thus accounting for a size reduction of 17 %.

With all slot loaded designs outlined above, size reduction is achieved at the expense of other parameters such as input impedance, bandwidth, Q factor, frequency ratio, axial ratio bandwidth, and manufacturing tolerances. The first trade-off to consider regards the input impedance. In the above designs, the patches are excited using a probe feed whose position is controlled by the square slot size. As the slot size increases the input impedance also increases and hence the 50 Ω feedpoint moves towards the slot. Practical size reduction is limited by the value of input impedance.

A further trade-off, specific to the dual frequency antenna is also apparent. It is reported that a relatively low frequency ratio range, from 1.276 to 1.281, exists for this design. This is due to the frequency ratio being largely controlled by the patch

aspect ratio. However, in order to achieve simultaneous impedance matching for both TM_{01} and TM_{10} modes, the patch length L must be comparable to the patch width W. As a consequence, for a fixed substrate thickness, any reduction in frequency will translate to a reduction in the electrical volume of the patch.

Considering the circular polarised design, a decrease in electrical volume of the substrate produces a reduction in axial ratio bandwidth with increasing slot size [128]. In this case, a reduction from in ARBW from 1.45% for a standard patch with truncated corners, to 1.33% for the square slot loaded design is reported. Conversely, it is found that the size of perturbation segment increases with increasing slot size, thus relaxing manufacturing tolerances.

3.5.1.2 Square-ring with cross Strip

A modification of the square slot loaded design has been suggested by Chen [71] which consists of a square ring structure with a cross strip to produce reduced size operation of a single frequency patch antenna. Two configurations are suggested, incorporating a centre-line cross-strip and a diagonal cross-strip, as shown in figures and 3.15, to achieve size reduction of 33% and 40% respectively. Circular polarisation is achieved by introducing a protruding stub to perturb the structure and thus excite two near-degenerate orthogonal modes. The patch is excited with a probe feed placed at an appropriate point along the cross strip.

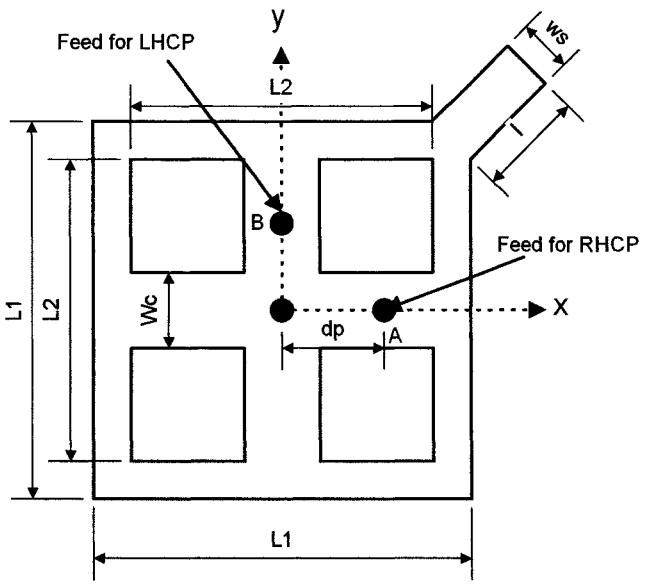

Figure 3.14: Square-ring microstrip antenna with centre-line cross strip

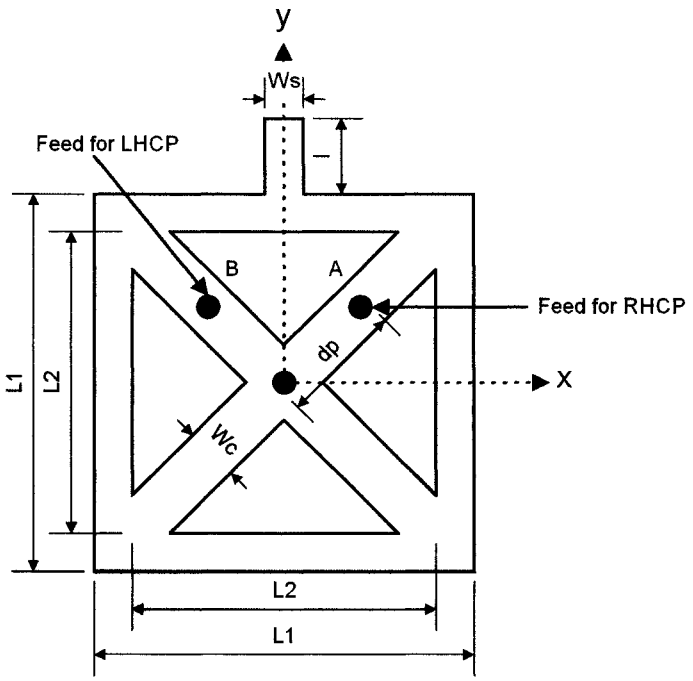

Figure 3.15: Square-ring microstrip antenna with diagonal cross strip

One of the problems of the square slot loaded design regards the input impedance. It was stated that as the slot size increases the 50 Ω feed position moves closer to the slot, thus only limited size reduction can be achieved. With the incorporation of a cross-strip structure, as L2 increases the feed position moves along the strip

towards the patch centre. This allows the square slot size to increase further, hence reducing the resonant frequency and antenna size further, whilst still maintaining input impedance matching.

Trade-offs associated with this design are similar to those for the square slot loaded patch, such as input impedance and axial ratio bandwidth. Primarily, achievable size reduction is limited by the value of input impedance at the feedpoint. As the slot size increases, the input impedance along the cross-strip increases, eventually reaching a value where a 50 Ω feedpoint cannot be found. A further trade-off of this design is a reduction in axial ratio bandwidth with increasing slot size. It is reported that this value decreases from 1.4%, for a standard nearly square patch, to 0.89% and 0.81% for figures 3.14 and 3.15 respectively. This compares to an axial ratio bandwidth of 1.33% for the square slot loaded design [128]. A major reason for the difference is attributed to the frequency selectivity of the protruding stub required to achieve circular polarisation as opposed to truncated corners.

3.5.1.3 Cross slot

Compact dual frequency operation of a patch antenna can also be achieved through the use of cross-slot loading inside a rectangular patch, as shown in figure 3.16 [129]. It could be argued that this design has evolved from the square slot loaded structure suggested by Chen [66]. From the research described in chapter 5 of this thesis, the square slot length Ls is largely responsible for frequency reduction of the TM_{01} mode, and has little effect on the TM_{10} mode. Conversely, the slot width Ws controls the frequency of the TM_{10} mode, with little effect on the TM_{01} mode.Given this fact, the slot geometry can be modified to create a cross-slot structure.

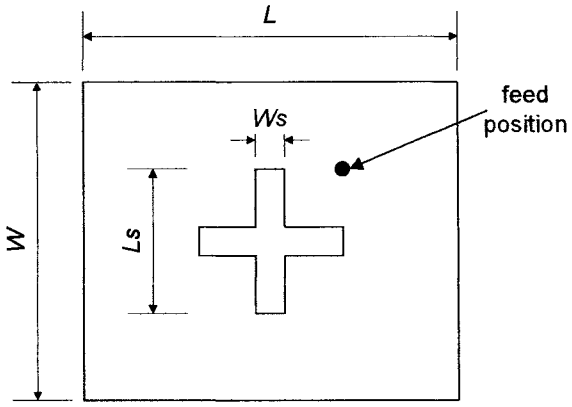

Figure 3.16: Cross-slot loaded rectangular patch

Using this structure, it is reported that dual frequency operation with each frequency being orthogonally polarised, a size reduction of 23% can be achieved. The cross-slot loading is responsible for size reduction, whilst the aspect ratio of the patch controls the frequency ratio.

As previously outlined, practical size reduction of square-slot loaded designs are controlled by the relationship between slot size and feed position. By employing cross-slot loading the slot length, Ls, is now allowed to increase further whilst the feedpoint can be moved closer to the patch centre without being inside the slot. Using this approach allows a further size reduction of 6% compared to that of Chen [66]. However, as with other slot loaded designs the maximum size reduction achievable is still limited by the input impedance value.

A further trade-off of this design regards the frequency ratio. For reasons similar to those relating to Chen [66], only a small frequency ratio range from 1.284 to 1.292 is achievable. Another trade-off involves a reduction in bandwidth for both frequencies, from 1.84% and 2.44% for a conventional unslotted dual frequency patch of the same dimensions L and W, to 1.38% and 1.82% for f_1 and f_2 respectively for the given design.

A modification of this design, which incorporates bent slot loading, as shown in figure 3.17 has been suggested by Wong et al [130] to produce compact dual frequency operation of a patch antenna.

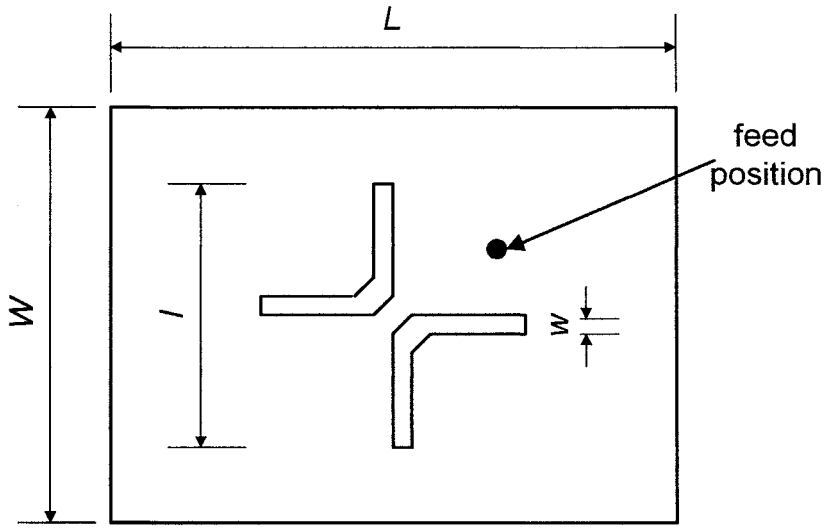

Figure 3.17: Patch with bent blots

The modified slot geometry produces different surface current paths for the TM_{01} and TM_{10} modes. This changes the feed position, and as a result size reduction of up to 32% can be achieved whilst still maintaining an input impedance of 50 Ω. A frequency ratio ranging from 1.292 to 1.378 is achievable, which is a slightly greater range than previous designs mentioned above. However, this design still suffers from the problem of reduced bandwidth, from 1.86% and 2.76% for a conventional unslotted dual frequency patch of the same dimensions L and W, to 1.46% and 1.83% for f_1 and f_2 respectively, for the given design, which is still comparable to previous designs.

3.5.1.4 H-shaped Patch

The designs considered so far have involved slot configurations placed inside the patch structure. A modification of these designs involve the use of rectangular slits cut into the centre of the non-radiating patch edge to produce an H-shape structure, as shown in figure 3.18. This technique was first employed by Palanisamy and

Garg [51] to produce a compact operation of a linear polarised patch antenna, by exciting the TM_{01} mode, achieving a reported size reduction of up to 46%.

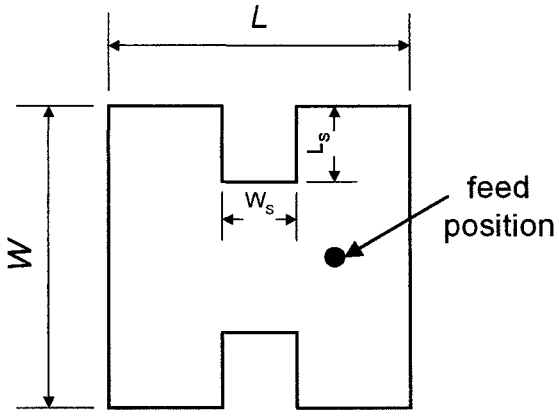

Figure 3.18: H-shaped microstrip patch

To excite the TM_{01} mode, the feedpoint is placed at an appropriate point along the $y = W/2$ axis. As with other slot loaded designs, the input impedance of the H-shape patch along the feed axis increases with increasing slot length. This is the major controlling factor for achievable size reduction. However due to the patch geometry, the feedpoint can be moved slightly closer to the patch centre and thus slightly greater size reduction can be achieved.

An extension of this technique has been reported by Wong and Wu [70] to produce compact circular polarised operation by incorporating a further pair of slots, as shown in figure 3.19. Circular polarisation is achieved by perturbing both the TM_{01} and TM_{10} modes with two pairs of slots of unequal lengths, and exciting both modes with a probe feed at an appropriate point along the patch diagonal.

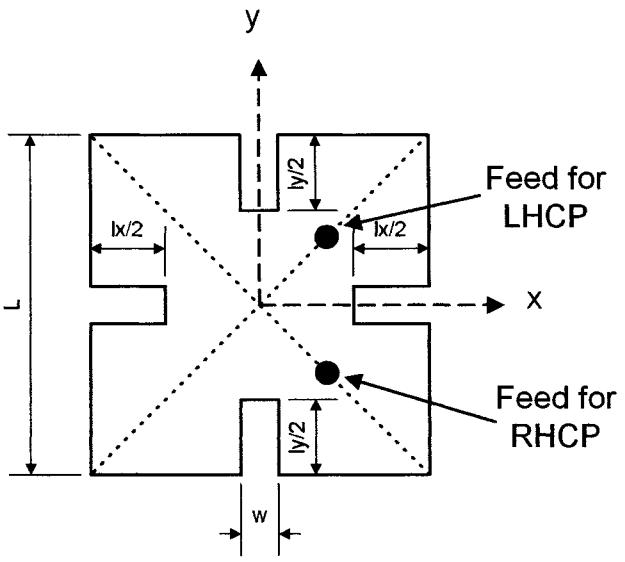

Figure 3.19: Single-feed small circularly polarised square microstrip antenna

In both designs, size reduction is achieved at the expense of input impedance, Q factor, axial ratio bandwidth and strict manufacturing tolerances. Considering input impedance, as with other slot loaded designs, it is found that the input impedance increases with slot size. This is one of the major limiting factors on achievable size reduction. Palinsbury and Garg [51] have reported that a Q factor of 127.8 can be achieved using an H-shape structure. This compares to a value of 68 for a conventional rectangular patch. From equation (2.13), it can thus be concluded that using an H-shape structure will reduce the antenna bandwidth. A similar trend can be predicted for similar circular polarised designs.

Regarding the axial ratio bandwidth, although no available literature exists, from Chapter 6, it is expected that this value will decrease with size reduction. With reference to the design suggested by Wong and Wu [70], the ratio of the slot lengths l_x and l_y required to produce circular polarisation is reported to be very small and further decreases with size reduction. This produces strict manufacturing tolerances.

To overcome this, a modified technique has been suggested by Chen et al [131], in which it is reported that by using inserted equal length slits at the patch corners, it is possible to obtain a size reduction of up to 36%. In this design circular polarisation is achieved through the use of truncated corners, which is reported to relax manufacturing tolerances, with the size of truncated corners increasing with slot size.

3.5.1.5 Inset microstripline-fed circular polarised microstrip antenna

In the previous examples, all of the antennas have been excited using a probe feed. A reduced size planar fed CP patch antenna with size reduction of up to 55% has been recently suggested by Chen et al [69]. The design combines ideas from [70] and [131] in a patch with truncated corners and incorporates them with an inset planar feed, as shown in figure 3.20. The suggested design embeds narrow slots of equal length on either side of the centre to produce size reduction, with the inset eed being responsible for input impedance matching.

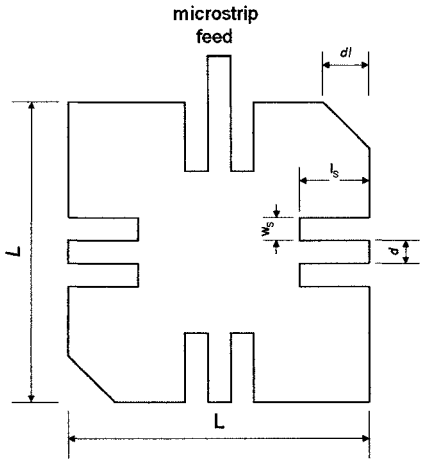

Figure 3.20: Inset-fed circular polarised H-shape patch

As with other slot loaded designs, a significant trade off of this design is an increase in input impedance with slot length. It is reported that the inset feed position moves closer to the centre of the patch with increased size reduction. A significant reduction in axial ratio bandwidth, from 1.45%, for a conventional

truncated corners patch, to 0.8% for the proposed structure, is also reported. It is also expected that size reduction produces an increased Q factor.

3.5.1.6 Meandered Patch Antenna

The slot loaded patch structures considered so far in this section are symmetrical about the x or y axis, as shown in figure 3.21a. As previously outlined, one such application of this type of configuration is to produce a dual frequency response by modifying the current paths of the TM_{01} and TM_{10} modes. In such designs, the slot sizes are fixed and the frequency ratio is controlled primarily by the aspect ratio of the patch, thus producing a limited frequency ratio range. To circumvent this it has been reported that a meandered patch structure can provide greater freedom [114]. Meandered patches could be categorised as antennas that have slits cut in the sides of the patch such that an asymmetrical structure is formed, as shown in figure 3.21b. Conversely, slot loaded designs could be considered as structures that do not compromise the symmetry of the patch. For illustrative purposes, the difference between slot loaded patches and meandered patch antennas is shown in figures 3.21a and b respectively.

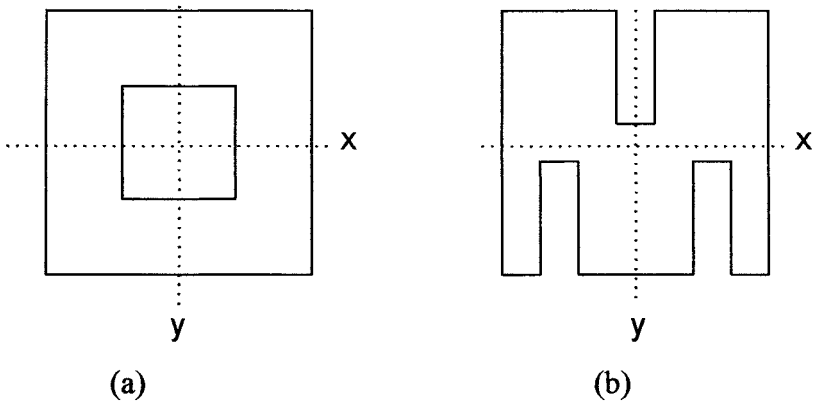

Figure 3.21: Difference between (a) slot loaded and (b) meandered patch

A technique suggested by Wu et al. [114], shown in figure 3.22, which involves the use of a meandered microstrip antenna has been shown to produce a dual frequency patch with a frequency ratio which is tuneable in the range 1.92 – 2.6. Size reduction of up to 50% is also achieved.

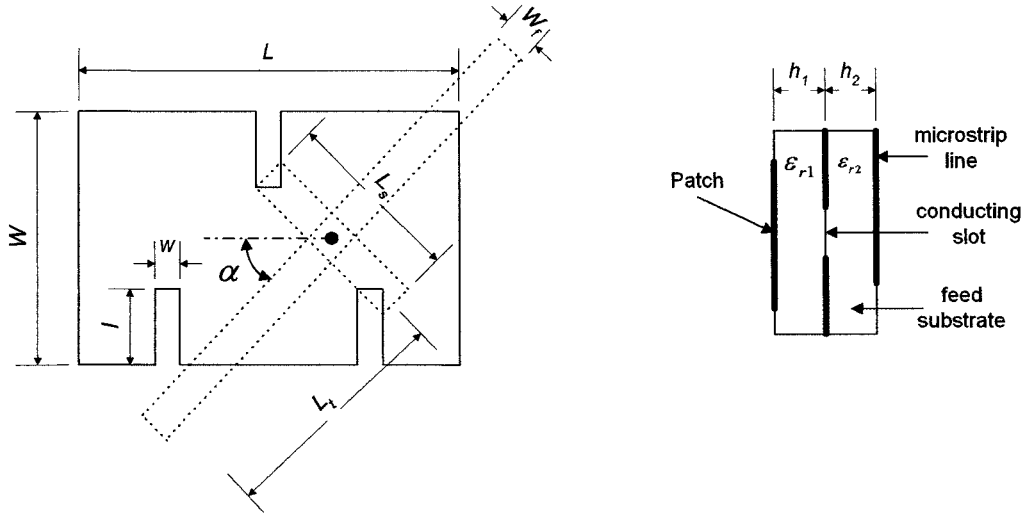

Figure 3.22: Meandered patch antenna

The inset slits lengthen the current path of the TM_{10} mode thus effectively lowering its resonant frequency. Conversely it has little effect on the resonant frequency of the TM_{01} mode. The frequency ratio is tuned by varying the slit lengths and separation between them. Impedance matching at both frequencies is achieved through the use of an aperture feed.

A significant trade-off of this design is a reduction in bandwidth from 1.66% and 2.71%, for a standard aperture-fed unslotted rectangular patch [114], to 1.58% and 2.05% for f_1 and f_2 respectively, for the proposed design. It is also reported, that as a consequence of the asymmetrical patch structure produced by the meandered patch, a significant increase in cross-polarisation radiation occurs in the H-plane. This can be attributed to the increased patch surface current component perpendicular to the main excitation direction.

For comparison, the surface current path of a square slot loaded and meandered patch antenna, determined using Ensemble [92] are illustrated in figure 3.23 below.

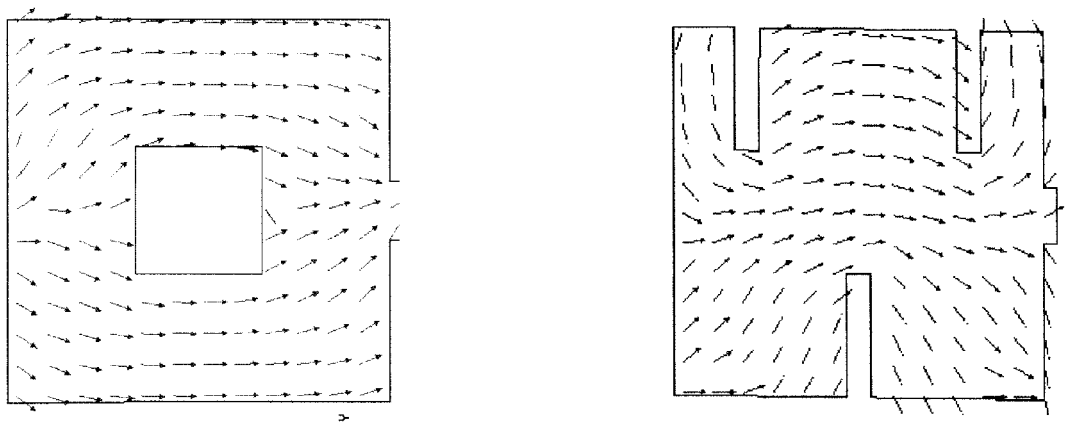

(a) (b)

Figure 3.23: Surface current path of (a) slot loaded and (b) meandered patch antennas

3.5.2 Modification of higher order modes

The dual frequency antennas reviewed thus far in this section has been limited to structures that produce orthogonally polarised frequencies. Such antennas operate by perturbing the current paths of the TM_{01} and TM_{10} modes. To produce a dual frequency response with both frequencies having the same polarisation sense requires a different technique. Two general approaches have been adopted by a number of authors. The first involves use of the TM_{01} and TM_{03} modes, whilst the second approach involves use of the TM_{01} together with the creation of an additional $TM_{0\delta}$ mode.

3.5.2.1 Modification of TM_{01} and TM_{03} modes

The configuration illustrated in figure 3.24, consisting of two narrow slots located close to the radiating patch edge has been used to produce dual frequency linear polarised operation of a patch antenna. This work was first suggested by Maci et al

[120] and later by Yazidi et al [121] in experimental form, with a more comprehensive study undertaken by Maci et al [132].

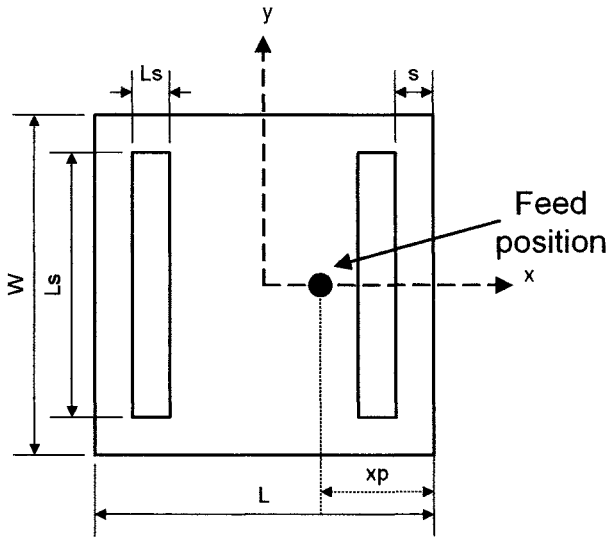

Figure 3.24: Dual band slot loaded patch

Locating slots close to the radiating patch edge, where the TM_{01} mode is at a minimum produce only minor perturbations of this mode. Thus the resonant frequency of this mode is only slightly affected. Conversely, the slots are positioned close to the current maxima of the TM_{03} mode, thus significant perturbation and frequency reduction of this mode occurs. Using this technique a frequency ratio tuneable from $1.6-2.0$ can be achieved. Simultaneous matching at both frequencies can be achieved by exciting with a probe or aperture feed at an appropriate point, with the correct position being determined by parametric analysis.

An extension of this work has been suggested by Lu et al [64] by incorporating edge loaded slots to reduce the size of a dual frequency patch. The slots parallel to the radiating edges are used to create the dual frequency response by perturbing the TM_{03} mode, whilst the edge loaded slots are responsible for modification of both the TM_{01} and TM_{03} modes and hence account for the size reduction. The patch configuration is illustrated in figure 3.25.

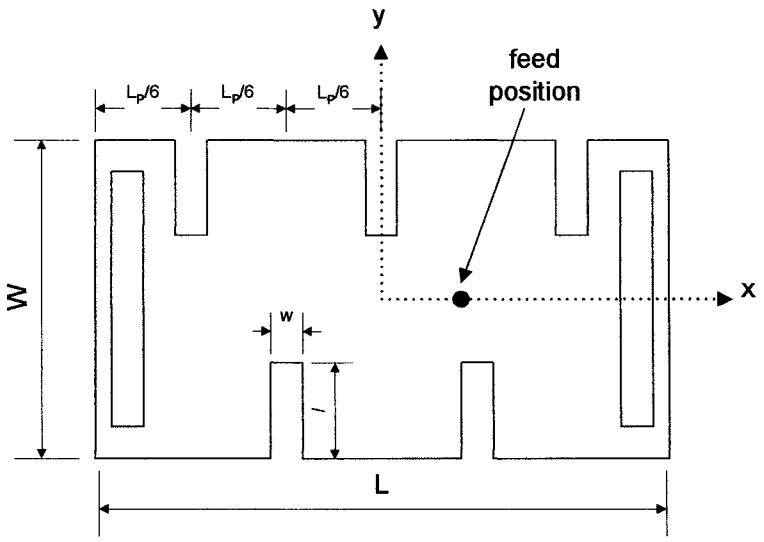

Figure 3.25: Reduced size dual frequency patch antenna

The above designs [120,121,132] have been used to produce a dual frequency response with both frequencies being linear polarised, by modifying the TM_{01} and TM_{03} modes. An extension of this work has been suggested by Yang and Wong [133] to produce circular polarised operation of both frequencies. This is achieved by placing slots at appropriate positions to perturb the current paths of the TM_{01}, TM_{10}, TM_{03} and TM_{30} modes. Two configurations have been proposed; the first uses four T-shaped slots, whilst the second incorporates four Y-shaped slots, as shown in figures 3.25(a) and (b) respectively. An additional slot is placed in the patch centre to split the first and third modes into two near-degenerate modes for dual-band circular polarisation. The patch is excited using a probe feed at an appropriate point along the diagonal axis of the patch.

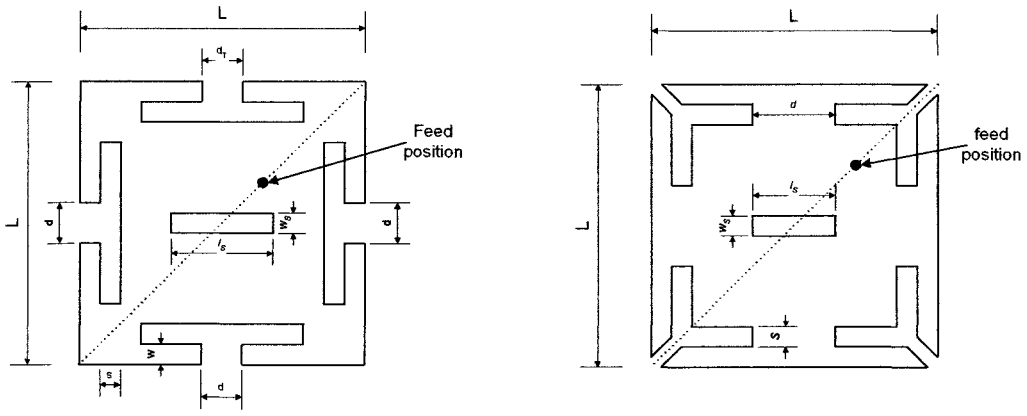

Figure 3.26: Dual-band CP patch designs

A significant trade-off associated with these designs is the high sensitivity of input impedance to feed position. For the case described by Maci et al [132] it is reported that a 1% error in the probe feed location causes a 5 dB increases in the input reflection coefficient level.

3.5.2.2 Creation of additional $TM_{0\delta}$ mode

In the above section it was stated that locating slots close to the radiating edge of a patch produces dual frequency operation with both frequencies having the same polarisation planes and broadside radiation [64,120,121,132,133]. This technique utilises the TM_{01} and TM_{03} modes to achieve a frequency ratio in the range 1.6 - 2.0. Recent research suggests that a dual frequency patch with a lower frequency ratio can be achieved through the creation of an additional mode. This mode lies between TM_{01} and TM_{02} modes, and has the same polarisation plane. One technique of creating the additional mode, which involves the location of bent slots close to the non-radiating edge, has been recently suggested by Wong and Sze [134] and is shown in figure 3.27. It is reported that a frequency ratio in the range 1.29 – 1.6 can be achieved using this technique. Impedance matching is achieved using a probe feed at an appropriate point along the $y = W/2$ axis.

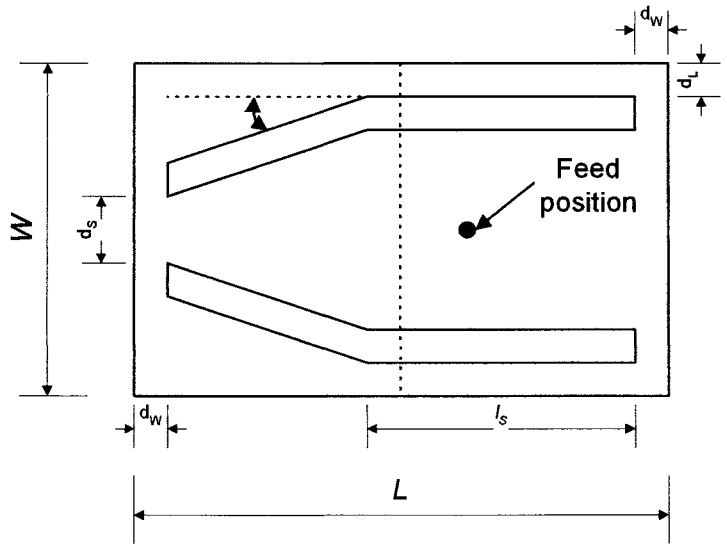

Figure 3.27: Dual frequency slotted rectangular patch antenna

Variations on this design, which incorporate different slot configurations close to the non-radiating edge have been proposed by a number of authors [135 - 140]. By modifying the slot geometry it is possible to produce dual frequency patches with different frequency ratios ranging from 1.07-1.63. This technique has also been employed to produce a wideband frequency response by exciting two frequencies close enough together to produce a single wideband frequency response.

3.6 Choice of Size Reduction Technique

Sections 3.3 – 3.5 has examined the use of shorting pin loading, slot loading and slot loaded ground plane in microstrip patch antennas.

Incorporating an edge-shorted design has been used to produce both compact and dual frequency patch antennas. Although this technique has significant advantages in terms of size reduction, it has a number of disadvantages both in terms of circuit and far-field characteristics. With reference to the circuit characteristics, the close proximity of the probe and shorting pin, together with the small diameter of these components required to excite the patch efficiently results in strict manufacturing tolerances. A further trade-off from such designs is a reduction in bandwidth. Considering the far-field response, it was found that the presence of a shorting plane / pin produces a dip in the E-plane polar response, together with large levels of cross-polarisation in the H-plane.

Slot loaded ground plane and slot loaded patch antennas both operate using similar principles. With reference to the slot loaded ground plane approach, it has been suggested that this approach has the advantage of increasing the antenna bandwidth. A major disadvantage of this approach however is a significant increase in back radiation at the expense of antenna gain.

It would therefore seem that the most promising method of producing planar fed compact antenna structures is through the employment of slot loading within a conventional patch. Using this technique, with correct positioning of slots with optimum dimensions, it is possible to produce reduced size linear and circular polarised antennas, dual frequency antennas and wideband antennas.

To produce compact patch antennas with linear polarisation the current path of the TM_{01} mode must be perturbed. With correct perturbation of the TM_{01} and TM_{10} modes compact circular polarised patch antennas can be designed. Perturbation of these two modes can also be used to produce compact dual frequency antennas with both frequencies being orthogonally polarised. In order to produce dual frequency antennas with the same polarisation sense, two approaches can be followed. The first involves modifying the current paths of TM_{01} and TM_{03} modes, whilst the latter involves the creation of an additional $TM_{0\delta}$ mode.

The slot loaded-patch also has another big advantage as it allows the possibility of realizing re-configurable antennas for future multi-system operations. This may be achieved by putting the Micromachined Electromechanical System (MEMS) capacitors or MEMS switches directly into the slots of the patch [141,142]. By varying the MEMS capacitors or MEMS switches, the antenna can be configured to operate at different frequency bandwidth the characteristics required by different systems. Though it is difficult to fabricate the MEMS device at this moment, this should be overcome in the near future with the rapid development of MEMS device fabrication technology.

Although significant research has been reported within the field of slot loaded patch antennas, a number of limitations of such designs still exists. Primarily, the vast majority of slot loaded designs are excited using a probe feed, and little research

exists into the use of planar fed designs. It has also been highlighted that current designs appear to suffer from a number of trade-offs including increased Q factor, reduced VSWR bandwidth, reduced axial ratio bandwidth, reduced gain, and stricter manufacturing tolerances. Moreover, research in this field is largely empirical with little theoretical knowledge available to support the design of such structures.

A major focus of this thesis is to therefore to address this knowledge gap. To achieve this, a rigorous analysis of slot loaded patch antennas is performed. From this, the effect of slot parameters on the antenna response, both in terms of circuit and far field characteristics is determined, with particular reference to the associated trade-offs of such designs. Using the knowledge obtained from this investigation, a design methodology is proposed that will give a framework for the design of slot loaded antennas for specific applications. Following this, new antenna structures are presented that overcome some of the trade-offs associated with existing structures.

3.7 Summary

A number of techniques for reducing the size of a microstrip patch antenna have been examined in this chapter. A brief overview of such different techniques has been reported in section 3.1. These included: the use of high permittivity substrate; shorted patch; folded patch; slot loaded patch; slot loaded ground plane; and various miscellaneous techniques. The focus of this thesis is to produce compact patch designs that do not compromise the planar structure of the microstrip antenna. The most suitable approaches were identified as the use of shorted patch, slot loaded ground plane and slot loaded patch. To this end, a review of such techniques was performed in sections 3.2-3.5 respectively. Section 3.6 has successfully argued that the use of slot loading offers the most suitable approach for the design of reduced size planar fed patch antennas.

CHAPTER 4

SEGMENTATION MODEL FOR ANALYSIS OF SLOT LOADED PATCH ANTENNAS

4.1 Introduction

Subsequent chapters within this thesis involve the design and analysis of slot loaded antennas similar to those illustrated in figure 4.1.

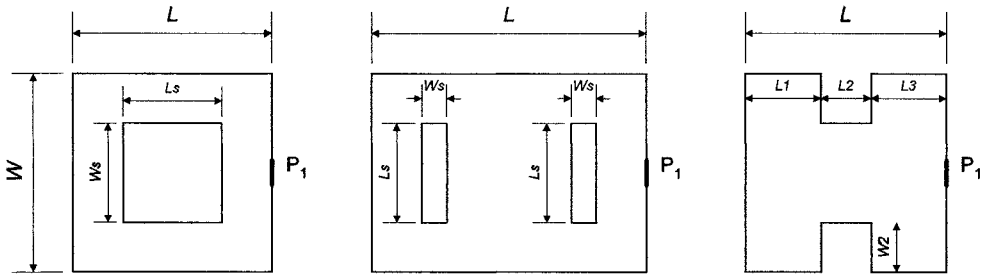

Figure 4.1: Slot loaded patch antenna structures

To facilitate this, the focus of this chapter is to develop a modelling technique that can be applied to such structures. The modelling approach will be used to determine the performance of the antennas in terms of circuit characteristics including resonant frequency, input impedance, and Q factor. A number of possible modelling approaches have been outlined in section 2.4, in which it was identified that the segmentation approach is the most appropriate method.

Following this brief introduction, section 4.2 presents a general overview of the modelling procedure. An integral part of the modelling process involves the development of expressions relating to the interaction between various ports on the

patch element. To achieve this requires the use of 2D Green's functions. Both of these are dealt with in section 4.3.

To test the validity of the developed expressions, section 4.4 applies this technique to a standard square patch antenna. To apply the segmentation approach, expressions relating to the synthesis between different segments are required, these are covered in section 4.5. To fully illustrate the modelling process and test its applicability a square patch antenna with square slot loading is analysed in section 4.6. In all cases the resonant frequency, input impedance and Q factor are obtained and a comparison is made with results obtained using practical measurements. Section 4.7 presents a summary of the main points from this chapter.

4.2 Modelling Overview

Analysing a patch antenna involves solving the wave equation (4.1) subject to given boundary conditions to determine the circuit parameters. If the patch has a simple geometry (i.e. rectangular, triangular, circular) the Green's function technique, which gives the voltage at any point for a unit source current excitation, gives an efficient approach. Using Green's functions, the patch is characterised in terms of an impedance matrix, from which parameters such as input impedance, resonant frequency Q factor and bandwidth can be determined.

If the circuit is complex, as in figure 4.2a, two possible approaches could be followed, namely the Segmentation[107,143-146] and Desegmentation[146-148] technique. The segmentation approach involves decomposing the patch into a number of simple segments for which Green's Functions are readily available, as shown in figure 4.2b. Conversely, the desegmentation technique, shown in figure 4.2c, involves subtracting regular shapes from the patch. The characteristics of the entire patch are then obtained by synthesising the characteristics of the segments. The choice of

either segmentation or desegmentation is determined by the patch shape and its decomposition.

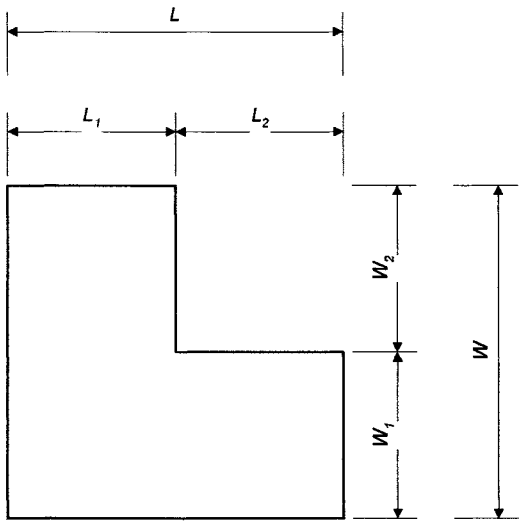

(a)

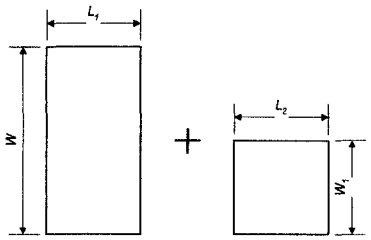

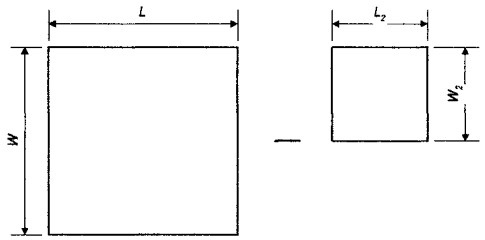

(b) (c)

Figure 4.2a-c: Principle of segmentation and desegmentation method:
(a) an example circuit pattern to which both segmentation and desegmenation method is suitable
(b) segmentation method by addition of patch segments
(c) desegmentation method by subtraction of segments

To apply either segmentation or desegmentation approach, multi-port network models of each segment must first be developed. Such models can be expressed in terms of s or z-parameters. Within this thesis z-parameters are employed as they can be derived directly from Green's Functions. Moreover, the required circuit characteristics of resonant frequency, input impedance, and Q factor can be obtained directly using this approach.

In short, the modelling approach followed in this section comprises of three stages:

1. The patch is decomposed into a number of regular elemental sections
2. Multi-port network models of each segment are developed
3. Synthesis of the entire structure is achieved using either segmentation or desegmentation approach

4.3 Multi-Port Network Model of Patch

To develop a multiport network model, Z-parameter expressions for the coupling between the external ports on the patch segment must be developed. With reference to figure 4.3, there are two problems regarding planar structures. The first constitutes a planar circuit loaded by current sources, as in figure 4.3a. This problem is described by a nonhomogenous Helmholtz differential equation with homogeneous boundary conditions. The second problem constitutes a planar circuit loaded with one or more ports, as illustrated in figure 4.3b. This problem is described by a homogenous Helmholtz differential equation with nonhomogeneous boundary conditions.

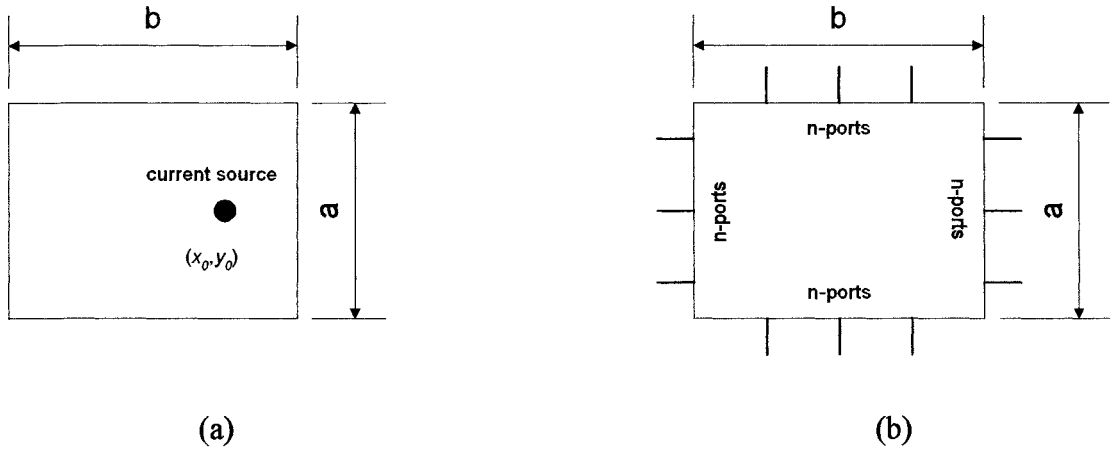

Figure 4.3: Planar structure (a) with ideal current source and (b) with n-ports

The latter problem is apparent when developing a multiport network circuit model of a patch antenna, hence the following section will concentrate on developing a procedure for solving n-port planar circuits.

4.3.1 Rectangular patch loaded with current sources

Figure 4.3a, represents a planar circuit loaded with a current source. The fields inside the this structure antenna are described by the following nonhomogeneous Helmholtz equation [107]:

$$\left(\frac{\partial^2}{\partial x^2}+\frac{\partial^2}{\partial y^2}+k^2\right)\phi(x,y)=f(x_0,y_0) \quad , \tag{4.1}$$

where:

$$f(x_0,y_0)=-j\omega\mu_0 J_z(x,y),$$

$$\phi(x,y)=E_Z(x,y), \tag{4.2}$$

$$k^2=\omega^2\mu_0\varepsilon_0\varepsilon_r(1-j\delta), \tag{4.3}$$

δ is the loss tangent of patch,

subject to the following boundary condition along the patch periphery:

$$\frac{\partial E_Z(C_p)}{\partial n}=0 \tag{4.4}$$

where C_p is the periphery of the patch.

The solution to this is based on a simpler problem for which the forcing function is an ideal current source injected normally into the patch. The forcing function now becomes

$$f(x_0,y_0)=-j\omega\mu h\delta(x,y-x_0,y_0), \tag{4.5}$$

where h is the substrate thickness, (x,y) is the observation point and (x_0,y_0) is the position of the unit point source, as shown in figure 4.4.

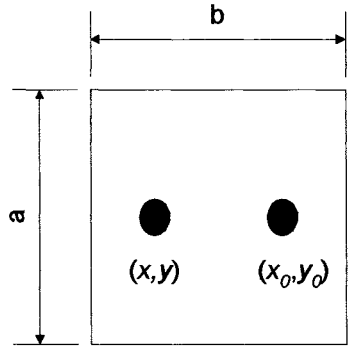

Figure 4.4 Planar structure with ideal current source

Equation (4.1) can now be rewritten as:

$$\left(\frac{\partial^2}{\partial x^2}+\frac{\partial^2}{\partial y^2}+k^2\right)\phi(x,y)=-j\omega\mu_0 h\delta(x,y-x_0,y_0)\,. \tag{4.6}$$

ϕ can be determined using the following relationship:

$$\phi(x,y)=G(x,y;x_0,y_0)\,. \tag{4.7}$$

The Green's function approach can then be applied.

4.3.2 Two-dimensional Green's Functions

$G(x,y;x_0,y_0)$ is the associated two-dimensional Greens Function. A suitable trial solution for this can be obtained by expanding it in terms of orthonormal eigenfunctions of the following related homogeneous helmholtz differential equation, thus:

$$G(x,y;x_0,y_0)=\sum_{m=1}^{\infty}\sum_{n=1}^{\infty}A_{mn}\phi_{mn}(x,y)\quad . \tag{4.8}$$

Substituting the trial solution (4.8) into (4.6) gives:

$$\sum_{m=1}^{\infty}\sum_{n=1}^{\infty}A_{mn}\phi_{mn}(x,y)=-j\varpi\mu_0 h\delta(x,y-x_0,y_0)\,. \tag{4.9}$$

In order to orthonormalise (4.9) the LHS must be multiplied by ϕ_{mn} * , thus giving:

$$\sum_{m=1}^{\infty}\sum_{n=1}^{\infty} A_{mn}\phi_{mn}(x,y)\phi_{mn}*(x_0,y_0) = -j\varpi\mu_0 h\delta(x,y-x_0,y_0)\phi_{mn}*(x_0,y_0).$$

(4.10)

Integrating both sides and making use of the following orthonormal relationship:

$$\int_a^b \phi_Z(x)\phi_Z*(x)dz = 1\ , \tag{4.11}$$

together with the property of the delta function:

$$\int_{-\infty}^{\infty}\delta(z-z_0)dz = 1, \tag{4.12}$$

results in the following:

$$A_{mn}(k_m{}^2 + k_n{}^2 - k^2) = -j\omega\mu_0\phi_{mn}*(x_0,y_0)\quad . \tag{4.13}$$

Thus:

$$A_{mn} = \frac{-j\omega\mu_0 h\phi_{mn}*(x_0,y_0)}{k_m{}^2 + k_n{}^2 - k^2}\ . \tag{4.14}$$

Introducing (4.14) into (4.8) gives:

$$G(x,y;x_0,y_0) = -j\omega\mu_0 h\frac{\phi_{mn}*(x_0,y_0)\phi_{mn}(x,y)}{k_m{}^2 + k_n{}^2 - k^2} \tag{4.15}$$

where ϕ_{mn} relate to the eigenfunctions of the patch, and is given in Appendix 4A by:

$$\phi_{m,n}(x,y) = k_{m,n}\cos\left(\frac{m\pi x}{a}\right)\cos\left(\frac{n\pi y}{b}\right). \qquad m,n = 0,1,2\ldots \tag{4.16}$$

4.3.3 Rectangular patch loaded with n-ports

Figure 4.3b Represents a patch antenna loaded with n-ports. The solution to this problem involves converting the nonhomogenous boundary conditions to homogenous ones, thus allowing the use of the Green's function approach. This can be achieved by replacing the boundary conditions on the patch periphery by

fictitious current distributions just inside the patch between the upper and lower conductors. With reference to figure 4.4, the source and observation points are situated on the periphery of the patch. For the solution of *n*-port planar structures, it is necessary to replace the unit point source, with an array of ideal current sources, each with a current density of $J_s(x_0, y_0)$ across the widths of each port. This relies on the fact that any Complicated solution can be constructed by a superposition of a number of simpler ones. If two ideal current sources are used at points x_1, y_1 and x_2, y_2 with amplitudes of $j_1(x_1, y_1)$ and $j_2(x_2, y_2)$ respectively, as shown below:

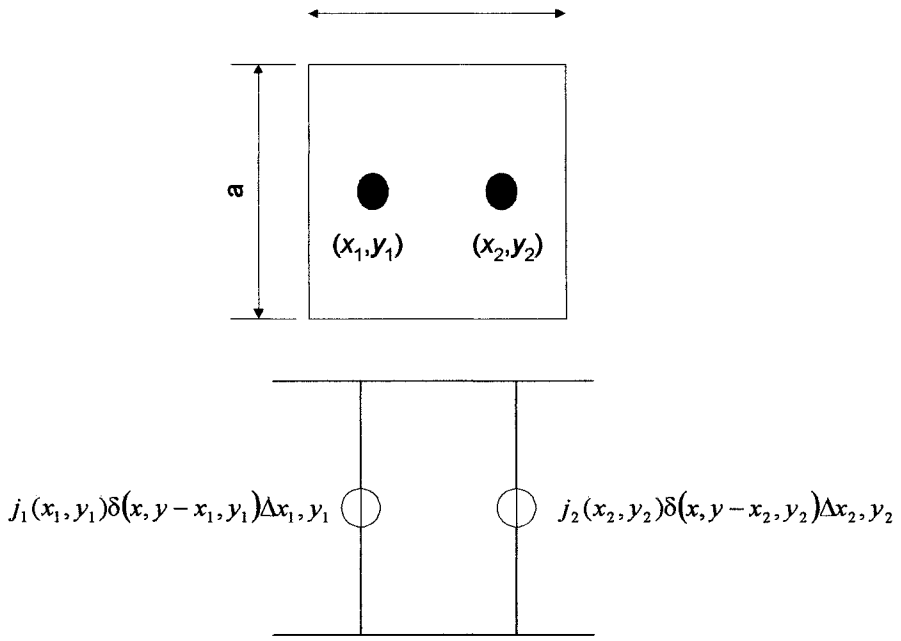

Figure 4.5: 2 Ideal current sources

The forcing function is given by [107]:

$$f(x,y) = -j\omega\mu_0[j_1(x_1,y_1)\delta(x,y-x_1,y_1)\Delta x_1,y_1 + j_2(x_2,y_2)\delta(x,y-x_2,y_2)\Delta x_2,y_2]. \tag{4.17}$$

If *n* ideal current sources are used, the forcing function f(z) can be constructed by the superposition of all of *n* ideal current sources, thus:

$$f(x_0, y_0) = -j\omega\mu_0 \int_{-\infty}^{\infty} Js(x_0, y_0)\delta(x, y - x_0, y_0)dx_0, y_0 \,. \tag{4.18}$$

The fields inside the patch shown in figure 4.3b, are thus given as:

$$\left(\frac{\partial^2}{\partial x^2} + \frac{\partial^2}{\partial y^2} + k^2\right)\phi(x, y) = -j\omega\mu_0 \int_{-\infty}^{\infty} Js(x_0, y_0)\delta(x, y - x_0, y_0)dx_0, y_0 \,, \tag{4.19}$$

where x, y is the observation point, and x_0, y_0 is the source point, and

$$V(x, y) = -hE_Z(x, y) \,, \tag{4.20}$$

$$k^2 = \omega^2\mu_0\varepsilon_0\varepsilon_r(1 - j\delta), \tag{4.21}$$

where h is the height of the substrate, and ϕ_{mn} was determined in (4.7).

The voltage at any point (x,y) due to a current source at (x_0,y_0) is given by [3]:

$$V(x, y) = \iint_{D_p} G(x, y; x_0, y_0).Js(x_0, y_0)dx_0dy_0 \,, \tag{4.22}$$

where D_p is the region inside the planar circuit, and G is the 2-dimensional Green's Function of the rectangular patch.

If the source and observation points are on the periphery of the patch, then the voltage is given by:

$$V = -\int_{C_p} G(x, y; x_0, y_0)J_S(x_0, y_0)dt \,, \tag{4.23}$$

where C_p is the patch boundary and t is a boundary tangent.

As the tangential component of the surface current density is only present at the ports, the line integral round the boundary can be replaced by a line integral over the port width:

$$V = -\sum_j \int_{W_j} G(x, y; x_0, y_0)J_S(x_0, y_0)dW_j \,, \tag{4.24}$$

The average voltage at port i due to current source at port j is given by:

$$Vi = -\frac{1}{Wi}\sum_{j}\int_{Wi}\int_{Wj} G(x,y;x_0,y_0)J_S(x_0,y_0)dW_i dW_j \quad , \tag{4.25}$$

where

$$I_j = -\int_{Wi} J_S(x_0,y_0)dW_j \, , \tag{4.26}$$

thus:

$$J_S = -\frac{I_j}{W_j} \quad , \tag{4.27}$$

Therefore:

$$V_i = \frac{1}{W_i}\sum_{j}\frac{I_j}{W_j}\int_{Wi}\int_{Wj} G(x,y;x_0,y_0)dW_i dW_j \, . \tag{4.28}$$

where (x,y) is the observation point (x,y), and (x_0,y_0) is the source point, and G is the associated 2D Green's functions derived in equation (4.15).

4.3.4 Z-parameters of 2-port network

The Z parameters of a 2 port network are given by:

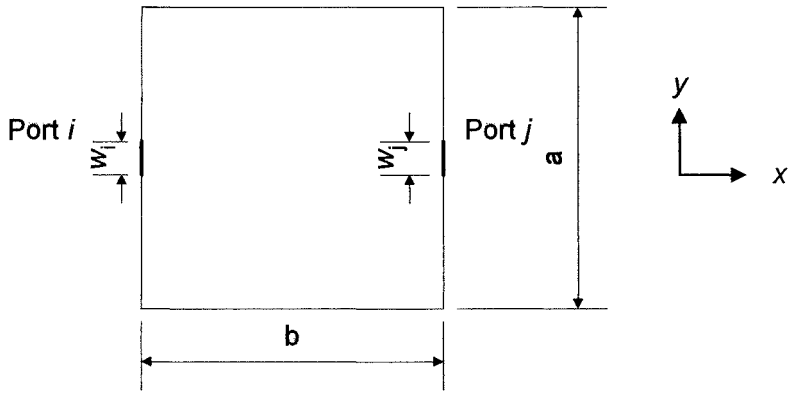

Figure 4.6: 2-port planar circuit

$$Z_{ii} = \frac{V_i}{I_i}\Big|_{Ij=0} \qquad Z_{ij} = \frac{V_i}{I_j}\Big|_{Ii=0}$$

$$Z_{ji} = \frac{V_j}{I_i}\Big|_{Ij=0} \qquad Z_{jj} = \frac{V_j}{I_j}\Big|_{Ii=0} \tag{4.29}$$

Substituting (4.28) into (4.29) gives:

$$Z_{ij} = \frac{V_i}{I_j}\Big|_{I_i=0} = \frac{1}{W_i W_j}\int_{Wi}\int_{Wj} G(x, y; x_0, y_0)\, dW_i dW_j = Z_{ji}\,, \tag{4.30}$$

Substituting (4.15) into (4.30) gives:

$$Z_{ij} = \frac{j\omega\mu_0 h}{ab W_i W_j}\int_{Wi}\int_{Wj}\sum_{m=0}^{\infty}\sum_{n=0}^{\infty}\sigma_m\sigma_n \frac{\cos(k_{xm}x_i)\cos(k_{yn}y_i)\cos(k_{xm}x_j)\cos(k_{yn}y_j)\;\; dW_i dW_j}{k_{xm}^{\;2} + k_{yn}^{\;2} - k^2}. \tag{4.31}$$

4.4 Analysis of Square Patch Antenna

To test the validity of the expressions developed above, the circuit characteristics of a rectangular patch antenna shown in figure 4.7 have been determined using the Green's Function approach (equation 4.31).

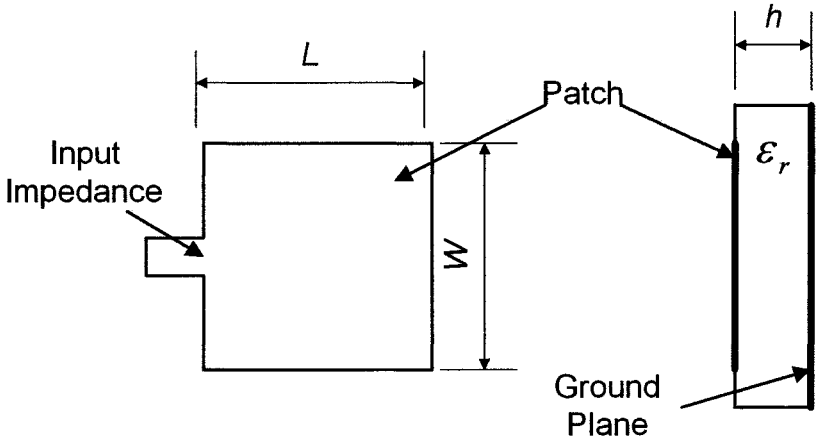

$\varepsilon_r = 2.33$, $h = 1.57$ mm, $L = W = 32$ mm

Figure 4.7: Single planar fed 1-port patch antenna

For convenience, the antenna was designed to operate at 3 GHz and fabricated on RT5870 with permittivity 2.33 and thickness 1.57mm.Using the analysis presented, the relationship between complex input impedance and frequency is determined. From this, the resonant frequency, input impedance and Q factor of the antenna is determined. To test the validity of the analysis, the practical results are also presented. With reference to figure 4.6, both ports are at the same point on the x axis, as shown in figure 4.8

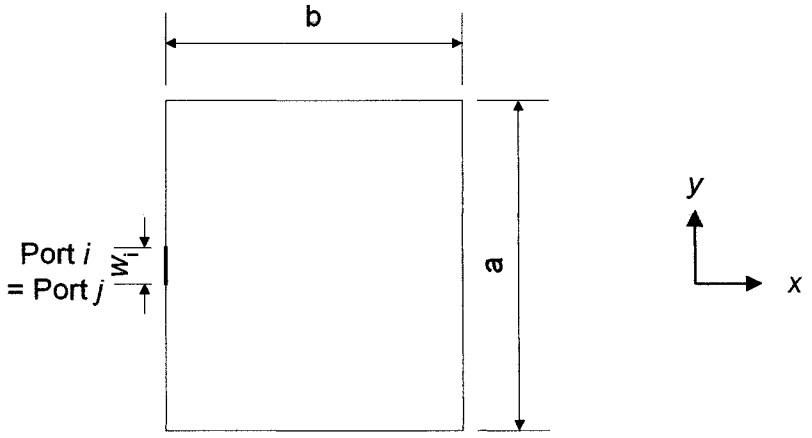

Figure 4.8: Port i and port j at same points on x axis

Port i is located at: $x_i, y_i \pm \frac{W_i}{2}$, Port j is located at: $x_j, y_j \pm \frac{W_j}{2}$

From (4.31) :

$$Z_{ii} = \frac{j\omega\mu_0 h}{ab2W_i}\sum_{m=0}^{\infty}\sum_{n=0}^{\infty}\sigma_m\sigma_n\left[\frac{\cos(k_{xm}x_i)\sin\left[k_{yn}\left(y_i+\frac{W_i}{2}\right)\right]}{k_{yn}} - \frac{\cos(k_{xm}x_i)\sin\left[k_{yn}\left(y_i-\frac{W_i}{2}\right)\right]}{k_{yn}}\right]^2 \left[\frac{1}{k_{xm^2}+k_{yn}{}^2-k^2}\right] \quad (4.32)$$

(for full derivation see Appendix 4B)

In the above equations the patch dimensions a and b include line extensions, ΔL, to account for fringing fields, and are given by:

$$a = L + \Delta L \quad \text{and} \quad b = W + \Delta L \tag{4.33}$$

where ΔL is given by equation (2.2) in Chapter 2.

k, k_{xm} and k_{yn} are the wavenumbers of the resonant modes and are given by:

$$k_{xm} = \frac{m\pi}{a} \qquad k_{yn} = \frac{n\pi}{b} \qquad k = \sqrt{\omega^2 \mu_0 \varepsilon_0 \varepsilon_r \left(1 - \frac{j}{Q}\right)} \tag{4.34}$$

Q represents total Q factor of the patch antenna and is given by equation (2.7) in Chapter 2.

In this analysis (equation 4.31), the upper limit on summation was taken to be m = n = 10, which was found to give good convergence. Graphs of real and imaginary input impedance versus frequency are shown in figure 4.9a and 4.9b respectively. For comparison practical results are also shown.

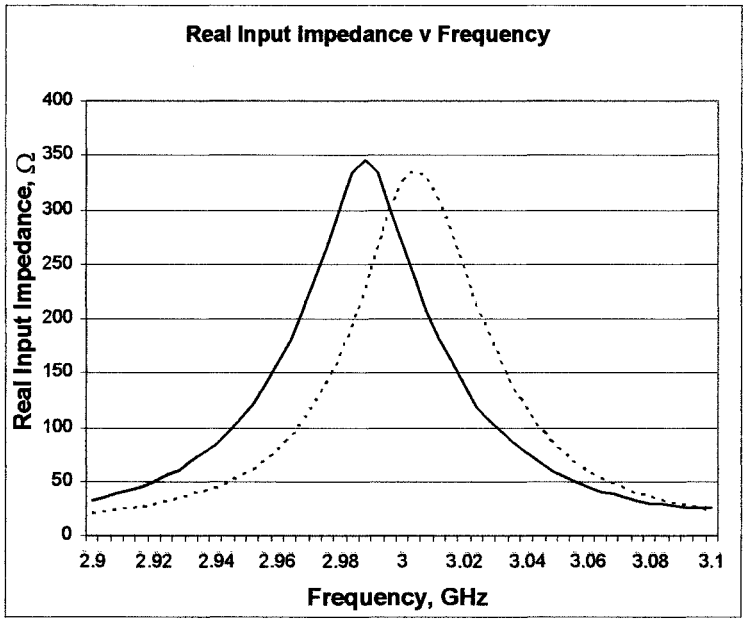

(a)

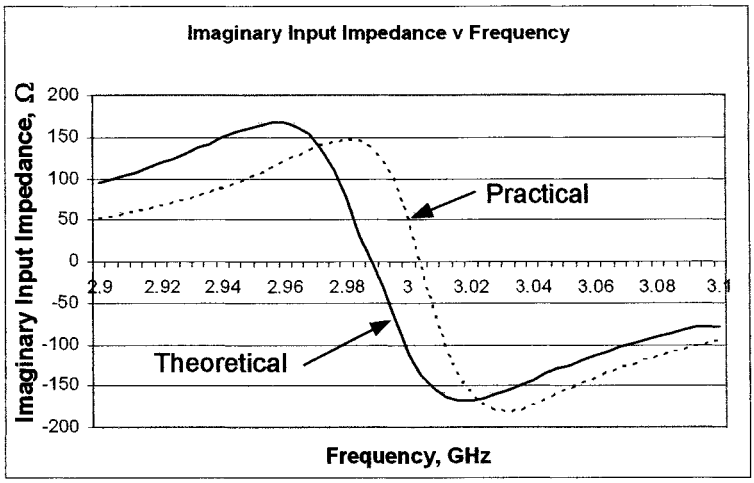

(b)

Figure 4.9: (a) Real and (b) imaginary input impedance of patch antenna

Figure 4.9 illustrates a difference of 20 MHz between theoretical and practical. This could be due to manufacturing tolerance. From the graphs in figure 4.9a and 4.9b, input impedance and Q factor can also be determined.

The input impedance of the patch occur when:

$$\text{Imag}\{Z_{in}\} = 0 \tag{4.35}$$

In Chapter 2, the Q-factor of the antenna was also defined in terms of the resonant frequency 'f_r' and the 3dB bandwidth 'Δf' by (2.13) in Chapter 2 as:

$$Q_t = \frac{f_r}{\Delta f} \tag{4.36}$$

where Δf is the 3 dB bandwidth and f_r is the centre frequency.

In Chapter 2, it was stated that the Q factor can be calculated directly using equations (2.7-2.12). However, this is only applicable to rectangular structures, and cannot be directly applied to complicated structures.

Modelling Technique	Resonant Frequency (GHz)	Input Impedance (Ω)	Q Factor Eqn (4.33)
Co-planar	2.998	345	56
Practical	3.004	336	57

Table 4.1: Circuit characteristics of square patch antenna obtained using both co-planar modelling and practical measurements

Table 4.1 demonstrates good agreement between predicted, and practical measurements in both cases although the theoretical prediction is slightly lower, which could be due to manufacturing tolerance, the approximate model of the fringing field extension and the empirical estimation of the effective dielectric constant.

4.5 Segmentation Technique

In this section, equation relating to the segmentation approach will be developed. For this purpose, the diagram in figure 4.10 will be considered. It consists of α, β and δ segments. The circuit characteristics of the δ segment can be determined by synthesising segments α and β.

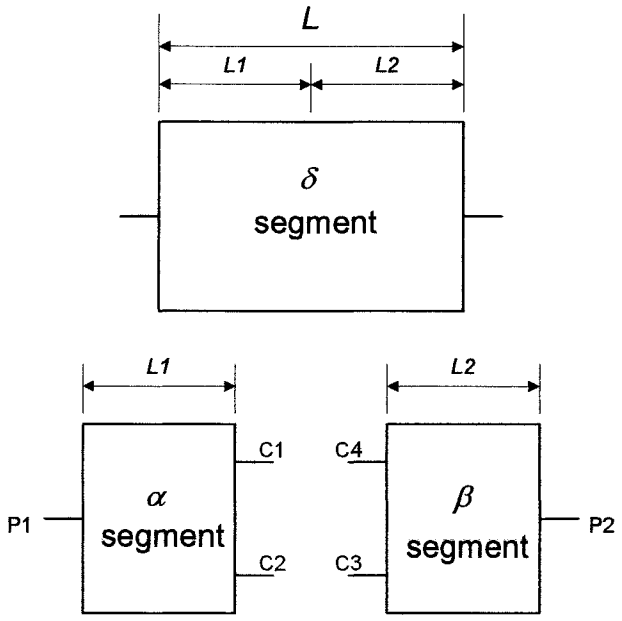

Figure 4.10: Synthesis of two segments

where P ports are external unconnected ports of each segment and C ports are internally connected ports.

Segments α and β can be independently described by:

$$\begin{bmatrix} V_p \\ V_c \end{bmatrix} = \begin{bmatrix} Z_{pp} & Z_{pc} \\ Z_{cp} & Z_{cc} \end{bmatrix} \begin{bmatrix} I_p \\ I_c \end{bmatrix} \tag{4.37}$$

where V_p, I_p and V_c, I_c are the voltages and currents at P and C ports respectively. For synthesising the segments α and β, two conditions must apply:

The voltages at connected ports are equal

$$\Gamma_1 V_c = 0 \tag{4.38}$$

The sum of currents at connected ports is zero

$$\Gamma_2 I_c = 0 \tag{4.39}$$

where Γ_1 and Γ_2 are two matrices with C/2 rows and C columns describing the connection topology.

Each row in these matrices describing the connection between the C ports is zero, except the two elements corresponding to the two connected ports. The two non-zero entries in a row are 1 and -1 for matrix Γ_1. For Γ_2 both entries are 1.

Assuming C_1 is connected to C_3, and C_2 to C_4:

$$\Gamma_1 = \begin{bmatrix} -1 & 0 & 0 & 1 \\ 0 & -1 & 1 & 0 \end{bmatrix} \tag{4.40}$$

$$\Gamma_2 = \begin{bmatrix} 1 & 0 & 0 & 1 \\ 0 & 1 & 1 & 0 \end{bmatrix} \tag{4.41}$$

The relationship between I_C and I_P is developed using (4.37) and (4.38):

From (4.37):

$$V_c = Z_{cp} I_p + Z_{cc} I_c \tag{4.42}$$

Thus:

$$0 = \Gamma_1 \left(Z_{cp} I_p + Z_{cc} I_c \right) \tag{4.43}$$

Combining (4.43) and (4.39), thus:

$$\begin{bmatrix} \Gamma_1 Z_{cc} \\ \Gamma_2 \end{bmatrix} Ic = \begin{bmatrix} -\Gamma_1 Z_{cp} \\ 0 \end{bmatrix} I_p \tag{4.44}$$

where 0 is a null matrix with C/2 rows and P columns.

The expression for input impedance of the complete network is derived using $Z_p = V_p / I_p$.

From (4.37):

$$V_p = Z_{pp} I_p + Z_{pc} I_c \tag{4.45}$$

$$Z_p = \frac{V_p}{I_p} = \frac{Z_{pp} I_p}{I_p} + \frac{Z_{pc} I_c}{I_p} = Z_{pp} + Z_{pc} \frac{I_c}{I_p} \tag{4.46}$$

From (4.44):

$$I_c = \begin{bmatrix} \Gamma_1 Zcc \\ \Gamma_2 \end{bmatrix}^{-1} \begin{bmatrix} -\Gamma_1 Zcp \\ 0 \end{bmatrix} Ip \tag{4.47}$$

Substituting (4.46) into (4.47) results in:

$$Z_p = Z_{pp} + Z_{pc} \begin{bmatrix} \Gamma_1 Z_{cc} \\ \Gamma_2 \end{bmatrix}^{-1} \begin{bmatrix} -\Gamma_1 Z_{cp} \\ 0 \end{bmatrix} \frac{I_p}{I_p} \tag{4.48}$$

$$Z_p = Z_{pp} - Z_{pc} \begin{bmatrix} \Gamma_1 Z_{cc} \\ \Gamma_2 \end{bmatrix}^{-1} \begin{bmatrix} \Gamma_1 Z_{cp} \\ 0 \end{bmatrix} \tag{4.49}$$

This gives the network impedance matrix of the synthesised shape. From figure 4.9, this gives:

$$Z_p = \begin{bmatrix} Z_{p1p1} & Z_{p1p2} \\ Z_{p2p1} & Z_{p2p2} \end{bmatrix} \tag{4.50}$$

where Z_{p1p1} and Z_{p2p2} give the input impedance at ports p_1 and p_2 respectively, and Z_{p1p2} and Z_{p2p1} gives the coupling between ports p_1 and p_2.

4.6 Application to Square Patch Antenna with Square-shaped Slot Loading

To fully illustrate the modelling process, the segmentation approach is used to analyse a square patch antenna with square slot loading, shown in figure 4.11. The model is implemented using MathCAD [149], and the resonant frequency, input impedance and Q factor are derived. To test the validity of the model, the results are then compared with those obtained using practical measurements.

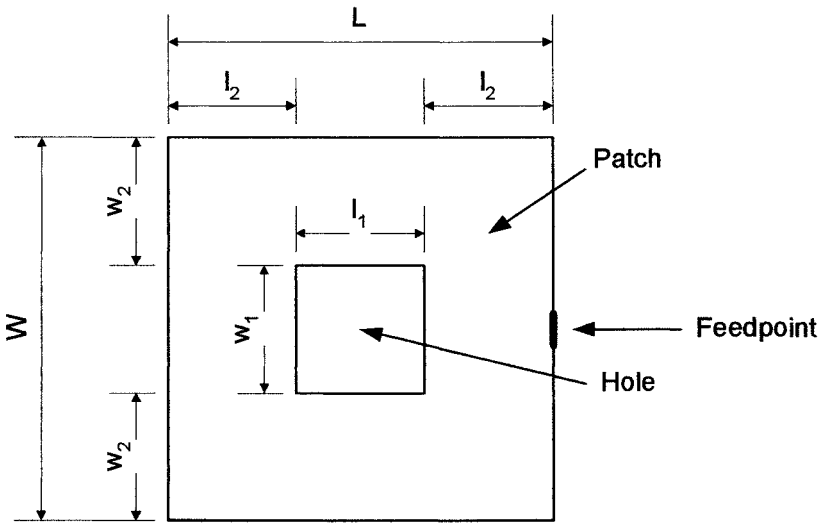

$\varepsilon_r = 2.33$, $h = 1.57$mm, $L = W = 30$mm, $l_1 = w_1 = 10$mm, $l_2 = w_2 = 10$mm

Figure 4.11: Square patch antenna with square slot loading

4.6.1 Patch decomposition and synthesis

Step 1: Patch Decomposition

The first stage in the modelling process is to decompose the patch into four elemental segments for which Green's Functions are available, as in figure 4.12a. As

the patch is symmetrical in both dimensions, it is possible to reduce the number of computations and thus reduce processing time, by synthesising the segments as in figures 4.12b-c, and following a two-stage process. The second stage, which is illustrated in figure 4.12b involves the synthesis of α_1 and β_1 segments to determine the impedance matrices of the γ_1 segment. The final stage, involves the determination of γ segment by combining γ_1 and γ_2 segments, as shown in figure 4.12c.

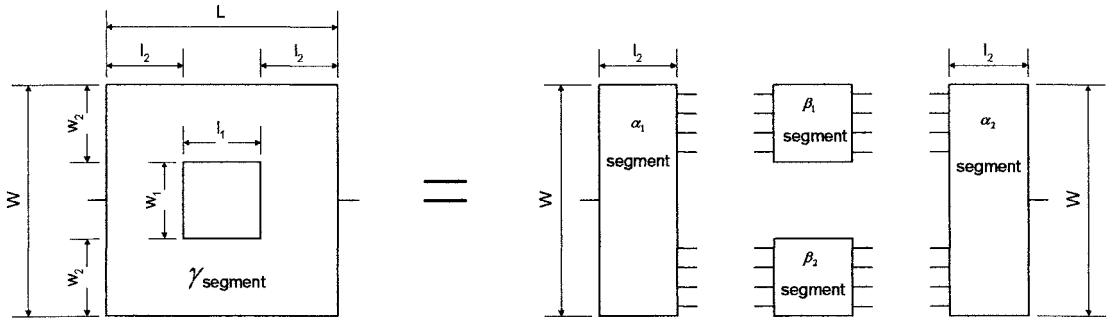

(a)

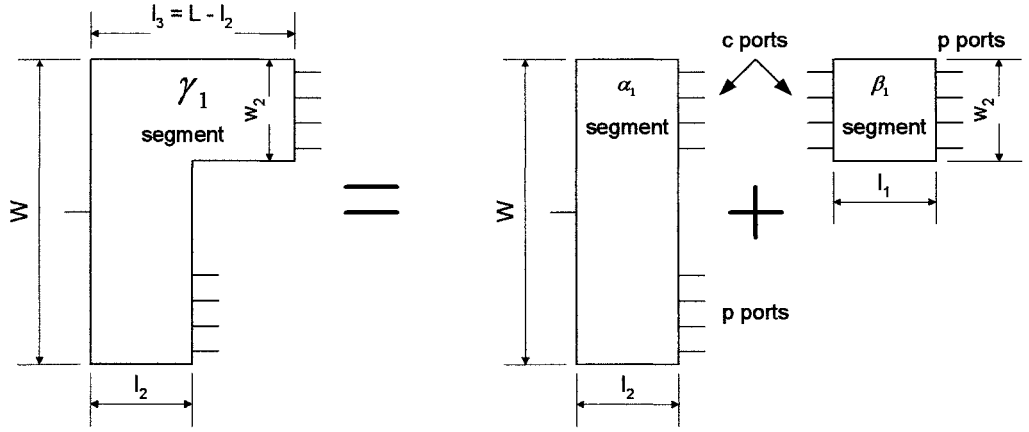

(b)

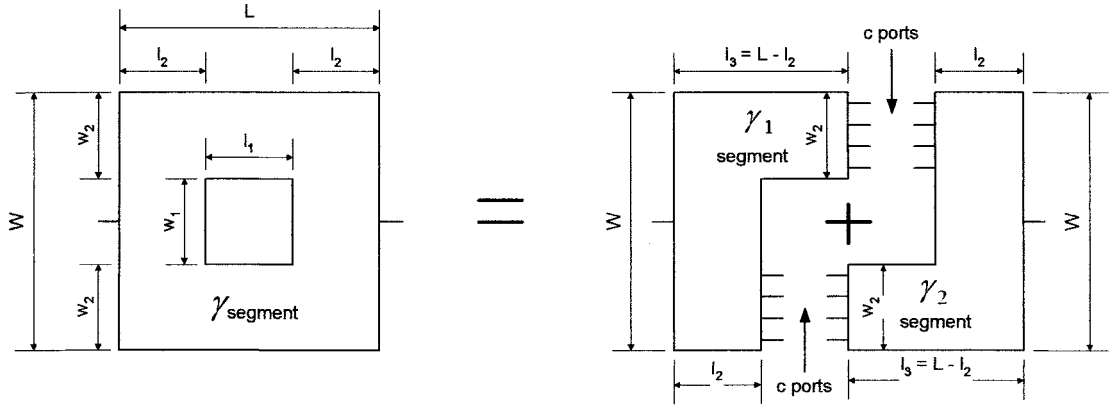

(c)

Figure 4.12: Decomposition and synthesis procedure
(a) Stage 1: patch decomposed into four rectangular segments
(b) Stage 2: synthesis of two segment into L-shaped segment and
(c) Stage 3: synthesis of two L-shaped segments into final design

Step 2: Determination of γ1 segment by synthesis of α_1 and β_1

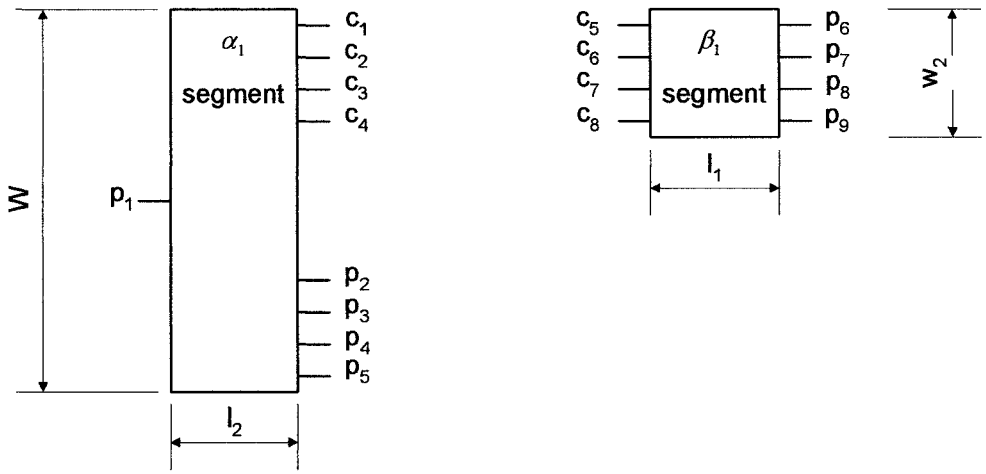

Figure 4.13: Ports of α_1 and β_1 segments

Figure 4.13 illustrates the port labelling of the α_1 and β_1 segments. The C-ports represent the connected ports of both segments and are arranged such that ports C_1 of the α_1 segment is connected to ports C_5 of the β_1 segment, C_2 is connected to C_6, etc... The P ports represent the unconnected ports of each segment.

Impedance Matrices of L-shape segments, γ_1 and γ_2:

The impedance matrix of the γ_1 segment is determined by synthesising α_1 and β_1 segments. The impedance matrix of the γ_2 segment is determined in a similar manner. However, due to the symmetry of the patch, it is only necessary to determine the impedance matrix of the γ_1 segment.

From (4.48) this is given by:

$$\gamma_1 Z_p = \gamma_2 Z_p = \gamma_1 Z_{pp} - \gamma_1 Z_{pc} \begin{bmatrix} \gamma_1 \Gamma_1 \gamma_1 Z_{cc} \\ \gamma_1 \Gamma_2 \end{bmatrix}^{-1} \begin{bmatrix} \gamma_1 \Gamma_1 \gamma_1 Z_{cp} \\ \gamma_1 0 \end{bmatrix} \qquad (4.50)$$

To achieve this requires the relevant impedance matrices $\gamma_1 Z_{pp}$, which represents the interaction between p ports on both segments and is given by:

$$\gamma_1 Z_{pp} = \begin{bmatrix} Z_{p1p1} & Z_{p2p1} & \cdots & Z_{p9p1} \\ Z_{p1p2} & Z_{p2p2} & \cdots & Z_{p9p2} \\ \vdots & \vdots & \ddots & \vdots \\ Z_{p1p9} & Z_{p2p9} & \vdots & Z_{p9p9} \end{bmatrix} \tag{4.51}$$

Note: from figure 4.13 the P ports (P_1 to P_5) on the α_1 segment and the P ports (P_6 to P_9) on β_1 segment are unconnected and hence the interaction between these ports equate to 0.

$\gamma_1 Z_{cp}$ represents the interaction between P ports on both segments and is given by:

$$\gamma_1 Z_{cp} = \begin{bmatrix} Z_{c1c1} & Z_{c1p2} & \cdots & Z_{c1p9} \\ Z_{c2p1} & Z_{c2p2} & \cdots & Z_{c2p9} \\ \vdots & \vdots & \ddots & \vdots \\ Z_{c8p1} & Z_{c8p2} & \vdots & Z_{p8p9} \end{bmatrix} \tag{4.52}$$

Note: from figure 4.13 the p ports (P_1 to P_5) on the α_1 segment and the C ports (C_5 to C_8) on β_1 segment are unconnected and hence the interaction between these ports equate to 0.

$\gamma_1 Z_{pc}$ represents the interaction between C and P ports on both segments. Due to the reciprocal nature of the ports, this is given by :

$$\gamma_1 Z_{pc} = \gamma_1 Z_{cp}^{\ T} \tag{4.53}$$

where T indicates the transpose of a matrix.

$\gamma_1 Z_{cc}$ represents the interaction between C ports on both segments and is given by:

$$\gamma_1 Z_{cc} = \begin{bmatrix} Z_{c1c1} & Z_{c2c1} & \cdots & Z_{c8c1} \\ Z_{c1c2} & Z_{c2c2} & \cdots & Z_{c8c2} \\ \vdots & \vdots & \ddots & \vdots \\ Z_{c1c8} & Z_{c2c8} & \vdots & Z_{c8c8} \end{bmatrix} \tag{4.54}$$

Note: from figure 4.13 the C ports (C_1 to C_4) on the α_1 segment and the C ports (C_5 to C_8) on β_1 segment are unconnected and hence the interaction between these ports equate to 0.

From equation (4.46-4.47) $\gamma_1\Gamma_1$ and $\gamma_1\Gamma_2$ has C/2 rows and C columns. From figure 4.13, assuming C_1 is connected to C_5, C_2 connected to C_6, etc.

$$\gamma_1\Gamma_1 = \begin{bmatrix} -1 & 0 & 0 & 0 & 0 & 0 & 0 & 1 \\ 0 & -1 & 0 & 0 & 0 & 0 & 1 & 0 \\ 0 & 0 & -1 & 0 & 0 & 1 & 0 & 0 \\ 0 & 0 & 0 & -1 & 1 & 0 & 0 & 0 \end{bmatrix} \tag{4.55}$$

$$\gamma_1\Gamma_2 = \begin{bmatrix} 1 & 0 & 0 & 0 & 0 & 0 & 0 & 1 \\ 0 & 1 & 0 & 0 & 0 & 0 & 1 & 0 \\ 0 & 0 & 1 & 0 & 0 & 1 & 0 & 0 \\ 0 & 0 & 0 & 1 & 1 & 0 & 0 & 0 \end{bmatrix} \tag{4.56}$$

$\gamma_1 0$ represents a null matrix and has C/2 rows and P columns and is given as:

$$\gamma_1 0 = \begin{bmatrix} 0 & 0 & 0 & 0 & 0 & 0 & 0 & 0 & 0 \\ 0 & 0 & 0 & 0 & 0 & 0 & 0 & 0 & 0 \\ 0 & 0 & 0 & 0 & 0 & 0 & 0 & 0 & 0 \\ 0 & 0 & 0 & 0 & 0 & 0 & 0 & 0 & 0 \end{bmatrix} \tag{4.57}$$

The final impedance matrix for the γ_1 (and γ_2) segment in figure 4.14, is given by (4.58):

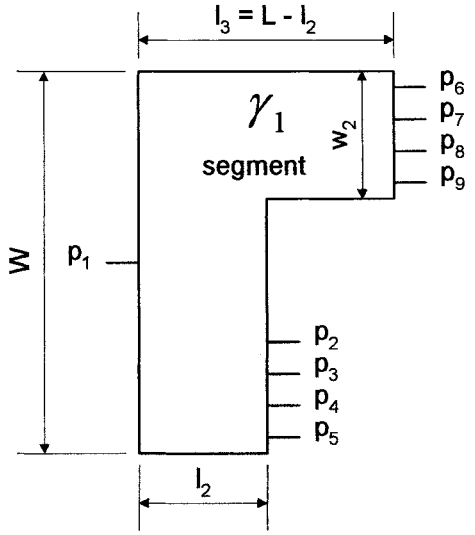

Figure 4.14: P Ports on γ_1 segment

$$\gamma_1 Z_p = \gamma_2 Z_p = \begin{bmatrix} Z_{p1p1} & Z_{p2p1} & \cdots & Z_{p9p1} \\ Z_{p1p2} & Z_{p2p2} & \cdots & Z_{p9p2} \\ \vdots & \vdots & \ddots & \vdots \\ Z_{p1p9} & Z_{p2p9} & \vdots & Z_{p9p9} \end{bmatrix} \tag{4.58}$$

Step 3: Determination of γ segment by synthesis of γ_1 and γ_2 segments

The Z-parameters of the final patch design can now be obtained by synthesising both γ_1 and γ_2 segments, as shown in figure 4.15.

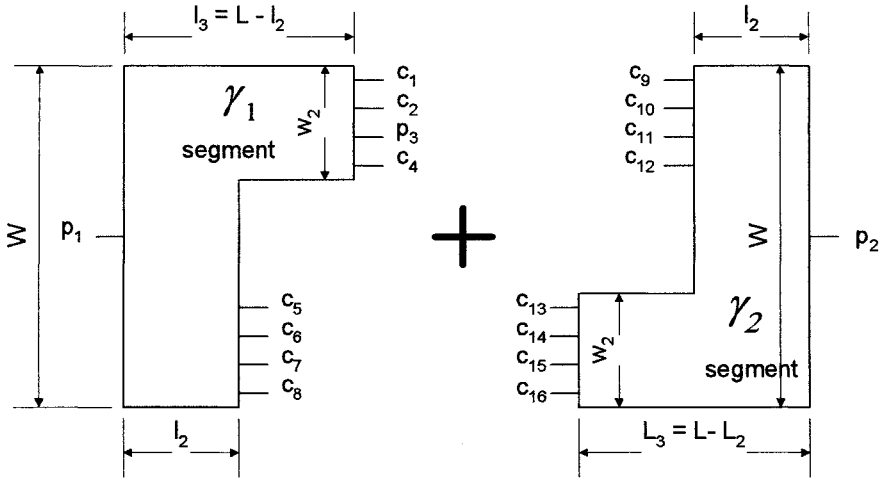

Figure 4.15: Synthesis of γ_1 and γ_2 segments

Equation (4.58) gives the impedance matrix of the γ_1 and γ_2 segments. To synthesise both segments requires that ports P_2 - P_9 on the γ_1 segment be renamed as ports $C_1 - C_8$. Similarly, ports $P_2 - P_9$ on the γ_2 segment are renamed as ports $C_9 - C_{16}$. The process of each stage is shown in steps 3.1 and 3.2 respectively.

Step 3.1: Impedance Matrices of γ_1 segment

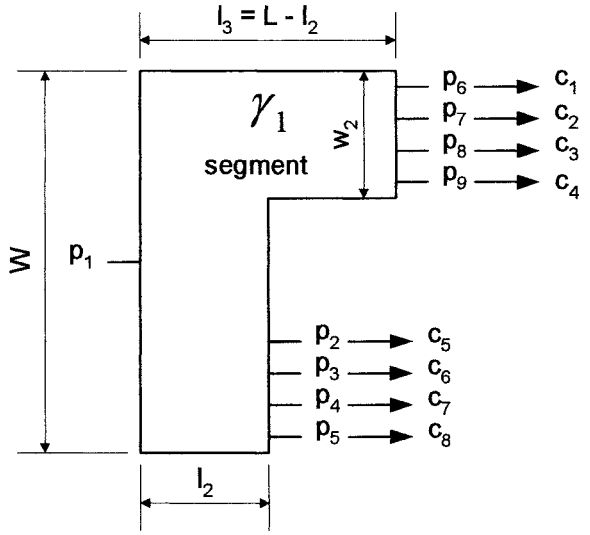

(a)

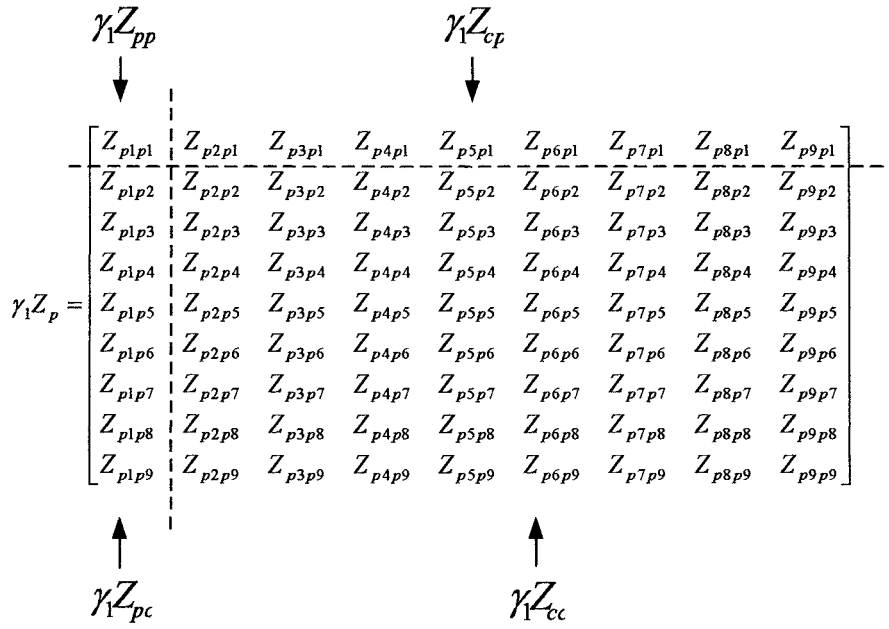

(b)

Figure 4.16: (a) Conversion of P ports to C ports on γ_1 segment (b) with relevant impedance matrix

Step 3.2: Impedance Matrices of γ_2 segment

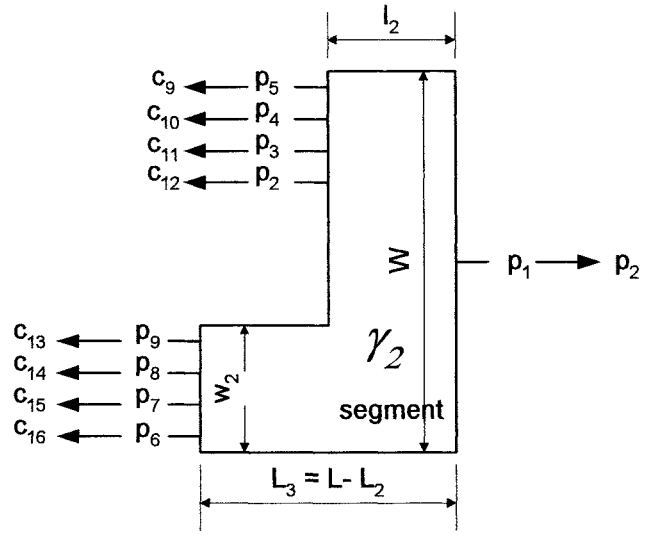

(a)

$$\gamma_2 Z_p = \begin{bmatrix} Z_{p1p1} & Z_{p2p1} & Z_{p3p1} & Z_{p4p1} & Z_{p5p1} & Z_{p6p1} & Z_{p7p1} & Z_{p8p1} & Z_{p9p1} \\ Z_{p1p2} & Z_{p2p2} & Z_{p3p2} & Z_{p4p2} & Z_{p5p2} & Z_{p6p2} & Z_{p7p2} & Z_{p8p2} & Z_{p9p2} \\ Z_{p1p3} & Z_{p2p3} & Z_{p3p3} & Z_{p4p3} & Z_{p5p3} & Z_{p6p3} & Z_{p7p3} & Z_{p8p3} & Z_{p9p3} \\ Z_{p1p4} & Z_{p2p4} & Z_{p3p4} & Z_{p4p4} & Z_{p5p4} & Z_{p6p4} & Z_{p7p4} & Z_{p8p4} & Z_{p9p4} \\ Z_{p1p5} & Z_{p2p5} & Z_{p3p5} & Z_{p4p5} & Z_{p5p5} & Z_{p6p5} & Z_{p7p5} & Z_{p8p5} & Z_{p9p5} \\ Z_{p1p6} & Z_{p2p6} & Z_{p3p6} & Z_{p4p6} & Z_{p5p6} & Z_{p6p6} & Z_{p7p6} & Z_{p8p6} & Z_{p9p6} \\ Z_{p1p7} & Z_{p2p7} & Z_{p3p7} & Z_{p4p7} & Z_{p5p7} & Z_{p6p7} & Z_{p7p7} & Z_{p8p7} & Z_{p9p7} \\ Z_{p1p8} & Z_{p2p8} & Z_{p3p8} & Z_{p4p8} & Z_{p5p8} & Z_{p6p8} & Z_{p7p8} & Z_{p8p8} & Z_{p9p8} \\ Z_{p1p9} & Z_{p2p9} & Z_{p3p9} & Z_{p4p9} & Z_{p5p9} & Z_{p6p9} & Z_{p7p9} & Z_{p8p9} & Z_{p9p9} \end{bmatrix}$$

$\gamma_2 Z_{pp}$ $\gamma_2 Z_{cp}$ $\gamma_2 Z_{pc}$ $\gamma_2 Z_{cc}$

(b)

Figure 4.17: (a) Conversion of P ports to C ports on γ_2 segment
(b) with relevant impedance matrix

Step 3.3: Impedance Matrices of γ_1 and γ_2 segments

The impedance matrix of the γ segment is determined by synthesising γ_1 and γ_2 segments. From (4.48) this is given by:

$$\gamma Z_p = \gamma Z_{pp} - \gamma Z_{pc}\begin{bmatrix}\gamma\Gamma_1\gamma Z_{cc}\\ \gamma\Gamma_2\end{bmatrix}^{-1}\begin{bmatrix}\gamma\Gamma_1\gamma Z_{cp}\\ \gamma 0\end{bmatrix} \tag{4.59}$$

To achieve this requires the relevant impedance matrices.

γZ_{pp} represents the interaction between P ports on both segments and is given by:

$$\gamma Z_{pp} = \begin{bmatrix} Z_{p1p1} & Z_{p2p1} \\ Z_{p1p2} & Z_{p2p2} \end{bmatrix} \tag{4.60}$$

Note: from figure 4.15 the ports P_1 on the γ_1 segment and port P_2 on γ_2 segment are unconnected and hence the interaction between these ports equate to 0.

γZ_{cp} represents the interaction between P ports on both segments and is given by:

$$\gamma Z_{cp} = \begin{bmatrix} Z_{c1p1} & Z_{c1p2} \\ Z_{c2p1} & Z_{c2p2} \\ Z_{c3p1} & Z_{c3p2} \\ Z_{c4p1} & Z_{c4p2} \\ Z_{c5p1} & Z_{c5p2} \\ Z_{c6p1} & Z_{c6p2} \\ Z_{c7p1} & Z_{c7p2} \\ Z_{c8p1} & Z_{c8p2} \end{bmatrix} \tag{4.61}$$

Note: from figure 4.15 port P_1 is unconnected to ports C_9 - C_{16}, hence the interaction between these ports equate to 0.

γZ_{pc} represents the interaction between C and P ports on both segments and is given by:

$$\gamma Z_{pc} = \gamma Z_{cp}^{\ T} \tag{4.62}$$

γZ_{cc} represents the interaction between C ports on both segments and is given by:

$$\gamma Z_{cc} = \begin{bmatrix} Z_{c1c1} & Z_{c2c1} & \cdots & Z_{c16c1} \\ Z_{c1c2} & Z_{c2c2} & \cdots & Z_{c16c2} \\ \vdots & \vdots & \ddots & \vdots \\ Z_{c1c16} & Z_{c2c16} & \vdots & Z_{c16c16} \end{bmatrix} \tag{4.63}$$

Note: from figure 4.15 ports C_1 to C_8 are unconnected to ports C_9 to C_{16}, hence the interaction between these ports equate to 0.

$\gamma\Gamma_1$ and $\gamma\Gamma_1$ has C/2 rows and C columns and were defined in (4.55) and (4.56). $\gamma 0$ represents a null matrix and has c/2 rows and p columns

$$\gamma 0 = \begin{bmatrix} 0 & 0 \\ 0 & 0 \\ 0 & 0 \\ 0 & 0 \end{bmatrix} \tag{4.64}$$

The final impedance matrix for the γ_1 (and γ_2) segment in figure 4.18, is given by:

$$\gamma Z_p = \begin{bmatrix} Z_{p1p1} & Z_{p2p1} \\ Z_{p1p2} & Z_{p2p2} \end{bmatrix} \tag{4.65}$$

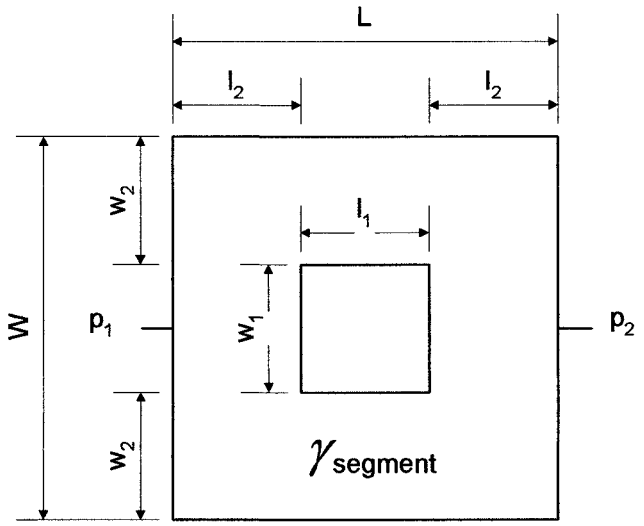

Figure 4.18: P ports on γ_1 segment

In order to apply the segmentation method described above, expressions relating to the interaction between the various ports on each segment must be developed. These expressions are then employed in the relevant impedance matrix. There are a number of expressions, with each depending on the position of the ports, together with the orientation of the patch, and are shown in appendix 4B.

4.6.2 Results

It is recommended [150] that the width of each port must be less than or equal to $\lambda_g / 20$, where λ_g is the wavelength of the fields in the substrate. With reference to figure 4.12c, in the initial formulation of the problem, 16 interconnecting C ports were chosen, each with a port width of 1mm. However, it was found that increasing the number of C ports to 32, and decreasing the port width to 0.5mm increases the accuracy of the computed results. Increasing the number of terms in the infinite also increases accuracy.

Graphs of real and imaginary input impedance versus frequency are shown in figure 4.19a and 4.19b respectively. For comparison practical results are also shown.

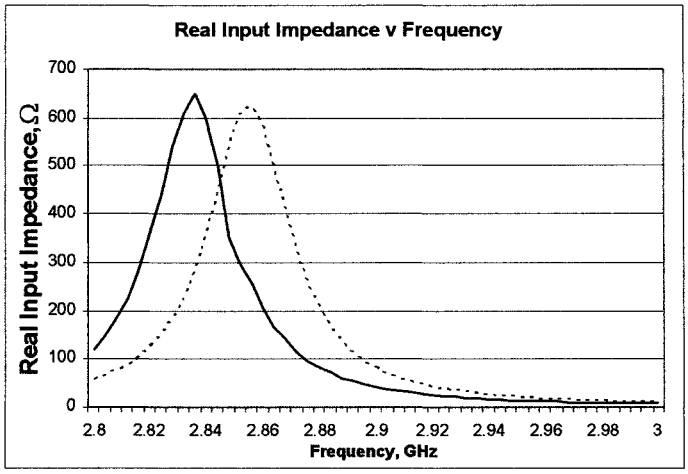

(a)

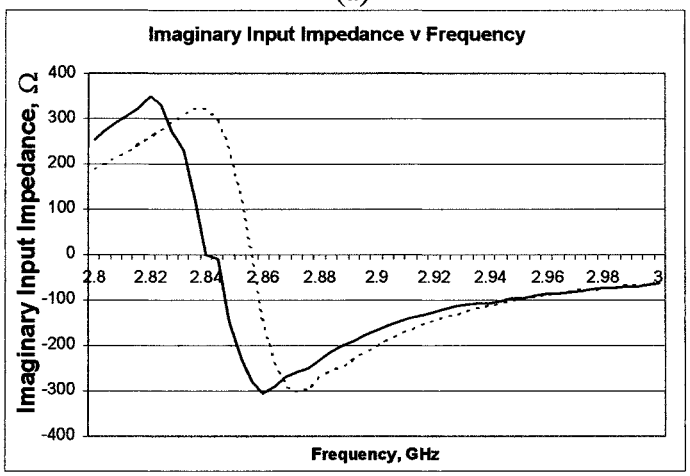

(b)

—— Equation 4.77 ------ Practical Results

Figure 4.19: (a) Real and (b) imaginary input impedance of patch antenna with square slot loading

Figure 4.19 illustrates a difference of 20 MHz between theoretical and practical. This could be due to manufacturing tolerance. From the graphs in figure 4.19a and 4.19b, input impedance and Q factor can also be determined using the same procedure outlined in section 4.4.

Modelling Technique	Resonant Frequency (GHz)	Input Impedance (Ω)	Q Factor
Segmentation	2.836	650	89
Practical	2.856	625	84

Table 4.2: Circuit characteristics of square slot loaded square patch antenna obtained using both segmentation and practical measurements

Table 4.2 demonstrates good agreement between predicted, and practical measurement in both cases although the theoretical prediction is slightly lower, which could be due to manufacturing tolerance, the approximate model of the fringing field extension and the empirical estimation of the effective dielectric constant.

4.7 Summary

This chapter has developed an efficient modelling procedure, based on the segmentation and co-planar modelling, that can be used to determine the circuit characteristics of slot loaded patch antennas. To confirm the applicability of this modelling procedure, two successful applications of this model have been demonstrated. Initially, the co-planar modelling technique was applied to a planar fed square patch antenna. The segmentation technique was then applied to analyse a square patch antenna with square slot loading. In both cases, good agreement with practical measurements for resonant frequency, input impedance and Q factor was demonstrated.

CHAPTER 5

DEVELOPMENT OF OPTIMISED SLOT LOADED STRUCTURE FOR PLANAR FED REDUCED SIZE LINEAR POLARISED PATCH ANTENNA

5.1 Introduction

Chapter 3 introduced the concept of slot loaded patch antennas in which it was stated that inserting slots within regular shaped patch antennas can be used to change the operation of a patch antenna. The insertion of slots results in perturbation of all TM_{mn} modes. The extent to which each mode is affected is dependant on slot shape, dimension and position. The insertion of slots also results in the creation of additional modes. By perturbation and / or creation of the correct mode, it is possible to produce compact linear polarised, compact dual frequency, compact circular polarised, and wideband patch antennas.

In the design of linear polarized patch antennas, a number of criteria in terms of circuit and far-field characteristics must be met. Considering the circuit characteristics, these include resonant frequency, input impedance, Q factor and VSWR Bandwidth. The relationship between these parameters is well established for conventional patch antennas. However, the same is not true of slot loaded patch designs. A detailed review of current work in this field was outlined in Chapter 3. Within this chapter, it was highlighted that current research is largely experimental, with no significant work existing on the design technique and moreover the associated trade-offs of such designs. To this end, the focus of this chapter is to fully investigate the use of slot parameters and their effect on patch performance in

terms of circuit characteristics. These include resonant frequency, input impedance, feed position and quality factor and are determined using the segmental approach outlined in Chapter 4. Using this knowledge, a design procedure is established to produce a new patch structure which is optimized for both size reduction and input impedance.

5.2 Square Patch Antenna with Rectangular Slot Loading

As described in section 3, inserting a single square slot in the centre of a rectangular patch has been used to produce reduced size single and dual frequency patch antennas. It could be argued that all subsequent slot loaded reduced patch antennas have evolved from this design. This technique is therefore of fundamental importance, hence detailed investigation of this design is required. This will provide greater understanding of the relationship between slot parameters and patch performance.

It is widely reported that inserting slots into principle patch shapes will increase the surface current path of the fundamental modes [44,58,62,64,114], and thus account for a lower operating frequency. To investigate this theory, a linear polarised square patch antenna with rectangular slot loading, as shown in figure 5.1, was analysed using the technique developed in Chapter 4.

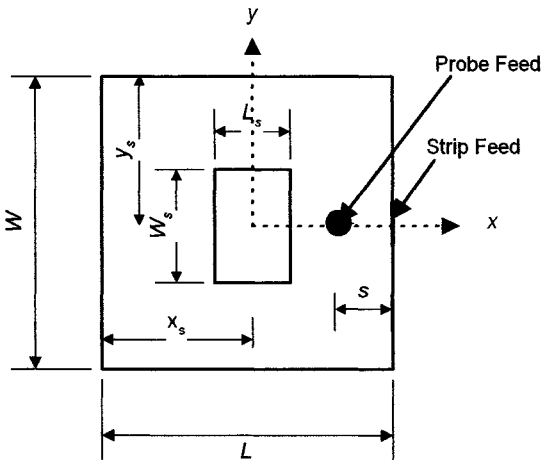

Figure 5.1: Square patch antenna with single square slot loading

The individual slot parameters are described by figure 5.1, and relate to slot length (L_s), slot width (W_s), slot position with respect to x direction (x_s) and slot position with respect to y direction (y_s). In all designs the patch dimensions, L and W, were fixed at 30 mm, on RTDuroid 5870 with a permittivity of 2.33 and thickness 1.57 mm, to give an unmodified resonant frequency of 3.17 GHz. The patch dimensions were arbitrary and chosen to keep the overall patch dimensions smaller to reduce manufacturing costs. The patch was excited using a 50 Ω microstrip feed at the patch edge ($x = 0, y = W/2$) to excite the TM_{01} mode. To this end, all results in this section refer to the effect on this mode. All simulation results are assuming that RTDuroid 5870 is used. . The relevant data for this substrate is shown in Appendix A.

5.2.1 Effect of slot length and width

To determine the effect of slot length and width, two sets of analyses were performed. The first involved parametric analysis to determine the effect of increasing slot length (L_s) for different values of slot width (W_s). The second experiment involved parametric analysis to determine the effect of increasing slot width (W_s) for different values of slot length (L_s). In both cases the slot position was placed in the patch centre, with x_s and y_s both fixed at 15 mm.

5.2.1.1 Effect on resonant frequency

The graphs in figure 5.2 illustrate the relationship between slot width and resonant frequency, for increasing values of slot length. These results were obtained using the following formulae:

The impedance matrix of the patch structure is given by (4.65)

$$\gamma Z_p = \begin{bmatrix} Z_{p1p1} & Z_{p2p1} \\ Z_{p1p2} & Z_{p2p2} \end{bmatrix} \tag{5.1}$$

from this, the input impedance can be determined using:

$$Z_{in} = \gamma Z_{p_{0,0}} = Z_{p1p1} \tag{5.2}$$

from (4.35) the resonant frequency of the patch occurs when:

$$\text{Imag}\{Z_{in}\} = 0 \tag{5.3}$$

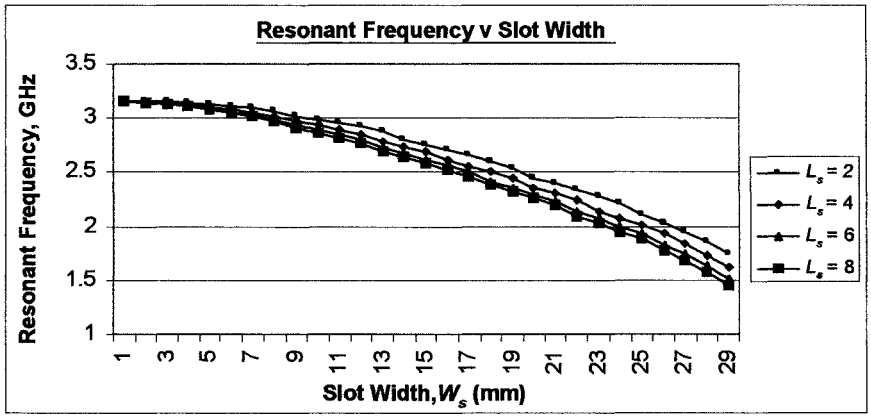

$L = W = 30$ mm, $x_s = y_s = 15$ mm, $\varepsilon_r = 2{,}33$, $h = 1.57$ mm

Figure 5.2: Resonant frequency of TM_{01} mode v slot width for increasing slot length

It is observed that for all values of slot length, there is a significant reduction in antenna resonant frequency with increased slot width. When case L_s = 8mm, the resonant frequency is reduced from 3.16 GHz to 1.4 GHz over a slot width of 0 mm to 29 mm, which corresponds to a size reduction of 81.37%.The relationship between slot length and resonant frequency, for increasing values of slot width, is illustrated in figure 5.3.

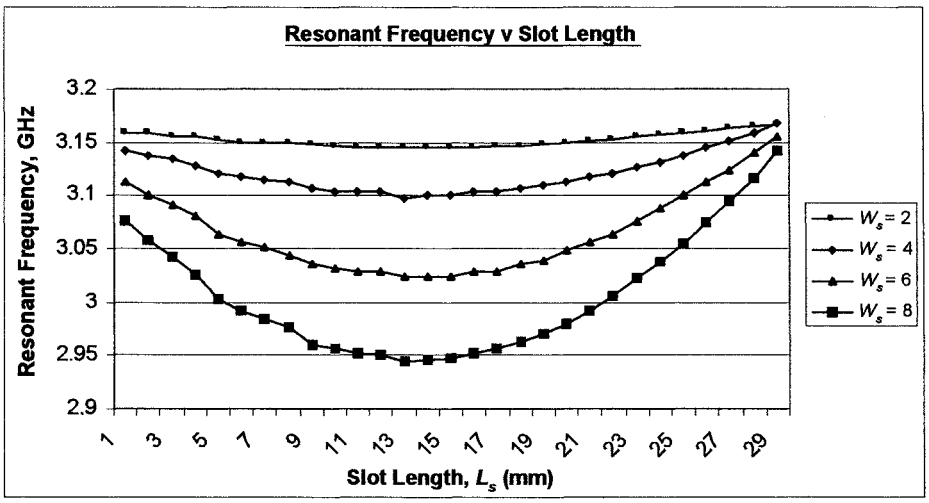

$L = W = 30$ mm, $x_s = y_s = 15$ mm, $\varepsilon_r = 2{,}33$, $h = 1.57$ mm

Figure 5.3: Resonant frequency of TM_{01} mode v slot length for increasing slot width

With a narrow slot width ($W_s = 2$ mm), it is observed that increasing slot length has negligible effect on the antenna resonant frequency, producing a frequency reduction of 30 MHz. It is also observed that for increased values of slot width, the value of slot length affects the resonant frequency. For the case of a large slot width ($W_s = 8$ mm), the resonant frequency is reduced from 3.05 GHz to 2.944 GHz, representing a frequency reduction of 106 MHz. However, this only equates to an antenna size reduction of 15.4%.

From the above results it can be concluded that slot width has greatest effect on the resonant frequency of the TM_{01} mode, whilst the slot length has negligible effect. The reason for this can be explained by referring to the current paths of different slot configurations, determined using Ensemble modelling package [92] and shown in figures 5.4a-c. To provide a reference the current path of an unslotted rectangular patch, fed at the edge in order to excite the TM_{01} mode, is illustrated in figure 5.4a.

Figure 5.4b shows the current path of a slotted patch antenna with the greatest slot dimension converse to the direction of current propagation. It can be seen that the

current path is only slightly lengthened. If a slot with an infinitesimal width could be produced it would be valid to assume that the current path of the TM_{01} mode would not be perturbed.

Figure 5.4c illustrates the effect on the current path of the TM_{01} mode of a slot loaded patch with the greatest slot dimension orthogonal to the direction of current propagation. It can be seen that the current path is lengthened as slot width is increased.

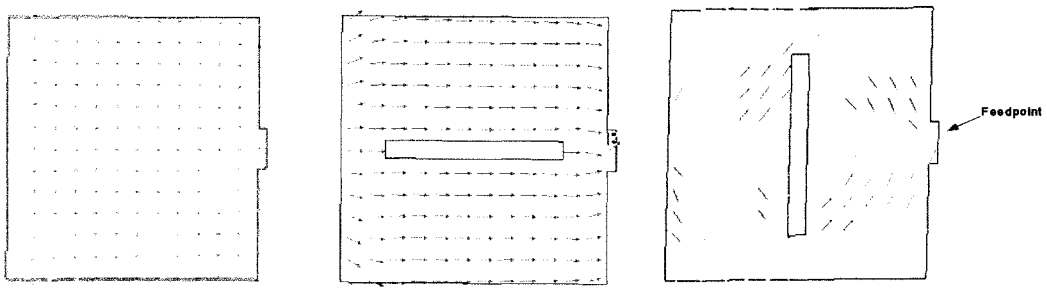

(a) (b) (c)

Figure 5.4 The effect of slot width on current path of TM_{01} mode

With reference to figures 5.2 – 5.4, it would appear that to achieve maximum frequency reduction and hence size reduction, the optimum values for slot length and slot width are $W_s = 29\text{mm}$ ($\approx W$) and $L_s = 15\text{mm}$ ($= L/2$). However, in practical systems other parameters such as input impedance and Q factor must also be considered.

5.2.1.2 Effect on input impedance

With reference to figure 5.4c, it can be seen that as slot width increases, the concentration of surface currents increases causing an increased current density around the slot, and hence lower input impedance at this point. As the feedpoint is a distance of $\lambda/4$ from this point, from transmission line theory, the input impedance can be expected to be significantly much higher (where λ is the wavelength is the patch).

Conversely, as shown in figure 5.4b, slot length appears to have negligible effect on the concentration of surface current and hence input impedance. To confirm this, figures 5.5-5.6 demonstrate the effect of slot width and length on antenna input impedance. The graph in figure 5.5 illustrates the relationship between slot width and input impedance, for increasing values of slot length. These results were obtained using the following formulation:

Equations (5.2) gives the input impedance as a function of frequency. Equation (4.35) is then used to obtain the real input impedance at resonance.

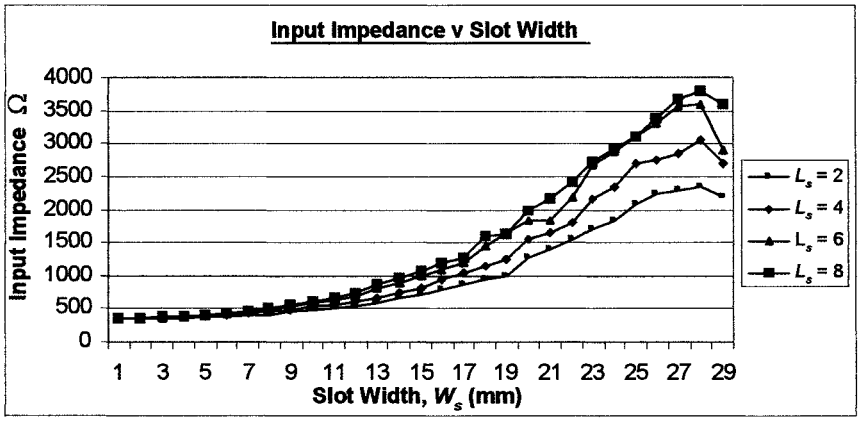

$L = W = 30$ mm, $x_s = y_s = 15$ mm, $\varepsilon_r = 2{,}33$, $h = 1.57$ mm

Figure 5.5: Input impedance of TM_{01} mode v slot width for increasing slot length

It is observed that for all values of slot length, there is a significant increase in antenna input impedance with slot width. This trend is true until the slot width approaches the patch width. At this point, there is a slight decrease in input impedance occurs, which could be due to a slight modelling inaccuracy. With reference to section 2.2.2, it was determined that for impedance matching using a quarter-wave planar matching network, the antenna input impedance must be constrained to below 500 Ω. From figure 5.5, this suggests a maximum slot width of 8 mm. With reference to figure 5.2, this equates to a resonant frequency of 2.954 GHz, producing a size reduction of 14.85%.

The relationship between slot length and input impedance, for increasing slot width, is illustrated in figure 5.6.

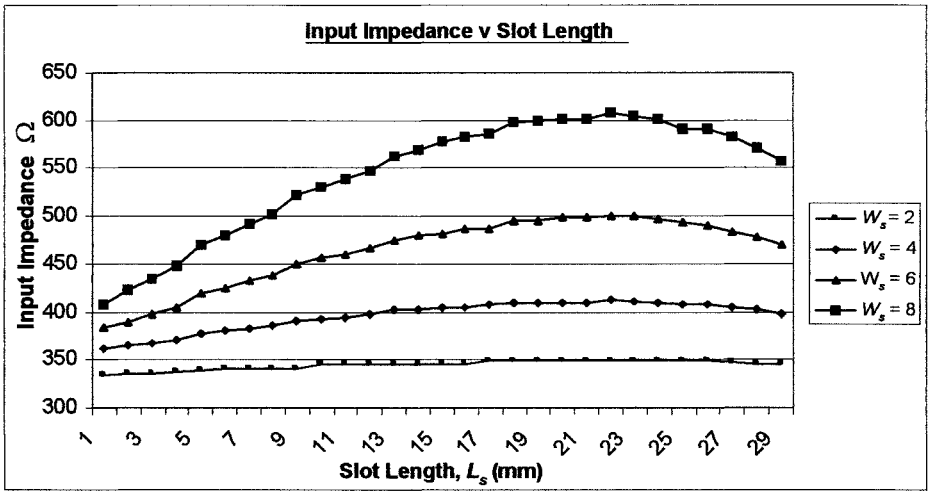

$L = W = 30$ mm, $x_s = y_s = 15$ mm, $\varepsilon_r = 2{,}33$, $h = 1.57$ mm

Figure 5.6: Input impedance of TM_{01} mode v slot length for increasing slot width

With a narrow slot width ($W_s = 2$mm), it is observed that increasing slot length has negligible effect on antenna input impedance. With increased slot width ($W_s = 8$mm), first observation suggests that increasing slot length significantly effects antenna input impedance, producing a maximum value of 600 Ω with slot length of 22 mm. However, this only represents an increase of 200 Ω, which is relatively small when compared to the effect of slot width. For a slot width of 8 mm, the current density at the slot edge increases, hence the impedance at this position is at a minimum. From figure 5.6, maximum input impedance at the feedpoint occurs when the slot length, L_s is approximately 23 mm. From transmission line theory, when the slot is placed at the position, as the feed position is approximately a distance of λ/4, the input impedance can be expected to be higher. As the slot length increases, the slot effectively moves closer to the feedpoint, hence the input impedance decreases.

From the above results, it can be concluded that slot width is the main slot parameter controlling antenna input impedance, with slot length having negligible

effect. This is due to the fact that slot width has a significant effect on the on the current path of the TM_{01} mode, whilst the slot length has negligible effect. With reference to figures 5.5 – 5.6, it would appear that to achieve optimum values of slot length and slot width in terms of input impedance are $W_s = 1\text{mm}$ and $L_s = 1\text{mm}$. However, selecting these values will have negligible effect on resonant frequency and size reduction.

5.2.1.3 Effect on Q factor

A further trade-off to be considered is the relationship between slot loading and Q factor. In general, the bandwidth of a patch is proportional to its volume [82], which was expressed in Chapter 2 as:

$$BW \sim volume = area * height = length * width * height \qquad (5.1)$$

By introducing slots, the excited volume of the patch effectively decreases, thus limiting bandwidth. The increased concentration of surface currents also increases the antenna frequency sensitivity, hence reducing its impedance bandwidth. It has already been established that slot width has a significant effect on the resonant frequency and hence patch size. Considering this, it can be predicted that slot width as opposed to slot length will be the controlling parameter for antenna Q factor. To confirm this prediction, the graphs in figure 5.6 demonstrate the effect of slot length and width on antenna Q factor. The graph in figure 5.7 illustrates the relationship between slot width and antenna Q factor, for increasing values of slot length. Figure 5.8 illustrates the relationship between slot length and antenna Q factor, for increasing values of slot width. These results were obtained by substituting (4.36) into (5.2).

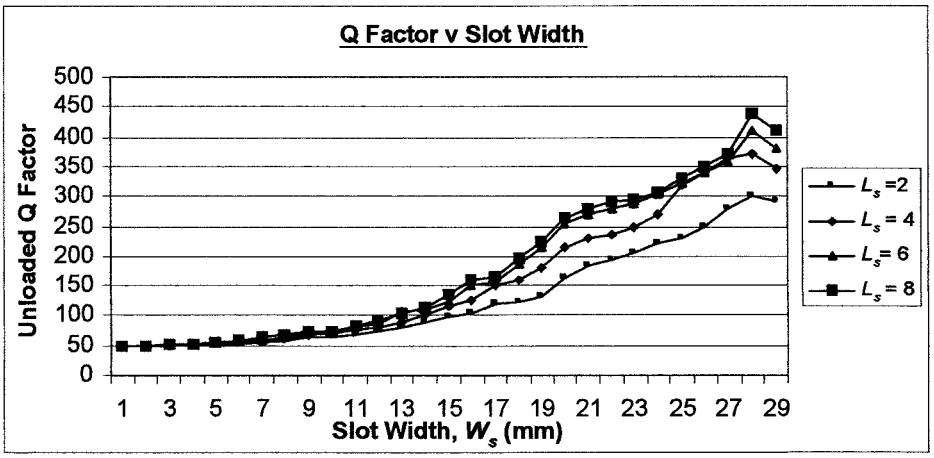

$L = W = 30$ mm, $x_s = y_s = 15$ mm, $\varepsilon_r = 2{,}33$, $h = 1.57$ mm

Figure 5.7: Unloaded Q factor of TM_{01} mode v slot width for increasing slot length

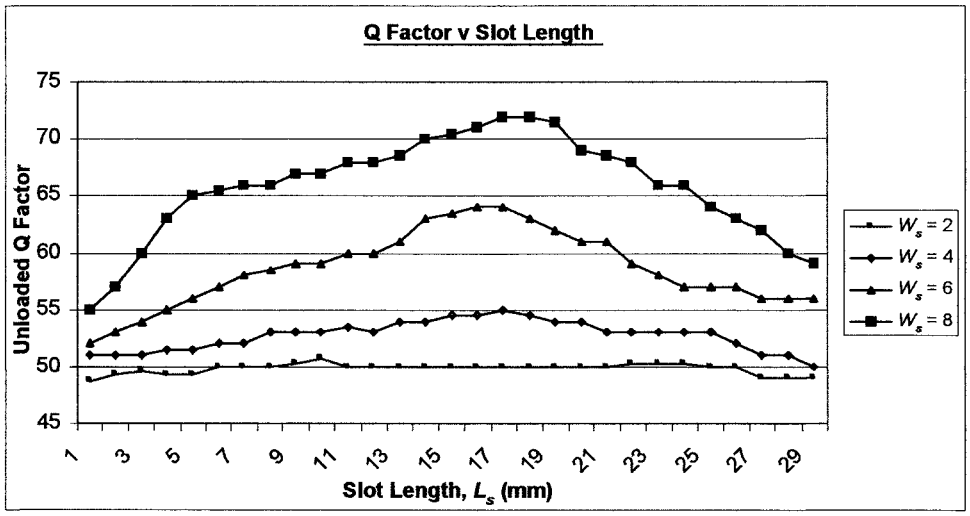

$L = W = 30$ mm, $x_s = y_s = 15$ mm, $\varepsilon_r = 2{,}33$, $h = 1.57$ mm

Figure 5.8: Unloaded Q factor of TM_{01} mode v slot length for increasing slot width

From figure 5.7, it is observed that for all values of slot length, there is a significant increase in antenna Q factor with increasing slot width. This trend is true until the slot width approaches the patch width. At this point, there is a slight decrease in input impedance occurs, which could be due to a slight modelling inaccuracy. Conversely, from figure 5.8, for a narrow slot width ($W_s = 2$mm), it observed that the antenna Q factor remains relatively constant with increasing slot length. With increased slot width, a slight increase in Q factor is observed, however

this only represents a maximum increase of 20, which is negligible. For a slot width of 8 mm, a maximum Q factor occurs when the slot length is approximately equal to L/2. The reason for this can be explained with reference to figure 5.3 and equation (2.15). Equation (2.15), states that the bandwidth is inversely proportional to the patch volume. Referring to figure 5.3, which illustrates the effect of slot length on resonant frequency, it can be seen that resonant frequency is also at its lowest value at this point, and hence the patch volume is smaller. Consequently, the antenna Q factor can be expected to increase.

From the above results, it can be concluded that slot width is the main slot parameter controlling antenna Q factor, with slot length having negligible effect. This is due to the fact that slot width has a significant effect on the on the current path of the TM_{01} mode, whilst the slot length has negligible effect. With reference to figures 5.7 – 5.8, it would appear that to achieve optimum values of slot length and slot width in terms of Q factor are $W_s = 1\text{mm}$ and $L_s = 1\text{mm}$. However, selecting these values will have negligible effect on resonant frequency and size reduction.

5.2.2 Effect of slot position

The review of slot loaded patch antennas, detailed in Chapter 3, highlighted that slot loaded compact designs operate by modifying the current path of the fundamental modes of a patch antenna. The majority of these designs involve the use of different shaped slots placed at some point along the central x or y axis of the patch, thus providing a symmetrical structure. This case is of especially important in circular polarized designs. To this end, the research presented thus far in this chapter has considered the effect of different slot parameters placed at the patch centre.

Chapter 3 also highlighted that it was also possible to produce compact linear polarised designs with both single and dual frequency response, through the use of offset slots. The following section presents an investigation of the effect of slot position on antenna response. Initially the effect of slot position, with respect to the

x direction, was investigated to determine the effect on antenna circuit characteristics. To enable this, parametric analysis for increasing values of slot width W_s, was performed on the patch configuration illustrated in figure 5.9.

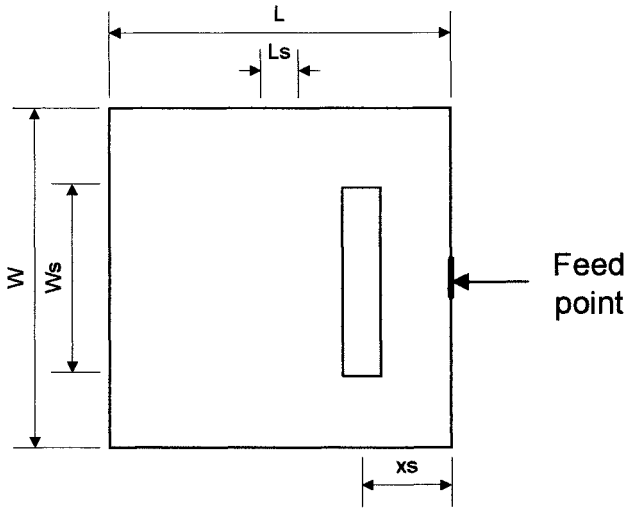

Figure 5.9: Patch configuration with slot offset in x direction

The patch was fabricated on RTDuroid 5870 with permittivity 2.33 and thickness 1.57 mm, with patch length L and width W both fixed at 30 mm. Regarding the slot length, L_s, the results from section 5.2.1, indicate that this parameter has negligible effect on the response of the TM_{01} mode. To this end, together with geometrical reasons, the value of L_s was fixed at 1 mm. To determine the effect of slot position, with respect to the y direction, the patch configuration illustrated in figure 5.10, was analysed. For geometrical reasons, the value of Ws was fixed at 1 mm.

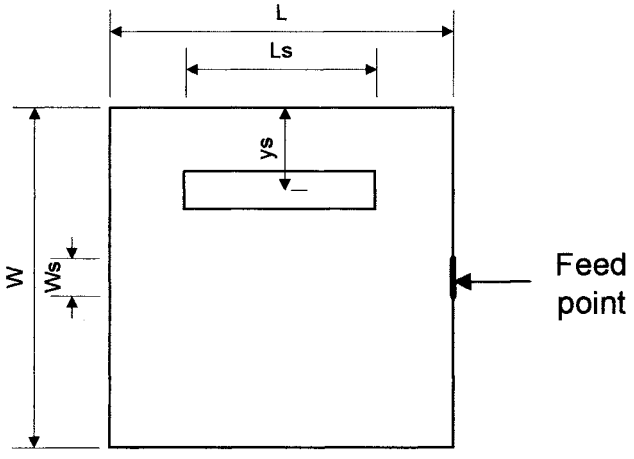

Figure 5.10: Patch configuration with slot offset in y direction

5.2.2.1 Effect on resonant frequency

The graph in figure 5.11a illustrates the relationship between slot position with respect to the x direction and resonant frequency, whilst figure 5.11b demonstrates the effect of slot position with respect to the y direction. These results were obtained using equations (5.1 – 5.3).

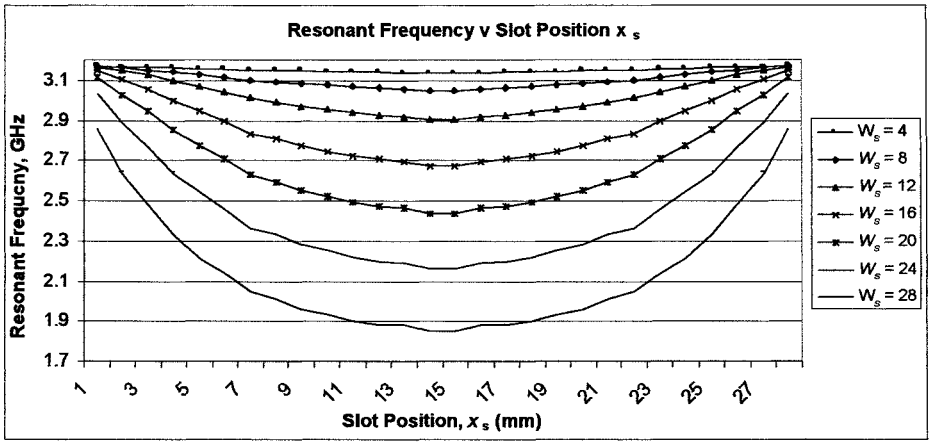

$L = W = 30$ mm, $L_s = 1$mm, $y_s = 15$ mm, $\varepsilon_r = 2{,}33$, $h = 1.57$ mm

(a)

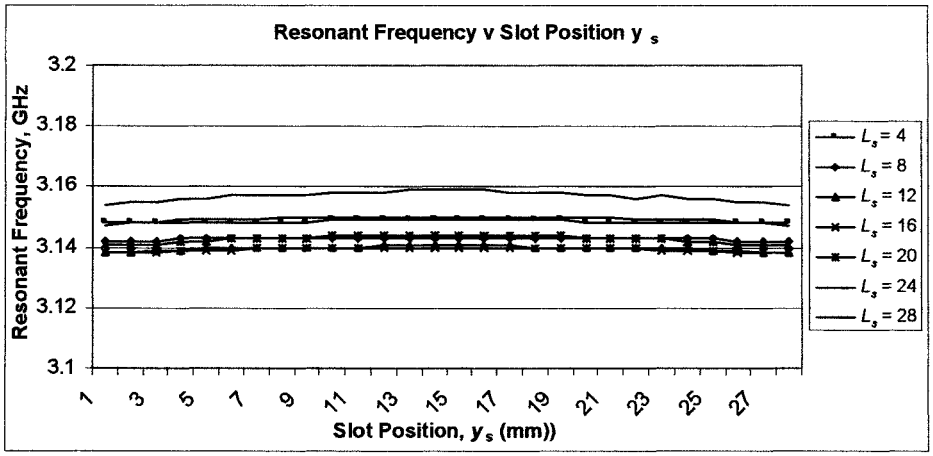

$L = W = 30$ mm, $W_s = 1$mm, $x_s = 15$ mm, $\varepsilon_r = 2{,}33$, $h = 1.57$ mm

Figure 5.11: (a) Effect of slot position w.r.t x axis on resonant frequency (b) effect of slot position w.r.t y axis on resonant frequency

From figure 5.11a, it can be seen that, for all values of slot width, maximum reduction in resonant frequency is achieved when $x_s = 14$ mm, i.e. along the central x

axis of the patch. Conversely, figure 5.11b, illustrates that, for all values of slot length, the slot position with respect to the y direction, has little effect on the resonant frequency of the TM_{01} mode.The reason for this trend can be explained with reference to the field configurations of a rectangular patch, as determined in section 2.2.2. The voltage and current distribution of the unperturbed TM_{01} mode of a rectangular patch without slot loading, with respect to the x direction, are illustrated in figure 5.12.

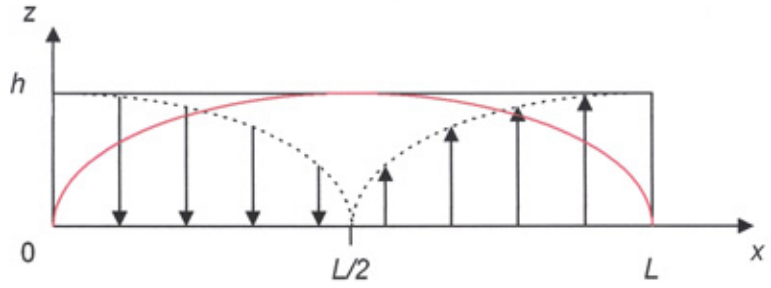

Voltage Distribution Current Distribution

Figure 5.12 Field configuration of TM_{01} mode

The basic principle of operation of compact slot loaded patch antennas is to reduce the resonant frequency of the fundamental mode by lengthening its current path. It can be seen that both the voltage and current distribution demonstrate a sinusoidal distribution in the x direction, with a single null-voltage point and current maxima along the central x axis and two voltage maxima and current minima existing at the patch edges. Hence, placing slots in the patch centre will have maximum effect on the current distribution of the fundamental TM_{01} mode, with the effect decreasing when the slot is moved towards the patch edges. Considering this, from figure 5.11 , it would appear that to achieve maximum frequency reduction and hence size reduction, the optimum value of slot position w.r.t the x axis if $x_s = L/2$, i.e. along the central x axis of the patch. However, in practical systems other parameters such as input impedance and Q factor must also be considered.

5.3.2.2 Effect on input impedance

The graph in figures 5.13a demonstrates the relationship between slot position with respect to the x direction and input impedance at the patch periphery, whilst figure 5.13b illustrates the effect of slot position with respect to the y direction. These results were obtained using the following formulation:

Equations (5.2) gives the input impedance as a function of frequency. Equation (4.35) is then used to obtain the real input impedance at resonance.

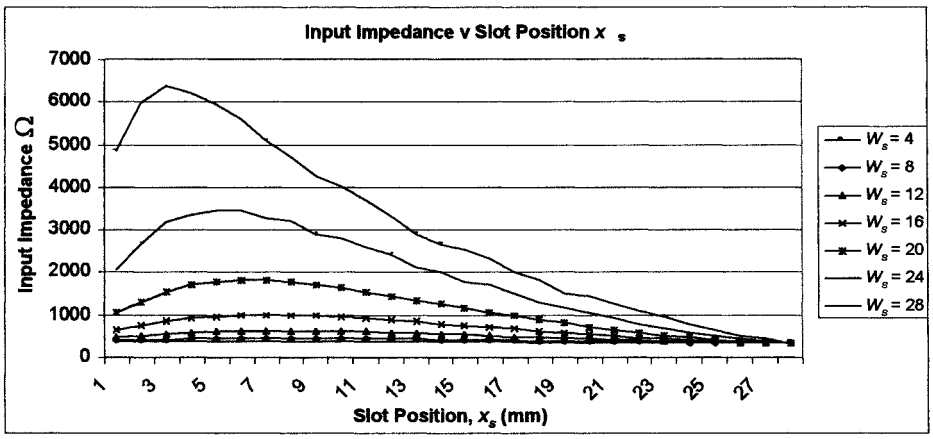

$L = W = 30$ mm, $L_s = 1$mm, $y_s = 15$ mm, $\varepsilon_r = 2{,}33$, $h = 1.57$ mm

(a)

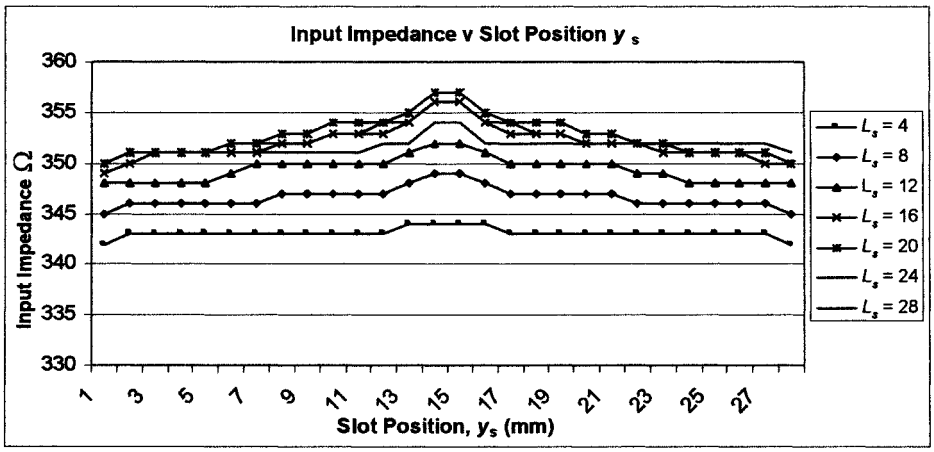

$L = W = 30$ mm, $W_s = 1$mm, $x_s = 15$ mm, $\varepsilon_r = 2{,}33$, $h = 1.57$ mm

(b)

Figure 5.13: (a) Effect of slot position w.r.t x axis on input impedance
(b): effect of slot position w.r.t y axis on input impedance

From figure 5.13a it can be seen the slot position has greatest effect on input impedance at resonance when the slot is placed close to the radiating patch edges.

Conversely, figure 5.13b, it can be seen that, for all values of slot length, the slot position w.r.t. the y axis has negligible effect on the input impedance at resonance. The reason for this is best explained with reference to figure 5.14a-c

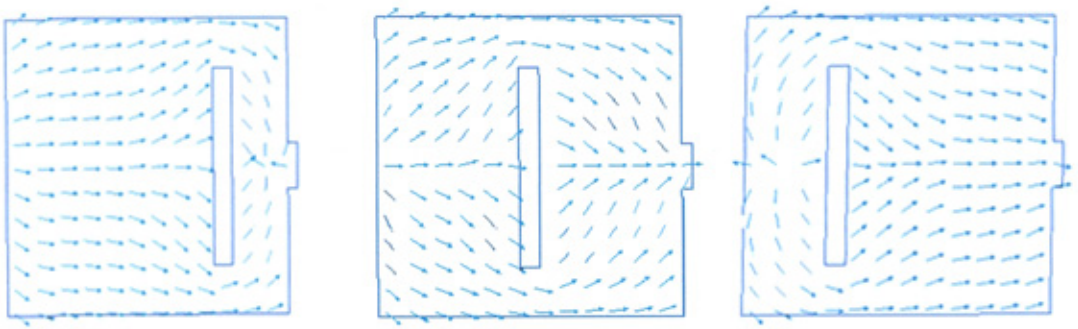

(a) (b) (c)

Figure 5.14: Effect of slot position w.r.t. x axis on TM_{01} current paths

When the slot is placed close to the planar feed, it can be seen that a significant increase in current density occurs around the feed position, as in figure 5.14a. As the slot moves away from the feed the current density near the feed decreases and hence the input impedance at this point also decreases, figure 5.14b and figure 5.14c. Considering this, it would appear that to achieve minimum input impedance, the slot should be placed at $x_s = 29$mm, i.e. close to the radiating patch edge opposite to the feed postion. However, selecting these values will have negligible effect on resonant frequency and size reduction.

5.2.2.3 Effect on Q Factor

The graph in figure 5.15a demonstrates the relationship between slot position with respect to the x direction and unloaded Q factor, whilst figure 5.15b illustrates the effect of slot position with respect to the y direction. These results were obtained by substituting (4.36) into (5.2).

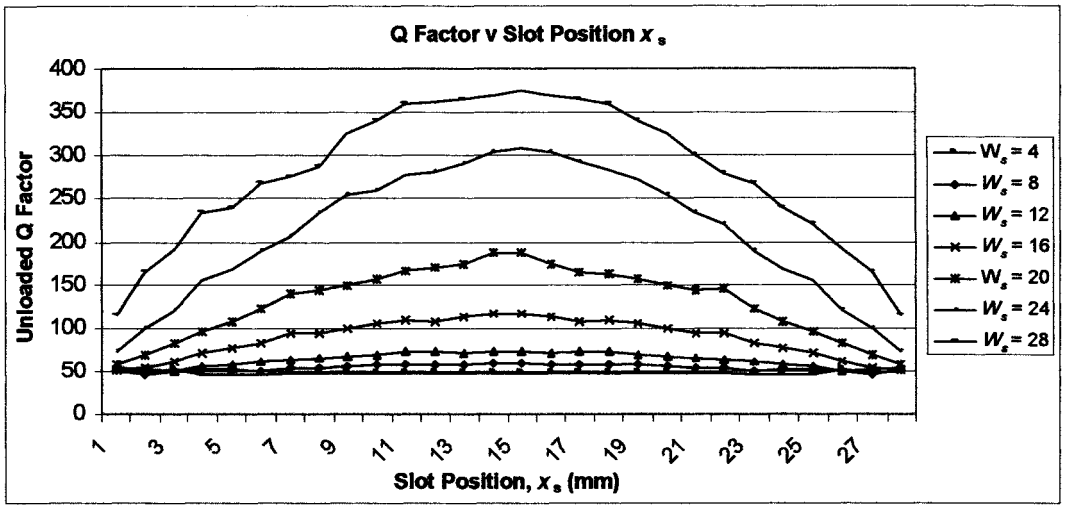

$L = W = 30$ mm, $L_s = 1$mm, $y_s = 15$ mm, $\varepsilon_r = 2{,}33$, $h = 1.57$ mm

(a)

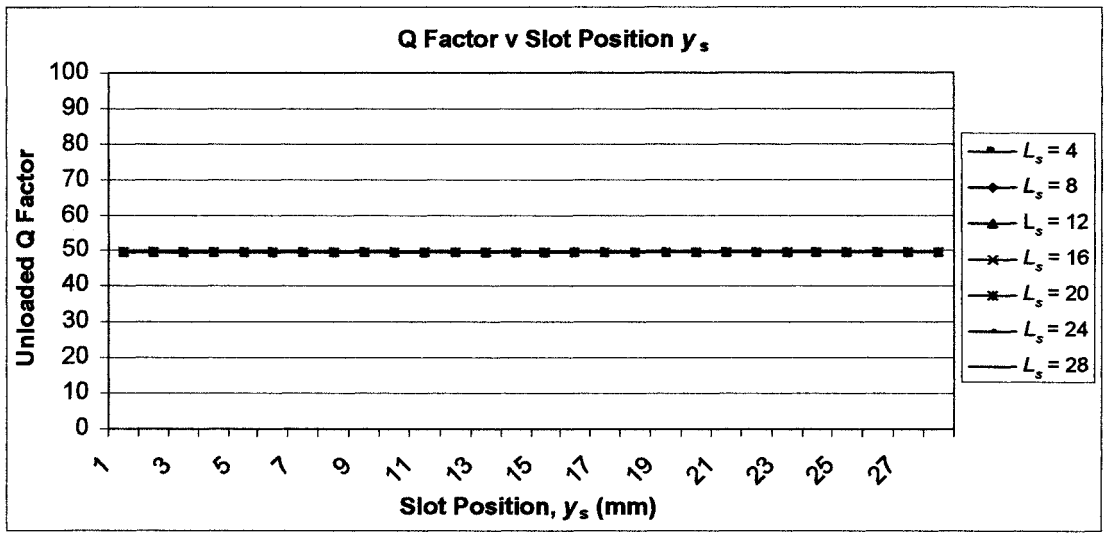

(b)

$L = W = 30$ mm, $W_s = 1$mm, $x_s = 15$ mm, $\varepsilon_r = 2{,}33$, $h = 1.57$ mm

Figure 5.15: (a) Effect of slot position w.r.t x axis on Q factor
(b): effect of slot position w.r.t. y axis on Q factor

From figure 5.15a, it can be seen that, for all values of slot width, maximum increase in Q factor of the TM_{01} mode is achieved when $x_s = 14$ mm, i.e. along the central x axis of the patch. For a slot position, x_s of 15 mm, i.e. slot placed in central x axis of the antenna, a maximum Q factor occurs. The reason for this can be explained with reference to figure 5.11a and equation (2.15). Equation (2.15), states that the bandwidth is inversely proportional to the patch volume. Referring to figure 5.11a, which illustrates the effect of slot length on resonant frequency, it can

be seen that resonant frequency is also at its lowest value at this point, and hence the patch volume is smaller. Consequently, the antenna Q factor can be expected to increase. Conversely, figure 5.15b, illustrates that, for all values of slot length, the slot position with respect to the y direction, has little effect on the Q factor.

It would therefore appear that to achieve optimum values of slot position in terms of Q factor are $x_s = 1$ mm or $x_s = 29$ mm, i.e. close to radiating patch edges. However, selecting these values will have negligible effect on resonant frequency and size reduction.

It can thus be concluded that placing slots of increasing width has maximum effect on the antenna Q factor when embedded along the central x axis of the patch. However, this has an undesirable effect on bandwidth. One reason for this, as previously determined is that inserting slots in a patch antenna will produce an increased concentration of surface currents, thus reducing the antenna frequency sensitivity and increasing the Q factor. The second reason can be explained by examining the current distribution of the TM_{01} mode of a standard unslotted patch antenna, as shown in figure 5.4a. It is observed that this follows a sinusoidal distribution along the x axis, with maximum current density at the centre.

5.2.3 Effect of slot parameters on patch design

The previous section has focussed on a rigorous investigation of a slot loaded square patch antenna, in particular the relationship between slot parameters and patch performance in terms of circuit characteristics. A number of significant findings have arisen from this study which will have a major impact on the design of slot loaded patch antennas. In particular the effect of slot length, width and position on the resonant frequency, input impedance, feed position and Q factor of the fundamental TM_{01} and TM_{10} modes was demonstrated. With reference to figure 5.16, it was found that in general the slot width W_s effects the TM_{01} mode, whilst

having little effect on the TM_{10} mode. Conversely, the slot length effects the TM_{10} mode and has negligible effect on the TM_{01} mode.

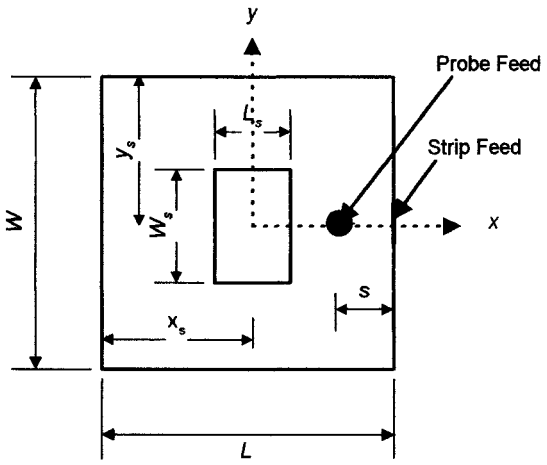

Figure 5.16: Square patch antenna with rectangular slot loading

Considering the TM_{01} mode, increasing slot width produces a reduction in resonant frequency and hence size reduction. However, this is achieved at the expense of increased input impedance and higher Q factor. The same relationship can also be expected to exist between slot length and the characteristics of the TM_{10} mode.

Regarding the slot position, the slot has maximum effect on the TM_{01} mode when it is positioned along the central x axis of the patch, with its effect decreasing as it moves towards the patch edge. The same relationship can also be expected to exist between y position and the characteristics of the TM_{10} mode.

The findings of this investigation can be summarised in the table 5.1. Only the effect on the TM_{01} mode is shown. For the effect on the TM_{10} mode the a similar trend exists with relevant orientation change.

L_s = Slot length, W_s = slot width, x_s = x position of slot, y_s = y position of slot,

Variable	**Frequency**	**Z_{in}**	**Q Factor**
$W_s \uparrow$	$f_{01} \downarrow$	$Z_{in01} \uparrow$	$Q_{01} \uparrow$

$L_s\uparrow$ $(L_s < L/2)$	$f_{01} \leftrightarrow$	$Z_{in01}\uparrow$	$Q_{01}\uparrow$
$(L/2 < L_s < 3L/4)$	$f_{01} \leftrightarrow$	$Z_{in01}\uparrow$	$Q_{01}\downarrow$
$(L_s > 3L/4)$	$f_{01} \leftrightarrow$	$Z_{in01}\downarrow$	$Q_{01}\downarrow$
$x_s\uparrow$ $(x_s < L/4)$	$f_{01}\downarrow$	$Z_{in01}\uparrow$	$Q_{01}\uparrow$
$(L/4 < x_s < L/2)$	$f_{01}\downarrow$	$Z_{in01}\downarrow$	$Q_{01}\uparrow$
$(L/2 < x_s < 3L/4)$	$f_{01}\uparrow$	$Z_{in01}\downarrow$	$Q_{01}\downarrow$
$(x_s > 3L/4)$	$f_{01}\uparrow$	$Z_{in01}\downarrow$	$Q_{01}\downarrow$
$y_s\uparrow$ $(y_s < L/2)$	$f_{01} \leftrightarrow$	$Z_{in01}\uparrow$	$Q_{01}\leftrightarrow$
$(y_s < L/2)$	$f_{01} \leftrightarrow$	$Z_{in01}\downarrow$	$Q_{01}\leftrightarrow$

Table 5.1: Effect of slot parameters on performance of TM_{01} mode

The use of compact slot loaded patch antennas has been the subject of many studies [44,58,62,64,114]. However, the majority of these designs are probe fed. One of the primary aims of this thesis is to investigate methods of producing reduced size patch antennas that are planar fed. This type of feed has inherent advantages over a probe feed as it not only eliminates drilling of holes and probe soldering, but also makes it simple adding a tuning device for impedance matching [151]. Moreover, the use of a planar feed allows easier manufacturing, robustness and ease of integration with associated microwave circuitry.

To design such an antenna, the goal is to achieve maximum frequency reduction for a fixed patch size, whilst maintaining an input impedance of practical value to allow the use of an impedance matching network, and maximising the impedance bandwidth and minimising antenna Q factor. From the investigation performed so far in this thesis significant trade-offs exist between all these performance characteristics and it is not possible to simultaneously optimise each one.

5.3 Optimised Design of Planar Fed H-Shaped Patch Antenna

The patch configuration considered thus far in this chapter, have involved the use of a single slot. However, examination of the TM_{01} mode current distribution of a rectangular patch antenna [92], shown in figure 5.17, is illustrated that as well as being greater along the $x = L/2$ axis, the current density also increases towards the non-radiating patch edge. This suggests that greater size reduction may be achieved by incorporating two slots and placing them towards each of the non-radiating patch edges.

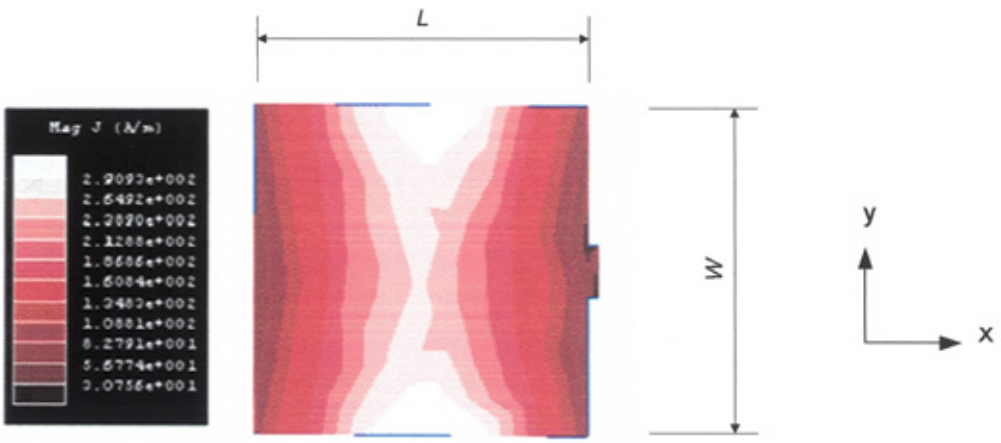

$L = W = 30$ mm, $\varepsilon_r = 2.33$, $h = 1.57$ mm

Figure 5.17: Current distribution of TM_{01} mode on rectangular patch antenna

5.3.1 Effect of slot parameters on patch performance

Figure 5.18 illustrates the proposed patch configuration. It consists of a square patch of dimensions $L = W$ and is fed by a microstrip-line fed which is impedance matched through the use traditional quarter-wave matching network. Two slot of dimensions L_s and $W_s/2$, separated by a distance s_y are embedded inside the patch at a distances x_s and y_s from the respective patch edges. As with single slot loaded

designs, trade-offs are expected to exists between size reduction, input impedance and Q factor. In order to demonstrate this, four examples are given below which clearly demonstrate the trade-offs between frequency reduction, input impedance and impedance bandwidth. The patch is designed for use on RTDuroid 5870. The relevant data for this substrate is shown in Appendix A.

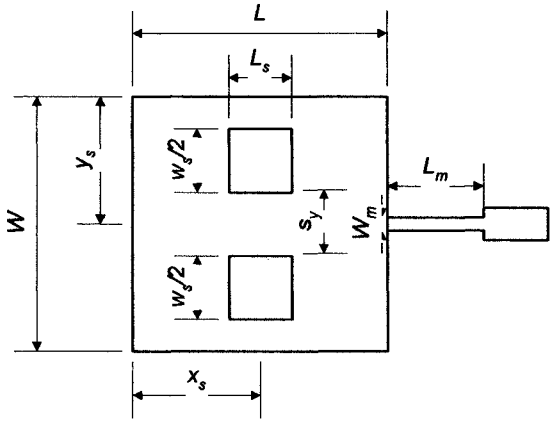

Figure 5.18: Proposed patch configuration

Once the choice of substrate is made, the design parameters are: L,W, L_s, W_s, x_s, y_s. Assuming L and W are fixed, the 4 controlling parameters, x_s, s_y, L_s and W_s. The graphs in figures 5.19 to 5.22 illustrate the effect of each parameter on (a) return loss and (b) input impedance as a function of frequency. To achieve this, the segmentation model outlined in Chapter 4 was first used to obtain the input impedance response as a function of frequency.

From this, the return loss as a function of frequency was determined using (5.4):

$$S_{11} = 20\log_{10}\left|\frac{|Z_{in} - Z_0|}{|Z_{in} + Z_0|}\right| \qquad (5.4)$$

where Z_{in} is assumed to be 50 Ω, and Z_0 is the input impedance of the patch antenna determined by equations (5.1 – 5.3).

The VSWR bandwidth, for a 2:1 ratio, of each design is also shown.

Effect of Increased L_s

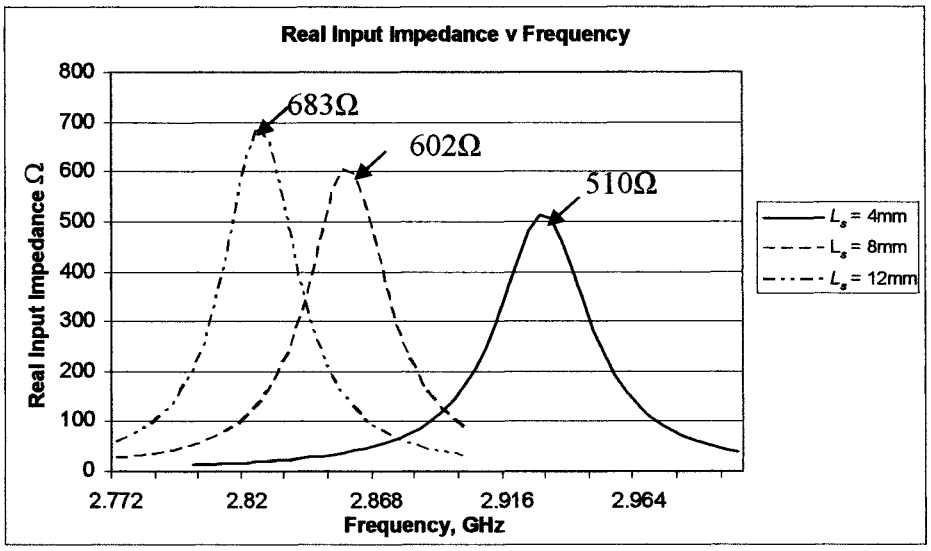

(a)

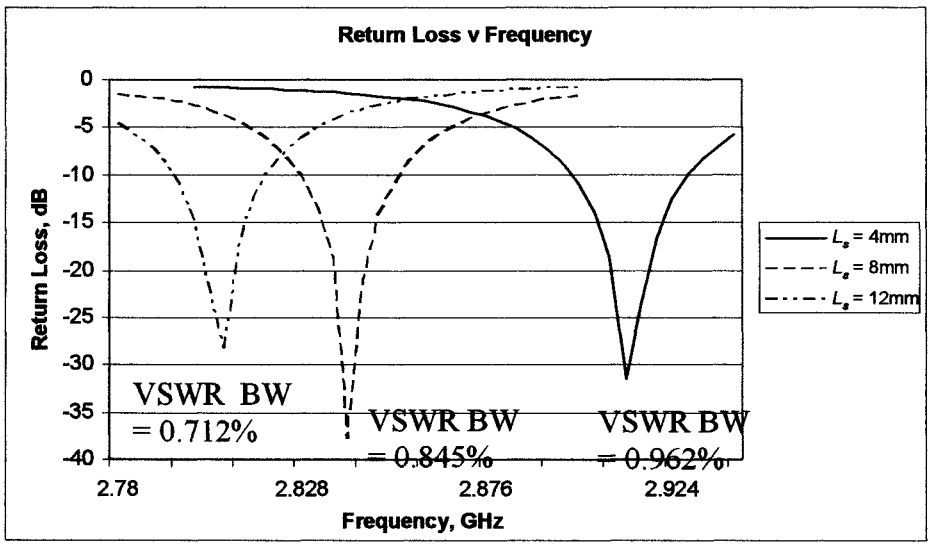

(b)

$L = W = 30$ mm, $x_s = 15$ mm, $y_s = 15$ mm, $s_y = 0$ mm, $W_s = 10$ mm, $\varepsilon_r = 2.33$, $h = 1.57$mm

Figure 5.19: Effect of slot length L_s on (a) input impedance and (b) return loss as a function of frequency

Effect of Increased W_s

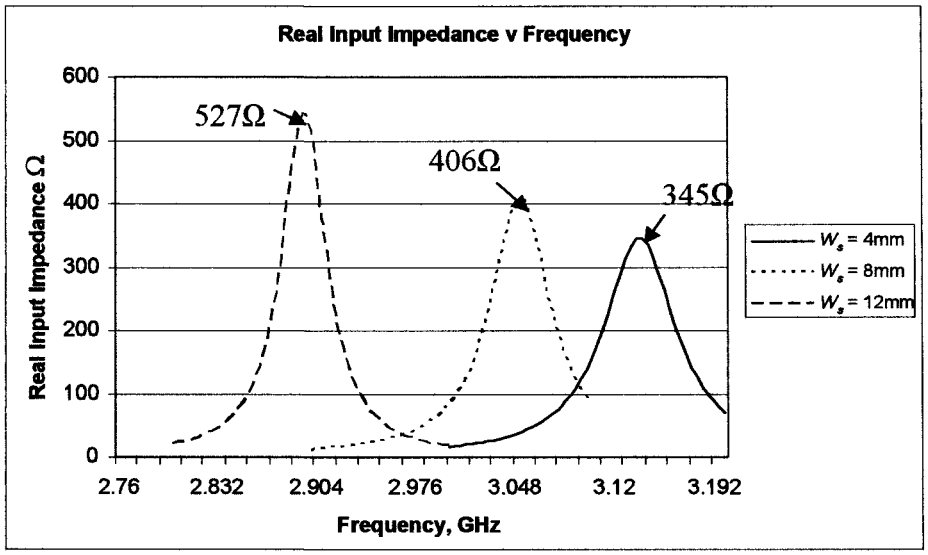

(a)

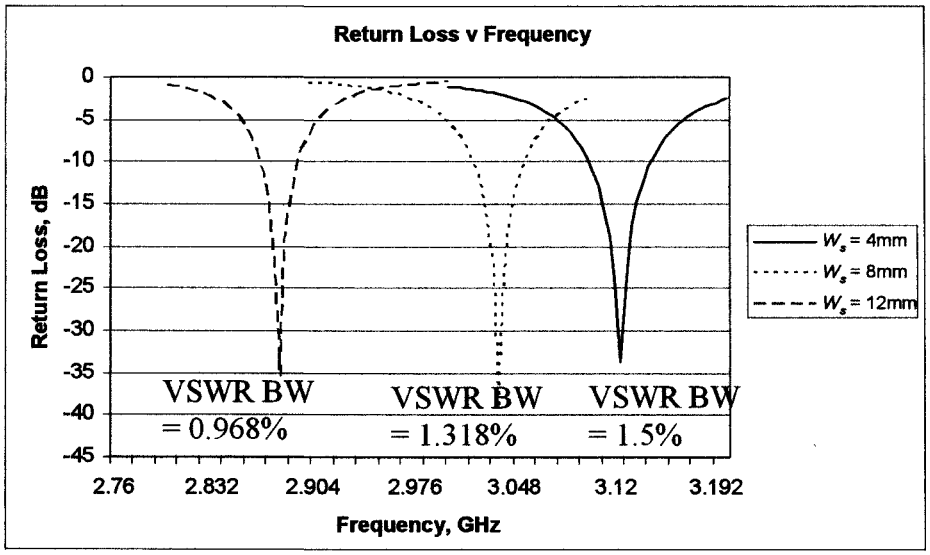

(b)

$L = W = 30$ mm, $x_s = 15$ mm, $y_s = 15$ mm, $s_y = 0$ mm, $L_s = 2$ mm, $\varepsilon_r = 2.33$, $h = 1.57$ mm

Figure 5.20: Effect of slot width W_s on (a) input impedance and (b) return loss as a function of frequency

Effect of Increased x_s

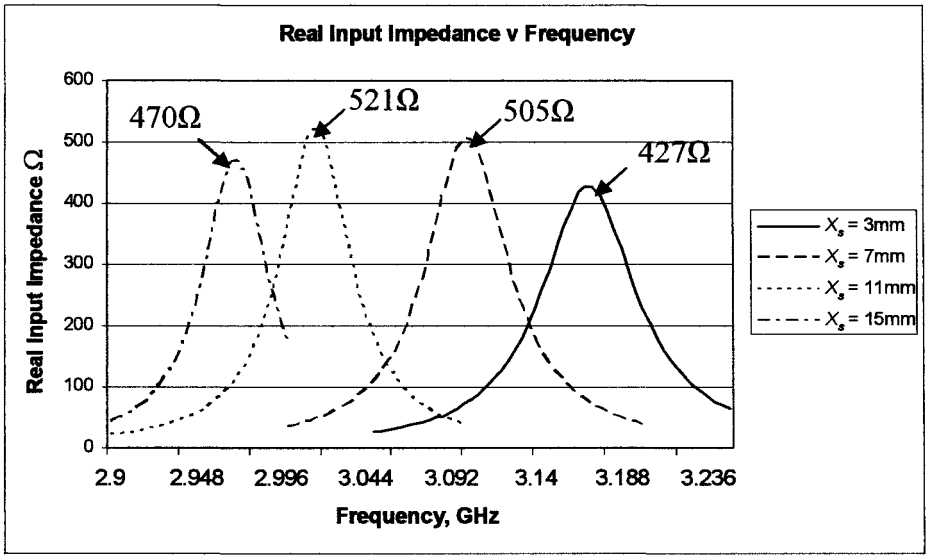

(a)

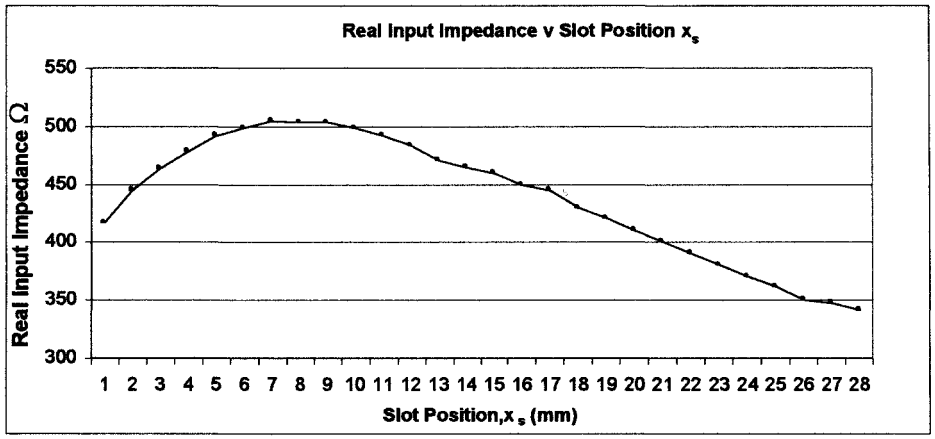

(b)

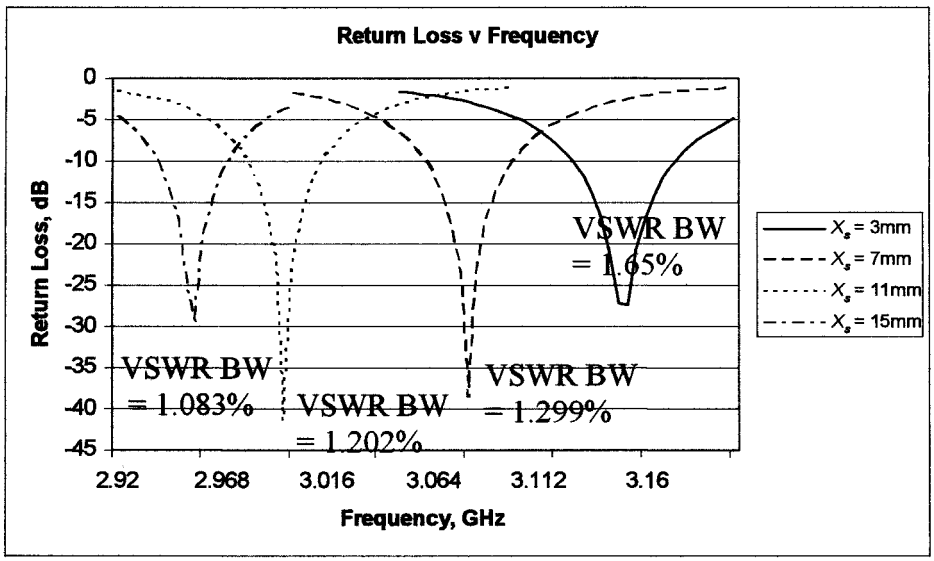

(c)

$L = W = 30$ mm, $y_s = 15$ mm, $s_y = 0$ mm, $W_s = 10$ mm, $L_s = 2$ mm, $\varepsilon_r = 2.33$, $h = 1.57$mm

Figure 5.21: Effect of slot position w.r.t. x axis, x_s on
(a) input impedance versus frequency
(b) input impedance versus x slot position (x_s)
(c) return loss as a function of frequency

Effect of Increased s_y

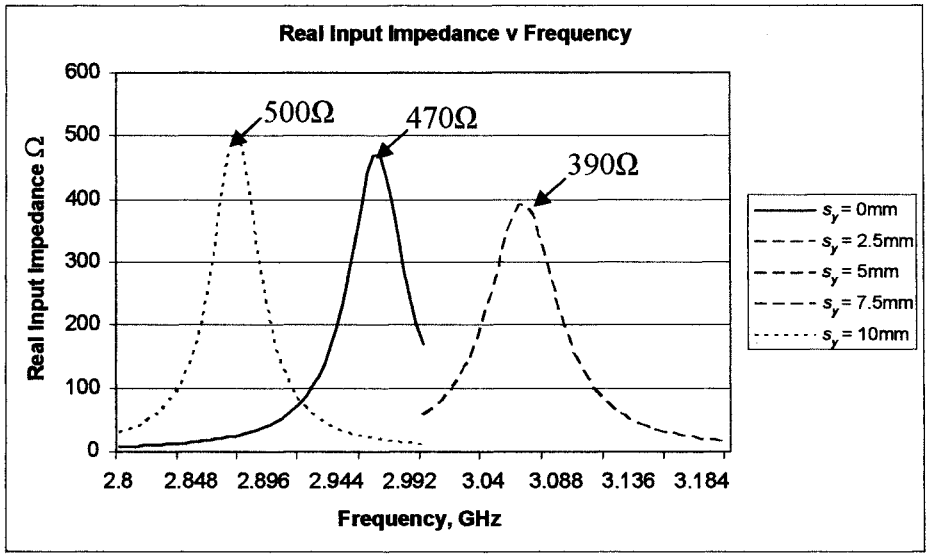

(a)

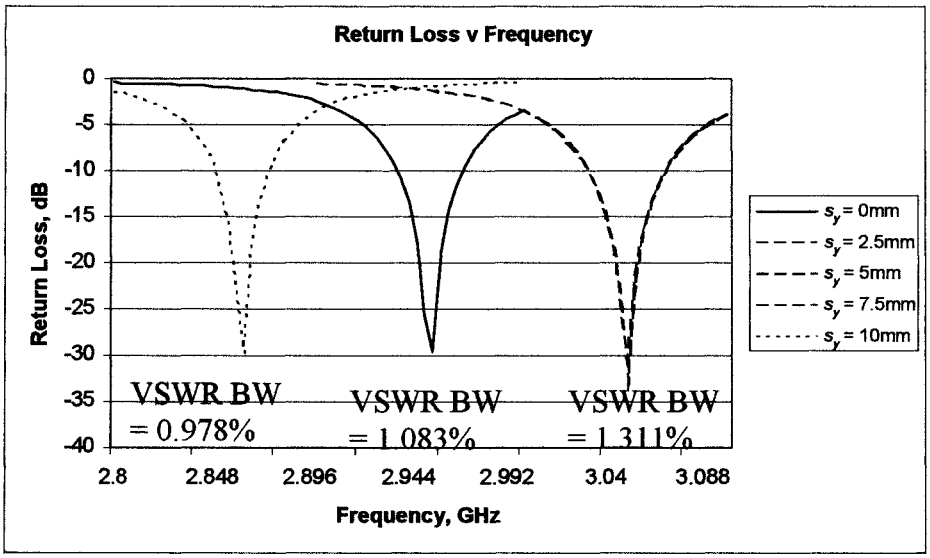

(b)

$L = W = 30$ mm, $x_s = 15$ mm, $W_s = 10$ mm, $L_s = 2$ mm, $\varepsilon_r = 2.33$, $h = 1.57$mm

Figure 5.22: Effect of slot separation along y axis, s_y on (a) Input impedance and (b) return loss as a function of frequency

From these figures, the following observations are essential for the future design of reduced size patch antennas:

- From figure 5.19a-b, by increasing slot length L_s, an input impedance of practical value can still be maintained, and only slight reduction in VSWR BW occurs. However, only a small reduction in resonant frequency is shown.

- From figure 5.20a-b, a significant reduction in resonant frequency can be achieved by increasing slot width W_s. However, a significant increase in input impedance occurs, causing problems regarding input impedance matching. A reduction in VSWR BW is also observed.

- From figure 5.21a-c, moving the slot towards the central x axis produces a reduction in resonant frequency, but at the expense of a reduced VSWR BW. From figure 5.21a-b, a maximum input impedance value occurs when the slot is placed close to the at a distance $x_s = L/4$ from the feedpoint. As the slot moves away from the patch edge the input impedance decreases with distance x_s. This is consistent with those results discussed previously in section 5.2.2.

- From figure 5.22, three distinct values of slot separation, sy, determine the patch performance.

  If $s_y = 0$:

  When the slots are placed next to each other, sy = 0mm, a certain value of resonant frequency, input impedance and VSWR BW is achieved.

  If $W + W_s/2 > s_y > 0$ mm:

  If the slots are separated ($s_y > 0$), a reduction in input impedance and increase in VSWR BW is achieved, at the expense of an increased

resonant frequency. The results for values of $s_y = 2.5$ mm, 5 mm and 7.5 mm, indicate that changing s_y within these limits has negligible effect on patch performance.

If $s_y = W + W_s/2$:

If the slots are separated by $W + W_s/2$, i.e. the slots are positioned at the non-radiating patch edge thus producing an H-shape structure, maximum reduction in resonant frequency occurs, but at the expense of increased input impedance and reduced VSWR BW.

The above examples clearly demonstrate that trade-offs exist between resonant frequency and VSWR BW. A trade-off between resonant frequency and input impedance also exists, however the relationship depends on the controlling slot parameter. If the slot area (L_s or W_s) or slot position with respect to the y axis is changed, a reduced resonant frequency produces an increased input impedance. However, if the slot position with respect to the x axis is changed a reduced resonant frequency does not automatically produce an increased input impedance.

5.3.2 Design Procedure

The patch designs outlined in section 5.2 clearly demonstrate the use of slot loading and associated trade-offs with such designs. All designs examined in section 5.2.3 are planar fed through the use of a traditional quarter-wave impedance matching network.

Using the knowledge obtained from this study, a new reduced size patch antenna based on the structure illustrated in figure 5.23 is presented and discussed, with particular reference to the associated design procedure. The new design presented in this section allows the use of a direct planar feed, thus removing the requirement for an external impedance matching network and hence further reducing overall

antenna size. Using this structure, a reduced size patch antenna with a operating frequency of 2.45 GHz and an input impedance of 50 Ω is subsequently presented and discussed.

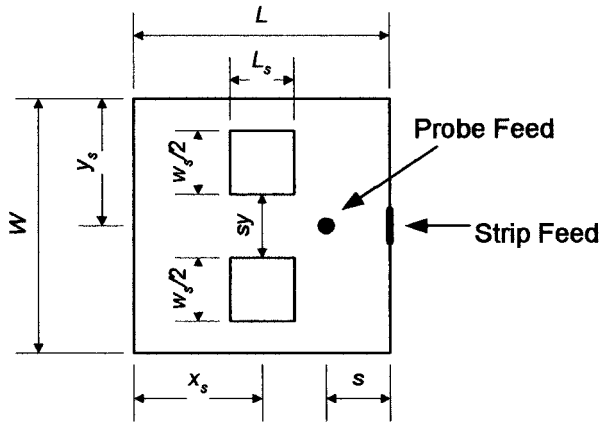

Figure 5.23: Patch configuration outline for optimisation of parameters

To achieve this, the goal is to produce maximum frequency and hence size reduction for a fixed patch size, whilst also maintaining an input impedance of 50 Ω to facilitate the use of a direct planar feed. The latter goal being achieved by the use of an inset feed. To independently achieve each goal the following actions could be taken.

To reduce the resonant frequency:

Increase x_s to $L/2$, Increase W_s to $W/2$, Increase s_y

To achieve impedance matching:

Reduce W_s, Reduce L_s, use probe or inset feed and increase s.

As can be seen, it is not possible to achieve both goals simultaneously. In this section, the effect of each parameter is examined in order to obtain the 'best' patch structure for the given application. The relevant equations used to generate each set of figures is shown directly below each graph.

1. Increase x_s

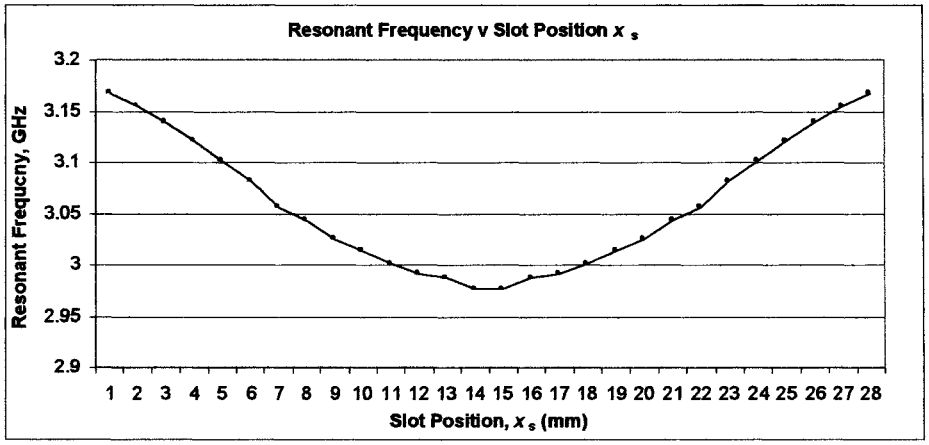

Equations (5.1) – (5.3)

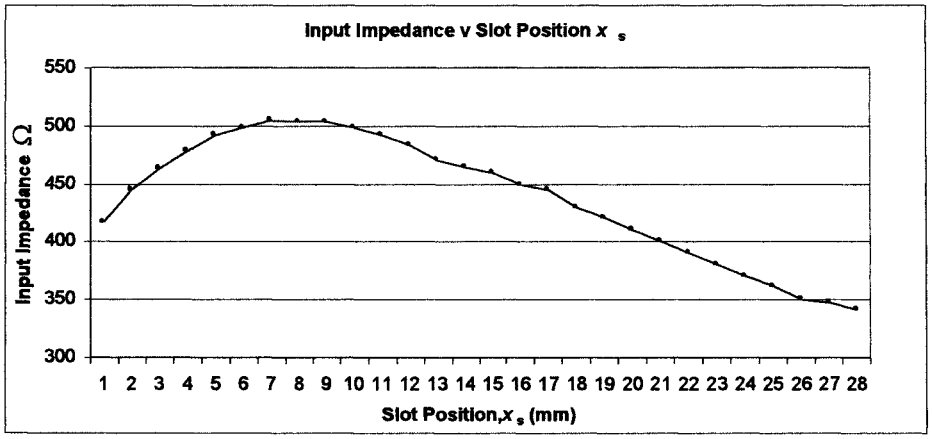

Equations (5.2) and (4.35)

$L = W = 30$ mm, $L_s = 1$ mm, $W_s = 10$ mm, $y_s = W/2$, $\varepsilon_r = 2.33$, $h = 1.57$mm

Figure 5.24: (a) Resonant frequency and (b) input impedance v slot position, x_s

From figure 5.24a, maximum reduction in resonant frequency is achieved when the slot is positioned along the central x axis of the patch.

Regarding the effect of the slot on the input impedance at the patch edge, from figure 5.24b, a maximum input impedance value occurs when the slot is placed at a distance $x_s = L/4$ from the feedpoint. As the slot moves away from the patch edge the input impedance decreases with distance x_s. It is also predicted that this trend occurs for the input impedance across the central x axis if a probe or inset feed is used.

These results are consistent with those described by figure 5.13a in section 5.2. This suggests that the optimum value of x_s in terms of resonant frequency and input impedance is $x_s = L/2$.

2. Increase s_y

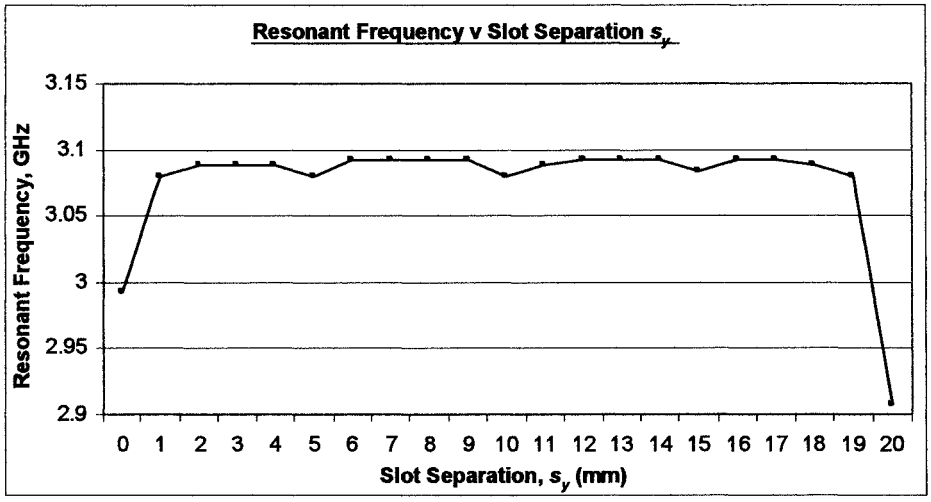

Equations (5.1) – (5.3)

$L = W = 30$ mm, $L_s = 1$ mm, $W_s = 10$ mm, $y_s = L/2$, $\varepsilon_r = 2.33$, $h = 1.57$mm

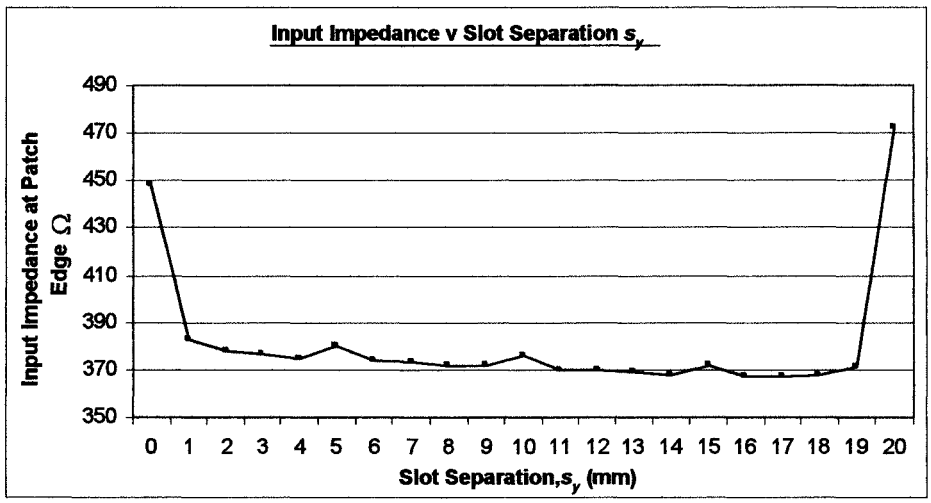

Equations (5.2) and (4.35)

$L = W = 30$ mm, $L_s = 1$ mm, $W_s = 10$ mm, $y_s = L/2$, $\varepsilon_r = 2.33$, $h = 1.57$mm

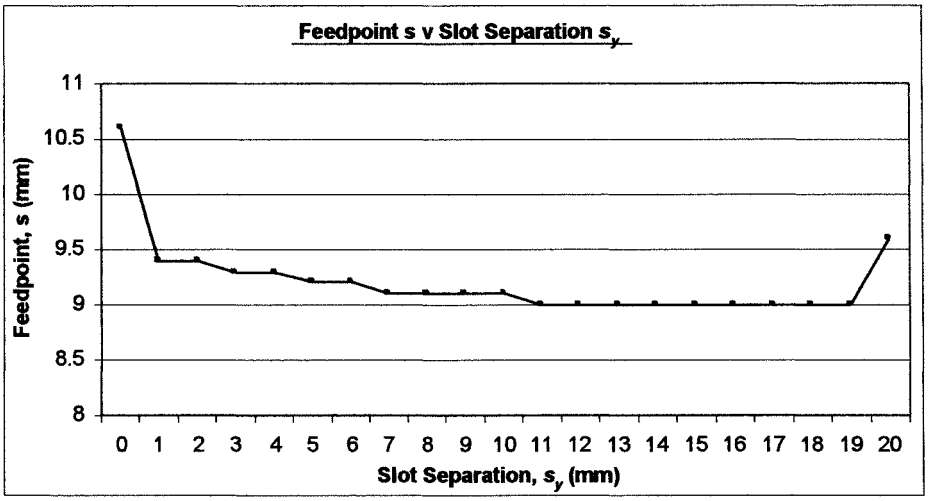

Equation (5.2)

$L = W = 30$ mm, $L_s = 1$ mm, $W_s = 10$ mm, $y_s = L/2$, $\varepsilon_r = 2.33$, $h = 1.57$mm

Figure 5.25: (a) Resonant frequency and (b) input impedance v slot position, s_y
(c) 50Ω feedpoint v slot separation, s_y

Figures 5.25a-c illustrates the effect of slot separation on the resonant frequency, input impedance at the patch edge and the 50 Ω feed position. From the above figures, as the slots are separated, whilst still inside the patch, the input impedance and feedpoint both decrease, but at the expense of an increased resonant frequency. Figure 5.25a illustrates that maximum size reduction can be achieved when the slots have maximum separation, i.e. are effectively placed at the non-radiating patch edge. However, a direct trade-off is an increased input impedance at the patch edge, which effectively limits the maximum size reduction when the patch is fed at the edge. Conversely, figure 5.25c, shows that the 50 Ω feedpoint for a probe excitation is not significantly affected by position of the slot in the y direction. This suggests greater size reduction can be achieved whilst still maintaining an input impedance of practical value if a probe or inset feed is used, as opposed to an edge-fed microstrip feed.

3. Decrease L_s

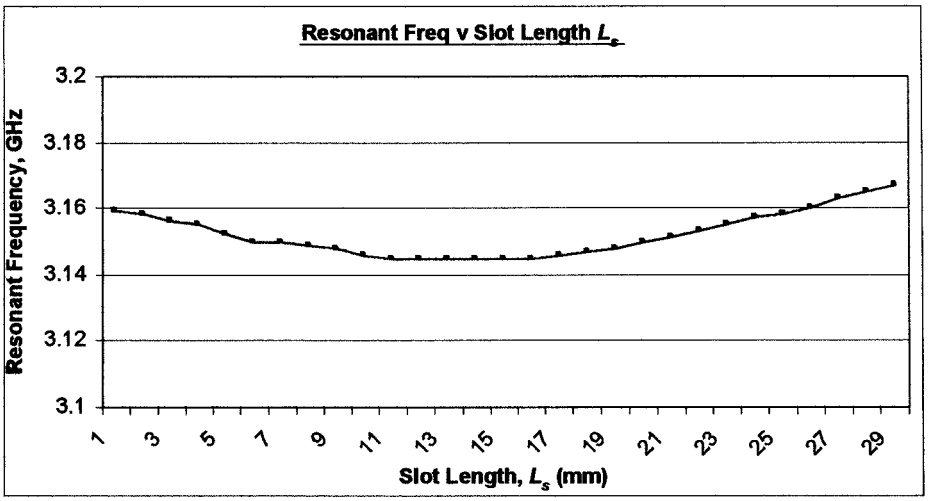

Equations (5.1) – (5.3)

$L = W = 30$ mm, $W_s = 10$ mm, $y_s = L/2$, $x_s = W/2$, $\varepsilon_r = 2.33$, $h = 1.57$mm

Figure 5.26: Resonant frequency v slot length, L_s

From figure 5.26, the effect of L_s on resonant frequency is negligible. The choice of L_s more concerned with impedance matching, with its value being determined by its effect on input impedance and feed position.

By choosing a large value of slot length, L_s, to excite this design with either a probe or inset feed, places a major constraint on practical size reduction. This is due to the fact that the probe feed position moves towards the patch centre with increasing slot size. A stage is reached where the feed position is inside the slot. By keeping L_s small the feed point can be moved closer to the patch centre without being inside the slot, without significantly effecting the resonant frequency.

4. Increase W_s

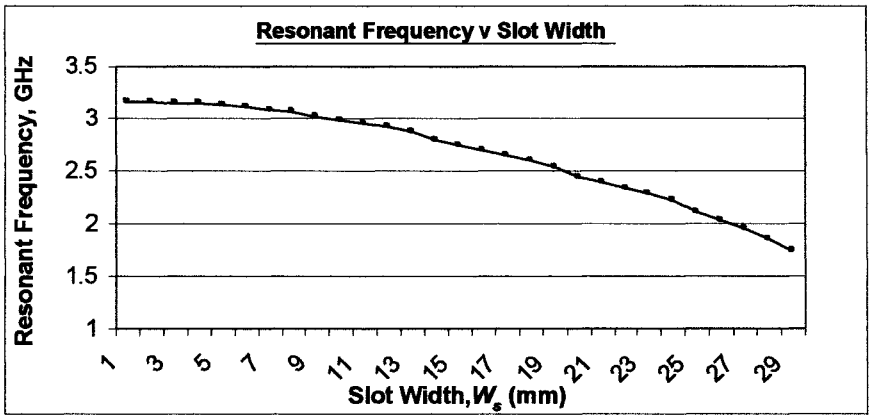

Equations (5.1) – (5.3)

$L = W = 30$ mm, $L_s = 1$ mm, $x_s = L/2$, $y_s = W/2$, $\varepsilon_r = 2.33$, $h = 1.57$mm

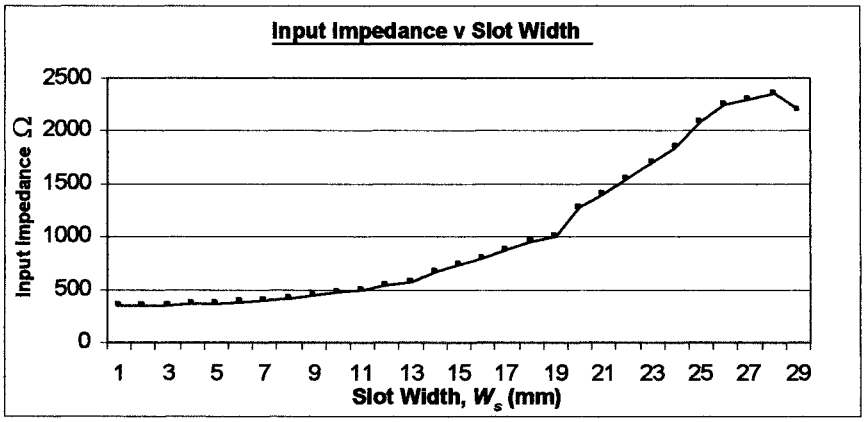

Equations (5.2) and (4.35)

$L = W = 30$ mm, $L_s = 1$ mm, $x_s = L/2$, $y_s = W/2$, $\varepsilon_r = 2.33$, $h = 1.57$mm

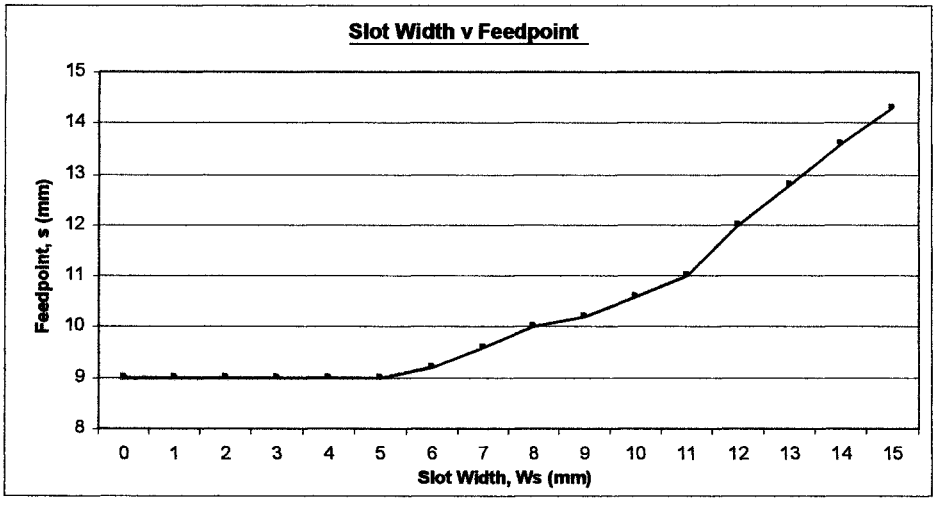

Equation (5.2)

$L = W = 30$ mm, $L_s = 1$ mm, $Y_f = W/2$, $\varepsilon_r = 2.33$, $h = 1.57$mm

Figure 5.27: (a) Slot width, W_s v resonant frequency
(b) slot width, W_s v input impedance at patch edge
(c): slot width, W_s v 50 Ω feedpoint

The graphs in figure 5.27a-c illustrate a direct trade-off between resonant frequency reduction and input impedance. Assuming all other values of slot parameters are fixed, increasing slot width, W_s produces a reduction in resonant frequency. However, the input impedance at both the patch edge and across all points along the central x axis increases. This has consequences for designs using both planar and probe feeds. For the case of edge fed planar feed design, the value of slot width is constrained by the maximum impedance value that can be practically matched due to the finite width of the impedance matching network. For the case of a probe feed, figure 5.27c illustrates that the 50 Ω feedpoint, s, increases with slot width until s is effectively inside the slot. This effectively places a constraint on the maximum size of slot width.

5.3.3 Optimum design

From the above results, a number of conclusions can be drawn on the size of the individual slot parameters to simultaneously achieve frequency reduction and impedance matching.

Firstly, a the value of slot length L_s should be kept to a minimum to achieve impedance matching by allowing the feed to move closer to patch centre without significantly affecting resonant frequency. Secondly, the slot/s should be positioned along the central x axis ($x_s = L/2$) to achieve maximum size reduction whilst also reducing the input impedance of the TM_{01} mode at all points across the $y = W/2$ axis. Finally, increasing the separation between slots across the y axis (s_y) so that the slots are placed at non-radiating patch edge greater frequency reduction can be achieved, whilst the feed position is closer to the patch edge, thus allowing more freedom to reduce the resonant frequency and still achieve impedance matching. The

optimum design therefore appears to be an H-shape structure symmetrical about the y axis, with thin slots, and excited by an inset feed, as shown in figure 5.28.

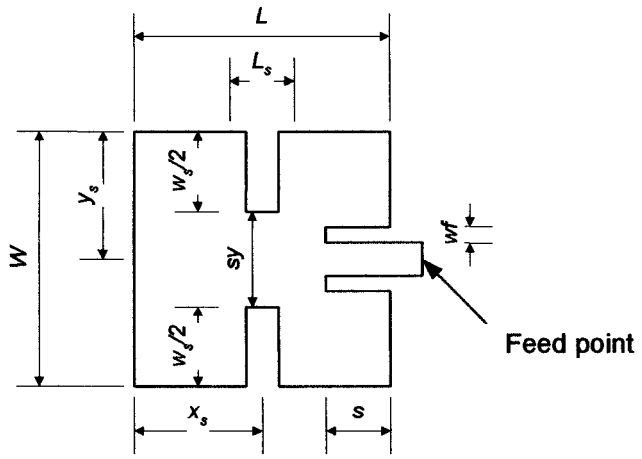

Figure 5.28: Optimised compact patch antenna design

5.3.4 Practical design and results

In view of the above results, in the subsequent design, the following values have been fixed:

$$L_s = 1 \text{ mm}, x_s = W/2, s_y = W + W_s/2$$

For ease of design the slot width W is equal to the slot length L.

The first stage in the design process was to determine the correlation between patch length L and slot length W_s, to achieve a target resonant frequency of 2.45 GHz. In all cases, the results were determined using an iterative application of the segmentation method outlined in Chapter 4. The slot length L_s was fixed at 1 mm, and the chosen duroid RT5870 has an ε_r of 2.33, with a substrate thickness of 1.57 mm. The results, seen in figure 5.29, suggest that a number of combinations of L and W_s can be used to produce a 2.45 GHz antenna, with a patch length L ranging from 20 mm to 38 mm.

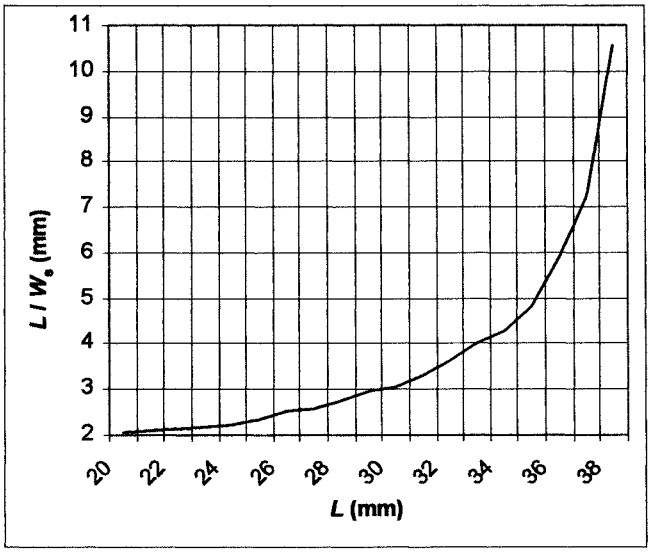

$L_s = 1$ mm, $x_s = L/2$, $y_s = W/2$, $\varepsilon_r = 2.33$, $h = 1.57$mm

Figure 5.29: Correlation between patch length and slot width for a 2.45 GHz patch

The next stage was to determine the inset feed position required to give an input impedance of 50 Ω at the desired frequency, whilst keeping the patch length to a minimum. To this end, a procedure similar to that described previously was carried out to determine the correlation between inset feed length, s, and input impedance for the different combinations of L and W_s. The results, shown in figure 5.30, illustrate the general relationship and indicate that a minimum patch length L of 30 mm is required to produce the desired input impedance.

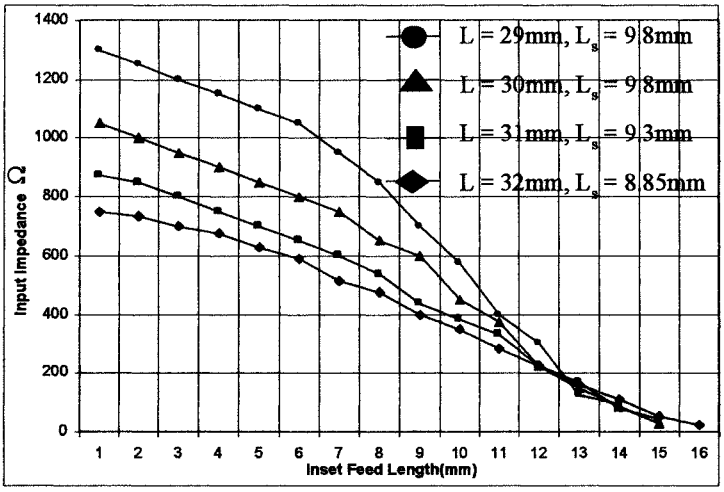

$x_s = L/2$, $y_s = W/2$, $\varepsilon_r = 2.33$, $h = 1.57$mm

Figure 5.30: Correlation between input impedance and inset feed length, s, at 2.45 GHz

Once L, W_s and s had been determined, slight retuning of W_s was required to account for the effect of the inset feed on the resonant frequency.

Using the above approach, a slot length L_s of 9.25 mm and inset feed length of 13.5 mm, with length L and width W each 30 mm, and a slot width W_s of 1 mm were shown to produce an antenna of minimum size with the required resonant frequency and input impedance.

Prototypes of the proposed design, together with a reference antenna were fabricated on RTDuroid 5870 with a permittivitty of 2.33 and a thickness of 1.57 mm. The proposed design, shown in figure 5.31a is excited using an inset feed, whilst the reference antenna, shown in figure 5.31b consisted of a square patch of $L = 39.4$ mm, fed by a quarter-wave matching network.

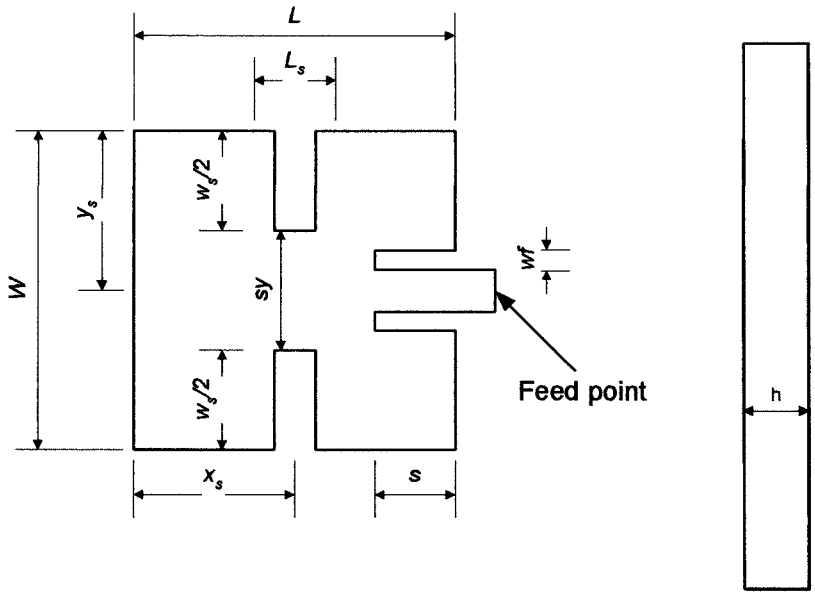

$L = 30$ mm, $W = 30$ mm, $x_s = 15$ mm, $y_s = 15$ mm, $s_y = 5.75$mm, $L_s = 1$mm, $W_s / 2 = 9.25$ mm, $s = 13.5$mm, $wf = 1.6945$ mm, $\varepsilon_r = 2.33$, $h = 1.57$mm

(a)

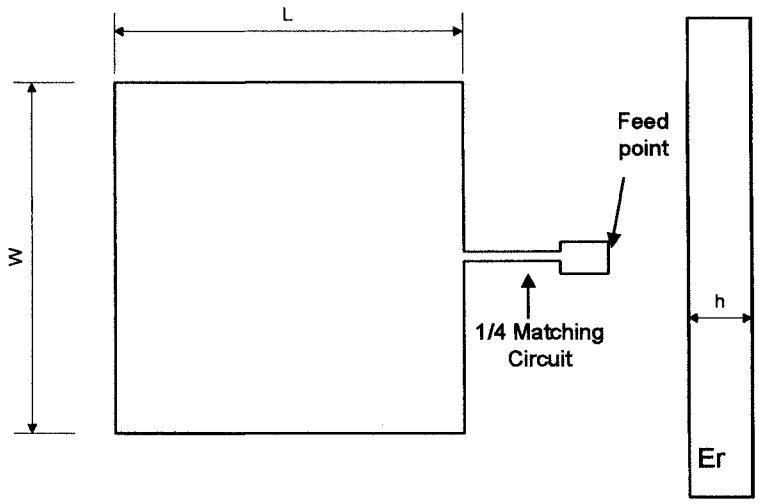

$L = W = 39.4$ mm, $\varepsilon_r = 2.33$, $h = 1.57$mm

(b)

Figure 5.31: Patch configurations for (a) proposed design and (b) reference antenna

Table 5.2 shows the practical results for proposed antenna designs, together with those of the reference antenna, which illustrate that size reduction of 55% has been achieved, at the expense other performance criteria. Considering the VSWR bandwidth, the results indicate that the reduced size designs suffers from a reduction when compared to a standard reference patch. The table also illustrates a reduced gain, which is attributed to the reduced patch volume.

	Proposed Design	**Reference Antenna**
Resonant Frequency, GHz	2.45	2.45
Size Reduction, %	55	0
Return Loss, dB	-23	-29
VSWR Bandwidth, %	1.22	1.904
Input Impedance, Ω	50	330
Measured Gain, dB	5.8	6.1
Patch Length *L* mm	30	39.4

Table 5.2: Practical results for inset fed compact patch designs

Plots of the radiation patterns, for proposed design are illustrated in Fig. 5.32.

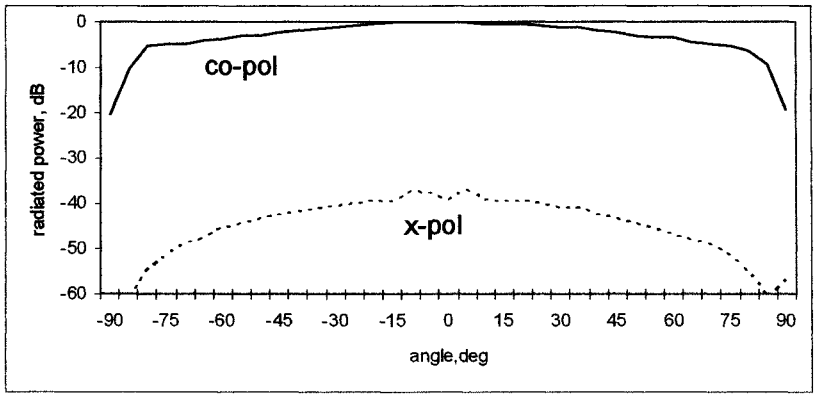

(a)

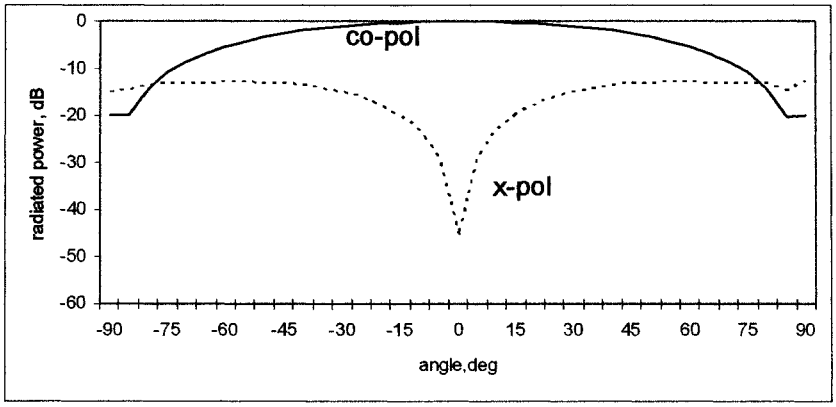

(b)

Figure 5.32: (a) E-plane and (b) H-plane radiation pattern for proposed design

Good broadside radiation is observed with a cross-polarisation level of below -20 dB in the E-plane, whilst a cross-polarisation level in the H-plane of below -10 dB is achieved.

5.4 Summary

Previous chapters have highlighted a lack of significant work on the trade-offs associated with compact slot loaded patch antennas, and moreover a lack of design technique. In this chapter, these knowledge gaps have been fully addressed. Initially a rigorous investigation of such a slot loaded design was performed in sections 5.2-5.3, which highlighted significant trade-offs in terms input impedance, Q factor and VSWR bandwidth. As the focus of this thesis in to design reduced size antennas

that are planar fed, the major trade-offs is the one that exists between reduced resonant frequency and increased input impedance. To overcome this, a design procedure was outlined in section 5.4 which was used to optimise a new structure for the desired resonant frequency reduction and input impedance. Using this technique, a patch antenna with a size reduction of 55% can be achieved which allows the use of a direct planar feed. This removes the need for a traditional $\lambda / 4$ matching network, thus further reducing the total element size.

CHAPTER 6

COMPACT CIRCULAR POLARISED PLANAR FED DESIGNS

6.1 Introduction

A number of techniques for modifying the frequency response of a patch antenna have been examined. It was determined that the most promising method of producing compact operation of a patch antenna was through the use of slot loading. Given that work in this field was largely empirical, a thorough investigation of the slot loading technique and its effect on both circuit characteristics was performed in Chapter 5. It was successfully demonstrated that with correct perturbation and excitation of the TM_{01} mode, compact linear polarised operation of a patch antenna can be designed.

The focus of the following chapter involve the design of planar fed reduced size patch designs with circular polarisation. One method of achieving this is through correct perturbation and excitation of the TM_{01} and TM_{10} modes. At present, the majority of work on compact slot loaded CP designs use a probe or aperture feed to excite the antenna, with little work existing on the use of a microstrip feed. The reason for this could be attributed to the relationship between slot loading and input impedance. It was determined in Chapter 5 that a trade-off of slot loaded designs is an increase in input impedance at the patch edge, thus causing problems regarding planar impedance matching.

Traditional methods of producing single-fed CP patch antennas include truncated corners, nearly square patch, and the cutting of a diagonal slot in the centre of a square patch [151]. In recent years, the use of slot loading has been used to reduce the size of the antenna element. To produce compact CP operation this technique

has been mainly applied to patch antennas with truncated corners [66-69] or square patch with unequal length slots [70] or tuning stubs [71]. The designs presented in this chapter are based upon a nearly square patch shape.

For efficient reduced size linear polarised planar fed design, the goals must be to achieve maximum frequency reduction whilst simultaneously achieving input impedance matching and maintaining a relatively wide impedance bandwidth. The design of a reduced size circular polarised patch antenna using a single feed is a more challenging problem. In addition to those mentioned above, further goals are to minimise the axial ratio, whilst simultaneously maximising the axial ratio bandwidth.

After this brief introduction, section 6.2 investigates a corner fed nearly square patch with square slot loading in order to produce a benchmark for subsequent designs. From this, any associated trade-offs arising from such designs can be determined. In section 6.3, a novel design for a reduced size nearly square patch is proposed. It is subsequently shown that the use of this arrangement reduces input impedance, whilst also increasing the axial ratio bandwidth. The design also benefits from improved manufacturing tolerances. In section 6.4, an alternate novel structure, based on the incorporation of triangular slot loading, is presented which offers a further improvement in CP performance. Section 6.5 summarises the main contributions from this chapter.

6.2 Corner fed Nearly Square CP patch with square slot loading

In Chapter 5, a detailed investigation of slot loading techniques to produce compact linear polarised patch antennas was carried out. It was highlighted that significant trade-offs from these designs include increased input impedance and Q factor. As the focus of this section is to develop compact circular polarised designs, the effect

of slot loading on axial ratio bandwidth and manufacturing tolerances must also be considered.

It was identified in Chapter 3 that all compact slot loaded designs evolved from regular shapes with square slot loading. To this end, an obvious starting point for producing compact CP designs is to embed a square slot in a nearly square patch, as shown in figure 6.1. The performance of this structure will provide a reference for subsequent designs in this chapter. The patch is designed for use on RTDuroid 5870. The relevant data for this substrate is shown in Appendix A.

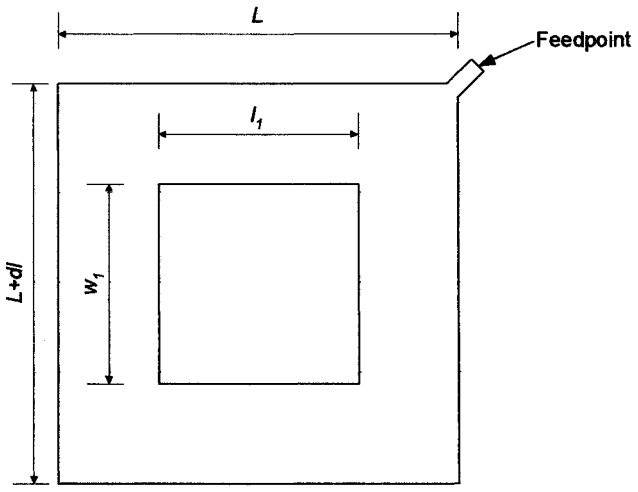

Figure 6.1: Corner fed square-slot loaded nearly square CP patch antenna

The nearly square microstrip patch has side lengths L and $L+dl$ and is printed on a substrate of thickness h and relative permittivity ε_r. The square-shape slot has equal dimensions l_1 and w_1. By increasing the slot size, l_1 and w_1, the current path of the fundamental TM_{01} and TM_{10} modes are lengthened, with l_1 largely controlling the TM_{01} mode current path and w_1 controlling the TM_{10} mode current path. The antenna is excited by a traditional quarter-wave planar matching network at the patch corner.

6.2.1 Patch design

To design a corner fed nearly square patch antenna a number of performance parameters must be determined. These include: axial ratio, axial ratio bandwidth,

resonant frequency, input impedance and Q factor. These parameters are controlled by the patch dimensions L, dl, L_s, W_s and feedpoint. To illustrate the design procedure, the following example is applied to a conventional corner fed nearly square patch with square slot loading, as shown in figure 6.1. To generate these results, the associated parameters with their fixed values are shown in table 6.1. The patch is designed for use on RTDuroid 5870. The relevant data for this substrate is shown in Appendix A.

6.2.1.1 Axial ratio and perturbation segment, *dl*

Assuming the slot is square, the axial ratio of the patch is controlled by the size of perturbation segment, *dl*. For efficient operation, an axial ratio of below 3 dB is required. To achieve this, plots of input impedance against frequency of the two fundamental modes are required. This has been determined by modifying the segmentation model approach described in section 4.6, to account for the ports positioned as shown in figure 6.2.

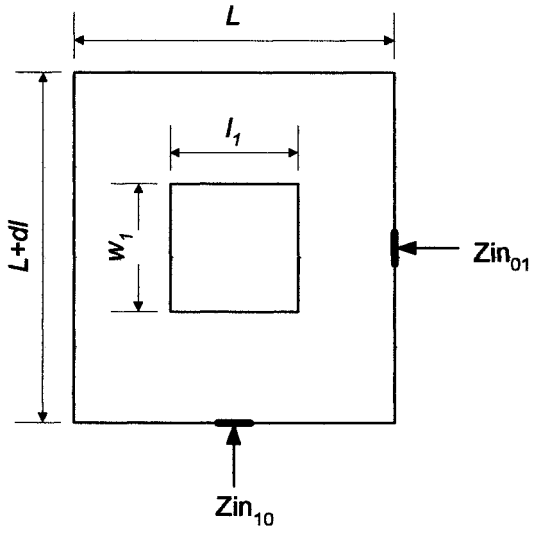

Figure 6.2: Port positions for determination of input impedance of fundamental modes

From empirical data, minimum axial ratio is achieved when the following conditions apply at a given frequency:

$$\frac{Zin_{01}\,\max}{2} = \frac{Zin_{10}\,\max}{2} \qquad (6.1)$$

where Z_{in01}max and Z_{in10}max represent the real input impedance at resonance of both fundamental TM_{mn} modes.

To achieve a good axial ratio, dl is increased until the above condition is met. The results are shown in figures 6.3a-c, with the corresponding graph of axial ratio versus frequency, determined using full-wave modelling software Ensemble [92] also displayed.

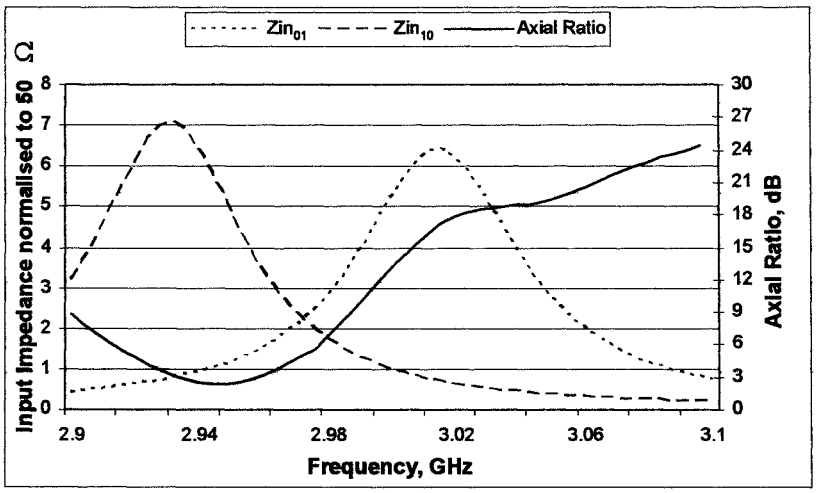

(a) $dl = 0.2$ mm

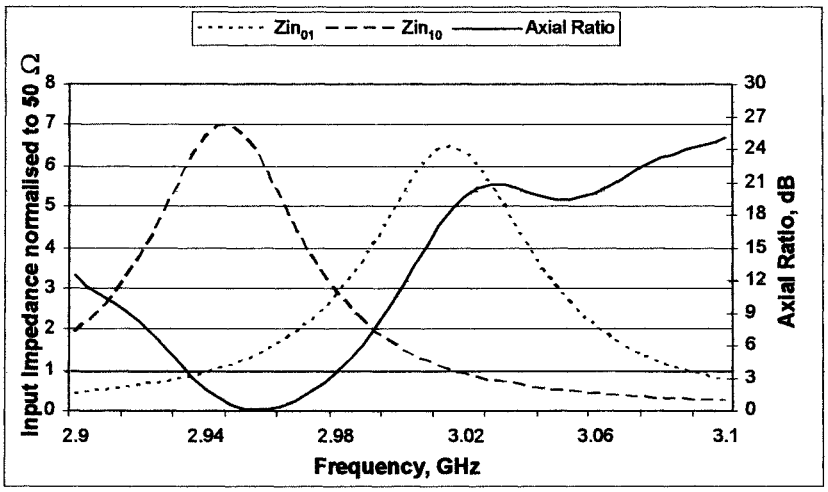

(b) $dl = 0.61$ mm

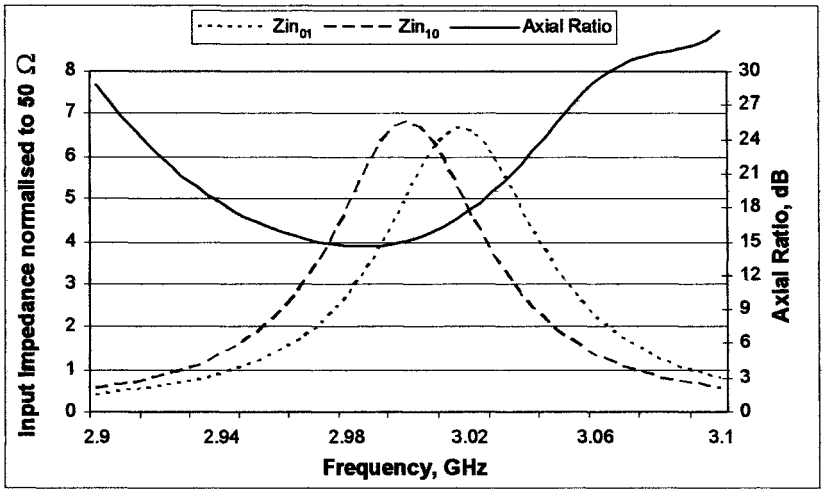

(c) $dl = 1$ mm

$\varepsilon_r = 2.33$, $h = 1.57$ mm, $L = 31.59$ mm, $l_1 = w_1 = 8$ mm

Figure 6.3(a-c): Normalised real input impedance of fundamental modes and axial ratio versus frequency for increasing perturbation size

The graph in figure 6.3b, illustrates that minimum axial ratio is achieved when Z_{in01} and Z_{in10} overlap at the 3 dB point at the desired frequency. This confirms that this approach offers a good approximation of the required perturbation length to achieve a good axial ratio.

6.2.1.2 Resonant frequency and input impedance

To determine the resonant frequency, input impedance and Q factor, graphs of real and imaginary input impedance against frequency are required. These have been determined using the segmentation model developed in section 4.6, with the feedpoint placed at the corner (as in figure 6.1), with the results shown in figure 6.4.

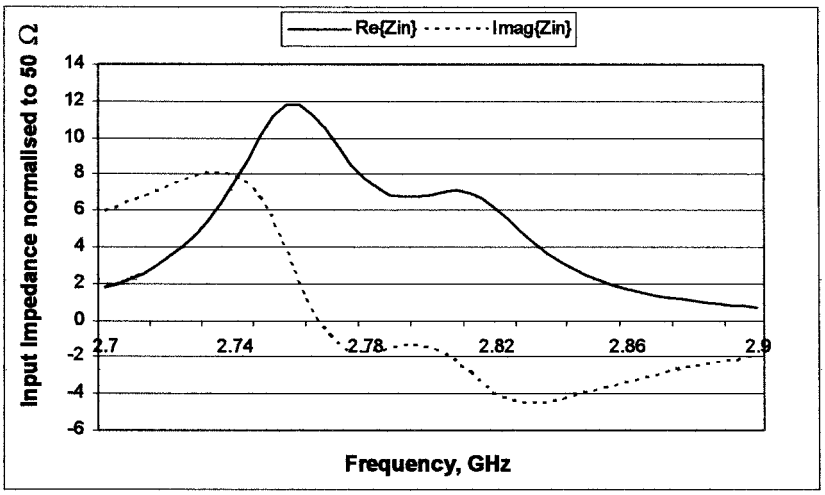

$\varepsilon_r = 2.33$, $h = 1.57$ mm, $L = 31.59$ mm, $dl = 0.71$ mm, $l_1 = w_1 = 8$ mm

Figure 6.4: Normalised real and imaginary input impedance of patch design

From the above graphs, the resonant frequency, input impedance and Q factor can be determined using the same procedure outlined in section 4.4.

6.2.2 Results and analysis

Several antennas with different slot sizes have been simulated, based on RTDuriod 5870 with permittivity of 2.33 and thickness 1.57 mm, with the corresponding CP performance shown in table 6.2.

$l_1 (= w_1)$ (mm)	dl (mm)	Frequency (GHz)	Input Impedance (Ω)	CP BW (3dB AR) (%)
0	0.71	2.95	310	1.2
4	0.71	2.925	330	0.92
8	0.61	2.805	400	0.7
12	0.41	2.639	750	0.59
16	0.21	2.396	1200	0.49

$\varepsilon_r = 2.33$, $h = 1.57$ mm, $L = 31.59$ mm

Table 6.1: Theoretical CP performance of corner fed square-slot loaded nearly square CP patch antenna

Although a significant frequency and hence size reduction is shown, it has been achieved at the expense of a number of other parameters. Primarily, as the slot size increases, the perturbation size reduces considerably. For the case of a standard CP patch without slot loading, the required perturbation size for the given design is 0.71 mm, which suggests strict manufacturing tolerances. For slot dimensions of l_1 = w_1 = 16 mm, the perturbation length, *dl* reduces to 0.21 mm, thus producing stricter tolerances. A further trade-off from the above design is a significant decrease in axial ratio bandwidth with slot size. For a slot size of $l_1 = w_1 = 16$ mm, a axial ratio bandwidth of 0.49% is achieved, compared with 1.2% for a standard unslotted design.

Considering the input impedance, the table illustrates a significant increase with slot size. For a slot size of $l_1 = w_1 = 16$ mm, an input impedance of 1200 Ω is produced at the feed-point. For such a high impedance value, the finite width of the required impedance matching network makes this design impossible to realise practically. This suggests that only limited size reduction can be achieved using the design presented in this section. This trend is consistent with those described for a linear polarised planar fed design, discussed in Chapter 5.

6.3 Offset Fed Nearly Square CP patch with star–shape slot loading (Design 1)

In the previous section, a typical reduced size nearly square patch with square-shaped slot loading was investigated, in which a number of trade-offs were found to exist. These included an increased input impedance, narrow axial ratio bandwidth and strict manufacturing tolerances. In this section a novel patch structure is presented. It is found that through the use of embedded star shaped slot loading and an offset planar feed, size reduction of up to 38% can be achieved with no significant

reduction in axial ratio bandwidth. It is also found that this design has relaxed manufacturing tolerances and lower input impedance.

The proposed compact CP patch design with star shaped loading and an offset feed is illustrated in figure 6.5. To generate these results, the associated parameters with their fixed values are shown in table 6.3. The patch is designed for use on RTDuroid 5870. The relevant data for this substrate is shown in Appendix A.

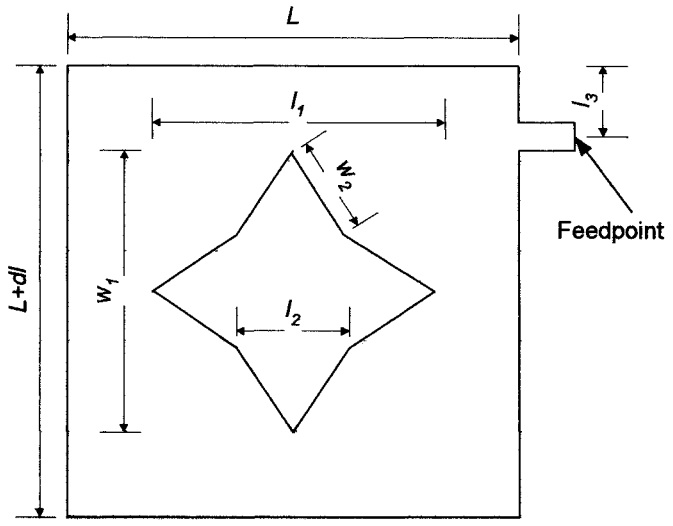

Figure 6.5: Proposed offset fed star-shaped loaded CP patch antenna design

It consists of a nearly square microstrip patch with side lengths L and $L+dl$ and is printed on a substrate of thickness h and relative permittivity ε_r. The star-shaped slot has equal dimensions l_2 and w_2. The patch antenna is excited by a traditional quarter-wave planar matching circuit, at a distance l_3 from the patch corner. By increasing the slot size, l_1 and w_1, the current path of the fundamental TM_{01} and TM_{10} modes are lengthened, with l_1 largely controlling the TM_{01} mode current path and w_1 controlling the TM_{10} current path. This results in a lowering of the patch operating frequency, which accounts for the size reduction. It is clear that both the star-shaped slot and offset feed both effect patch performance. To this end, in the following sections the effect of these two design features are investigated both independently and simultaneously.

6.3.1 Effect of Star-shaped slot loading on corner fed nearly square CP patch

The effect of the star-shaped slot has been determined by comparing the performance of a corner fed nearly square patch with Star-shaped with that of the corner fed nearly square patch with Square-shaped slot loading described in section 6.2. Both designs are shown in figures 6.6a and 6.6b respectively.

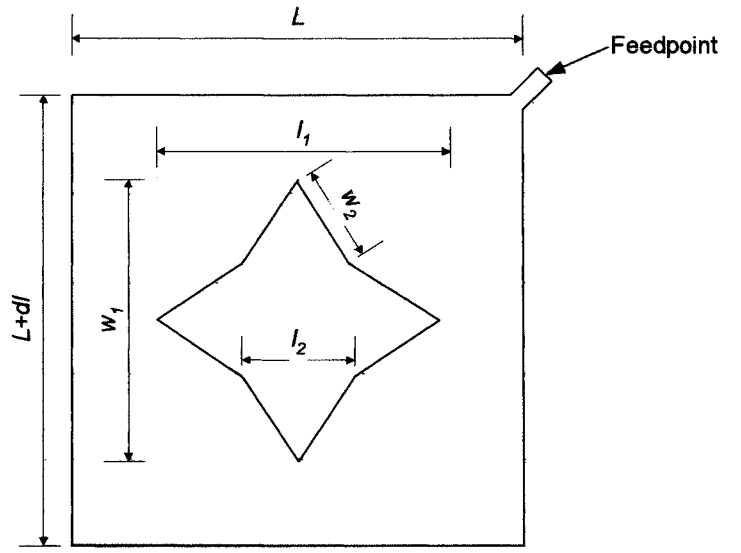

(a)

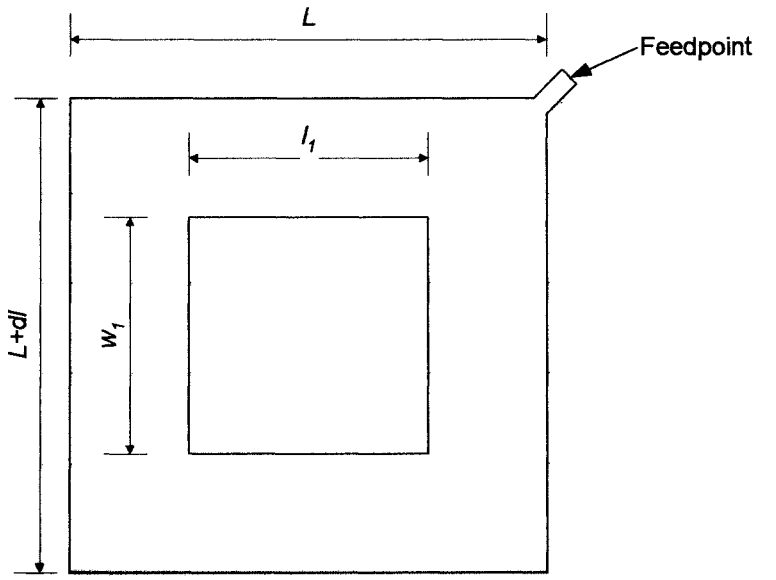

(b)

Figure 6.6: Corner fed CP patch designs with (a) star-shaped slot loading and (b) square-shaped slot loading

6.3.1.1 Patch modelling procedure

To design the structure in figure 6.6a, the segmentation approach developed in Chapter 4 is applied. This involves decomposing the structure into regular segments then synthesising each one to obtain the original structure. Using this approach, the input impedance and Q factor can be determined. To determine the required perturbation size, dl, the approach described in section 6.2 is applied.

Patch Decomposition Procedure:

To model the patch, the patch must first be decomposed into regular segments. The patch is firstly into four elemental segments, as illustrated in figure 6.7b. Decomposing the patch in this manner takes advantage of its symmetrical structure in both x and y directions. This gives four elements of equal shape and dimensions, thus reducing the number of required computations. As each elemental segment in figure 6.7b is irregular, each segment must be further decomposed into five further segments for which Green's functions are available, as illustrated in figure 6.7c.

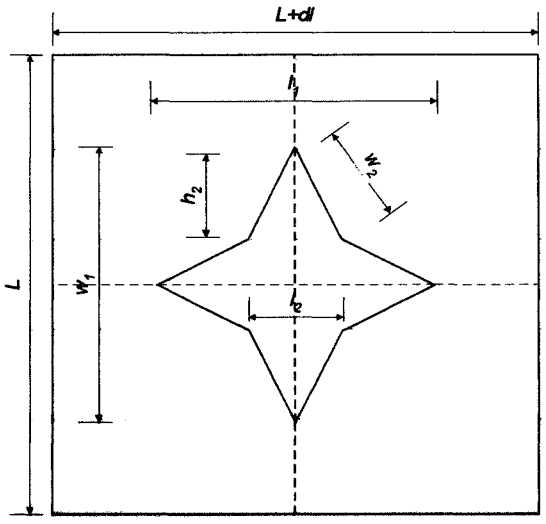

(a)

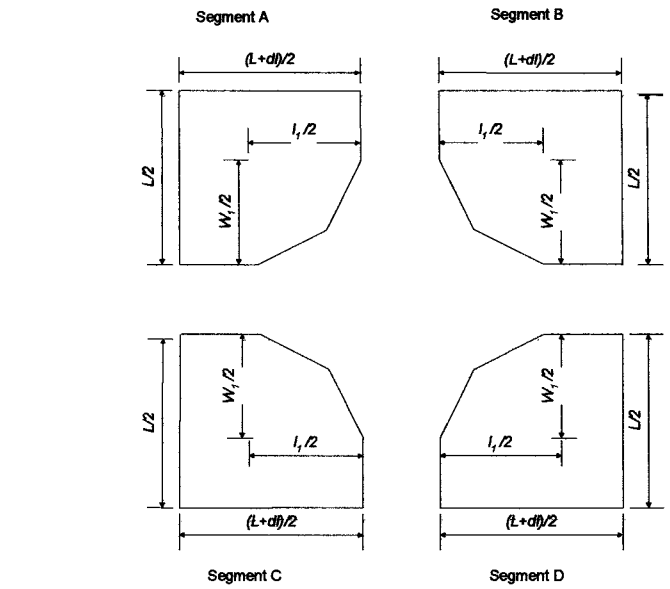

(b)

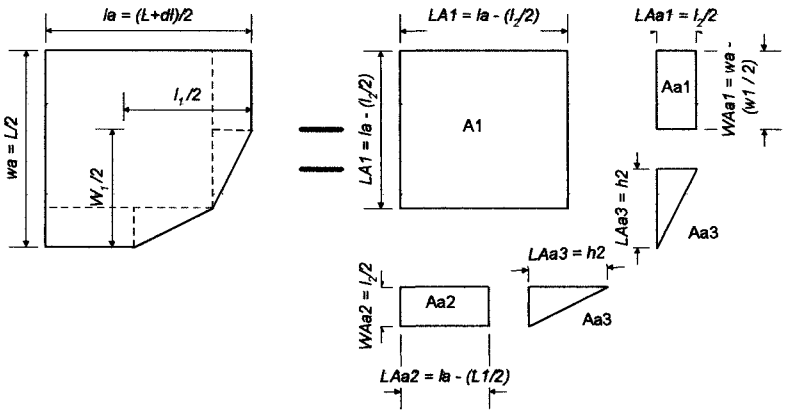

(c)

Figure 6.7: Decomposition of patch structure
(a) patch structure
(b) patch decomposed into 4 equal segments
(c) decomposition of individual segment into regular shaped segments

Patch Synthesis Procedure:

To synthesise the patch, a five-step procedure has been developed. An overview of this approach is illustrated in figure 6.8a-e, whilst a more detailed explanation follows.

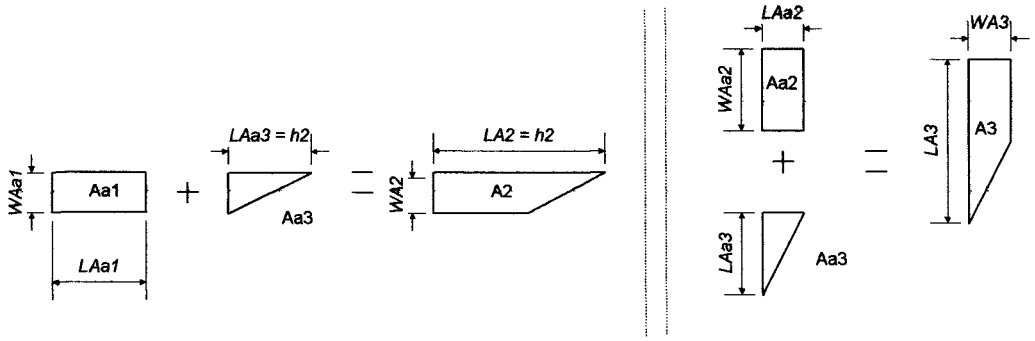

(i) (ii)

(a) Step 1

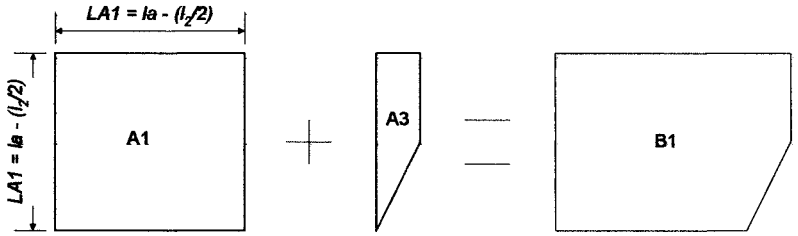

(b) Step 2:

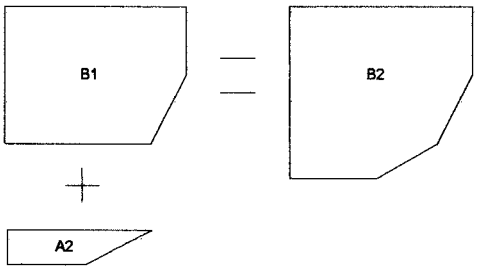

(c) Step 3

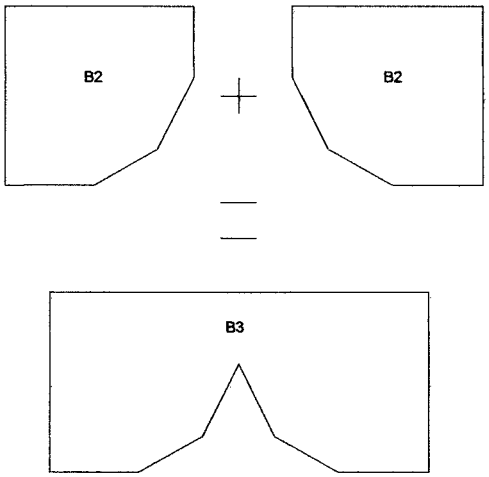

(d) Step 4

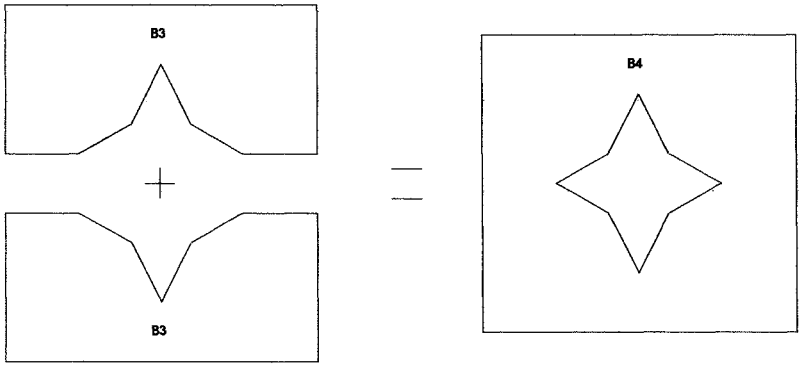

(e) Step 5

Figure 6.8: Synthesis process

Step 1:

Part (i): Determination of A2 segment by synthesis of Aa1 and Aa3 segments:

With reference to figure 6.9a, the impedance matrices of segment A2 is determined by synthesising segments Aa1 and Aa3.

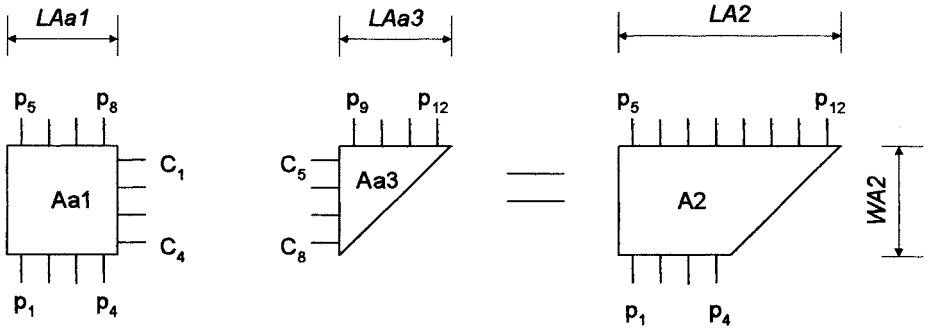

Figure 6.9: Ports of Aa1, Aa3 and A2 segments

Figure 6.9 illustrates the port labelling of the Aa1, Aa3 and A2 segments. The C-ports represent the connected ports of segments Aa1 and Aa3 and are arranged such that ports C_1 of the Aa1 segment is connected to ports C_5 of the Aa3 segment, C_2 is connected to C_6, etc... The P ports represent the unconnected ports of each segment.

The interaction between ports was defined in (4.30) as:

$$Z_{ij} = \frac{V_i}{I_j}\Big|_{I_i=0} = \frac{1}{W_i W_j}\int\int_{WiWj} G(x,y;x_0,y_0)dW_i dW_j = Z_{ji} \qquad (6.2)$$

G is the associated 2D Green's function for the shape, which for a square is as defined in Chapter 4. The Green's function for a triangle is given by [153]:

$$G(x,y;x_0,y_0)=\frac{j\omega\mu d}{2}\sum_{m=0}^{\infty}\sum_{n=0}^{\infty}\frac{\sigma_m\sigma_n T(x_0,y_0)T(x,y)}{(m^2+n^2)\pi^2-a^2k^2} \tag{6.3}$$

where,

$$T=\cos\left(\frac{m\pi x}{a}\right)\cos\left(\frac{n\pi y}{a}\right)-1^{m+n}\cos\left(\frac{n\pi x}{a}\right)\cos\left(\frac{m\pi y}{a}\right) \tag{6.4}$$

The impedance matrix of the A2 segment is determined by synthesising Aa1 and Aa3 segments. From (4.49) this is given by:

$$A2Z_p=A2Z_{pp}-A2Z_{pc}\begin{bmatrix}A2\Gamma_1 A2Z_{cc}\\ A2\Gamma_2\end{bmatrix}^{-1}\begin{bmatrix}A2\Gamma_1 A2Z_{cp}\\ A20\end{bmatrix} \tag{6.5}$$

where:

$A2Z_{pp}$ represents the interaction between P ports on segments Aa1 and Aa3

$A2Z_{cp}$ represents the interaction between C and P ports

$A2Z_{pc}$ represents the interaction between P and C ports

$A2Z_{cc}$ represents the interaction between C ports

Part (ii): Determination of A3 segment by synthesis of Aa2 and Aa3 segments:

To determine the impedance matrices of the A3, segments Aa2 and Aa3 are synthesised, as illustrated in figure 6.10. A similar procedure to that described in part (i) is then followed.

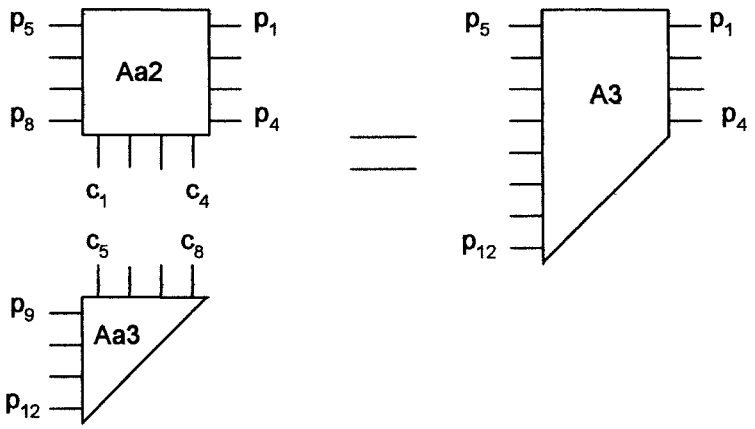

Figure 6.10: Ports of Aa2, Aa3 and A3 segments

The impedance matrix of the A3 segment is determined by synthesising Aa2 and Aa3 segments. From (4.49) this is given by:

$$A3Z_p = A3Z_{pp} - A3Z_{pc}\begin{bmatrix} A3\Gamma_1 A3Z_{cc} \\ A3\Gamma_2 \end{bmatrix}^{-1}\begin{bmatrix} A3\Gamma_1 A3Z_{cp} \\ A30 \end{bmatrix} \qquad (6.6)$$

where:

$A3Z_{pp}$ represents the interaction between P ports on segments Aa1 and Aa3

$A3Z_{cp}$ represents the interaction between C and P ports

$A3Z_{pc}$ represents the interaction between P and C ports

$A3Z_{cc}$ represents the interaction between C ports

Step 2: Determination of B1 segment by synthesis of A1 and A3 segments:

To synthesise segments A1 and A3 requires that ports P_5 - P_{12} on segment A3 be renamed as ports C_9 - C_{16}, as illustrated in figure 6.11a-b.

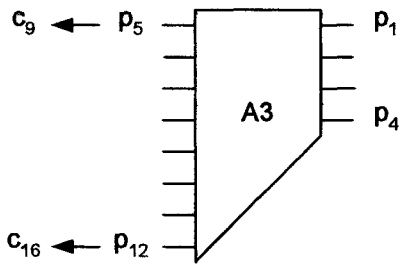

(a)

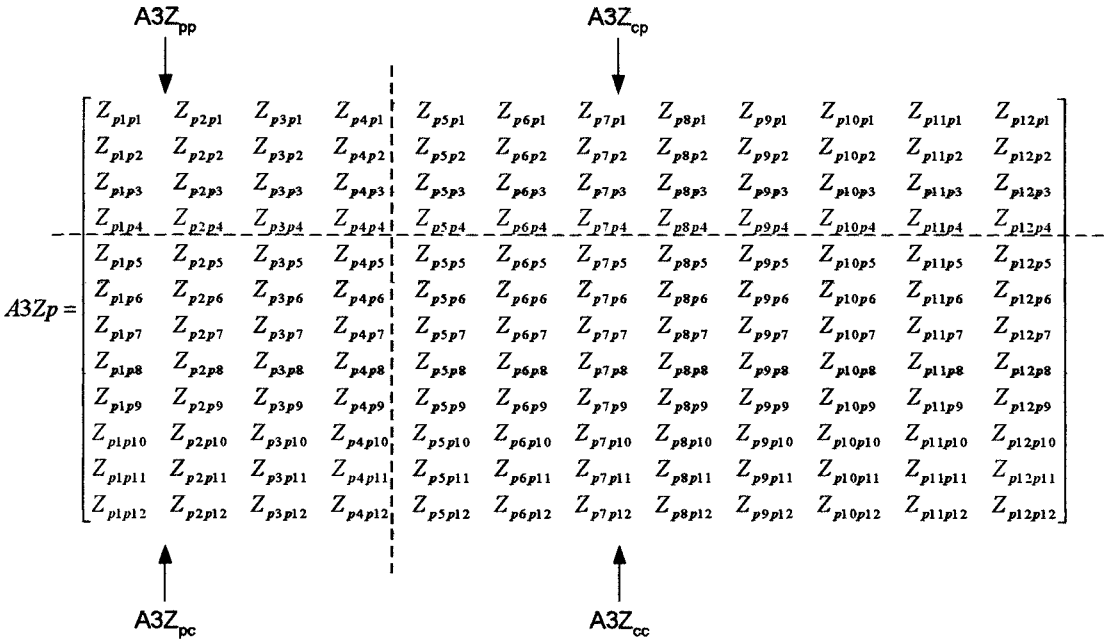

(b)

Figure 6.11: (a) Conversion of P ports to C ports on A3 segments
(b) with relevant impedance matrix

Figure 6.12 illustrates the port labelling of the A1 and A3 segments. Note that port p_{13} is used to determine the input impedance at the feedpoint.

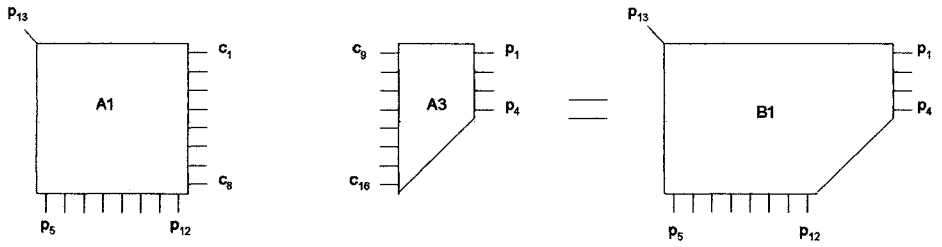

Figure 6.12: Ports of A1 and A3 segments

The impedance matrix of the B1 segment is determined by synthesising A1 and A3 segments. From (4.49) this is given by:

$$B1Z_p = B1Z_{pp} - B1Z_{pc}\begin{bmatrix} B1\Gamma_1 B1Z_{cc} \\ B1\Gamma_2 \end{bmatrix}^{-1}\begin{bmatrix} B1\Gamma_1 B1Z_{cp} \\ B10 \end{bmatrix} \qquad (6.7)$$

where:

$B1Z_{pp}$ represents the interaction between P ports on segments A1 and A3

$B1Z_{cp}$ represents the interaction between C and P ports

$B1Z_{pc}$ represents the interaction between P and C ports

$B1Z_{cc}$ represents the interaction between C ports

Step 3: Determination of B2 segment by synthesis of B1 and A2 segments:

To synthesise segments B1 and A2 requires that port P_{13} on B1 segment be renamed port P_5, ports P_5 - P_{12} on segment B1 be renamed as ports C_1 - C_8, as illustrated in figure 6.13a-b.

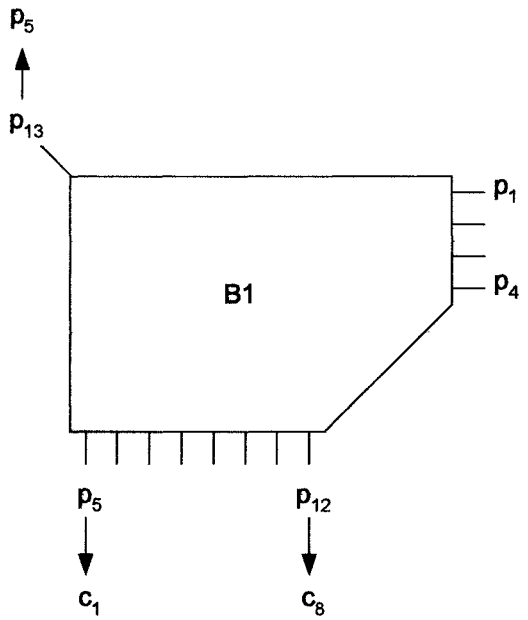

(a)

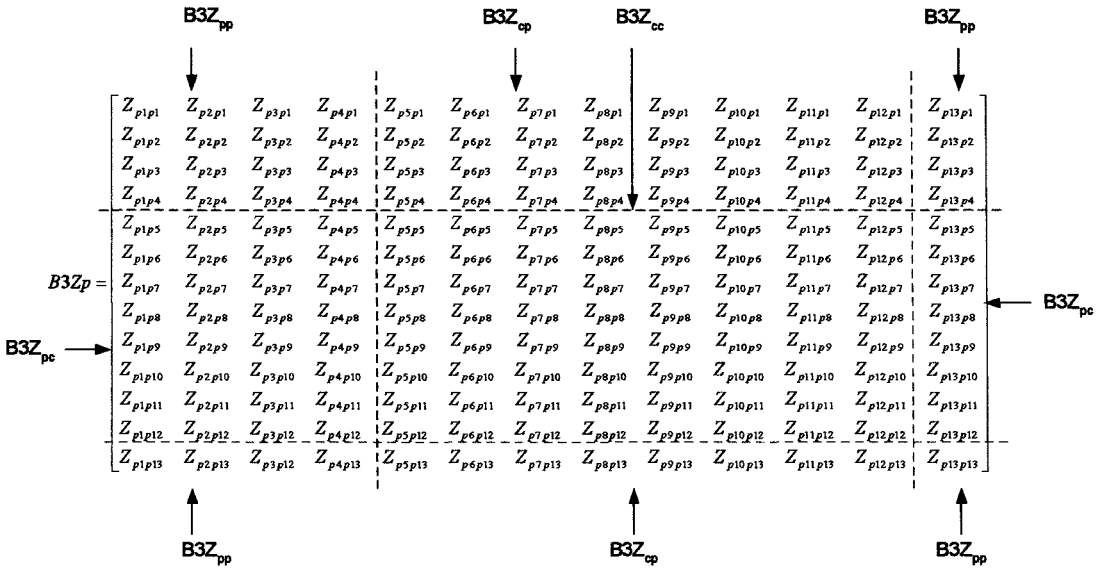

$$B3Z_{pp} = \begin{bmatrix} Z_{p1p1} & Z_{p2p1} & Z_{p3p1} & Z_{p4p1} & Z_{p13p1} \\ Z_{p1p2} & Z_{p2p2} & Z_{p3p2} & Z_{p4p2} & Z_{p13p2} \\ Z_{p1p3} & Z_{p2p3} & Z_{p3p3} & Z_{p4p3} & Z_{p13p3} \\ Z_{p1p4} & Z_{p2p4} & Z_{p3p4} & Z_{p4p4} & Z_{p13p4} \\ Z_{p1p13} & Z_{p2p13} & Z_{p3p13} & Z_{p4p13} & Z_{p13p13} \end{bmatrix}$$

$$B3Z_{cc} = \begin{bmatrix} Z_{p5p5} & Z_{p6p5} & Z_{p7p5} & Z_{p8p5} & Z_{p9p5} & Z_{p10p5} & Z_{p11p5} & Z_{p12p5} \\ Z_{p5p6} & Z_{p6p6} & Z_{p7p6} & Z_{p8p6} & Z_{p9p6} & Z_{p10p6} & Z_{p11p6} & Z_{p12p6} \\ Z_{p5p7} & Z_{p6p7} & Z_{p7p7} & Z_{p8p7} & Z_{p9p7} & Z_{p10p7} & Z_{p11p7} & Z_{p12p7} \\ Z_{p5p8} & Z_{p6p8} & Z_{p7p8} & Z_{p8p8} & Z_{p9p8} & Z_{p10p8} & Z_{p11p8} & Z_{p12p8} \\ Z_{p5p9} & Z_{p6p9} & Z_{p7p9} & Z_{p8p9} & Z_{p9p9} & Z_{p10p9} & Z_{p11p9} & Z_{p12p9} \\ Z_{p5p10} & Z_{p6p10} & Z_{p7p10} & Z_{p8p10} & Z_{p9p10} & Z_{p10p10} & Z_{p11p10} & Z_{p12p10} \\ Z_{p5p11} & Z_{p6p11} & Z_{p7p11} & Z_{p8p11} & Z_{p9p11} & Z_{p10p11} & Z_{p11p11} & Z_{p12p11} \\ Z_{p5p12} & Z_{p6p12} & Z_{p7p12} & Z_{p8p12} & Z_{p9p12} & Z_{p10p10} & Z_{p11p12} & Z_{p12p12} \end{bmatrix}$$

$$B3Z_{pc} = \begin{bmatrix} Z_{p1p5} & Z_{p2p5} & Z_{p3p5} & Z_{p4p5} & Z_{p13p5} \\ Z_{p1p6} & Z_{p2p6} & Z_{p3p6} & Z_{p4p6} & Z_{p13p6} \\ Z_{p1p7} & Z_{p2p7} & Z_{p3p7} & Z_{p4p7} & Z_{p13p7} \\ Z_{p1p8} & Z_{p2p8} & Z_{p3p8} & Z_{p4p8} & Z_{p13p8} \\ Z_{p1p9} & Z_{p2p9} & Z_{p3p9} & Z_{p4p9} & Z_{p13p9} \\ Z_{p1p10} & Z_{p2p10} & Z_{p3p10} & Z_{p4p10} & Z_{p13p10} \\ Z_{p1p11} & Z_{p2p11} & Z_{p3p11} & Z_{p4p11} & Z_{p13p11} \\ Z_{p1p12} & Z_{p2p12} & Z_{p3p12} & Z_{p4p12} & Z_{p13p12} \end{bmatrix} \qquad B3Z_{cp} = B3Z_{pc}^{\ T}$$

(b)

Figure 6.13: (a) Conversion of P ports to C ports on B1 segment (b) with relevant impedance matrix

It is also required that ports $P_1 - P_4$ on A2 segment be renamed ports $P_6 - P_9$, and ports $P_5 - P_{12}$ on A2 segment be renamed $C_9 - C_{16}$, as illustrated in figure 6.14a-b.

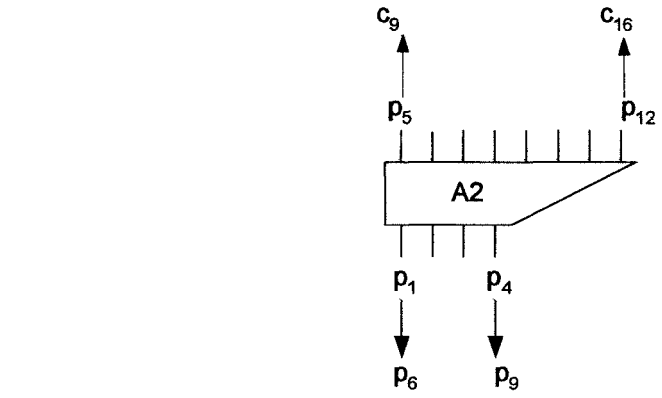

(a)

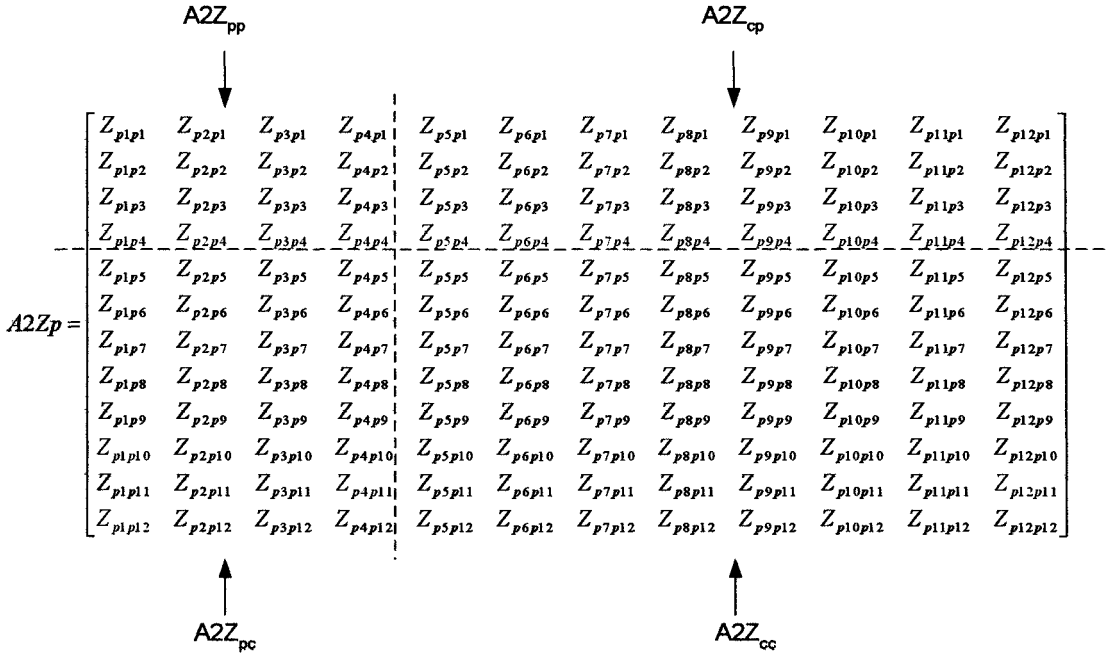

(b)

Figure 6.14: (a) Conversion of ports on A2 segment
(b) with relevant impedance matrix

Figure 6.15 illustrates the port labelling of the B1 and A2 segments. Note that port P_5 is used to determine the input impedance at the feedpoint.

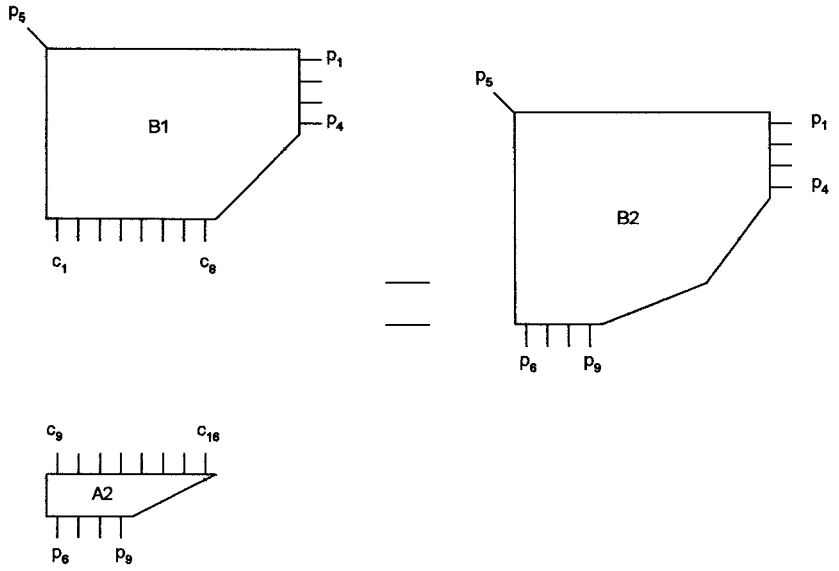

Figure 6.15: Ports of B1 and A2 segments

The impedance matrix of the B2 segment is determined by synthesising B1 and A2 segments. From (4.49) this is given by:

$$B2Z_p = B2Z_{pp} - B2Z_{pc}\begin{bmatrix} B2\Gamma_1 B2Z_{cc} \\ B2\Gamma_2 \end{bmatrix}^{-1}\begin{bmatrix} B2\Gamma_1 B2Z_{cp} \\ B20 \end{bmatrix} \qquad (6.8)$$

where:

$B2Z_{pp}$ represents the interaction between P ports on segments B1 and A2

$B2Z_{cp}$ represents the interaction between C and P ports

$B2Z_{pc}$ represents the interaction between P and C ports

$B2Z_{cc}$ represents the interaction between C ports

Step 4: Determination of B3 segment by synthesis of B2a and B2b segments:

The impedance matrices of the B3 segment is determined by synthesising segments B2a and B2b. To achieve this requires that ports P_1 - P_4 on segment B2a be renamed as ports C_1 - C_4, ports $P_6 - P_9$ on B2a segment be renamed ports $P_1 - P_4$, as illustrated in figure 6.16a-b

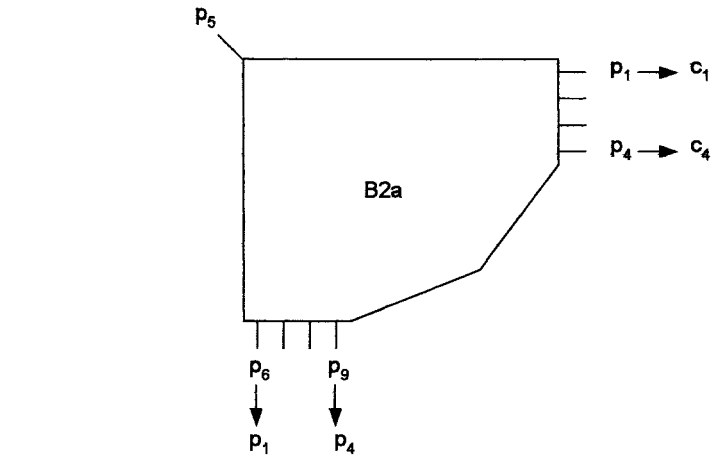

(a)

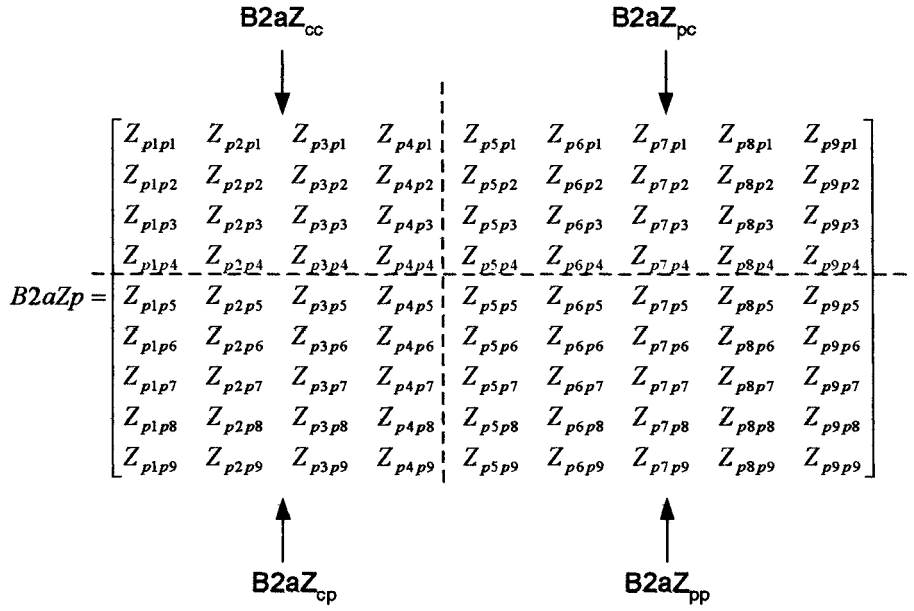

(b)

Figure 6.16: (a) Conversion of ports on B2a segment
(b) with relevant impedance matrix

It is also required that ports $P_1 - P_4$ on B2b segment be renamed $C_5 - C_8$, as illustrated in figure 6.17a-d. Note that in segment B2b, port P_5 is no longer required, hence all interactions between this and other ports are ignored in later steps.

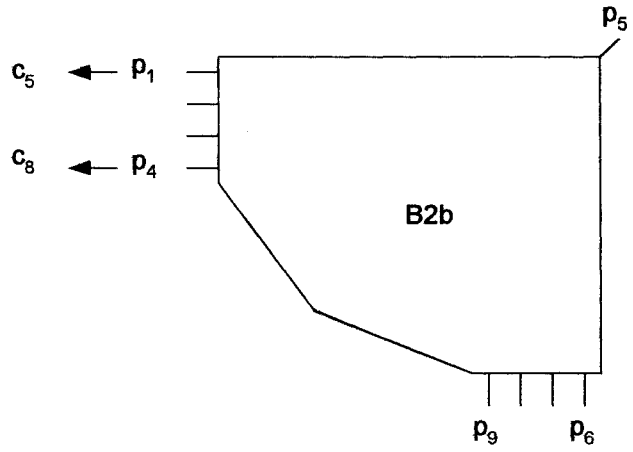

(a)

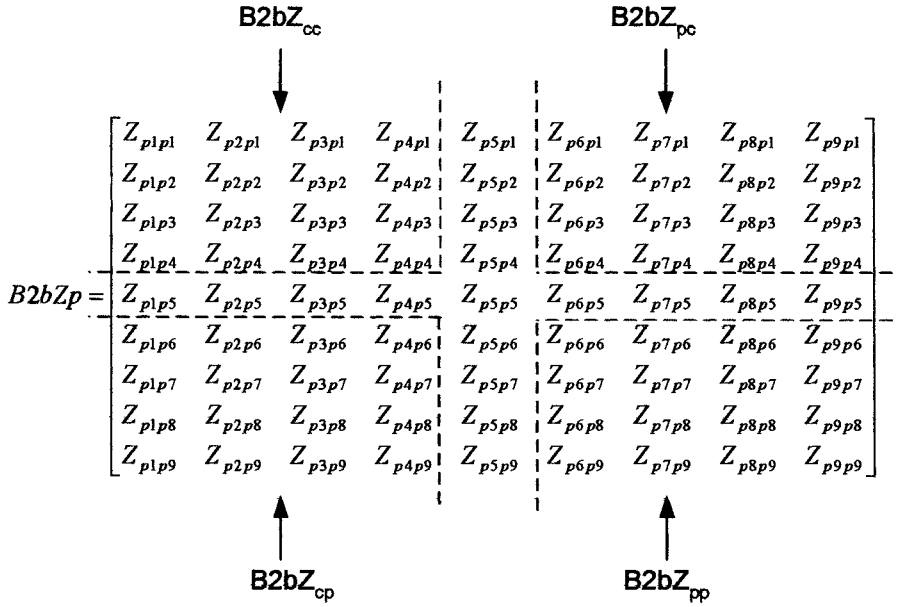

(b)

Figure 6.17: (a) Conversion of ports on B2b segment
(b) with relevant impedance matrix

With reference to equation 6.1, to determine the required perturbation length, the Real Input Impedance of the TM_{01} mode ($Re\{Z_{in01}\}$) is required. To enable this port C_1 on the B2a segment is also used as an unconnected P port (P_{10}). A similar procedure to those described above is then followed.

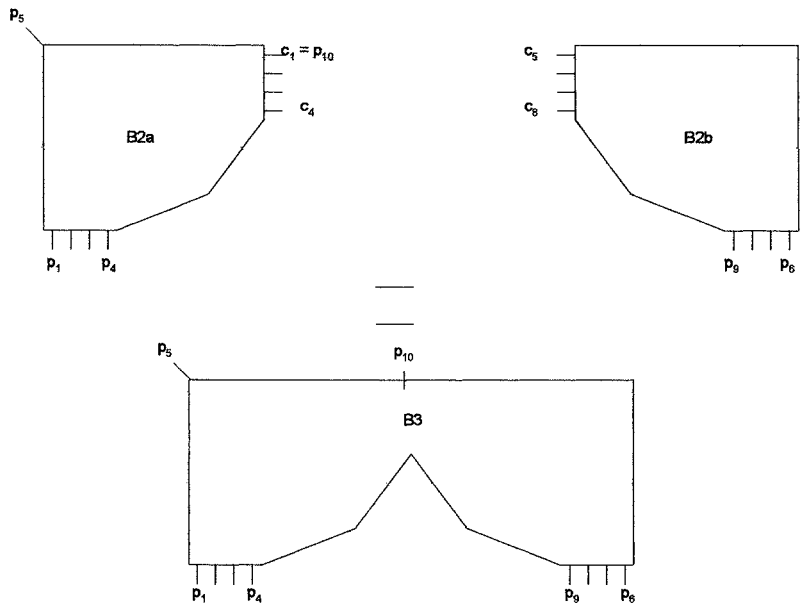

Figure 6.18: Ports on B2a and B2b segments

From (4.49) this is given by:

$$B3Z_p = B3Z_{pp} - B3Z_{pc}\begin{bmatrix} B3\Gamma_1 B3Z_{cc} \\ B3\Gamma_2 \end{bmatrix}^{-1}\begin{bmatrix} B3\Gamma_1 B3Z_{cp} \\ B30 \end{bmatrix} \qquad (6.9)$$

where:

$B3Z_{pp}$ represents the interaction between P ports on segments B2a and B2b

$B3Z_{cp}$ represents the interaction between C and P ports

$B3Z_{pc}$ represents the interaction between P and C ports

$B3Z_{cc}$ represents the interaction between C ports

Step 5: Determination of B4 segment by synthesis of B3a and B3b segments:

The impedance matrices of the B4 segment is determined by synthesising segments B3a and B3b. To achieve this requires that ports P_1 - P_4 and ports P_6-P_9 on segment B3a be renamed as ports C_1 - C_8, port P_5 and port P_{10} on segment B3a is also renamed as port P_1 and P_2 respectively, as illustrated in figure 6.19a-b.

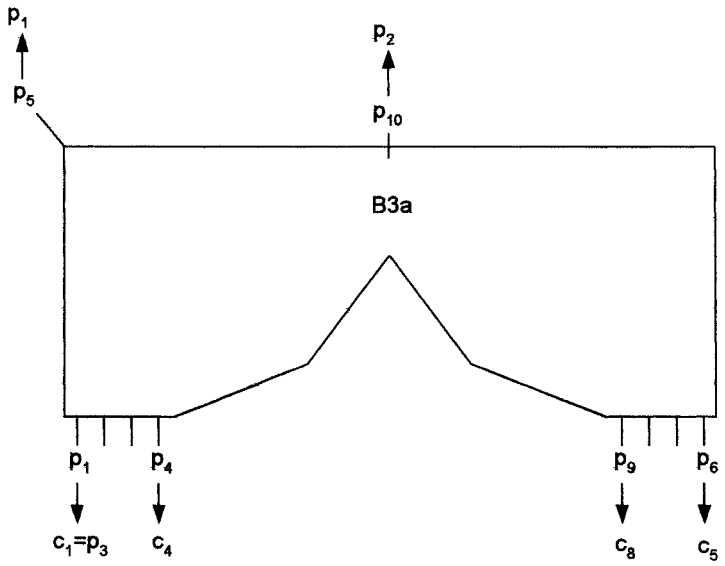

(a)

$$B3aZp = \begin{bmatrix} Z_{p1p1} & Z_{p2p1} & \cdots & Z_{p10p1} \\ Z_{p1p2} & Z_{p2p2} & \cdots & Z_{p10p2} \\ \vdots & \vdots & \ddots & \vdots \\ Z_{p1p10} & Z_{p2p10} & \vdots & Z_{p10p10} \end{bmatrix}$$

$$B3aZ_{pp} = \begin{bmatrix} Z_{p5p5} & Z_{p5p10} & Z_{p5p1} \\ Z_{p10p5} & Z_{p10p10} & Z_{p10p1} \\ Z_{p1p5} & Z_{p1p10} & Z_{p1p1} \end{bmatrix}$$

$$B3aZ_{pc} = \begin{bmatrix} Z_{p5p1} & Z_{p5p2} & Z_{p5p3} & Z_{p5p4} & Z_{p5p6} & Z_{p5p7} & Z_{p5p8} & Z_{p5p9} \\ Z_{p10p1} & Z_{p10p2} & Z_{p10p3} & Z_{p10p4} & Z_{p10p6} & Z_{p10p7} & Z_{p10p8} & Z_{p10p9} \\ Z_{p1p1} & Z_{p1p2} & Z_{p1p3} & Z_{p1p4} & Z_{p1p6} & Z_{p1p7} & Z_{p1p8} & Z_{p1p9} \end{bmatrix}$$

$$B3aZ_{cp} = B3aZ_{pc}^{T}$$

$$B3aZ_{cc} = \begin{bmatrix} Z_{p1p1} & Z_{p2p1} & \cdots & Z_{p9p1} \\ Z_{p1p2} & Z_{p2p2} & \cdots & Z_{p9p2} \\ \vdots & \vdots & \ddots & \vdots \\ Z_{p1p9} & Z_{p2p9} & \vdots & Z_{p9p9} \end{bmatrix}$$

(b)

Figure 6.19: (a) Conversion of ports on B3a segment
(b) with relevant impedance matrix

It is also required that ports $P_1 - P_8$ on B3a segment be renamed as ports $C_9 - C_{16}$, illustrated in figure 6.20a-b.

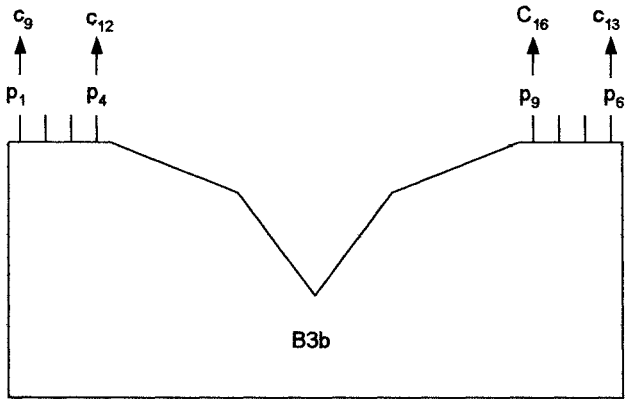

(a)

$$B3bZp = \begin{bmatrix} Z_{p1p1} & Z_{p2p1} & \cdots & Z_{p9p1} \\ Z_{p1p2} & Z_{p2p2} & \cdots & Z_{p9p2} \\ \vdots & \vdots & \ddots & \vdots \\ Z_{p1p9} & Z_{p2p9} & \vdots & Z_{p9p9} \end{bmatrix} = B3bZ_{cc}$$

(b)

Figure 6.20: (a) Conversion of ports on B3b segment
(b) with relevant impedance matrix

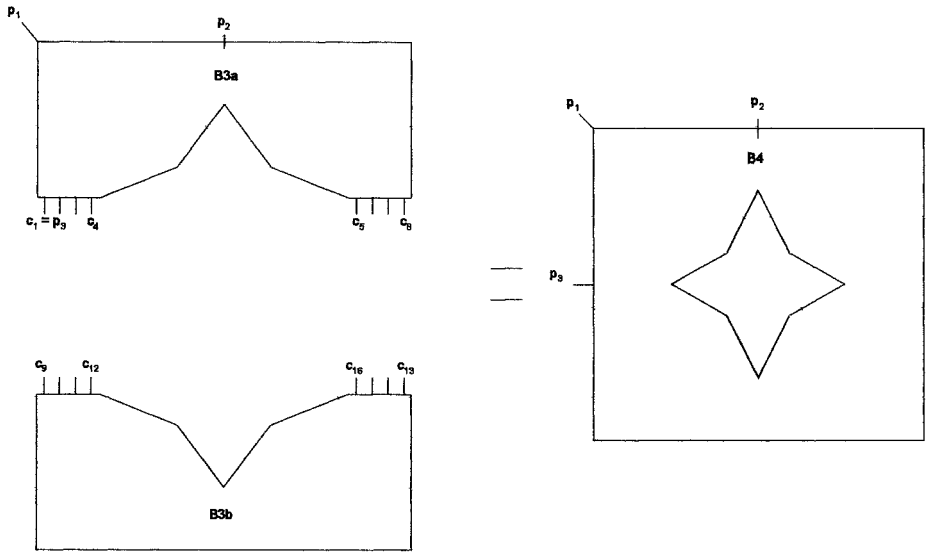

Figure 6.21: Ports on B3a and B3b segments

The impedance matrix of the B4 segment is determined by synthesising B3a and B3b segments. From (4.49) this is given by:

$$B4Z_p = B4Z_{pp} - B4Z_{pc}\begin{bmatrix} B4\Gamma_1 B4Z_{cc} \\ B4\Gamma_2 \end{bmatrix}^{-1}\begin{bmatrix} B4\Gamma_1 B4Z_{cp} \\ B40 \end{bmatrix} \qquad (6.10)$$

where:

$B4Z_{pp}$ represents the interaction between P ports on segments B3a and B3b

$B4Z_{cp}$ represents the interaction between C and P ports

$B4Z_{pc}$ represents the interaction between P and C ports

$B4Z_{cc}$ represents the interaction between C ports

6.3.1.2 Results and analysis

The CP performance of the corner fed nearly square patch with star-shaped slot loading (figure 6.6a) and square-shaped slot loading (figure 6.6b). The patch dimensions l_1 and dl have been determined using the segmentation procedure together with the procedure defined by equation 6.1. The corresponding CP performance, determined using full-wave analysis [92] are shown in tables 6.4a and 6.4b respectively.

l_1 (= w_1) (mm)	*dl* (mm)	Frequency (GHz)	Input Impedance (Ω)	CP BW (3dB AR) (%)
0	0.71	2.95	310	1.2
4	0.71	2.926	307	0.92
8	0.61	2.824	360	0.75
12	0.41	2.639	430	0.72
16	0.21	2.406	1100	0.54

$\varepsilon_r = 2.33$, h = 1.57 mm, L = 31.59 mm

(a)

l_1 (= w_1) (mm)	dl (mm)	Frequency (GHz)	Input Impedance (Ω)	CP BW (3dB AR) (%)
0	0.71	2.95	310	1.2
4	0.71	2.925	330	0.92
8	0.61	2.805	400	0.7
12	0.41	2.639	750	0.59
16	0.21	2.396	1200	0.49

$\varepsilon_r = 2.33$, $h = 1.57$ mm, $L = 31.59$ mm

(b)

Table 6.2: Theoretical CP performance for slot loaded designs (a) corner fed CP design with star-shaped loaded patch (b) corner fed CP patch design with square-shaped slot loading

It can be seen that significant size reduction can be achieved using either design. The results also indicate that the perturbation size and resonant frequency are comparable for both designs. However, by using a star-shaped slot a results in a lower input impedance than the corresponding square-slot loaded design. This is more apparent as the slot size increases. For example, with a slot length, l_1, of 12 mm, using a star-shaped slot produces an input impedance of 430 Ω, compared to 750 Ω for a square-shaped slot. The results also demonstrate that a slight increase in Axial Ratio Bandwidth can also be achieved using star-shaped loading. These two facts could be attributed to the fact the star-shaped slot does not produce such a sharp transition in the current path.

6.3.2 Effect of Offset Feed on Nearly Square CP Patch with Star-shaped Slot Loading

To further improve the performance of the antenna, the use of an offset feed is considered in this section, as shown in figure 6.22.

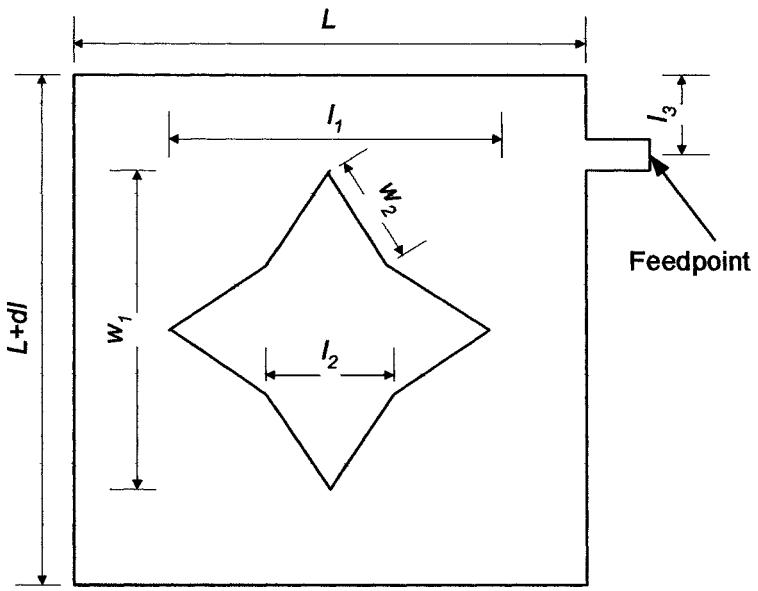

Figure 6.22: Star-shaped slot loaded CP patch design with offset feed

As a consequence of slot loading there are two problems to be considered. Namely, the position of the offset feedpoint and amount of perturbation segment with slot dimensions.

Regarding the feedpoint, the first consideration is to determine the position of the offset feed, l_3, at which the input impedance is purely real, whilst still exciting both TM_{01} and TM_{10} modes, such that good CP performance is achieved. For the proposed offset fed nearly square patch, exciting the patch close to the corner, the input impedance is inductive. As the offset feed distance, l_3 increases a point is reached where the input impedance is purely real, with no imaginary component. As l_3 is increases further the input impedance becomes capacitive, eventually reaching a position where both TM_{mn} modes cannot be excited. From table 6.4a, experimental results indicate that this value, l_3, required to achieve a purely real input impedance increases with slot dimensions l_1 and w_1.

Regarding the relationship between slot size and perturbation segment, for reasons described in section 6.3.1, experimental results indicate that this decreases with increased slot size.

To determine the required slot dimensions and feed position, an iterative application of full-wave modelling using Ensemble software [92] was employed. To determine the effect of the offset feed, the performance of the offset fed design is compared with that of a star-shaped slot loaded patch with a corner feed, developed in section 6.3.1.

l_1 (= w_1) (mm)	l_3 (mm)	*dl* (mm)	Frequency (GHz)	Input Impedance (Ω)	CP BW (3dB AR) (%)
0	4	0.81	2.95	245	1.5
4	4	0.81	2.94	250	1.4
8	4.5	0.71	2.826	290	1.2
12	5	0.51	2.643	330	1.1
16	5.5	0.41	2.409	475	1.1

$\varepsilon_r = 2.33$, $h = 1.57$ mm, $L = 31.59$ mm
(a)

l_1 (= w_1) (mm)	*dl* (mm)	Frequency (GHz)	Input Impedance (Ω)	CP BW (3dB AR) (%)
0	0.71	2.95	310	1.2
4	0.71	2.976	307	0.92
8	0.61	2.824	360	0.75
12	0.41	2.639	430	0.72
16	0.21	2.406	900	0.54

$\varepsilon_r = 2.33$, $h = 1.57$ mm, $L = 31.59$ mm
(b)

Table 6.3: Theoretical CP performance for star-shaped slot loaded designs with (a) offset feed and (b) corner feed

Regarding the effect of the offset feed, it can be seen from tables 6.5a and 6.5b, that for both corner and offset feed positions, there is a reduction in axial ratio bandwidth with increased slot size. However, this effect is not as significant for the offset fed design. For the case of the offset feed, with large slot size, l_1 and w_1 = 16 mm, the axial ratio bandwidth remains above 1%.

An added advantage of using an offset feed regards the input impedance of the antenna. For regular slot loaded patch antennas, a trade-off of embedded slots is an

increased input impedance at the patch corner. As the slot size increases, the input impedance reaches a value where traditional quarter-wave impedance matching cannot be practically achieved. The use of an offset feed significantly reduces the impedance, thus allowing greater size reduction whilst still allowing planar impedance matching. This is demonstrated in table 6.3, which shows that the offset-fed patch has a lower input impedance than the corner fed design. This becomes more apparent as the slot size increases. For slot length l_1 of 16 mm, using an offset feed produces an input impedance of 475 Ω, compared to an impedance of 1100 Ω with a corner feed.

Moreover, it can also be seen that the use of an offset feed increases the length of perturbation segment, *dl*, which implies a relaxed manufacturing tolerance.

When compared to the original nearly square CP patch with square slot loading described in section 6.2, significant improvement in patch performance is achieved using Design 1. For convenience, the results of both these structures are reproduced in tables 6.4a and b respectively.

l_1 (= w_1) (mm)	l_3 (mm)	*dl* (mm)	Frequency (GHz)	Input Impedance (Ω)	CP BW (3dB AR) (%)
0	4	0.81	2.95	245	1.5
4	4	0.81	2.94	250	1.4
8	4.5	0.71	2.816	290	1.2
12	5	0.51	2.643	330	1.1
16	5.5	0.41	2.39	475	1.1

$\varepsilon_r = 2.33$, $h = 1.57$ mm, $L = 31.59$ mm

(a)

l_1 (= w_1) (mm)	*dl* (mm)	Frequency (GHz)	Input Impedance (Ω)	CP BW (3dB AR) (%)
0	0.71	2.95	310	1.2
4	0.71	2.925	330	0.92
8	0.61	2.805	400	0.7
12	0.41	2.639	750	0.59
16	0.21	2.396	1200	0.49

$\varepsilon_r = 2.33$, $h = 1.57$ mm, $L = 31.59$ mm

(b)

Table 6.4: Theoretical CP performance for slot loaded designs (a) Design 1: proposed star-shaped loaded patch with offset feed. (b) corner fed square-shaped slot loaded patch (Reference Antenna)

The results in table 6.6 highlight a number of key advantages of the proposed design in terms of axial ratio bandwidth, input impedance and manufacturing tolerances. Considering the axial ratio bandwidth, for both the proposed and reference antennas, this value decreases with increased slot size. However, the reduction is not as significant for the proposed design 1. For the case of a large slot size, l_1 ($= w_1$) = 16 mm, the axial ratio bandwidth remains above 1.1%, which is still comparable to a regular unslotted corner fed nearly square patch . It is also observed that the proposed design has a larger perturbation segment, which implies a relaxed manufacturing tolerance.

Regarding the effect of both designs on input impedance, the table confirms that the proposed design has a lower input impedance than the square-shaped slot loaded design. This becomes more apparent as slot size increases, and hence resonant frequency decreases. To achieve a resonant frequency of approximately 2.4 GHz, the proposed design 1 has an input impedance of 475 Ω, compared to 1200 Ω for the square-shaped design.

6.3.3 Practical Implementation of Proposed Design 1

Several star-shape loaded designs have been successfully implemented. Figure 6.23 illustrates the measured axial ratio versus frequency for two typical designs with l_1 = w_1 = 8 mm (Antenna A), and $l_1 = w_1$ = 16 mm (Antenna B). To provide a reference, a conventional corner fed nearly square CP patch was also fabricated and tested. The axial ratio bandwidth, is also shown on the diagram.

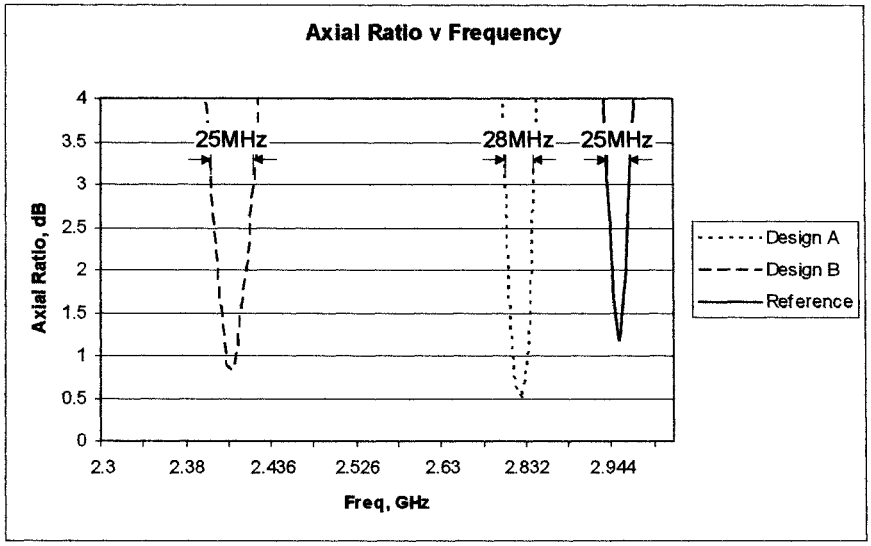

$L = 31.39$mm, $\varepsilon_r = 2.33$, $h = 1.57$mm.
Design A: $dl = 0.71$, $l_1 = 8$mm, $w_1 = 8$mm, $l_3 = 4.5$
Design B: $dl = 0.41$, $l_1 = 16$mm, $w_1 = 16$mm, $l_3 = 5.5$
Reference Antenna: $dl = 0.71$mm

Figure 6.23: Measured axial ratio for the proposed antenna (Design 1) with various slot dimensions;

The operating frequency, defined as the frequency with minimum axial ratio in the operating bandwidth, is 2.826 GHz for Antenna A and 2.409 GHz for Antenna B. This corresponds to a size reduction of 13% and 38% respectively, when compared with the reference antenna. Regarding the axial ratio bandwidth, design has a bandwidth of 28MHz, whilst both design B and the reference antenna have a bandwidth of 25MHz. These results demonstrate that size reduction can be achieved with no reduction in ARBW. The above results are summarised in table 6.7, together with the predicted theoretical results determined in section 6.3.2.

	Reference		**Design A**		**Design B**	
	Theoretical	**Practical**	**Theoretical**	**Practical**	**Theoretical**	**Practical**
Frequency (GHz)	2.952	2.95	2.816	2.82	2.39	2.409
AR BW (MHz)	34	25	33	28	25	25

Table 6.5: Comparison between theoretical and practical results for offset-fed star shaped slot loaded CP patch designs

Table 6.7 shows a slight difference in resonant frequency and axial ratio bandwidth for predicted and theoretical results. This could be due to manufacturing tolerances, the approximate model of the fringing field extension and the empirical estimation of the effective dielectric constant.

Antenna B achieves the largest size reduction and hence only the radiation pattern of this design is shown. With reference to figure 6.24a and 6.24b, good LHCP radiation is achieved with cross polarisation levels of below 20 dB is demonstrated in both *E* and *H*-planes respectively. A measured gain of 6.3 dB is also achieved.

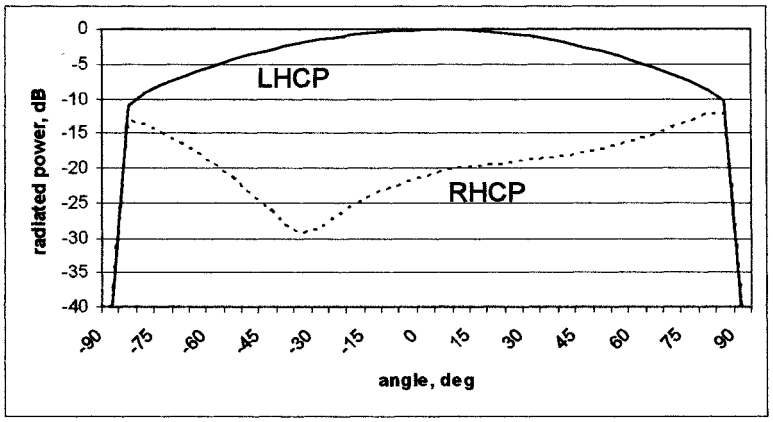

(a)

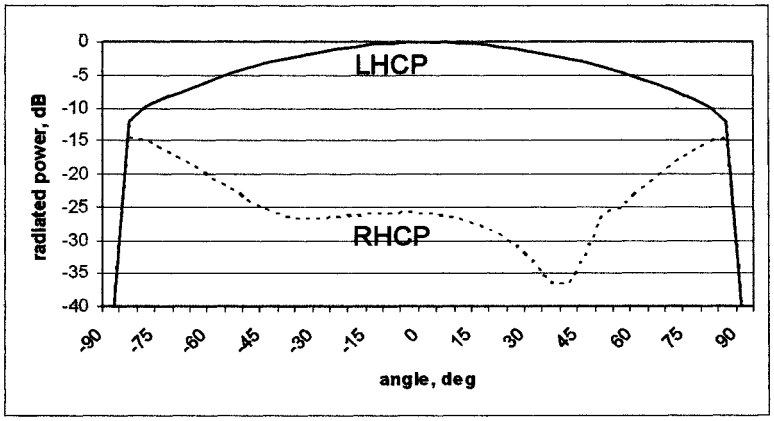

(b)

Figure 6.24: Measured radiation patterns in two orthogonal planes for antenna B, (a) x-z plane. (b) y-z plane

6.4 Offset Fed Nearly Square CP patch with triangular–shape slot loading - Design 2

6.4.1 Patch Design and Results

In this section, it is demonstrated that by embedding four right angle triangular slots in a nearly square patch antenna, size reduction of up to 43% can be achieved. Combined with the use of an offset feed, this design offers similar performance in terms of manufacturing tolerances and axial ratio bandwidth, to the star shaped slot loaded design described in section 6.3.

The proposed compact CP design 2 is shown in figure 6.25. To generate these results, the associated parameters with their fixed values are shown in table 6.8. The patch is designed for use on RTDuroid 5870. The relevant data for this substrate is shown in Appendix A.

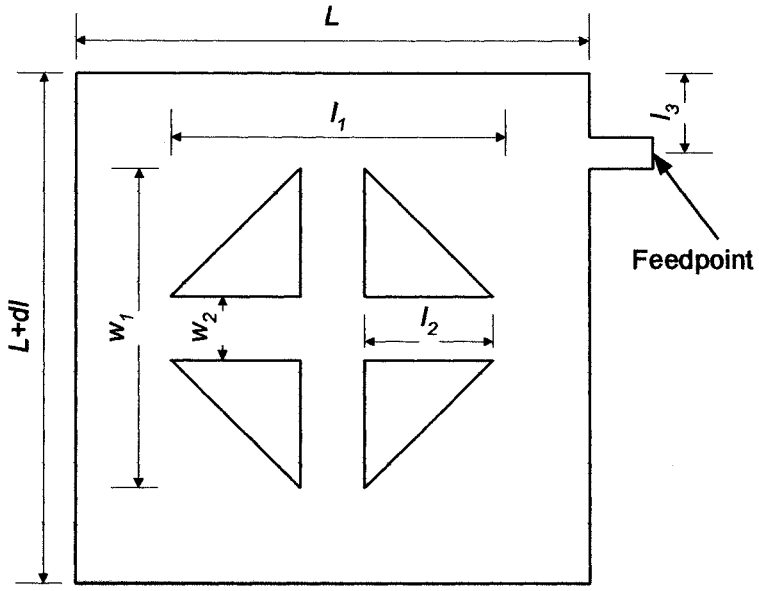

Figure 6.25: Proposed offset fed triangular-shaped slot loaded nearly square CP (Design 2)

The nearly square patch has side lengths L and $L+dl$, and is printed on a substrate of permittivity ε_r and thickness h. The patch is excited by the use an offset feed, at a distance l_3 from the patch corner. The triangular slots are of length l_2, and are separated by width w_2. By increasing the slot size, l_1 and w_1, the current path of the

fundamental TM_{01} and TM_{10} modes are lengthened, with l_1 largely controlling the TM_{01} mode current path and w_1 controlling the TM_{10} current path. This results in a lowering of the patch operating frequency, which accounts for the size reduction. The corresponding CP performance of typical designs, determined using full-wave analysis [92], are shown in table 6.5a. For reference, the performance of the offset fed star-shape loaded patch described in section 6.3 is shown in table 6.6b. Whilst the performance of a corner fed square slot loaded nearly square patch described in section 6.2 is also shown in table 6.6c.All patches were fabricated on RTDuroid with a permittivity of 2.33 and thickness of 1.57 mm.

l_1 (= w_1) (mm)	l_3 (mm)	dl (mm)	Frequency (GHz)	Input Impedance (Ω)	CP BW (3dB AR) (%)
0	4	0.81	2.95	235	1.5
4	4	0.81	2.94	245	1.4
8	4.5	0.71	2.87	270	1.35
12	5	0.51	2.682	360	1.25
16	5.5	0.41	2.422	510	1.2

$\varepsilon_r = 2.33$, $h = 1.57$ mm, $L = 31.59$ mm, $w_2 = 1$ mm
(a)

l_1 (= w_1) (mm)	l_3 (mm)	dl (mm)	Frequency (GHz)	Input Impedance (Ω)	CP BW (3dB AR) (%)
0	4	0.81	2.95	245	1.5
4	4	0.81	2.94	250	1.4
8	4.5	0.71	2.816	290	1.2
12	5	0.51	2.643	330	1.1
16	5.5	0.41	2.39	475	1.1

$\varepsilon_r = 2.33$, $h = 1.57$ mm, $L = 31.59$ mm
(b)

l_1 (= w_1) (mm)	dl (mm)	Frequency (GHz)	Input Impedance (Ω)	CP BW (3dB AR) (%)
0	0.71	2.95	310	1.2
4	0.71	2.925	330	0.92
8	0.61	2.805	400	0.7
12	0.41	2.639	750	0.59
16	0.21	2.396	1200	0.49

$\varepsilon_r = 2.33$, $h = 1.57$ mm, $L = 31.59$ mm
(c)

Table 6.6:Theoretical CP performance for
(a) proposed offset fed triangular-shaped slot loaded nearly square CP patch (Design 2)
(b) offset fed star-shaped slot loaded nearly square CP patch antenna (Design 1)
(c) corner fed square-shaped slot loaded nearly square CP patch antenna (reference)

When compared to the corner fed square-shaped slot loaded nearly square patch (reference) in table 6.6c, the proposed triangular-shaped slot loaded design (Design 2) in table 6.6a offers a number of advantages in terms of axial ratio bandwidth, input impedance and manufacturing tolerances. Considering the axial ratio bandwidth, for both the designs, this value decreases with increased slot size. However, the Reduction is not as significant for the proposed design 2. For the case of a large slot size, l_1 ($= w_1$) = 16 mm, the axial ratio bandwidth remains above 1.2%, which is still comparable to a regular unslotted corner fed nearly square patch. It is also observed that the proposed Design 2 has a larger perturbation segment for all values of slot size, which implies a relaxed manufacturing tolerance.

Regarding the effect of both designs on input impedance, the table confirms that the proposed design has a lower input impedance than the square-shaped slot loaded design. This becomes more apparent as slot size increases, and hence resonant frequency decreases. To achieve a resonant frequency of approximately 2.4 GHz, the proposed design has an input impedance of 510 Ω, compared to 1200 Ω for the square-shaped design.

Comparing the performance of the triangular-shaped (Design 2) and star-shaped slot loaded design (Design 1) in tables 6.5a and 6.5c respectively, the former design appears to offer a slight improvement in axial ratio bandwidth, but a slight increase in input impedance, whilst the size of the perturbation segment is the same for both designs.

6.4.2 Practical Implementation of Proposed Design 2

Several proposed antennas with different slot dimensions have been fabricated and tested. All patches were fabricated on RTDuroid with a permittivity of 2.33 and thickness of 1.57 mm. Figure 6.26 illustrates the measured axial ratio versus frequency for two typical designs with $l_1 = w_1 = 8$ mm (Antenna C), and $l_1 = w_1 = 16$ mm (Antenna D), together with a conventional corner fed nearly square CP patch antenna as a reference. To provide a reference, a conventional corner fed nearly square CP patch was also fabricated and tested. The axial ratio bandwidth, is also shown on the diagram.

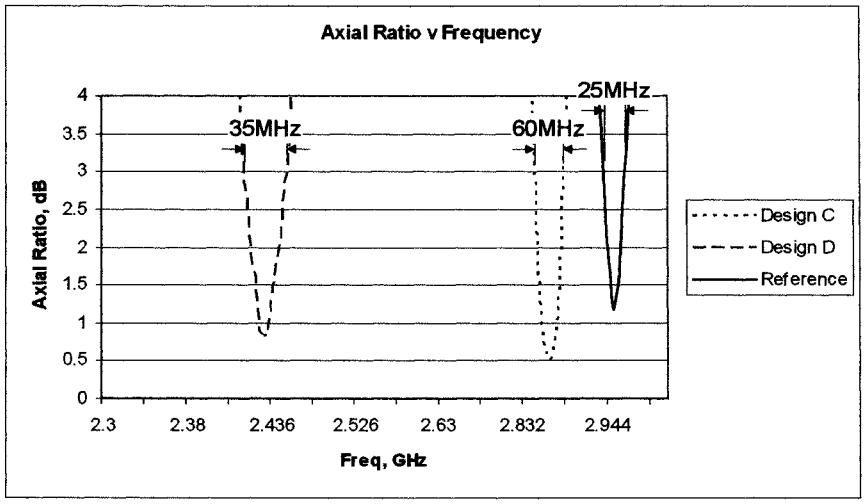

$L = 31.59$ mm, $\varepsilon_r = 2.33$, $h = 1.57$ mm.
Design C: $dl = 0.71$ mm, $l_1 = 8$ mm, $w_1 = 8$ mm, $l_2 = 1.5$ mm, $w_2 = 1$ mm, $l_3 = 4.5$ mm
Design D: $dl = 41$ mm, $l_1 = 16$ mm, $w_1 = 16$ mm, $l_2 = 7.5$ mm, $w_2 = 1$ mm, $l_3 = 5.5$ mm,
Reference Antenna: $dl = 0.71$mm

Figure 6.26: Measured axial ratio for the design 2 with various slot dimensions;

The operating frequency, defined as the frequency with minimum axial ratio in the operating bandwidth, is 2.874 GHz for Antenna C and 2.428 GHz for Antenna B. This corresponds to a size reduction of 19% and 43% respectively, when compared with the reference antenna. Regarding the axial ratio bandwidth, design has a bandwidth of 60MHz, design B has a bandwidth of 35MHz and the reference antenna has a bandwidth of 25 MHz. These results demonstrate that size reduction

can be achieved with no reduction in ARBW. The above results are summarised in table 6.7, together with the predicted theoretical results determined in section 6.3.1.

	Reference		Design A		Design B	
	Theoretical	**Practical**	**Theoretical**	**Practical**	**Theoretical**	**Practical**
Frequency (GHz)	2.952	2.95	2.87	2.874	2.422	2.488
AR BW (MHz)	34	25	40	60	29	35

Table 6.7: Comparison between theoretical and practical results for offset-fed triangular shaped slot loaded CP patch designs

Table 6.7 shows a slight difference in resonant frequency and axial ratio bandwidth for predicted and theoretical results. This could be due to manufacturing tolerances, the approximate model of the fringing field extension and the empirical estimation of the effective dielectric constant.

Antenna D achieves the largest size reduction and hence only the radiation pattern of this design is shown. With reference to figure 6.27a and 6.27b, good LHCP radiation is achieved with cross polarisation levels of below 20 dB is demonstrated in both E and H-planes respectively. A measured gain of 6.2 dB is also achieved.

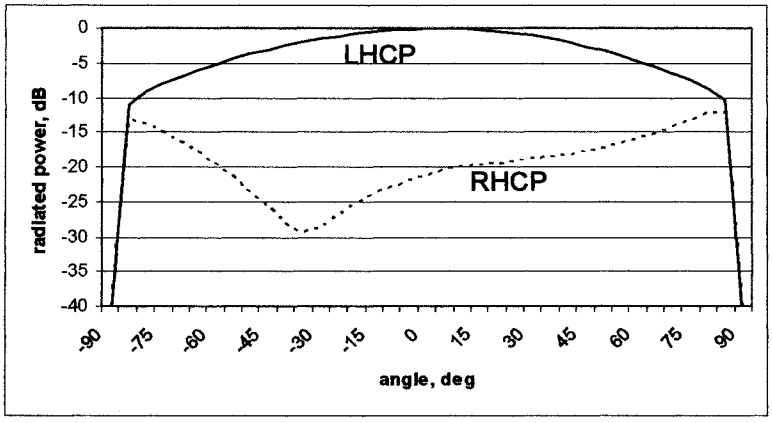

(a)

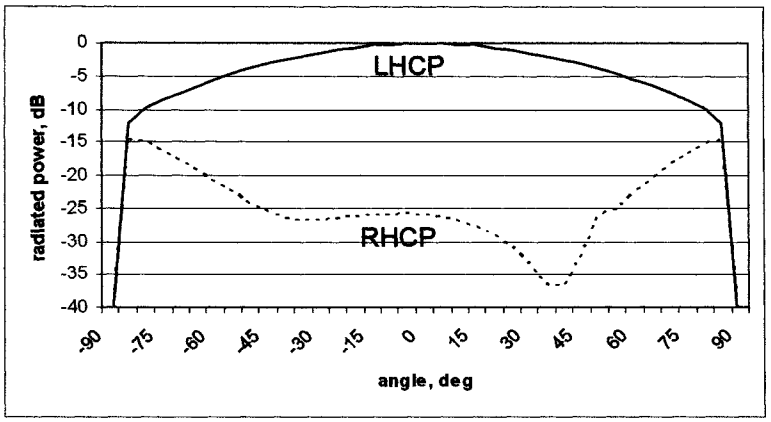

(b)

Figure 6.27: Measured radiation patterns in two orthogonal planes for antenna D. (a) x-z plane. (b) y-z plane

6.5 Summary

This chapter has highlighted the lack of work on reduced size planar fed nearly square CP patch antennas. The reasons for this has been determined in section 6.2 which examined the use of square slot loading within a corner fed nearly square patch. It was subsequently shown that this design suffers from an increased input impedance, reduced axial ratio bandwidth and strict manufacturing tolerances. To overcome these problems, two novel offset fed structures with different types of slot loading have been presented and discussed. The first design incorporates star-shape slot loading with an offset feed and has been shown to produce a size reduction of up to 38%, with a with no significant reduction in axial ratio bandwidth and has relaxed manufacturing tolerances. A lower value of input impedance has also been achieved. The second design incorporating triangular slot loading and an offset feed achieves slightly increased size reduction of up to 43% and provides similar benefits in terms of CP performance.

CHAPTER 7

COMPACT PLANAR FED DESIGNS BASED ON CREATION OF $TM_{0\delta}$ MODE

7.1 Introduction

A detailed review of present methods of reducing the size of a patch antenna was outlined in Chapter 3. Within this chapter, it was highlighted that little significant research existed on the design technique of such antennas and moreover the associated trade-offs of such antennas. This knowledge gap has been addressed in chapter 5 which fully investigated the use of slot loading on patch performance. One of the major findings of this study was a significant increase in patch input impedance with size reduction. As a consequence, the majority of compact designs are excited using either a probe feed, with little work existing on the use of a planar feed.

This has been addressed in Chapters 5 and 6 in which planar fed compact patch antennas with linear and circular polarisation were designed. However, in these cases, an impedance matching network or an inset feed was required to facilitate the use of a planar feed. In these designs (and those in current literature) size reduction has been achieved by operating the patch using the fundamental TM_{01} / TM_{10} mode and modifying its current patch. It has been shown in Chapter 5 that due to the impedance response of these modes it is not possible to achieve both size reduction and still achieve the required input impedance to allow the use of a direct 50 Ω planar feed.

To overcome this problem, two novel designs, based on the structure in figure are presented. As explained in Chapter 3, Wong and Sze [134] suggested that by inserting bent slots close to the non-radiating edge a patch, dual frequency operation

a patch antenna can be achieved. This structure operates by creating an additional $TM_{0\delta}$ mode, with a resonant frequency between the TM_{01} and TM_{02} mode. Impedance matching is achieved using a probe feed at an appropriate point along the $y = W/2$ axis. It is found that by inserting two narrow rectangular slits cut into one of the radiating edges patch edge and parallel to the non-radiating edge, as shown in figure 7.1, an additional $TM_{0\delta}$ mode is created. Using this structure, an additional $TM_{0\delta}$ mode can be created, with a resonant frequency below the fundamental TM_{01} mode, thus lending itself to the design of a reduced size patch antenna.

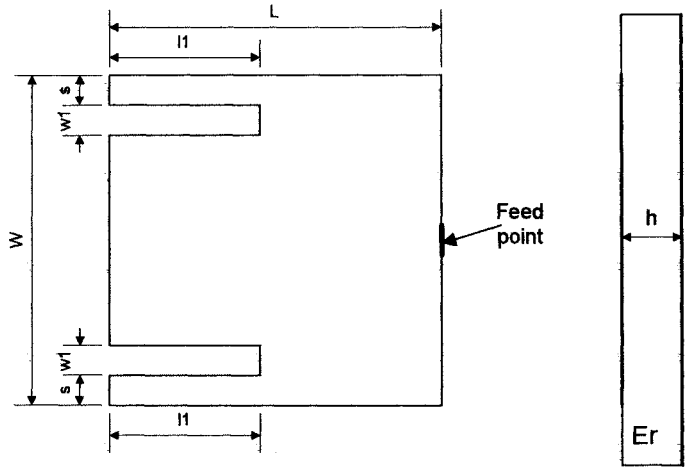

Figure 7.1: New patch structure to create additional mode

The current path of this mode, determined using Ensemble software [92], together with that of the fundamental TM_{01} mode, is shown in figures 7.2a and 7.2b respectively.

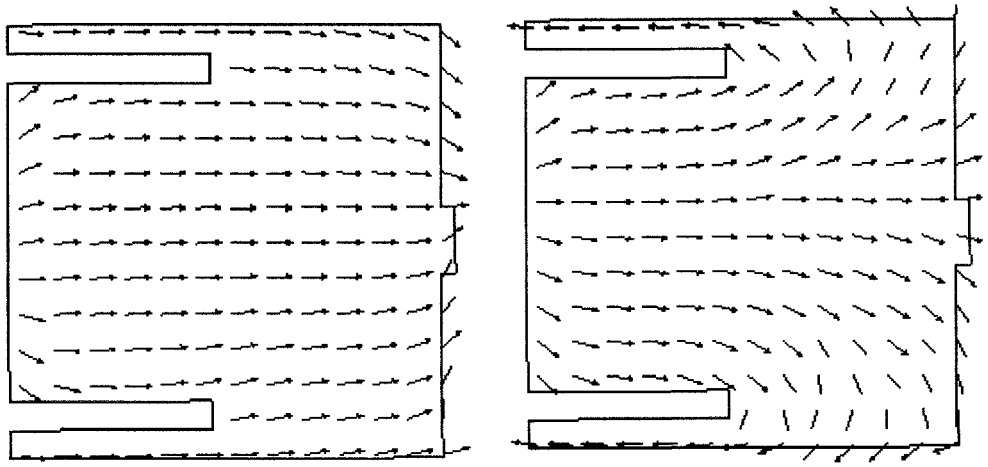

(a) TM_{01} mode
(frequency = 3.19GHz)

(b) $TM_{0\delta}$ mode
(frequency = 2.86GHz)

Figure 7.2: Current path of (a) $TM_{0\delta}$ and (b) TM_{01} modes

As can be seen, the $TM_{0\delta}$ mode follows a different current path to the TM_{01} mode and is thus expected to have a different frequency and impedance response. It is subsequently shown that this mode has a different frequency and impedance response to the fundamental mode. It is also shown in this chapter that with correct selection of slot parameters to excite the correct mode / (s), it is possible to design both single and dual frequency compact patch antennas with a direct planar feed.

7.2 Segmentation Analysis of Proposed Patch

To analyse the structure shown in figure 7.1, the segmentation approach developed in Chapter 4 is applied. Section 7.2.1 fully illustrates the modelling procedure, required to determine the impedance matrix. In section 7.2.2., the antenna is simulated for resonant frequency, input impedance and Q factor. To test the validity of the model, the results are then compared with those obtained using practical measurements.

7.2.1 Patch Decomposition and Synthesis

To model the patch shown below is a four-step procedure, as illustrated in figure 7.3a-d.

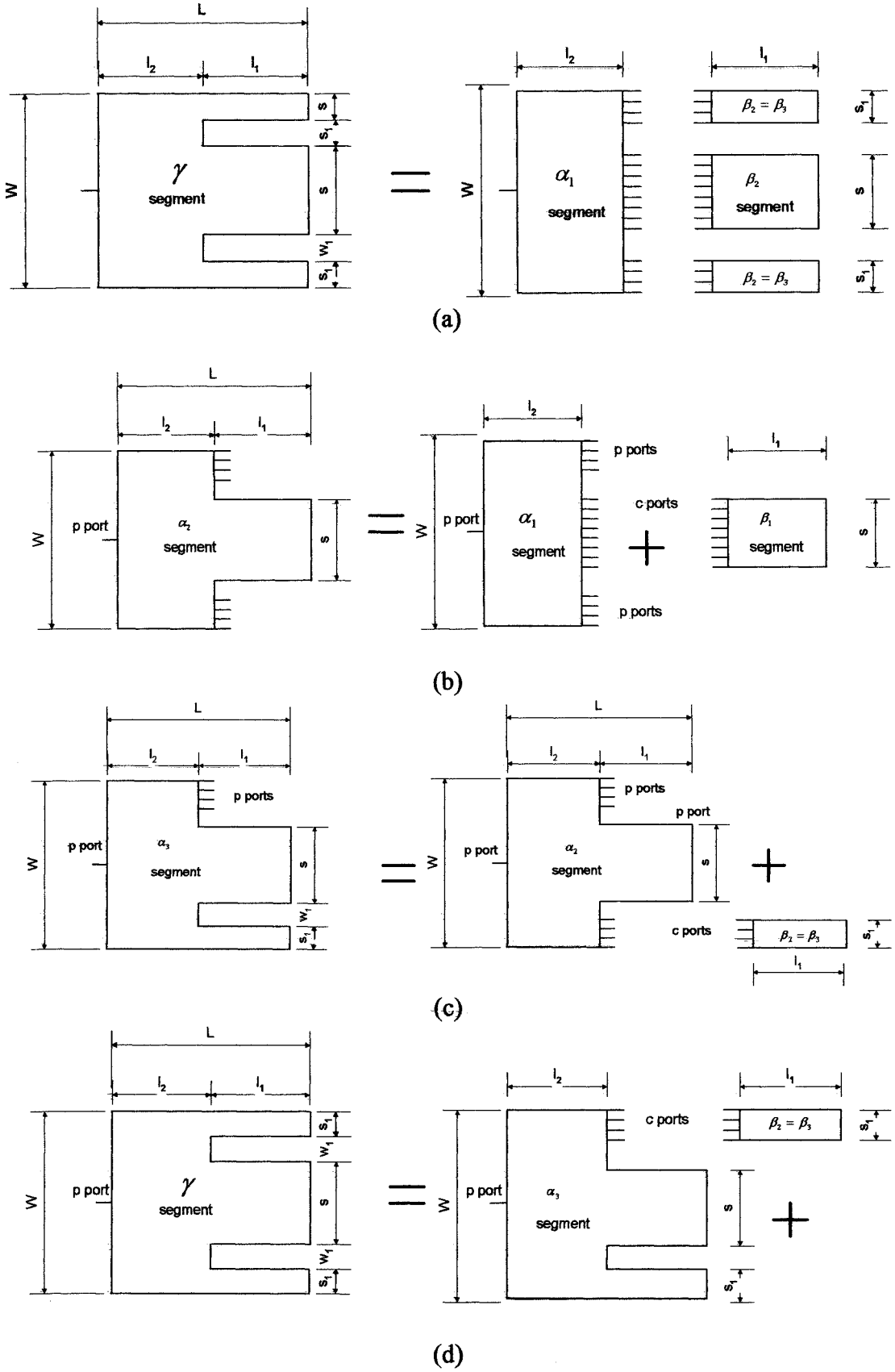

Figure 7.3: Decomposition and synthesis procedure
(a) Step 1: patch decomposed into four rectangular segments
(b) Step 2: synthesis of α_1 and β_1 segments
(c) Step 3: synthesis of α_2 and β_2 segments
(d) Step 4: synthesis of α_3 and β_3 segments

Step 1: Patch Decomposition

The first stage in the modelling process is to decompose the patch into four elemental segments for which Green's Functions are available, as in figure 7.3a. As the patch is symmetrical about the x axis, decomposing the patch in this manner means β_2 and β_3 segments are of equal size with the same number of ports. This will reduce the number of computations required. Steps 2 to 4 involve the synthesis of individual elements, as illustrated in figure 7.3b – 7.3d, to obtain the impedance matrix of the final structure.

Step 2:Determination of α_2 segment by synthesis of α_1 and β_1 segments:

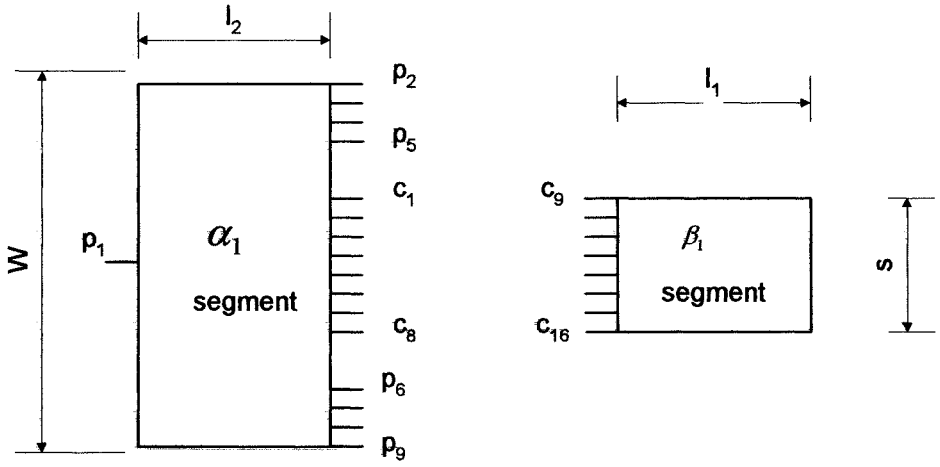

Figure 7.4: Ports of α_1 and β_1 segments

Figure 7.4 illustrates the port labelling of the α_1 and β_1 segments. The C-ports represent the connected ports of both segments and are arranged such that ports C_1 of the α_1 segment is connected to ports C_9 of the β_1 segment, C_2 is connected to C_{10}, etc... The P ports represent the unconnected ports of each segment. The impedance matrix of the α_2 segment is determined by synthesising α_1 and β_1 segments. From (4.49) this is given by:

$$\alpha_2 Z_p = \alpha_2 Z_{pp} - \alpha_2 Z_{pc} \begin{bmatrix} \alpha_2 \Gamma_1 \alpha_2 Z_{cc} \\ \alpha_2 \Gamma_2 \end{bmatrix}^{-1} \begin{bmatrix} \alpha_2 \Gamma_1 \alpha_2 Z_{cp} \\ \alpha_2 0 \end{bmatrix} \qquad (7.1)$$

where:

$\gamma_2 Z_{pp}$ represents the interaction between P ports on both segments

$\gamma_2 Z_{cp}$ represents the interaction between C and P ports on both segments

$\gamma_2 Z_{pc}$ represents the interaction between C and P ports on both segments

$\gamma_2 Z_{cc}$ represents the interaction between C ports on both segments

Step 3:Determination of α_3 segment by synthesis of α_2 and β_2 segments:

To synthesise the α_2 and β_2 segments requires that ports P_2 - P_5 on the α_2 segment be renamed as ports $C_1 - C_4$., as illustrated by figure 7.5a-b.

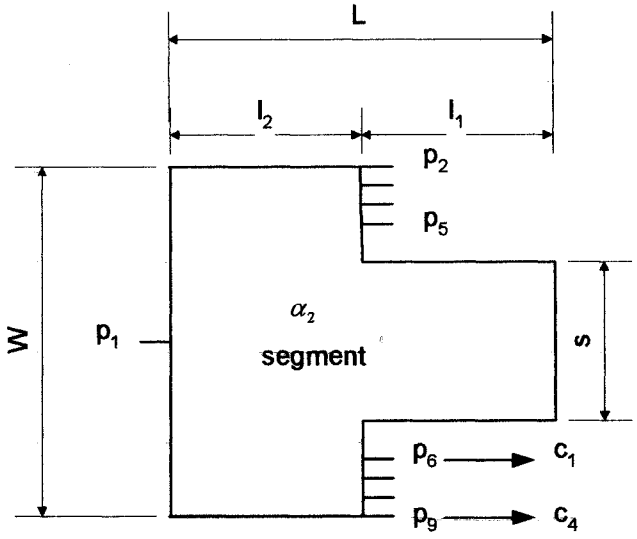

(a)

$$\alpha_2 Z_p = \left[\begin{array}{cccc|cccc} Z_{p1p1} & Z_{p2p1} & Z_{p3p1} & Z_{p4p1} & Z_{p5p1} & Z_{p6p1} & Z_{p7p1} & Z_{p8p1} & Z_{p9p1} \\ Z_{p1p2} & Z_{p2p2} & Z_{p3p2} & Z_{p4p2} & Z_{p5p2} & Z_{p6p2} & Z_{p7p2} & Z_{p8p2} & Z_{p9p2} \\ Z_{p1p3} & Z_{p2p3} & Z_{p3p3} & Z_{p4p3} & Z_{p5p3} & Z_{p6p3} & Z_{p7p3} & Z_{p8p3} & Z_{p9p3} \\ Z_{p1p4} & Z_{p2p4} & Z_{p3p4} & Z_{p4p4} & Z_{p5p4} & Z_{p6p4} & Z_{p7p4} & Z_{p8p4} & Z_{p9p4} \\ Z_{p1p5} & Z_{p2p5} & Z_{p3p5} & Z_{p4p5} & Z_{p5p5} & Z_{p6p5} & Z_{p7p5} & Z_{p8p5} & Z_{p9p5} \\ \hline Z_{p1p6} & Z_{p2p6} & Z_{p3p6} & Z_{p4p6} & Z_{p5p6} & Z_{p6p6} & Z_{p7p6} & Z_{p8p6} & Z_{p9p6} \\ Z_{p1p7} & Z_{p2p7} & Z_{p3p7} & Z_{p4p7} & Z_{p5p7} & Z_{p6p7} & Z_{p7p7} & Z_{p8p7} & Z_{p9p7} \\ Z_{p1p8} & Z_{p2p8} & Z_{p3p8} & Z_{p4p8} & Z_{p5p8} & Z_{p6p8} & Z_{p7p8} & Z_{p8p8} & Z_{p9p8} \\ Z_{p1p9} & Z_{p2p9} & Z_{p3p9} & Z_{p4p9} & Z_{p5p9} & Z_{p6p9} & Z_{p7p9} & Z_{p8p9} & Z_{p9p9} \end{array}\right]$$

$\alpha_2 Z_{pp}$ $\alpha_2 Z_{cp}$ $\alpha_2 Z_{pc}$ $\alpha_2 Z_{cc}$

(b)

Figure 7.5: (a) Conversion of p ports to c ports on α_2 segment
(b) with relevant impedance matrix

Figure 7.6 illustrates the port labelling of the α_2 and β_2 segments. The C-ports represent the connected ports of both segments and are arranged such that ports C_1 of the α_2 segment is connected to ports C_5 of the β_2 segment, C_2 is connected to C_6, etc... The P ports represent the unconnected ports of each segment.

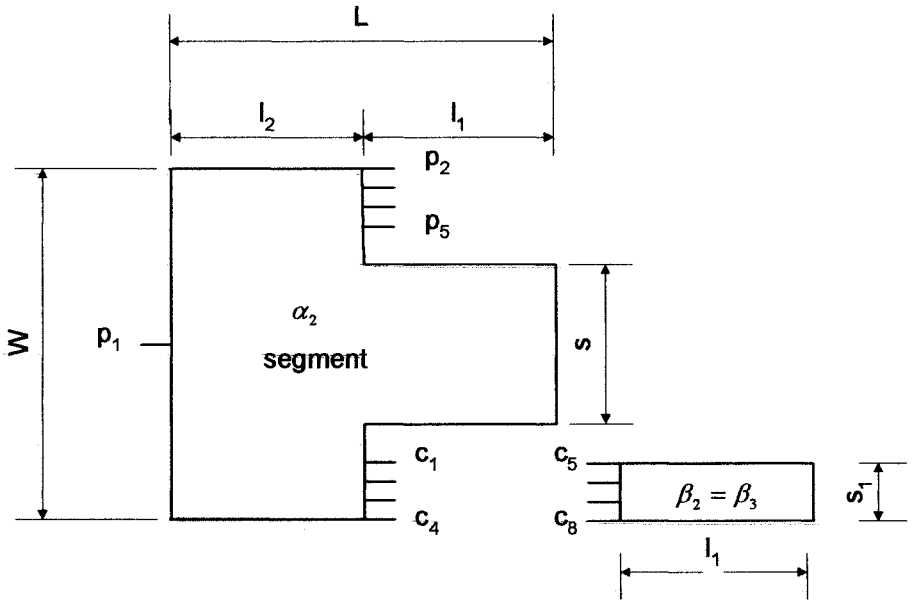

Figure 7.6: Ports of α_2 and β_2 segments

The impedance matrix of the α_3 segment is determined by synthesising α_2 and β_2 segments. From (4.49) this is given by:

$$\alpha_3 Z_p = \alpha_3 Z_{pp} - \alpha_3 Z_{pc} \begin{bmatrix} \alpha_3 \Gamma_1 \alpha_3 Z_{cc} \\ \alpha_3 \Gamma_2 \end{bmatrix}^{-1} \begin{bmatrix} \alpha_3 \Gamma_1 \alpha_3 Z_{cp} \\ \alpha_3 0 \end{bmatrix} \qquad (7.2)$$

Step 4:Determination of γ segment by synthesis of α_3 and β_3 segments:

To synthesise α_3 and β_3 segments, requires that ports P_2 - P_5 on the α_3 segment be renamed as ports $C_1 - C_4$., as illustrated by figure 7.7a-b.

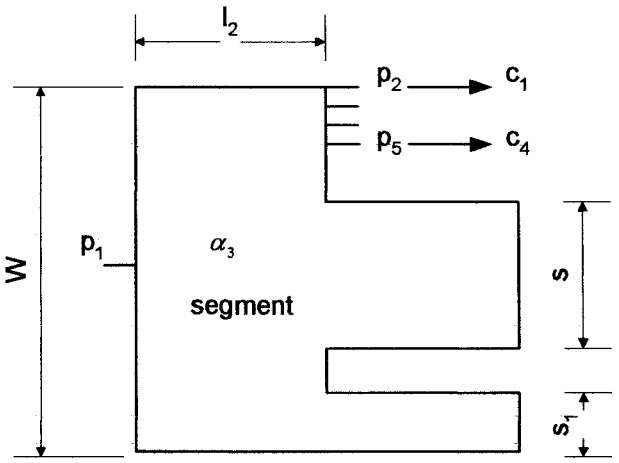

(a)

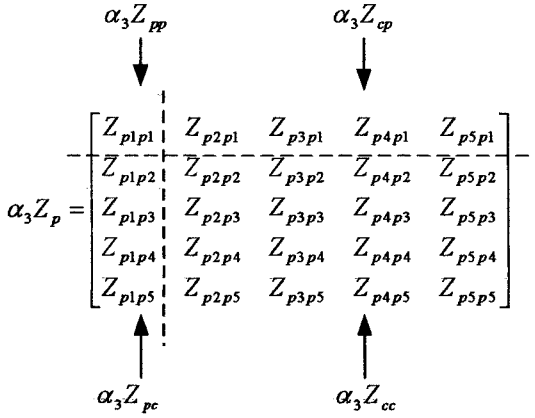

(b)

Figure 7.7: (a) Conversion of P ports to C ports on α_3 segment
(b) with relevant impedance matrix

The Z-parameters of the final patch design can now be obtained by synthesising both α_3 and β_3 segments, as shown in figure 7.8.

Figure 7.8 illustrates the port labelling of the α_3 and β_3 segments. The C-ports represent the connected ports of both segments and are arranged such that ports C_1 of the α_3 segment is connected to ports C_5 of the β_3 segment, C_2 is connected to C_6, etc... The P ports represent the unconnected ports of each segment.

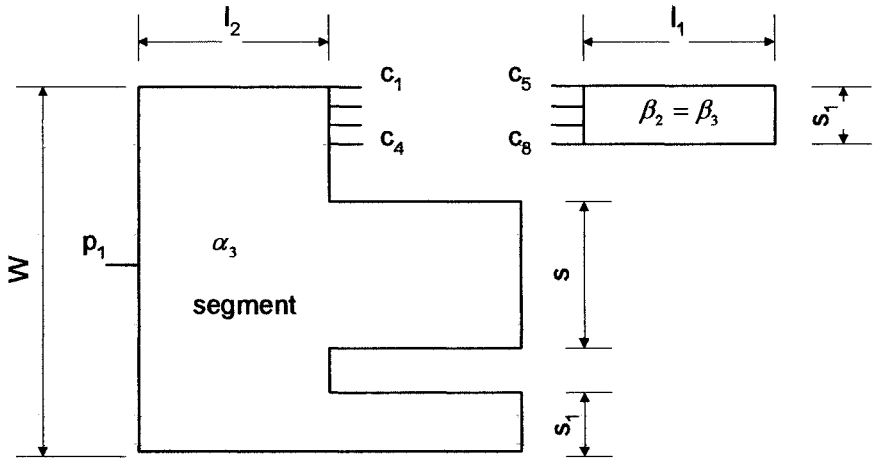

Figure 7.8: Ports of α_2 and β_2 segments

The impedance matrix of the γ segment is determined by synthesising α_3 and β_3 segments. From (4.67) this is given by:

$$\gamma Z_p = \gamma Z_{pp} - \gamma Z_{pc}\begin{bmatrix}\gamma\Gamma_1\gamma Z_{cc}\\ \gamma\Gamma_2\end{bmatrix}^{-1}\begin{bmatrix}\gamma\Gamma_1\gamma Z_{cp}\\ \gamma 0\end{bmatrix} \tag{7.3}$$

where

γZ_{pp} represents the interaction between P ports on both segments

γZ_{cp} represents the interaction between C and P ports on both segments

γZ_{pc} represents the interaction between P and C ports on both segments

γZ_{cc} represents the interaction between C ports on both segments

The expressions for the interaction between ports have been developed previously in Chapter 4, and are given in Appendix 4B.

7.2.2 Simulated and Practical Results

With reference to figure 7.3, in the initial formulation of the problem, the following number of interconnecting ports were shown to give improved results:

- from figure 7.4, 8 C interconnecting C ports between α_1 and β_1 segments, each with a port width of 0.1 mm.

- from figure 7.5, 4 C interconnecting C ports between α_2 and β_2 segments, each with a port width of 0.1 mm.
- From figure 7.7, 4 C interconnecting C ports between α_3 and β_3 segments, each with a port width of 0.1 mm.

Graphs of real and imaginary input impedance versus frequency are shown in figure 7.9a and 7.9b respectively. For comparison the frequency response of a conventional square patch with the same length and width.

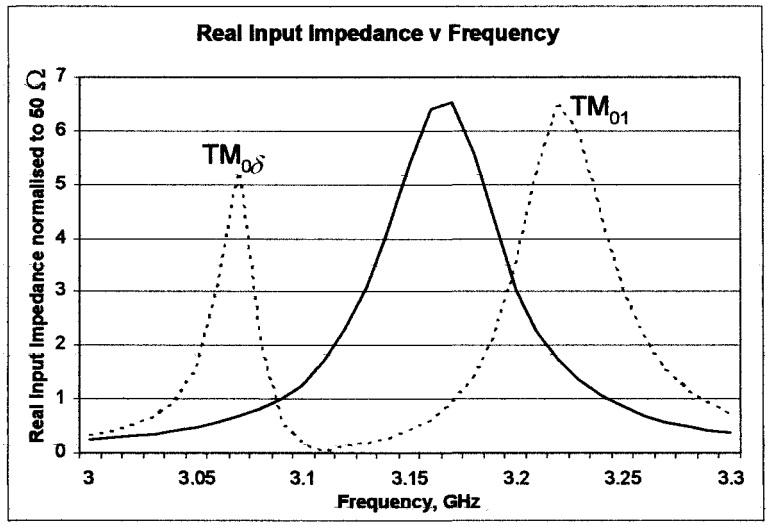

(a)

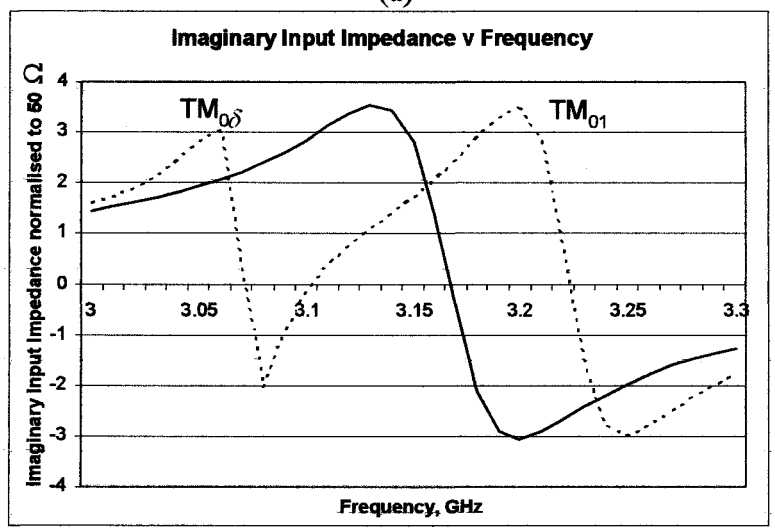

(b)

$\varepsilon_r = 2.33$, $h = 1.57$ mm, $L = W = 30$ mm, $l_1 = 16$ mm, $w_1 = 1$ mm, $s = 1$mm

——— conventional square patch antenna ------ slot loaded design

Figure 7.9: Comparison of frequency response of proposed slot loaded patch design and conventional square patch antenna
(a) real and (b) imaginary input impedance

From the graphs in figure 7.9, the resonant frequency, input impedance and Q factor of this mode can be determined using the same procedure outlined in section 4.4. These are illustrated in table 7.1.

	f_{01} (GHz)	Z_{in01} (Ω)	Q_{01}	$f_{0\delta}$ (GHz)	$Z_{in0\delta}$ (Ω)	$Q_{0\delta}$
Proposed Design	3.22	322	53	3.07	262	140
Conventional Square Patch	3.17	327	52	NA	NA	NA

Table 7.1: Circuit characteristics of compact patch antenna obtained using both segmentation and practical measurements

The results clearly indicate that the insertion of slots parallel to the non-radiating edges creates an additional $TM_{0\delta}$ mode.

7.3 Compact Patch Antenna Analysis and Design

In this section, a comprehensive evaluation of the effect of slot parameters on the circuit characteristics is presented and discussed. It is demonstrated that with proper selection of inserted slits, together with slot loading of correct dimensions, a patch antenna can be designed to operate using this $TM_{0\delta}$ mode, with a resonant frequency below that of the fundamental mode, thus reducing the element size. An input impedance of 50 Ω can also be achieved, which facilitates the use of a direct planar feed, thus removing the requirement for an external matching network. Following this, the design technique and results for the two configurations are detailed, in which it is demonstrated that size reduction of up to 40% can be achieved. The patch is designed for use on RTDuroid 5870. The relevant data for this substrate is shown in Appendix A.

7.3.1 Patch Design A

The first design is shown in figure 7.10.

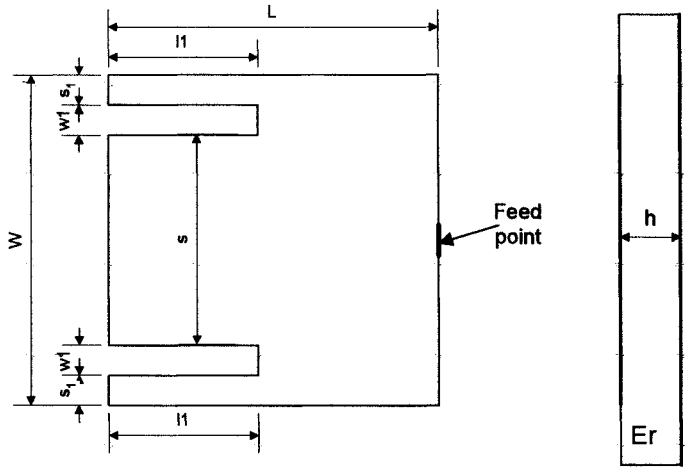

Figure 7.10: Compact patch configuration - Design A

In patch antenna design, important circuit considerations are resonant frequency, input impedance and Q factor. Assuming the patch length and width are fixed, these characteristics are controlled by slot length, l_1, slot width, w_1, and slot distance from the edge, s. To this end, the following section will perform a detailed parametric analysis on each of the aforementioned slot dimensions, modelling the effect on circuit characteristics. To achieve this, the modelling procedure described in section 7.2.1 has been employed.

7.3.1.1 Effect of slot parameters on resonant frequency

Figure 7.11a-b illustrates the effect of slot length on resonant frequency of the $TM_{0\delta}$ mode. In figure 7.11 (a), the slot distance from the relative patch edge, s_1, is fixed at 1 mm, and parametric analysis is performed on slot length l_1 for increasing values of slot width w_1. In figure 7.11 (b), the slot width w_1 is fixed at 1 mm, and parametric analysis is performed on slot length, for decreasing values of slot separation, s.

To provide a reference, the effect of slot length on the circuit characteristics of the fundamental TM_{01} (f_{01}) mode is also shown. In this case, the values of s_1 and w_1 were fixed at 1 mm.

These results were obtained using the following formulae:

The impedance matrix of the patch structure is given by (7.3). From this, the input impedance can be determined using:

$$Z_{in} = \gamma Z_{p_{0,0}} = Z_{p1\,p1} \tag{7.4}$$

from (4.35) the resonant frequency of the patch occurs when:

$$\text{Imag}\{Z_{in}\} = 0 \tag{7.5}$$

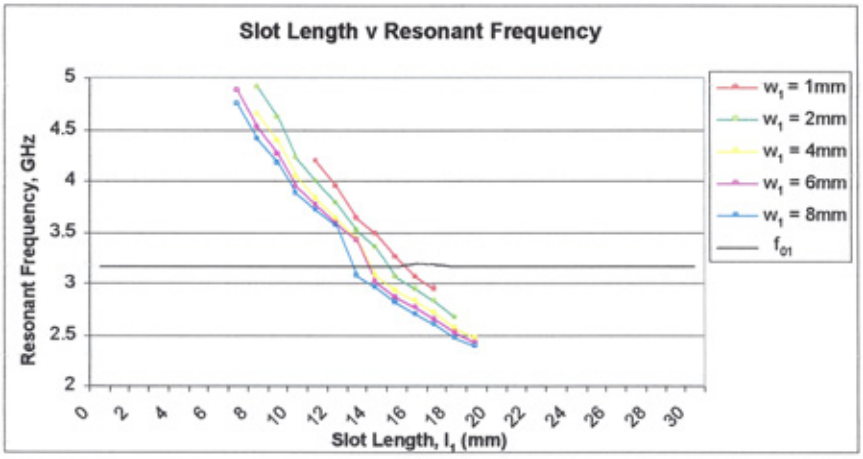

$\varepsilon_r = 2.33$, $h = 1.57$ mm, $L = W = 30$ mm, $s_1 = 1$ mm

(a)

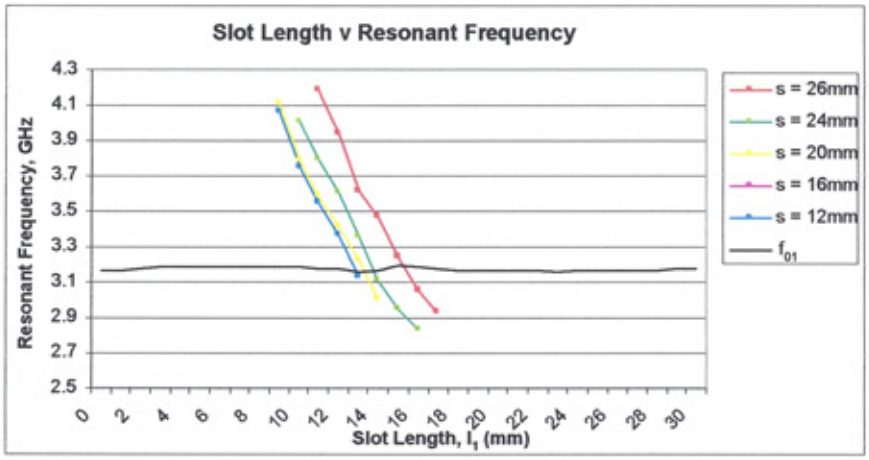

$\varepsilon_r = 2.33$, $h = 1.57$ mm, $L = W = 30$ mm, $w_1 = 1$ mm

(b)

Figure 7.11: Effect of slot length l_1 on resonant frequency
(a) parametric Analysis w_1
(b) parametric Analysis s

Considering the effect on the TM_{01} mode, the graphs illustrate that the slot length has negligible effect on this mode. From the analysis of slot loading on the TM_{01} mode detailed in Chapter 5, this relationship has already been determined.

Analysing the effect of slot length on the $TM_{0\delta}$ mode, the first point of note is that to create an additional $TM_{0\delta}$ mode the slot length must take on a certain value. Both graphs confirm the theory stated previously about the current path taken by the $TM_{0\delta}$ mode. This is evidenced by the fact that resonant frequency decreases with slot length l_1. It can also be seen that when the slot length l_1 is approximately equal to half of the patch length, the resonant frequency of the TM_{01} and $TM_{0\delta}$ mode are approximately equal. This suggests that the length of current path taken by both modes are approximately equal at this point, further confirming the prediction regarding the $TM_{0\delta}$ current path.

From figure 7.11a, it can also be seen that by increasing the slot width, this effectively lengthens the current path of the $TM_{0\delta}$ mode, and hence reducing its resonant frequency. This trend is expected given the current path of this mode. From figure 7.11b, as the slot separation s decreases, the slots effectively move closer together. When this occurs, there is less degree of freedom to tune the frequency of the $TM_{0\delta}$ mode with increasing values of s. Furthermore, in order to create the additional mode, the value of slot length becomes increasingly critical.

7.3.1.2 Effect of slot parameters on Input Impedance

Figure 7.12a-b illustrates the effect of slot length on input impedance of the $TM_{0\delta}$ mode. In figure 7.12(a), the slot distance from the relative patch edge, s_1, is fixed at 1 mm, and parametric analysis is performed on slot length l_1 for increasing values of slot width. In figure 7.12 (b), the slot width w_1 is fixed at 1mm, and parametric analysis is performed on slot length, for decreasing values of slot

separation, s. In both graphs only values of slot length required to create the additional $TM_{0\delta}$ mode, determined in figure 7.11, are illustrated.

To provide a reference, the effect of slot length on the circuit characteristics of the fundamental TM_{01} mode is shown. In this case, the values of s_1 and w_1 were fixed at 1 mm.

These results were obtained using the following formulation:

Equations (7.4) gives the input impedance as a function of frequency. Equation (4.35) is then used to obtain the real input impedance at resonance.

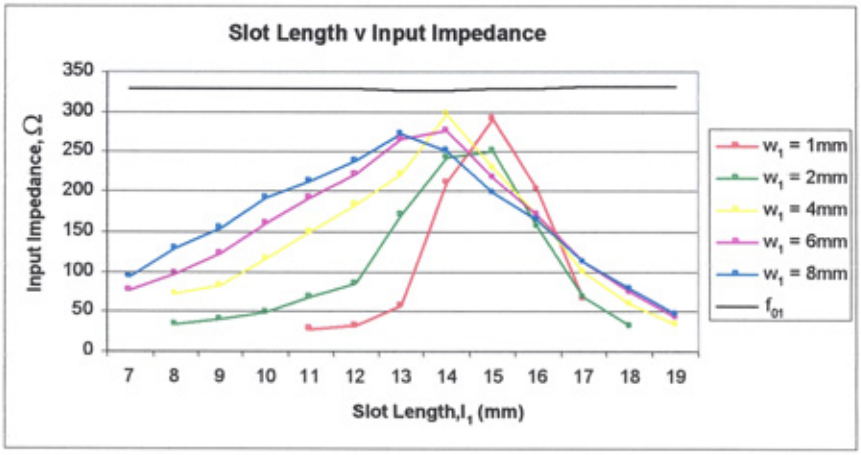

$\varepsilon_r = 2.33$, $h = 1.57$ mm, $L = W = 30$ mm, $s_1 = 1$ mm

(a)

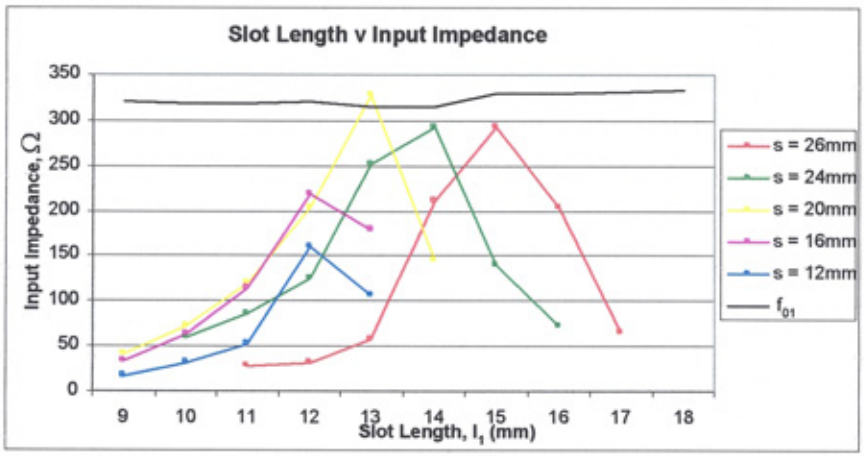

$\varepsilon_r = 2.33$, $h = 1.57$ mm, $L = W = 30$ mm, $w_1 = 1$ mm

(b)

Figure 7.12: Effect of slot length l_1 on input impedance
(a) parametric analysis w_1
(b) parametric analysis s

Considering the effect of slot length on the input impedance of the TM_{01} mode, the graphs illustrate that the slot length has negligible effect on this mode. Regarding the effect on the $TM_{0\delta}$ mode, from figure 7.12, two distinct trends are evident, depending on the values of slot length. Firstly, the value of input impedance appears to increase in value with slot length, this occurs until the value of l_1 is approximately equal to the patch length L. At this point, the input impedance of the $TM_{0\delta}$ mode is approximately equal to that of the TM_{01} mode. When the slot length s greater than half patch length L, the input impedance of the $TM_{0\delta}$ mode decreases with increasing slot length.

Regarding the effect of slot width on the input impedance of the $TM_{0\delta}$ mode, increasing the slot length effectively narrows the path for the current flow. Given the fact that an inverse relationship exists between patch width and input impedance for a standard patch antenna operating in the TM_{01} mode, a similar relationship is expected to exist for the $TM_{0\delta}$ mode between slot width and input impedance. This is evidenced by figure 7.12a, which illustrates that for a given slot length the input impedance of the $TM_{0\delta}$ mode increases with slot width.

7.3.1.3 Effect of slot parameters on Q factor

Figure 7.13a-b illustrates the effect of slot length on Q factor of the $TM_{0\delta}$ mode. In figure 7.13 (a), the slot distance from the relative patch edge s_1 is fixed at 1 mm, and parametric analysis is performed on slot length l_1 for increasing values of slot width. In figure 7.13 (b), the slot width w_1 is fixed at 1mm, and parametric analysis is performed on slot length, for decreasing values of slot separation. In both graphs only values of slot length required to create the additional $TM_{0\delta}$ mode, determined in figure 7.11, are illustrated.

To provide a reference, the effect of slot length on the Q factor of the fundamental TM_{01} mode is shown. In this case, the values of s_1 and w_1 were fixed at 1mm.

These results were obtained by substituting (4.36) into (7.4).

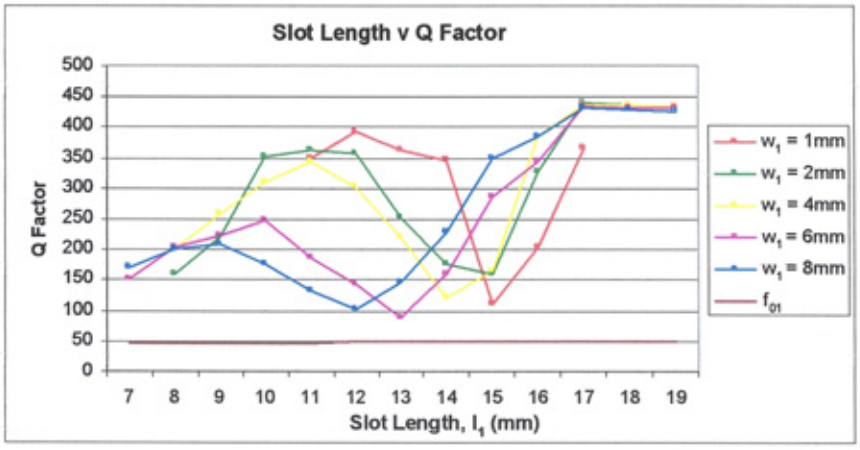

$\varepsilon_r = 2.33$, $h = 1.57$ mm, $L = W = 30$ mm, $s_1 = 1$ mm
(a)

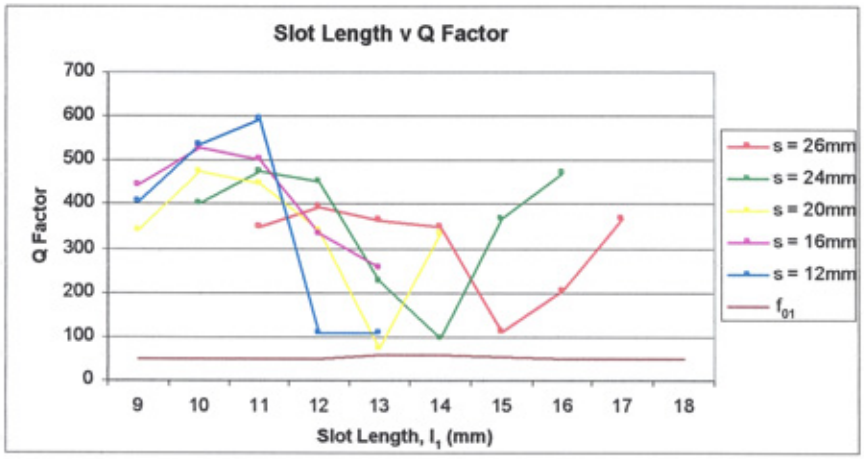

$\varepsilon_r = 2.33$, $h = 1.57$ mm, $L = W = 30$ mm, $w_1 = 1$ mm
(b)

Figure 7.13: Effect of slot length l_1 on Q factor
(a) parametric analysis w_1
(b) parametric analysis s

As with previous trends, the slot length has negligible effect on the Q factor of the TM_{01} mode. From figure 7.13a-b, as with the case of resonant frequency and input impedance one definite trend is evident. Namely, the Q factor of the $TM_{0\delta}$ mode appears to approach that of the TM_{01} mode when the slot length is approximately equal to half the patch length.

7.3.1.4 Patch A design procedure

From the results described above it can be seen that there are a number of parameters that affect the resonant frequency, input impedance and Q factor of the

$TM_{0\delta}$ mode. In fact there is no one unique solution for a given design. However, a number of general conclusions about the general effect of slot parameters on patch design can be established.

With reference to the value of slot separation, from figure 7.11b, placing the slots close to the non-radiating edges of the patch increases the effect of slot length on resonant frequency. This gives greater freedom to tune the frequency of the $TM_{0\delta}$ mode. In view of this, for ease of design s_1 has been fixed at 1 mm in the following designs.

Considering the effect of slot width, from figures 7.12a-b, for a given slot length, the input impedance of the $TM_{0\delta}$ mode appears to increase with slot width. Given that the aim of this patch design is to achieve low input impedance of 50 Ω for direct planar matching, it is felt that the value of w_1 should be kept below 4 mm. In view of the constraints on slot separation and slot width, for design purposes only graphs of slot length versus resonant frequency and input impedance $TM_{0\delta}$ characteristics are required. For convenience, these are reproduced in figures 7.14a-b.

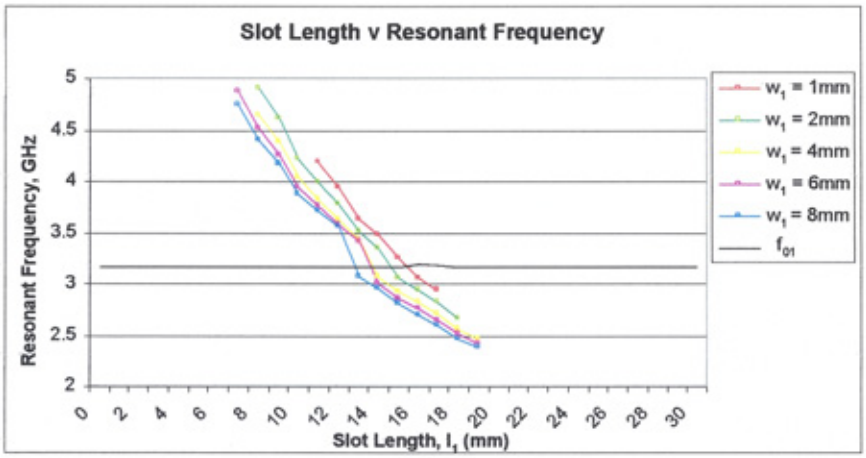

$\varepsilon_r = 2.33$, $h = 1.57$ mm, $L = W = 30$ mm, $s_1 = 1$ mm

(a)

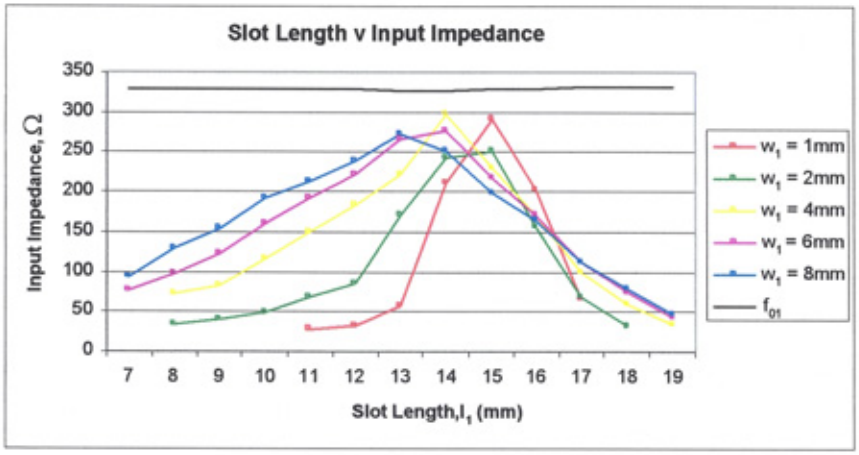

$\varepsilon_r = 2.33$, $h = 1.57$ mm, $L = W = 30$ mm, $s_1 = 1$ mm
(b)

Figure 7.14: Effect of slot length l_1 on (a) resonant frequency and (b) input impedance (parametric analysis w_1)

The first design, shown in Figure 7.15, consists of a square patch of length L, with two peripheral slits of length l_1 and width w_1 parallel to the non-radiating patch edge, separated by distance s from each other and at a distance s_1 from each relative patch edge. The patch is directly excited by a 50 Ω planar microstrip feed-line.

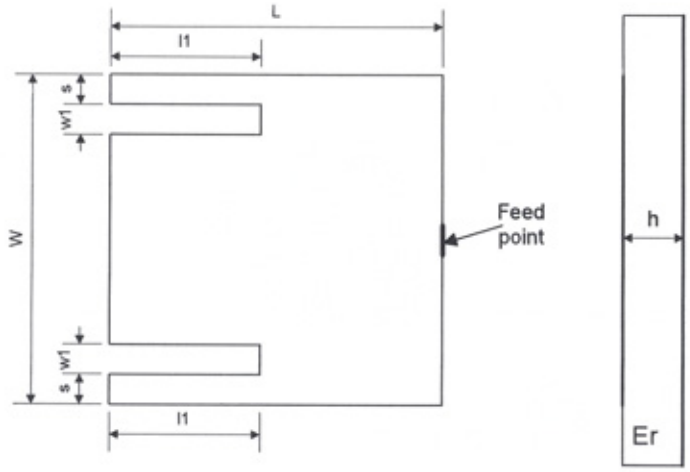

Figure 7.15: Patch design A

When designing the reduced size antenna, maximum reduction in resonant frequency must be achieved whilst simultaneously achieving an input impedance of 50 Ω. From figures 7.14a, it is shown that to create a TM_{08} below the fundamental TM_{01}

mode, the slot length must be greater than half the patch length. At this stage, from figure 7.14b, the input impedance decreases with slot length. For ease of design and proof of concept, it has been decided to keep slot width fixed at 2 mm, and simply increase the slot length until the impedance is reduced to the required value. The value of slot length then determines the resonant frequency, and hence size reduction.

7.3.1.5 Practical results and discussion

Prototypes of the proposed design (Design A), together with a reference antenna were fabricated on RTDuroid 5870 with a permittivitty of 2.33 and a thickness of 1.57 mm. Design A was fed with a direct 50 Ω microstrip-line with patch dimensions as shown in figure 7.16a. The reference antenna, shown in figure 7.16(b) was a square patch of $L = 30$ mm, fed by a quarter-wave matching network.

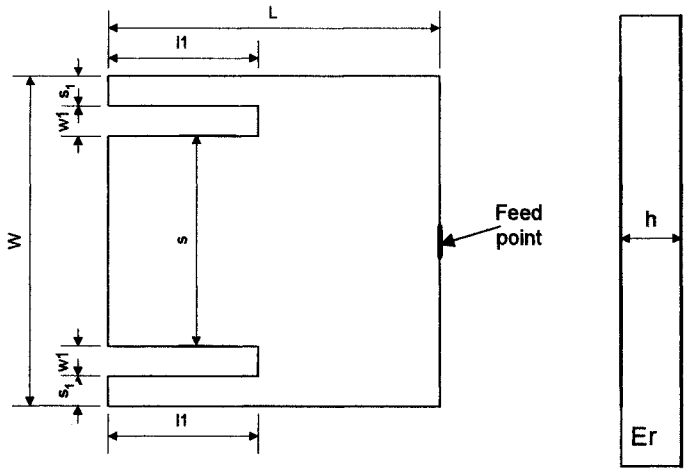

$L = 30$ mm, $W = 30$ mm, $l_1 = 17.1$ mm, $w_1 = 2$ mm, $s = 24$ mm, $s_1 = 1$ mm, $\varepsilon_r = 2.33$, $h = 1.57$ mm

(a)

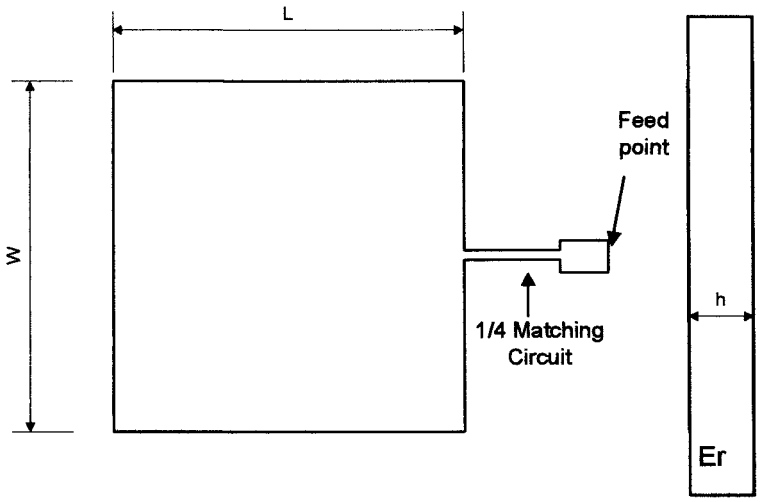

$L = W = 30$ mm, $\varepsilon_r = 2.33$, $h = 1.57$ mm

(b)

Figure 7.16: Patch configurations for (a) design A and (b) reference antenna

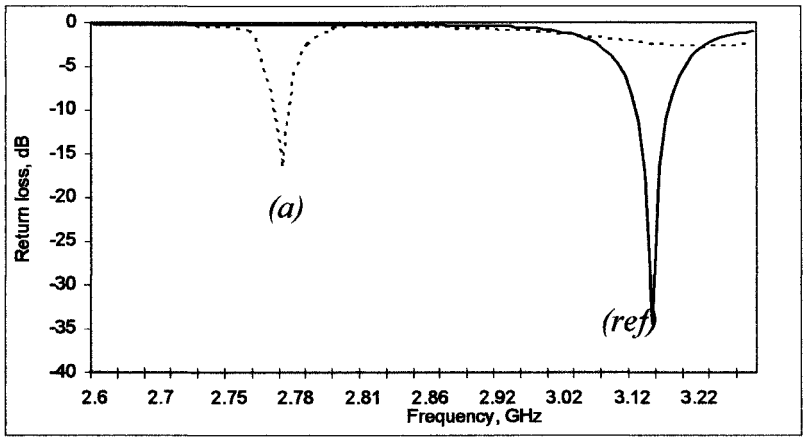

Figure 7.17: Return loss v frequency for (a) design A, and (b) reference antenna (*ref*)

Figure 7.17 shows the return loss versus resonant frequency for both antennas. It can be seen that the proposed design achieves a resonant frequency of 2.772 GHz with a return loss of better than -15 dB. This corresponds to a size reduction of 12% in terms of area.

Table 7.2 show the practical results for the proposed antenna designs, together with the reference antenna. Plots of the radiation patterns for both designs are illustrated in Fig. 7.18.

	Design A	Reference Antenna
Resonant Frequency (GHz)	2.778	3.15
Size Reduction (%)	12	NA
Return Loss (dB)	-16.5	-35
VSWR Bandwidth (%)	1.25	1.904
Input Impedance (Ω)	50	330
Measured Gain (dB)	4.2	6.1

Table 7.2: Practical results for design A

The table illustrates that size reduction of 12% has been achieved, but at the expense of decreased gain and reduced bandwidth. Considering the VSWR bandwidth, the results indicate that the proposed design suffers from a reduction when compared to a standard reference patch. This trend is evident for slot loaded compact antennas discussed in Chapter 5, in which it was described that an inverse relationship exists between VSWR BW and size reduction. The table also illustrates a reduced gain, which is attributed to the reduced patch volume.

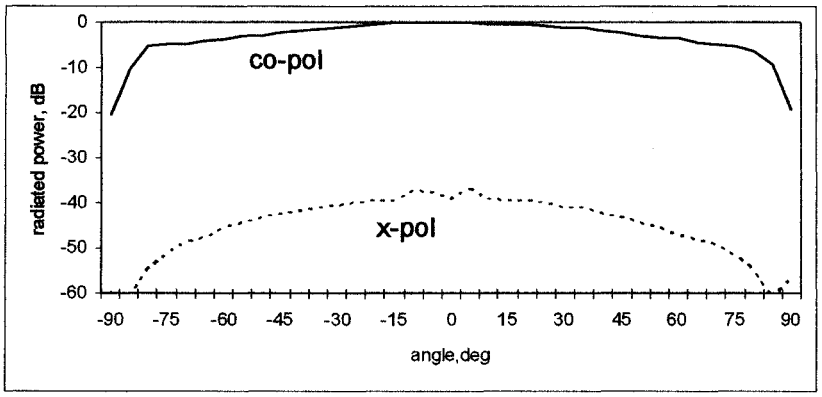

(a)

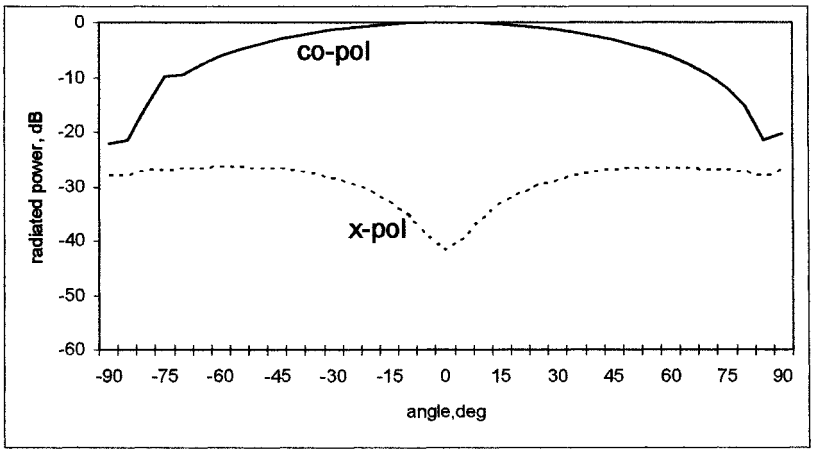

(b)

Figure 7.18: Radiation pattern for design A (a) E-plane and (b) H-plane

Figure 7.18(a) and (b) show the E-plane and H-plane radiation for design A. Good broadside radiation is observed with a cross-polarisation level of below -20 dB in both the E and H-planes, relative to co-polar on-axis.

7.3.2 Patch Design B

An extension of this design, which incorporates a further slot, of length l_2 and width w_2 placed in the patch centre, is shown in Figure 7.19. This technique has been used in other designs to lower the resonant frequency of the fundamental mode(s) by lengthening its current path [51,66,70,71,128,130]. A direct trade-off of this is a significant increase in input impedance with slot length l_2. However, in this design, the centre slot is used to perturb the current path of the $TM_{0\delta}$ mode. It is subsequently shown in section 7.3.3 that greater size reduction can be achieved using this structure.

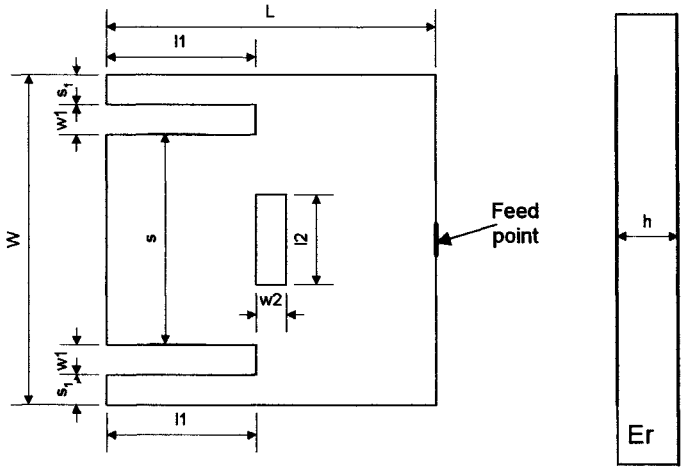

Figure 7.19: Compact patch configuration – design B

The purpose of the following section, is to determine the effect of the centre slot dimensions on circuit characteristics: resonant frequency, input impedance and Q factor. From results obtained in Chapter 5 the effect of slot dimensions on TM_{01} mode was investigated. It was concluded that slot width has little effect on the current path of the TM_{01} mode, and hence resonant frequency, input impedance and Q factor. As the purpose of the design in this section is to lengthen the current path of the $TM_{0\delta}$ mode slot width also has little effect on the $TM_{0\delta}$ mode, hence the main controlling parameter for this mode is the slot length l_2. Considering these factors, the slot width w_2 was fixed at 1 mm. To this end, the effect of slot length l_2 on the aforementioned circuit characteristics is performed. It is subsequently shown that employment of this patch structure can produce element size reduction of up to 40%, whilst still allowing the use of a direct planar feed.

Figure 7.20 – 7.22 illustrate the effect of centre slot length l_2 on the resonant frequency, input impedance and Q factor of the $TM_{0\delta}$ mode respectively. To achieve this, the modelling procedure described in section 7.2.1 has been employed. In all cases, the values of all other patch parameters are fixed at values shown. The patch is designed for use on RTDuroid 5870. The relevant data for this substrate is shown in Appendix A.

7.3.2.1 Effect of l_2 on resonant frequency

The graph in figure 7.20, illustrates the effect of slot length l_2 on resonant frequency, confirming the prediction that the insertion of a centre slot lengthens the current path of the additional $TM_{0\delta}$, thus reducing its resonant frequency. These results were obtained using equation (7.4).

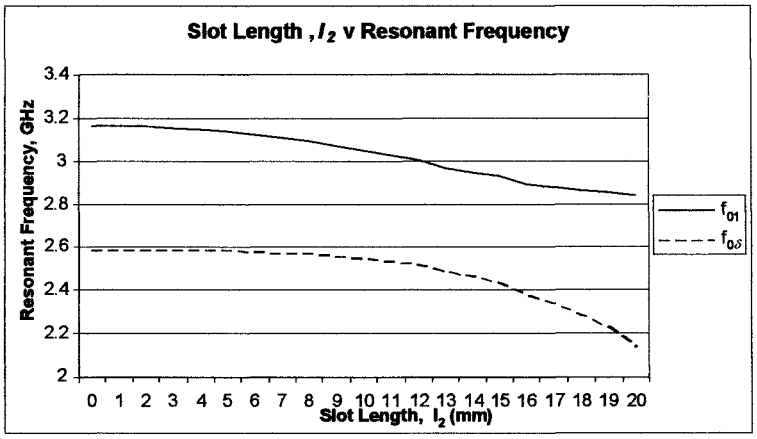

$\varepsilon_r = 2.33$, $h = 1.57$ mm, $L = W = 30$ mm, $l_1 = 18$ mm, $w_1 = 2$ mm, $s = 24$ mm, $s_1 = 2$ mm, $w_2 = 1$ mm

Figure 7.20: Effect of slot length l_2 on resonant frequency of TM_{01} and $TM_{0\delta}$ mode

7.3.2.2 Effect of l_2 on input impedance

The graph in figure 7.21, illustrates the effect of slot length l_2 on input impedance, and indicates an increase in input impedance of both modes with slot length. The relationship between slot length and TM_{01} characteristics have already been determined in Chapter 5. However, as the patch is operating in the $TM_{0\delta}$ mode, the effect on this mode is of more interest. These results were obtained using the following formulation. Equations (7.4) gives the input impedance as a function of frequency. Equation (4.35) is then used to obtain the real input impedance at resonance.

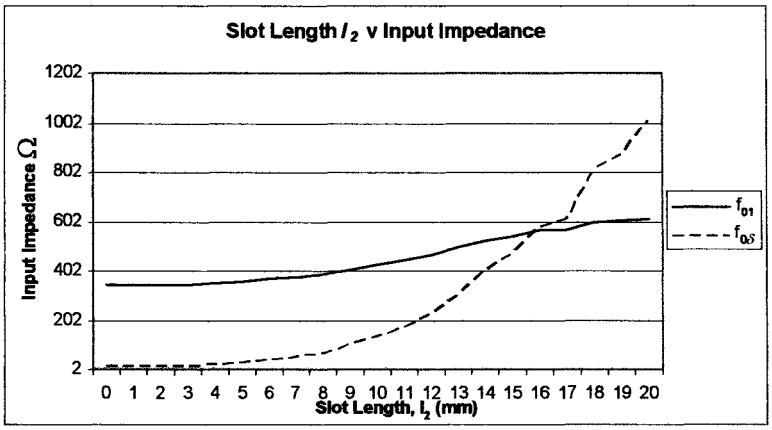

$\varepsilon_r = 2.33$, $h = 1.57$ mm, $L = W = 30$ mm, $l_1 = 18$ mm, $w_1 = 2$ mm, $s = 24$ mm, $s_1 = 2$ mm, $w_2 = 1$ mm

Figure 7.21: Effect of slot length l_2 on input impedance of TM_{01} and $TM_{0\delta}$ mode

7.3.2.3 Effect of l_2 on Q factor

The graph in figure 7.22 illustrates the effect of slot length on the Q factor of both modes. It can be seen that the TM_{01} Q factor increases with slot length, which is consistent with the results determined in Chapter 5. This represents one of the fundamental problems with reduced size slot loaded patch designs. Conversely, the Q factor of the $TM_{0\delta}$ mode appears to decrease with slot length. This relationship provides increased bandwidth, which is a major benefit for practical applications. These results were obtained by substituting (4.36) into (7.4).

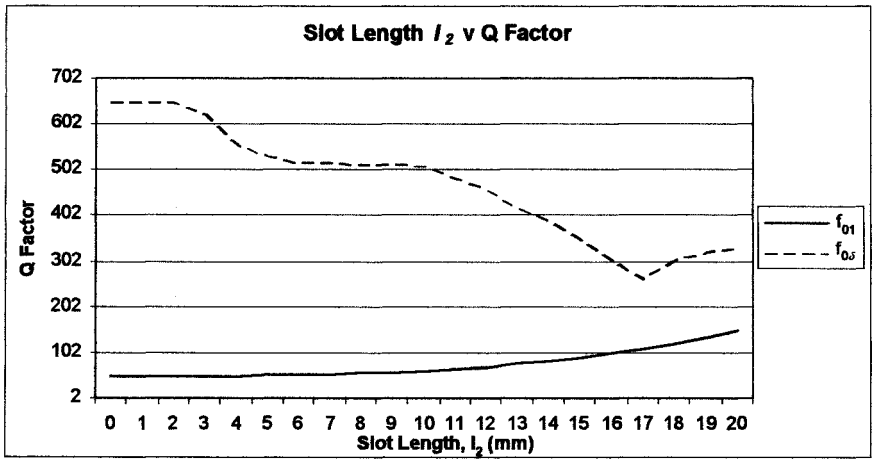

$\varepsilon_r = 2.33$, $h = 1.57$ mm, $L = W = 30$ mm, $l_1 = 18$ mm, $w_1 = 2$ mm, $s = 24$ mm, $s_1 = 2$ mm, $w_2 = 1$ mm

Figure 7.22: Effect of slot length l_2 on Q factor of TM_{01} and $TM_{0\delta}$ mode

7.3.2.4 Patch B Design Procedure

The results in the above section illustrate that a reduction in frequency and Q factor occur with increased centre slot length l_2. However, an increased input impedance also occurs with slot length. For practical applications, an input impedance of 50 Ω is required. For designs purposes the results in table 7.3, illustrate the correlation between side slot lengths l_1, centre slot length l_2 required to produce the required value of input impedance of approximately 50 Ω for the $TM_{0\delta}$ mode. It can be seen that increasing the side slot lengths l_1, can compensate for an increased input impedance with centre slot length l_2.

l_2 (mm)	l_1 (mm)	Input Impedance (Ω)	Frequency (GHz)
0	17.1	51	2.928
2	17.1	53	2.926
4	17.3	51	2.924
6	17.6	54	2.734
8	18.8	48	2.64
10	20	50	2.476
12	21	54	2.388

$\varepsilon_r = 2.33$, $h = 1.57$ mm, $L = W = 30$ mm, $w_1 = 2$ mm, $s = 24$ mm, $s_1 = 2$ mm, $w_2 = 1$ mm

Table 7.3: Correlation between l_1 and l_2

Using this table, a typical patch antenna operating in the $TM_{0\delta}$ mode has been implemented.

7.3.2.5 Practical results and discussion

Prototypes of the proposed design (Design B), together with a reference antenna were fabricated on RTDuroid 5870 with a permittivitty of 2.33 and a thickness of 1.57 mm. Design B was fed with a direct 50 Ω microstrip-line with patch dimensions as shown in figure 7.23a. The reference antenna, shown in figure 7.23(b) was a square patch of $L = 30$ mm, fed by a quarter-wave matching network

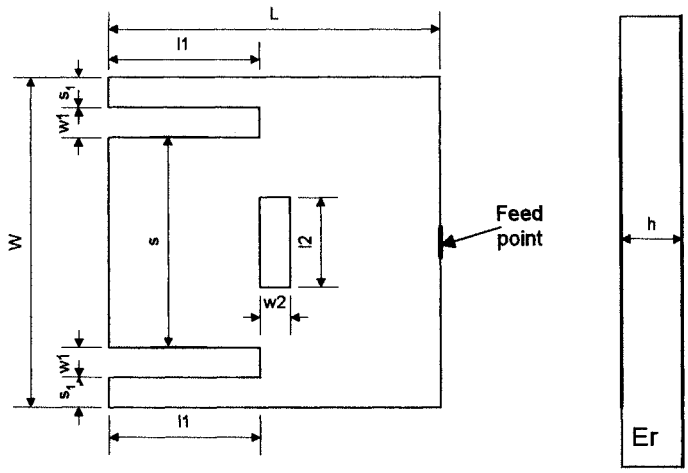

$L = 30$ mm, $W = 30$ mm, $l_1 = 21$ mm, $w_1 = 2$ mm, $s = 24$ mm, $s_1 = 1$ mm, $l_2 = 12$ mm, $w_2 = 1$ mm, $\varepsilon_r = 2.33$, $h = 1.57$ mm

(a)

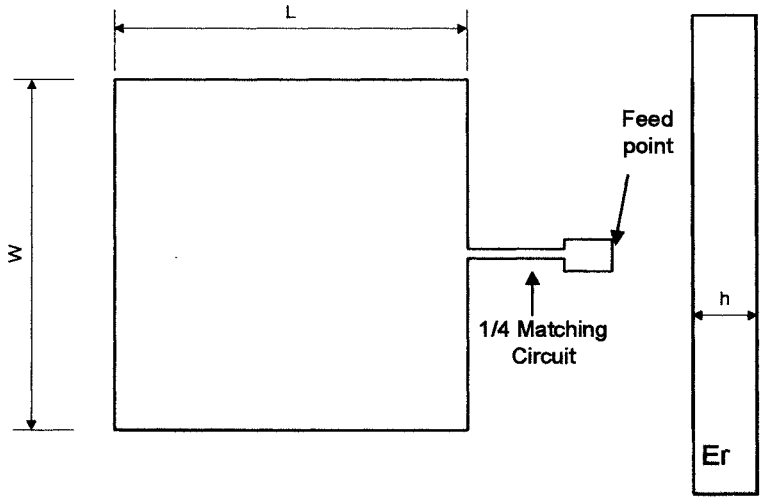

$L = W = 30$ mm, $\varepsilon_r = 2.33$, $h = 1.57$ mm

(b)

Figure 7.23: Patch configurations for (a) design B, and (b) reference antenna

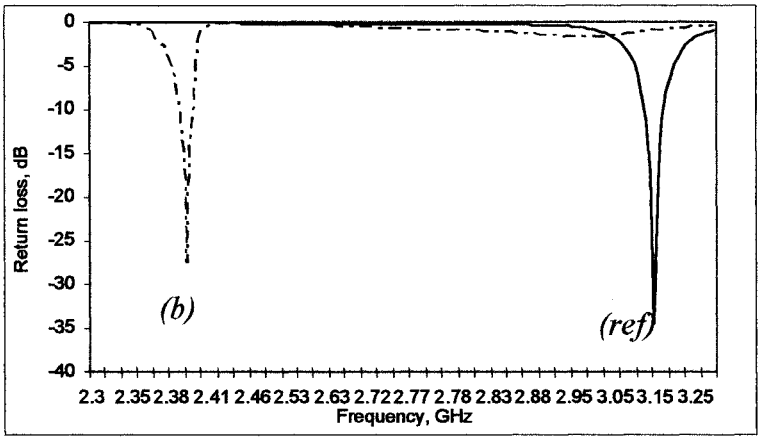

Figure 7.24: Return loss v frequency for design B (*b*) and reference antenna (*ref*)

Figure 7.24 shows the return loss versus resonant frequency for both antennas. It can be seen that the proposed design achieves a resonant frequency of 2.338 GHz with a return loss of better than -15 dB. This corresponds to a size reduction of 40% in terms of area.

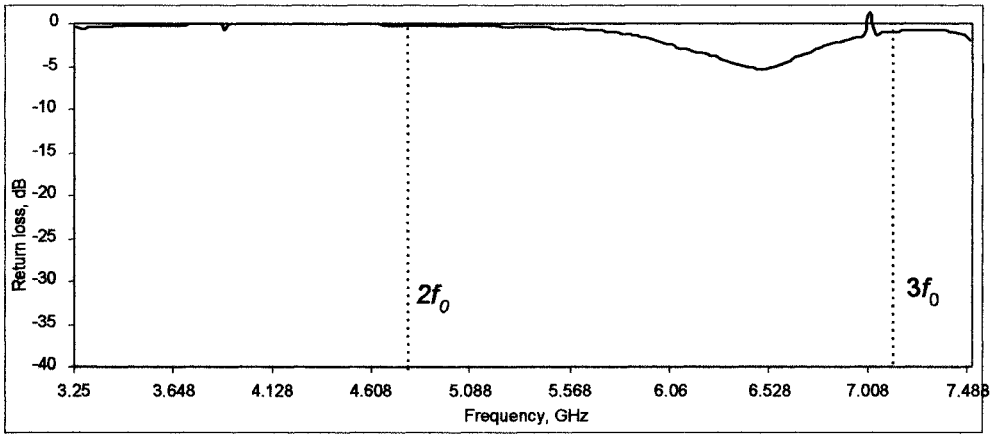

Figure 7.25: Return loss v frequency for design B

An additional benefit of design B is its ability to suppress the 2nd and 3rd order harmonics, as illustrated in figure 7.22. A return loss of -0.1 dB and -1.22 dB at the 2nd (4.776 GHz) and 3rd (7.164 GHz) harmonic is achieved. This is very useful in amplifier-type active integrated antenna applications where the antenna is directly integrated with high-efficiency power amplifiers. In this case, the antenna should

suppress higher order harmonics, as required by the high-efficiency operation of the power amplifier [154].

Table 7.4 show the practical results for both antenna designs, together with the reference antenna. Plots of the radiation patterns are illustrated in figure 7.26.

	Design B	**Reference Antenna**
Resonant Frequency (GHz)	2.338	3.15
Size Reduction (%)	40	NA
Return Loss (dB)	-35	-35
VSWR Bandwidth (%)	1.4	1.904
Input Impedance (Ω)	50	330
Measured Gain (dB)	3.7	6.1

Table 7.4: Practical results for design B

The table illustrates that size reduction of 12% has been achieved, but at the expense of decreased gain and reduced bandwidth. Considering the VSWR BW, the results indicate that the proposed design suffers from a reduction when compared to a standard reference patch. This trend is evident for slot loaded compact antennas discussed in Chapter 5, in which it was described that an inverse relationship exists between VSWR BW and size reduction. However, a major benefit of Design B is a wider BW compared to Design A shown in section 7.3.1. This confirms the trend stated in the results regarding the effect of the centre slot on the antenna Q factor described by figure 7.22. The table also illustrates a reduced gain, which is attributed to the reduced patch volume.

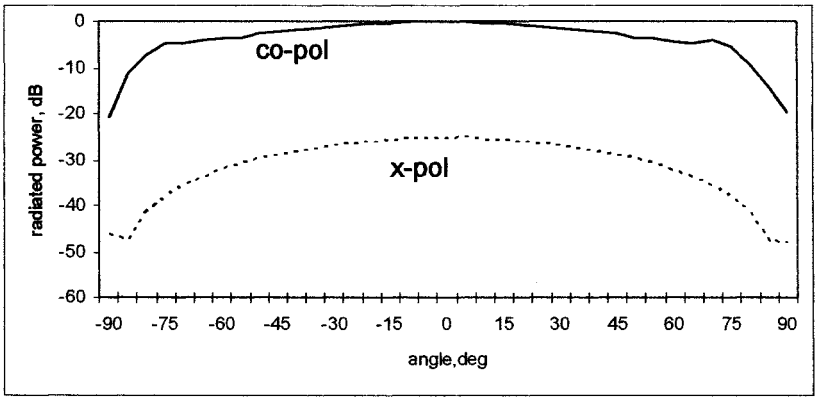

(a)

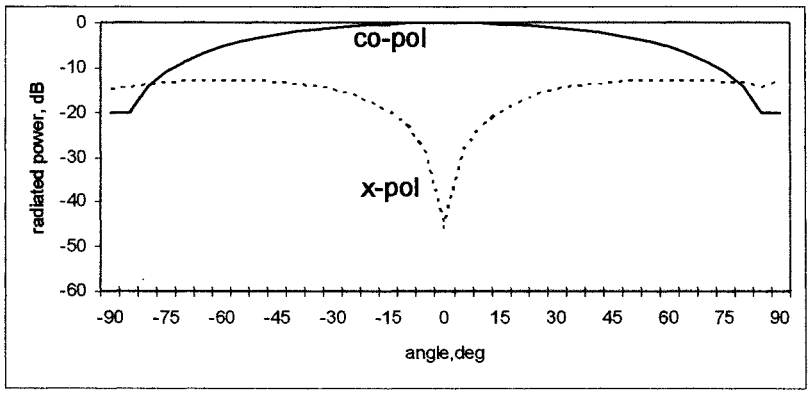

(b)

Figure 7.26: Radiation pattern for design B (a) E-plane (b) H-plane

The radiation patterns for design B are shown in figure 7.26(a) and (b). Good broadside radiation is achieved in both planes. The cross-polarisation level in the E and H-planes are below -20 dB and -10 dB respectively, relative to co-polar on-axis.

7.4 Compact Dual Frequency Antenna Analysis and Design

The technique of embedding slots inside a microstrip antenna to produce a dual frequency response, with both frequencies having the same polarisation sense, was introduced in chapter 3. To produce a large frequency ratio the TM_{01} and TM_{03} modes are used [64,120,121,132,133]. To achieve this, narrow slots are positioned parallel to the radiating edges of a rectangular patch. To produce a lower frequency

ratio, the existing TM_{01} mode together with the creation of an additional $TM_{0\delta}$ mode, which has a resonant frequency at a value between that of the TM_{01} and TM_{02} modes, are used. This is achieved by embedding bent slots along the non-radiating patch edges [134-140].

A major design problem is the difficulty in achieving a suitable impedance match at both frequencies. It was reported in Chapter 3 that the feed position required to produce optimum impedance matching at both frequencies simultaneously is highly sensitive. As a consequence, present dual frequency designs are excited using a probe feed, and no work exists at present on the use of a planar fed.The design presented in this section produces a dual frequency antenna with a reduced feed position sensitivity. It is found that this design lends itself to the use of an inset planar feed with a relatively simple impedance matching procedure.

7.4.1 Patch Design

The patch design consists of two stages. The first stage involves the creation of an additional $TM_{0\delta}$ resonant mode at a frequency above the fundamental TM_{01} mode, with the same polarisation sense and the same value of input impedance. This is achieved by using the structure shown in figure 7.4. The second stage is to simultaneously reduce the input impedance of both modes to 50 Ω at resonance through the use of an inset feed. The final structure is shown in figure 7.27. To achieve this, the modelling procedure outlined in section 7.2.1 has been employed. The patch is designed for use on RTDuroid 5870. The relevant data for this substrate is shown in Appendix C.

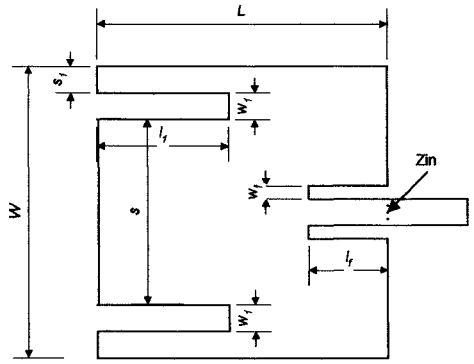

Figure 7.27: Inset fed dual frequency patch antenna structure

The first point to note in the design process is the effect of slot separation on the patch design. From the results in figure 7.6b in section 7.3, an important trend was illustrated. With reference to the value of slot separation, from figure 7.11b, placing the slots close to the non-radiating edges of the patch increases the effect of slot length on resonant frequency. This gives greater freedom to tune the frequency of the $TM_{0\delta}$ mode. In view of this, for ease of design s_1 has been fixed at 1 mm in the following designs.

Stage 1: Creating two resonant modes with equal input impedance

The requirement to achieve impedance matching of both TM_{01} and $TM_{0\delta}$ modes effectively places a constraint on the value of slot width w_1. From the analysis performed in Chapter 5, increasing slot width produces an increase in input impedance of the TM_{01} mode. As the slot width increases further, a stage is reached where the input impedance is too high for traditional impedance matching. A further reason for placing a limit on the value of slot width, is the fact that the resonant frequency of the TM_{01} mode remains unaffected. In this design, experimental results indicate that the value of slot width should not exceed 3 mm. Placing this constraint on the value slot width is beneficial from a designers point of view, as only the effect of slits on the additional mode need be considered. This reduces the complexity of the design process.

Regarding the effect of slot length l_1, it has previously been determined that in order to create an additional $TM_{0\delta}$ mode, the slot length l_1, must take on a value of between 40% L and 56% L. By increasing l_1 within these constraints can produce a frequency ratio of between 1.03 ~ 1.2. This is illustrated in figure 7.28, which illustrates the relationship between slot length l_1 and resonant frequencies of the TM_{01} (f_{01}) and $TM_{0\delta}$ ($f_{0\delta}$) modes, together with the frequency ratio (FR). These results were obtained using equation (7.4) – (7.5)

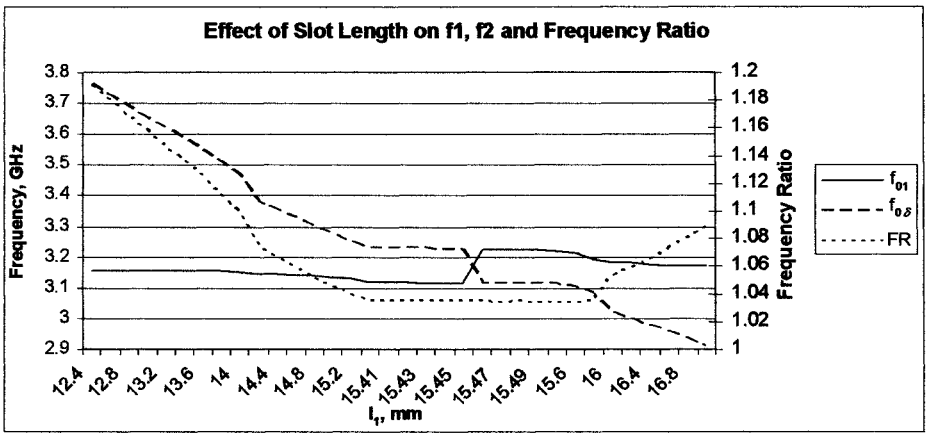

$\varepsilon_r = 2.33$, $h = 1.57$ mm, $L = 30$ mm, $W = 30$ mm, $w_1 = 1$ mm, $s = 1$ mm, $l_f = 0$ mm, $w_f = 0$ mm

Figure 7.28: Effect of slot length l_1 on resonant frequency of TM_{01} and $TM_{0\delta}$ modes and frequency ratio (FR)

The graph in figure 7.29 illustrates the relationship between slot width and input impedance of both modes, at the patch edge. It can be seen that increasing the value of w_1 results in an increased input impedance of the $TM_{0\delta}$ ($Z_{in0\delta}$), whilst the TM_{01} (Z_{in01}) remains largely unchanged. These results were obtained by substituting (4.36) into (7.4).

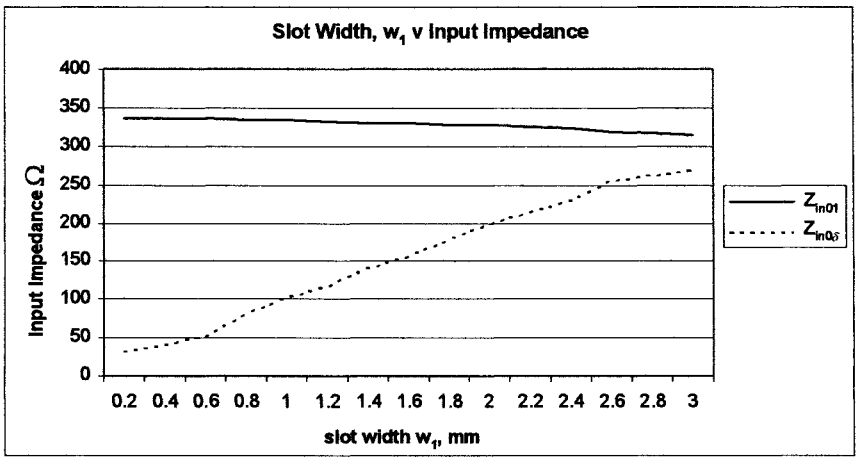

$\varepsilon_r = 2.33$, $h = 1.57$ mm, $L = 30$ mm, $W = 30$ mm, $l_1 = 13.6$ mm, $w_1 = 1$ mm, $s = 1$ mm, $l_f = 0$ mm, $w_f = 0$ mm

Figure 7.29: Correlation between w_1 and input impedance of TM_{01} (Z_{in01}) and $TM_{0\delta}$ ($Z_{in0\delta}$) modes

Stage 2: Reducing Input Impedance at both Frequencies to 50 Ω

The final stage in the design process involves the use of an inset feed. It is found that increasing the inset feed length, l_f, can simultaneously reduce the input impedance at both frequencies to 50 Ω. The inset feed has a slight effect on both resonant frequencies and thus slight tuning is required. These results were obtained by substituting (4.36) into (7.4).

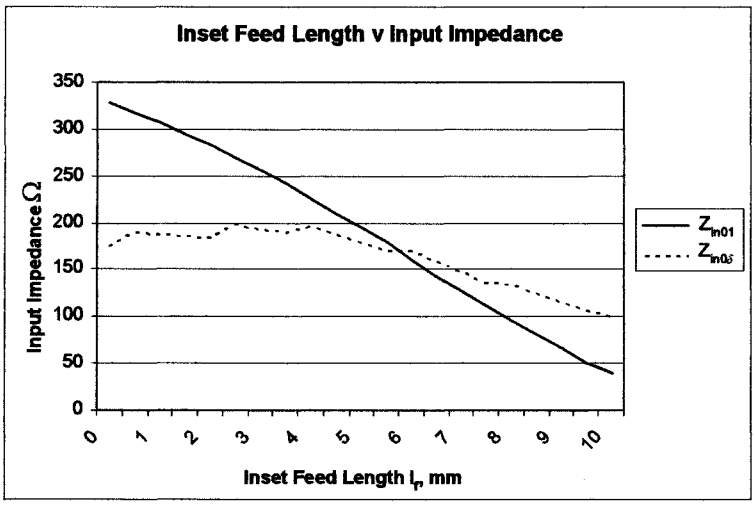

$\varepsilon_r = 2.33$, $h = 1.57$ mm, $L = 30$ mm, $W = 30$ mm, $l_1 = 14$ mm, $w_1 = 1$ mm, $s = 1$ mm, $w_f = 1.6945$ mm

Figure 7.30: Effect of inset feed length l_f on input impedance

7.4.2 Practical Results and Discussion

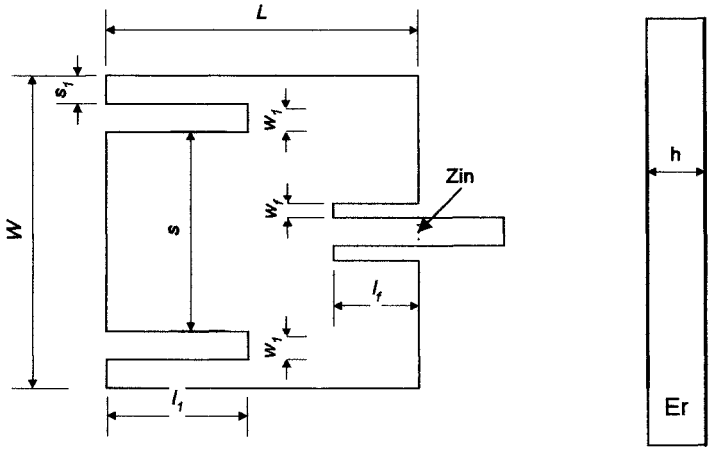

$L = 30$ mm, $W = 30$ mm, $l_1 = 13.6$ mm, $w_1 = 1$ mm, $s = 1$ mm,
$l_f = 10$ mm, $w_f = 1.6945$ mm, $\varepsilon_r = 2.33$, $h = 1.57$ mm

Figure 7.31: Patch configuration for inset fed dual frequency patch antenna

A prototype of a typical proposed design, with operating frequencies of 3.2 GHz and 3.55 GHz was fabricated on RTDuroid 5870 with a permittivity of 2.33 and thickness of 1.57 mm. The antenna dimensions were as shown in figure 7.29 and the patch was fed with a 50 Ω inset-fed microstrip-line. Figure 7.32 shows the return loss versus resonant frequency. A return loss of greater than -15 dB has been achieved at both resonant frequencies.

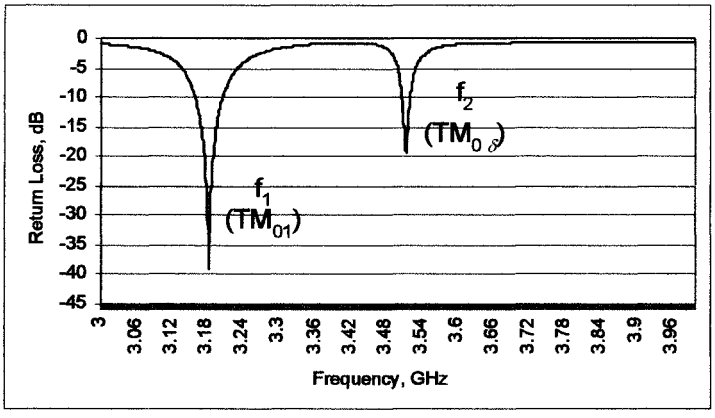

$L = 30$ mm, $W = 30$ mm, $l_1 = 13.6$ mm, $w_1 = 1$ mm, $s = 1$ mm,
$l_f = 10$ mm, $w_f = 1.6945$ mm, $\varepsilon_r = 2.33$, $h = 1.57$ mm

Figure 7.32: Return loss v frequency for f_1 ($TM_{0\delta}$) and f_2 (TM_{01})

Plots of the radiation patterns for the design frequencies are illustrated in figures and 7.34 respectively. Figure 7.33 (a) and (b) shows the E-plane and H-plane radiation for the TM_{01} mode at f_1. Figure 7.34 (a) and (b) show the radiation patterns for the $TM_{0\delta}$ mode at f_2. Good broadside radiation and cross-polarisation levels of below -20 dB have also been achieved at both design frequencies in the E and H- planes.

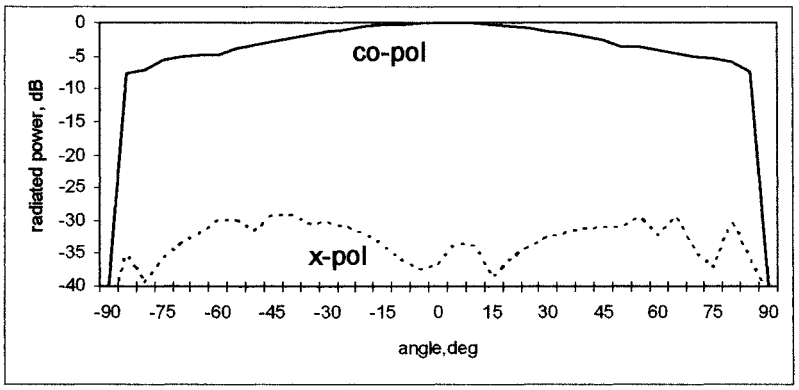

(a)

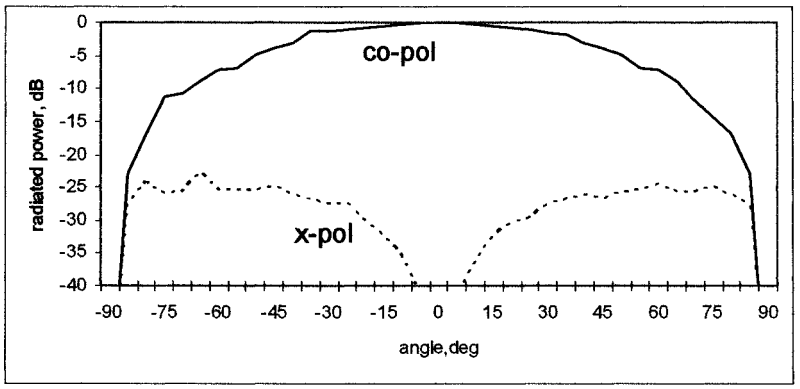

(b)

Figure 7.33: Radiation pattern for f_1 ($TM_{0\delta}$ mode) (a) E-plane and (b) H-plane

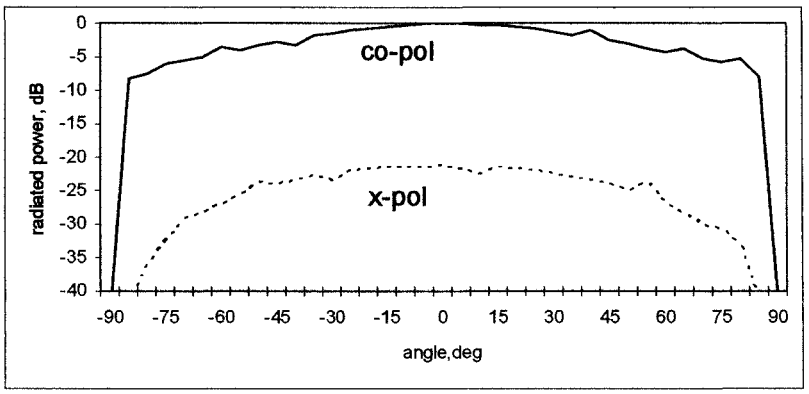

(a)

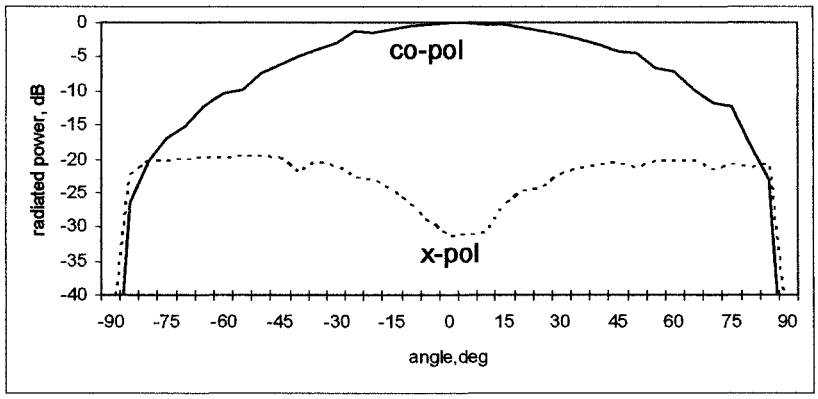

(b)

Figure 7.34: Radiation pattern for f_2 (TM_{01} mode) E-plane and (b) H-plane

The practical results of the dual frequency patch design are shown in table 7.5, which illustrate that the design has been achieved at the expense of other parameters.

	f_1 (GHz)	f_2 (GHz)
Resonant Frequency (GHz)	3.18	3.51
Return Loss (dB)	-38	-18.6
VSWR Bandwidth (%)	1.57	0.41
Input Impedance (Ω)	50	50
Gain (dB)	5.9	5.1

$L = 30$ mm, $W = 30$ mm, $l_1 = 13.6$ mm, $w_1 = 1$ mm, $s = 1$ mm,
$l_f = 10$ mm, $w_f = 1.6945$ mm, $\varepsilon_r = 2.33$, $h = 1.57$ mm

Table 7.5: Operating parameters for dual frequency patch design

Firstly, it can be seen that the gain is decreased from 6.1 dB for a typical single frequency antenna to 5.9 dB and 5.1 dB for this design. This is attributed to the reduced patch volume. It is also noted that, due to the increased antenna Q factor, the VSWR BW is reduced from 1.904% for a typical single frequency antenna to 1.57% and 0.41% for the two resonant frequencies in the proposed design.

7.5 Summary

The analysis, design technique and practical implementation of a novel antenna structures have been presented and discussed. It has been shown that with correct selection of slot dimensions and positions, a number of compact antenna designs can be produced. The use of this structure has been applied to produce patches with a single or dual frequency response. It has been demonstrated that for the single frequency design, a size reduction of up to 40% can be achieved when compared to a standard patch antenna.

In all cases, the antenna is excited using a 50 Ω planar feed. The use of a planar feed represents a significant advantage as it makes these designs suitable for integration with associated microwave circuitry and can also be easily extended for incorporation into antenna arrays. Moreover, the absence of an external impedance transformer is also a significant advantage as it further reduces the overall element size.

CHAPTER 8

CONCLUSION AND FURTHER RESEARCH

8.1 Conclusion

The primary goal of this research work was to investigate the use of planar fed compact microstrip patch antennas. A promising technique involves the use of slot loading to achieve such designs. Subsequent investigation of current methods of this technique identified a number of knowledge gaps in this field and established the need for detailed analysis of the full impact of slot loading on antenna performance. As a result of this work, novel designs for planar fed slot loaded compact patch antennas have been proposed. New designs for both linear and circular polarised single frequency antennas have been proposed, together with a dual frequency design.

Miniaturising an antenna effects its radiation characteristics [1 – 9], and influence its bandwidth, gain, efficiency and polarisation purity. Moreover, it is not always easy to feed a small antenna efficiently [10]. With this in mind, detailed understanding of the most important patch antenna characteristics in relation to miniaturisation techniques have been examined. Specific attention has been paid to the field distribution and radiation characteristics of different TM_{mn} modes.

A number of possible techniques for producing a reduced size planar fed patch antenna have been examined. These included: the use of shorting pin loaded patches; high permittivity substrates; folded patches; slot loaded ground plane; and the use of slot loaded patch. The use of high permittivity substrate allows size reduction, but at the expense of reduced bandwidth, increased dielectric losses and increased cost. Employing a folded patch structure also allows size reduction, but at the expense of

increased antenna volume and more complex manufacturing process. Incorporating shorting pin loading has been shown to reduce the antenna resonant frequency by a factor of $0.38f_{01}$.However, trade-offs of this approach include reduced E-plane gain and a dip in the H-plane radiation pattern. Moreover, strict manufacturing tolerances produce difficulties in exciting the antenna efficiently. The use of slot loaded ground plane and slot loaded patch both operate using a similar principle. By insertion of slot of correct size, shape and position it is possible to produce reduced size, dual frequency and wideband patch antennas. However, a significant trade-off, specific to the slot loaded ground plane approach, is the presence of back-radiation. In view of this, it has been successfully argued that the most promising method of achieving size reduction whilst allowing the use of a planar feed is through the use of slot loading.

To analyse slot loaded structures, a mathematical model has been developed to determine the performance slot loaded antennas. The most applicable modelling approach, in terms of accuracy and computer time, was the segmentation technique. The validity of the model was tested by analysing a square patch antenna with square slot loading. A comparison between the results determined using the developed model and those obtain using practical results provided confidence in the modelling procedure.

Using this model, a rigorous investigation of a slot loaded square patch antenna was performed, to determine the relationship between slot parameters and patch performance in terms of circuit characteristics. This study has addressed a major knowledge gap in the design of slot loaded patch antennas. From this investigation, a number of significant findings arose, which have a major effect on the design of slot loaded patch antennas. Primarily, the insertion of slots results in perturbation of all TM_{mn} modes. The extent to which each mode is affected is dependant on slot shape, dimension and position. In general, the slot length is largely responsible for

changes in the TM_{0n} characteristic, whilst the slot width largely effects the TM_{m0} modes. It has also been shown that significant trade-offs of reduced size slot loaded designs is an increased input impedance and higher Q factor. The relationship between slot size and Q factor has a limiting effect on antenna bandwidth. Moreover, the increased input impedance produce a constraint on practical size reduction due to the difficulty in producing optimum impedance matching. It has been demonstrated that for a typical square patch antenna with square slot loading, a maximum practical size reduction of only 14.85% can be achieved whilst still maintaining an input impedance value low enough to allow the use of a planar feed. To overcome this, a design procedure has been established and subsequently used for the design of a linear polarised patch antenna with a size reduction of 55%, whilst still allowing the use of a planar feed.

Further designs have also been implemented which achieve significant size reduction which also overcoming some of the trade-offs of previous designs.

In recent years, the use of slot loading has been used to reduce the size of the antenna element. To produce compact CP operation this technique has been mainly applied to patch antennas with truncated corners [66-69] or square patch with unequal length slots [70]. At present, little work exists on the use of slot loaded nearly square CP patch antennas. One of the major reasons for this is due to the high sensitivity of patch dimensions required to produce good CP performance, resulting in strict manufacturing tolerances. Another disadvantage of the nearly square CP patch antenna is a relatively narrow axial ratio compared to designs with truncated corners. This problem has been addressed, with the design of two novel reduced size circular polarised designs. It has been shown both of these achieve size reduction of up to 43% with relaxed manufacturing tolerances and no significant reduction in axial ratio bandwidth.

Although these designs are planar fed, as with standard size patch antennas, they still require an impedance matching network, which increases the total element size. Further designs have been proposed, which completely remove the problem of impedance matching by the development of novel antenna structures with an input impedance of 50 Ω. Using this approach, two new designs for a novel compact planar-fed microstrip patch antenna have been presented and discussed, which achieve size reduction of up to 40%. These designs also have the advantage of suppressing 2^{nd} and 3^{rd} order harmonics, thus being useful for active integrated antennas in high-efficiency radio transmitters.

A further reduced size patch with a dual frequency response has also been designed using a similar approach. Both frequencies have the same polarisation sense and an input impedance of 50 Ω at both design frequencies is achieved using a relatively simple impedance matching procedure.

Overall, this thesis has addressed a major knowledge gap in the field of reduced size slot loaded microstrip patch antennas. As a result of this, greater understanding of the design procedures and associated trade-offs from such designs are known. Using this knowledge, novel structures that overcome some of the associated problems of current designs have been presented.

8.2 Recommendations For Further Research

Based upon the experience and knowledge acquired during this research, several areas for further research can be suggested. These are:-

- The work determined the relationship between slot parameters and patch performance in terms of resonant frequency, input impedance, Q factor and feed position. It was subsequently argued that size reduction is achieved at the expense of some of these parameters. A useful extension to this study

would be to investigate the use of optimisation techniques to allow the designer to produce a slot loaded antenna with the required patch performance. A possible optimisation technique could be the use of genetic algorithms.

- The focus of this thesis has mainly focussed on the effect of slot parameters on the circuit characteristics. It would be useful to extend this to investigate the effect on the far-field response of the antenna.
- Chapter 6 presented novel structures for planar fed reduced size circular polarised patch antennas. These designs are both excited using a planar feed via a quarter-wave impedance matching network. A possible avenue for further work would be to investigate ways of producing a similar antenna response, but with a 50 Ω input impedance. This would remove the need for a matching circuit and thus reduce the element size further.
- Within Chapter 7 a novel design for a dual frequency planar fed patch antenna was presented with both frequencies having the same polarisation sense and being linear polarised. The design was achieved by using slots to create an additional $TM_{0\delta}$ mode, whilst also having little effect on the TM_{01} mode. To extend this work, it would be interesting to investigate the placement of slots to create an additional $TM_{\delta 0}$ mode orthogonal to the $TM_{0\delta}$ mode. This would allow the design of dual frequency circular polarised antenna. This design would also lend itself to an antenna with a dual frequency dual polarised response.
- Two applications of the reduced size patch antennas developed in this thesis is in the fields of both near-field antenna measurements and microwave imaging. Traditional Far-Field measurement techniques for large antennas at high frequencies suffer from large distance at which measurements have to be taken. To overcome this, much research into the development of close

range measuring techniques exists. One such approach uses a holographic approach to reconstruct the far-field response using measurements taken in the near-field. In such a system, a waveguide or microstrip patch is typically used as the probe antenna. The accuracy of the result is inversely related to the size of the probe antenna. It is predicted that using patch antenna whose size is significantly less than half-wavelength, improved results can be obtained. An extension of this technique has also been shown to exist for use in the field of microwave imaging of objects. A further avenue for research would be to incorporate the antenna structures developed in this thesis into such a system.

References

[1] L. Lewin, "Radiation from discontinuities in stripline," Proc. IEE, 107C, p163-170, 1960

[2] E. Chang, S.A. Long and W.F. Richards, "An experimental investigation of electrically thick rectangular microstrip antennas," IEEE Transactions Antennas & Propagation, **AP-34**, (6), p767-772,1986

[3] J.M. Griffin and J.R. Forrest, "Broadband circular disc microstrip antenna," Electronic Letters, **18**, p26-29, 1982

[4] K.S. Fong, H.F. Hues and M.J. Withers, "Wideband multilayer coaxial fed microstrip antenna element," Electronic Letters, **21**, p497-499, 1985

[5] P.S. Hall, "Probe compensation in thick microstrip patches," Electronic Letters, **23**, p606-607, 1987

[6] D.R. Poddar, J.S. Chatterjee and S.K. Chowdhury, "On some broad band microstrip resonators," IEEE Transaction on Antennas & Propagation, AP-31, p606-607, 1983

[7] J.S. Chatterjee, "Conically depressed microstrip patch antenna," IEE Proceedings H, p193-196, 1983

[8] A. Sabban, "New broadband stacked two layer microstrip antenna," IEEE AP-S Symposium, Houston, p63-66, 1983

[9] P.S. Hall, C. Wood and C. Garrett, "Wide bandwidth microstrip antennas for circuit integration," Electronic Letters, **15**, p458-460, 1979

[10] D.H. Schaubert and F.G. Farrar, "Some conformal printed circuit antenna designs," Proceedings Workshop of Printed Antenna Technology, New Mexico State University, p5.1-5.21, 1979

[11] G. Kumar and K.C. Gupta, "Non-radiating edge and four edges gap coupled multiple resonator broad band microstrip antennas," IEEE Transactions on Antennas & Propagation, **AP-33**, p173-177, 1985

[12] P.S. Bhatnagar, P.S. Daniel, J.P. Mahdjoubi and C. Terret, "Hybrid edge, gap and directly coupled triangular microstrip antenna," Electronic Letters, **22**, p853-855, 1986

[13] C.K. Aanandan and K.G. Nair, "A compact broad band microstrip antenna," Electronic Letters, **22**, p1064-1065, 1986

[14] C. Wood, "Improved bandwidth of microstrip antennas using parasitic elements," IEE Proceedings, **127H**, p231-234, 1980

[15] C. Prior and P.S. Hall, "Microstrip disc antenna with short circuit annular ring," Electronic Letters, **21**, p719-721, 1985

[16] C. Wood, "Curved microstrip lines as compact wideband circular polarised antennas," IEE J. MOA, **3**, p5-13, 1979

[17] P.S. Hall and C.J. Prior, "Radiation control in corporately fed microstrip patch arrays," JINA 86, p271-275, 1986

[18] A. Henderson and J.R. James, "Design of microstrip antenna feeds- Pt. 1: Estimation of radiation loss and design implications," IEE Proceedings, **128H**, (1), p19-25, 1981

[19] Y.T. Lo, D. Soloman and W.F. Richards, "Theory and experiment on microstrip antennas," IEEE Transaction Antennas & Propagation, **AP-27**, p137-145, 1979

[20] J.R. James, P.S. Hall and C. Wood, "Microstrip antenna theory and design," IEE Peter Peregrinus,1981

[21] P.S. Hall and J.R. James, "Design of microstrip antenna feeds- Pt. 2: Performance limitations of triplate corporate feeds," IEE Proceedings, **128H**, p.26-34, 1981

[22] A. Rogers, "Wideband squintless linear arrays," Marconi Rev., **87**, p221-243, 1972

[23] J.C. Williams, "Cross fed printed aerials," Proceedings 7th European Microwave Conference, Copenhagen, p292-296, Sept. 1977

[24] A.G. Derneryd, "Linearly polarised microstrip antennas," IEEE Transactions on Antennas & Propagation, **AP-24**, p846-851, 1976

[25] M. Tiuri, J. Henrikson and S. Tallquist, "Printed circuit radio link antenna," 6th European Microwave Conference, Rome, p280-282, Sept. 1976

[26] R. Hill, "Printed planar resonant arrays," ICAP 87, York, IEE Int. Conference on Antennas & Propagation, p473-476, 1987

[27] R. Dumanchin, "Microstrip aerials," French Patent Application 855234, 1959

[28] J.R. James and P.S. Hall, "Microstrip antennas and arrays: Pt. 2: New design technique," IEE J. MOA, p175-181, 1977

[29] E.R. Cashen, R. Frost and D.E. Young, "Improvements relating to aerial arrangements," British Provisional Patent (EMI Ltd) Specification 1294024

[30] T. Metzler, "Microstrip series arrays," IEEE Transaction Antennas & Propagation, **AP-29**, p174-178, 1981

[31] H.G. Oltman, "Electromagnetically coupled microstrip dipole antenna elements," 8th European Microwave Conference, Paris, p281-285, Sept. 1978

[32] N.G. Alexopoulus and D.R. Jackson, "Fundamental superstrate (cover) effects on printed circuit antennas," IEEE Transaction on Antennas & Propagation, **AP-32**, p807-816, 1984

[33] J.R. James, C.M. Hall and G. Andrasic, "Microstrip elements and arrays with dielectric overlays," IEE Proc., **133**, H, (6), p474-482,1986

[34] R.P. Owens and A.C. Smith, "Dual band, dual polarised microstrip antenna for X band satellite communications," Military Microwaves Conference, Brighton, p323-328, June 1986

[35] D.M. Pozar, "Microstrip antenna aperture coupled to a microstrip line," Electronic Letters, **21**, p49-50, 1985

[36] A.C. Buck and D.M. Pozar, "Aperture coupled microstrip antenna with a perpendicular feed," Electronic Letters, **22**, p125-126, 1986

[37] T. Teshirogi, M. Tanaka and W. Chujo, "Wideband circularly polarised array with sequential rotation," Proceedings ISAP, Tokyo, Japan, p117-120, Aug. 1985

[38] A.K. Skrivervik, J.-F. Zurcher, O. Staub and J.R. Mosig, "PCS Antenna Design: The Challenge of Miniaturization," IEEE Antennas and Propagation Magazine, **43** (4), p12-27, August 2001

[39] H.A. Wheeler, "Fundamental Limitations of Small Antennas," Proceedings of the IRE, **35**, pp1479-1484, December 1947

[40] R.E. Collin, "Minimum Q of Small Antennas," Journal of Electromagnetic Waves and Applications, **12**, pp1369-1393, 1998

[41] R.F. Harrington, "Effect of Antenna Size on Gain, Bandwidth and Efficiency," Journal of Research of the National Bureau of Standards - D. Radio Propagation, 64D, pp151-155, January-February 1960

[42] K. Fujimoto, A. Henderson, K. Hirasawa, J.R. James, Small Antennas, New York, John Wiley and Sons, Research Studies Press, 1987

[43] K. Fujimoto and J.R. James, Mobile Antenna Systems Handbook, Norwood, MA, USA, Artech House, 1994

[44] S. Dey and R. Mittra, 'Compact microstrip patch antenna,' Microwave Opt. Technol. Lett. **13**, p12-14, Sept. 1996

[45] R. Waterhouse, "Small microstrip patch antenna," Electron. Lett., **31** (8), p604-605, April 1995

[46] D. Singh, P. Gardner & P.S. Hall, "Miniaturised microstrip antenna for MMIC applications," Electronic Lett., **33** (22), p1830-1831, Oct. 1997

[47] K.L. Wong and S.C. Pan, "Compact triangular microstrip antenna," Electronic Lett., **33** (6), p433-434, March 1997

[48] S.K Satpathy, G. Kumar & K. P. Ray, "Compact shorted variations of triangular microstrip antennas," Electronic Lett., **34** (8), p709-711, April 1998

[49] S.K. Satpathy, K. P. Ray & G. Kumar, "Compact shorted variations of circular microstrip antennas," Electronic Lett., **34** (2), p137-138, Jan. 1998

[50] K.L. Wong and W.S. Chen, "Compact microstrip antenna with dual frequency operation," Electron. Lett., **33**, p646-647, April 1997

[51] V. Palanisamy & R.Garg, "Rectangular Ring and H-Shape Microstrip Antennas - Alternatives to Rectangular Patch Antenna," Elec. Letters, **21** (19), p10-12, 12th Sept. 1985

[52] R. Chair, K.M. Luk and K.F. Lee, "Small dual patch antenna," Electron.Lett. **35**, p762-764, May 1999

[53] K.M. Luk, R. Chair and K.F. Lee, "Small rectangular patch antenna," Electron. Lett. **34**, p2366-2367, Dec. 1999

[54] J.S. Kuo and K.L. Wong, , "A compact microstrip antenna with meandering slots in the ground plane," Microw. Opt. Technol. Lett. **29**, p95-97, April 20, 2001

[55] S. Dey and R. Mittra, "Compact microstrip patch antenna," Microwave Opt. Technology Letters, **13**, p12-14, Sept. 1996

[56] J.S. Kuo and K.L. Wong, "A Compact Microstrip Antenna with Meandering Slots in the Ground Plane," Microwave and Optical Technology Letters, **29**, p95-97, April 2001

[57] T.W. Chiou and K.L. Wong, "Designs of compact microstrip antennas with a slotted ground plane," IEEE Antennas and Propagation Soc. Int. Symp. Digest, p 732-734, 2001

[58] K.L. Wong, C.L. Tang, and H.T. Chen, "A compact meandered circular microstrip antenna with a shorting pin," Microwave Optical Technology Letters, **15**, 147-149, June 20, 1997

[59] C.K. Wu, K.L. Wong, and W.S. Chen, "Slot-coupled meandered microstrip antenna for compact dual frequency operation," Electronic Letters, **34**, p1047-1048, May 1998

[60] S. Dey and R. Mittra, 'Compact microstrip patch antenna,' Microwave Opt. Technol. Lett. **13**, p12-14, Sept. 1996

[61] K.L. Wong, C.L. Tang and H.T. Chen, "A compact meandered circular microstrip antenna with a shorting pin," Microwave and Optical Technology Letters, **15**, p147-149, June 1997

[62] J. George, M. Deepukumar, C.K. Aanandan, P. Mohanan and K.G. Nair, "New compact microstrip antenna," Electronic Letters, **32**, p508- 509, March 1996

[63] Chun-Kun Wu, Kin-Lu Wong & Wen-Shyang Chen, "Slot coupled meandered microstrip antenna for compact dual-frequency operation", Electron. Letters, **34** (11), p1047-1048, May 1998,

[64] J. H. Lu & K.L. Wong, "Slot-loaded, meandered rectangular microstrip antenna with compact dual-frequency operation," Electron. Lett., **34** (11), p1048-1050, May 1998

[65] P.C. Sharma, K.C. Gupta, "Analysis and optimized design of single feed circular polarised microstrip antenna," IEEE Trans. Antennas Propog., **29**, p949-955, 1983

[66] W.S. Chen, C.K. Wu, K.L. Wong, "Single-feed square-ring microstrip antenna with truncated corners for compact circular polarisation operation', Electron. Lett.,**34**, p1045-1047, 1998

[67] W.S. Chen, C.K. Wu, K.L. Wong, "'Compact circular polarised microstrip antenna with bent slots," Electron. Lett., **34**, p1278-1279, 1998

[68] W.S. Chen, K.C. Wu, K.L. Wong, "Novel Compact Circular Polarized Square Microstrip Antenna," IEEE Trans. Antennas Propog., **49**, p340-342, 2001

[69] W.S. Chen, K.L. Wong, C.K. Wu, "Inset Microstripline-Fed Circularly Polarized Microstrip Antenna," IEEE Trans. Antennas Propog., **48**, p1253-1254, 2000

[70] K.L. Wong, J.Y. Wu, "Single-feed small circular-polarised square microstrip antenna," Electron. Lett.,**33**, p1833-1834, 1998

[71] W.S. Chen, C.K. Wu, K.L. Wong, "Square-Ring Microstrip Antenna with a Cross-Strip for Compact Fed Circularly Polarized Operation," IEEE Trans. Antennas Propog., **47**, p1566-1567, 1999

[72] L.J. Chu, "Physical Limitations on Omni-Directional Antennas," Journal of Applied Physics, **19**, p1163-1175, December 1948

[73] J.S. McLean, "A Re-Examination of the Fundamental Limits on the Radiation Q of Electrically Small Antennas," IEEE Transactions on Antennas and Propagation, **AP-44**, p672-675, May 1996

[74] R.E. Collin and S. Rothschild, "Evaluation of Antenna Q," IEEE Transactions on Antennas and Propagation, **AP-12**, p23-27, 1964

[75] R.L. Fante, "Quality Factor of General Ideal Antennas," IEEE Transactions on Antennas and Propagation, **AP-17**, pp151-155, March 1969

[76] D.M. Pozar, "Microstrip Antennas," Proc. IEEE, **80** (1), p79-81, January 1992

[77] I. J. Bahl and P. Bhartia, Microstrip Antennas, Artech House, Dedham, MA, USA, 1980

[78] K.R. Carver and J.W. Mink, "Microstrip Antenna Technology," IEEE Trans. Antennas Propagat., **AP-29** (1), p2-24, January 1981

[79] P.B. Katehi and N.G. Alexopoulos, "On the Modeling of Electromagnetically Coupled Microstrip Antennas – The Printed Strip Dipole," IEEE Trans. Antennas Propagat., **AP-32** (11), p1179-1186, November 1984

[80] J.R. James and P.S. Hall, Handbook of Microstrip Antennas, Vols. 1 and 2, Peter Peregrinus, London, UK, 1989

[81] G. Gronau and I. Wolff, "Aperture-Coupling of a Rectangular Microstrip Resonator," Electronic Letters, **22**, p554-556, May 1986

[82] C.A. Balanis, Antenna Design Analysis And Design, 2nd Edition, John Wiley & Sons, New York, 1997

[83] H.G. Oltman and D.A. Huebner, "Electromagnetically coupled microstrip dipoles," IEEE Transactions Antennas & Propagation, **AP-29**, p151-157, January 1981

[84] P.B. Katehi and N.G. Alexopoulos, "On the modelling of electromagnetically coupled microstrip antennas - The printed strip dipole," IEEE Transactions Antennas & Propagation, **AP-32**, p1179-1186, November 1984

[85] E.O. Hamerstad, "Equations for Microstrip Circuit Design," Proc. Fifth European Microwave Conf., p268 –272, September 1975.

[86] Microstrip Antenna Theory and Design, J.R. James, P.S. Hall and C. Wood, Peter Peregrinus Ltd., England, 1981

[87] R.J. Collier & P.D. White, "Surface Waves in Microstrip Circuits," Proc. 6th European Microwave Conference, p632-636, 1976

[88] K.R. Carver & J.W. Mink, "Microstrip Antenna Technology," IEEE Trans. Antennas Propogat., **AP-29** (1), p2-24, January 1981

[89] P.S. Hall and C. Wood, Microstrip Antenna Theory and Design, J.R. James, Peter Peregrinus Ltd., England, 1981

[90] R.E. Munson, "Conformal Microstrip Antennas and Phased Arrays," IEEE Transactions on Antennas and Propagation, **22**, p74-78, Jan. 1974

[91] J.D. Woermbke, "Soft Substrates Conquer Hard Designs," Microwaves Journal, p89-98, January 1982

[92] Ansoft Ensemble® V.7 – Method of Moments 2.5 D EM Field Solver

[93] T. Miligan and H.Shrank, "Antennas Designers Notebook," IEEE Antennas and Propagation Magazine, **38** (3), p76-82, June 1996

[94] C.A. Balanis, "Antenna Theory Analysis and Design," John Wiley and Sons Ltd., USA, 1982

[95] D.M. Pozar and S.M. Voda, "A Rigorous Analysis of a Microstripline Fed Patch Antenna," IEEE Transactions on Antennas and Propagation, **35**(12), p1343-1349, 1987,

[96] C. Scott, The Spectral Domain Method on Electromagnetics, Artech House, Inc., USA, 1989

[97] Y.T. Lo, D.D. Harrison, G.A. Deschamps and F.R. Ore, "Study of microstrip antennas, microstrip phased arrays and microstrip feed networks," Rome Air Development Centre Tech. Rep. **TR-77-406**, Oct. 1977

[98] K.R. Carver and E.L. Coffey, "Theoretical investigation of the microstrip antenna," Physic. And Sci. Lab., New Mexico State Univ., Las Cruces, Tech. Rep. **PT-00929**, Jan. 1979

[99] K.R. Carver, "A modal expansion theory for the microstrip antenna," in Dig. Int. Symp. Antennas Propagat. Soc., Seattle, WA, pp101-104, June 1979

[100] K.R. Carver, "Practical analytical techniques for the microstrip antenna," in Proc. Workshop Printed Circuit Antenna Tech. New Mexico State Univ., Las Cruces, p 7/1-20, Oct. 1979,

[101] Y.T. Lo, D. Solomon and W.F. Richards, "Theory and experiment on microstrip antennas," IEEE Transactions on Antennas and Propagation, **AP-27** (2), p137-145, March 1979

[102] W. F. Richards and Y.T. Lo, "An improved theory for microstrip antennas and applications," in Dig. Int. Symp. Antennas Propagat. Soc., Seattle, WA, p113-116, June 1979

[103] W.F. Richards, Y.T. Lo, P. Simon and D.D. Harrison, "Theory and applications for microstrip antennas," in Proc. Workshop Printed Circuit Antenna Tech. New Mexico State Univ., Las Cruces, p 8/1-23, Oct. 1979

[104] A.R. Van de Capelle, "Theoretical investigations of microstrip antennas," in Proc. Workshop Printed Circuit Antenna Tech. New Mexico State Univ., Las Cruces, p 11/1-8, Oct. 1979

[105] E. Van Lil, R. Van Loock and A. Van de Capelle, "Design models for rectangular microstrip resonator antennas," in Dig. Int. Symp. Antennas Propagat.,Soc., College Park, MD, p264-267, May 1978,

[106] K.F. Lee and W. Chen, Advances in Microstrip and Printed Antennas, John Wiley and Sons, Inc., USA, 1997

[107] T. Okoshi, Planar Circuits for Microwaves and Lightwaves, Springer-Verlag, England, 1985

[108] D.H. Schaubert, F.G. Farrar, A. Sindoris, S.T. Hayes, "Microstrip Antennas with Frequency Agility and Polarisation Diversity," IEEE Transactions on Antennas and Propagation, **AP-29** (1), p118-123, January 1981

[109] Skriverik, J.F. Zurcher, O. Staub and J.R. Mosig, "PCS Antenna Design: The Challenge of Miniaturisation," IEEE Antennas and Propagation Magazine, **43** (4), p12-27, August 2001

[110] K.L. Wong, Compact and Broadband Microstrip Antennas, John Wiley and Sons, Inc., USA, 2003

[111] K.L. Wong and H.C. Tung, "A Compact Patch Antenna an Inverted U-Shaped Radiating Patch," IEEE Antennas and Propagation Society Int. Symposium Digest, p728-731, 2001

[112] J.S. Kuo and K.L. Wong, "A Dual-Frequency L-Shaped Patch Antenna," Microwave and Optical Technology Letters, **27**, p177-179, Nov. 5, 2000

[113] J.S. Kuo and K.L. Wong, "Dual-Frequency operation of a Planar Inverted L Antenna with a Tapered Patch Width," Microwave and Optical Technology Letters, **28**, p126-127, Jan. 2001

[114] Chun-Kun Wu, Kin-Lu Wong & Wen-Shyang Chen, "Slot coupled meandered microstrip antenna for compact dual-frequency operation", Electron. Letters, **34** (11) p1047-1048, May 1998

[115] C. Borja, J. Romeu, "On the behaviour of kock island fractal boundary microstrip patch antenna," IEEE Transactions on Antennas and Propagation, **51** (6), p1281-1291, June 2003,

[116] K.L. Wong and Y.F. Lin, "Small broadband rectangular microstrip antenna with chip resistor loading," Electron. Letters, **33**, p1593-1594, Sept. 1997

[117] S. Pioch and J. Laheurte, "Size reduction of microstrip antennas by means of periodic metallic patterns," Electron. Letters, **39** (13), p959-961, 2002

[118] J. Row, "Patch antenna fed by shorted coplanar microstrip line," Electronic Letters, **39** (13), p958-959, 2003

[119] M. Sanad, "Effect of the shorting posts on short circuit microstrip antennas," Proceedings IEEE Antennas and Propagation Symposium, p794-797, 1994

[120] S. Maci, G.B. Gentili & G. Avtiabile, "Single-layer Dual Frequency Patch Antenna," Elec. Letters, 5th Aug, **29** (16), p1441-1443, 1993

[121] M.E. Yazidi, M. Himdi & J.P. Daniel, "Aperture Coupled Microstrip Antenna for Dual Frequency Operation," Electron. Letters, **29** (17), p1506-1508, 19th Aug. 1993

[122] K.L Wong and W.S. Chen, "Compact Microstrip Antenna with Dual Frequency Operation," Electron. Letters, **33**, p646p647, April 1997

[123] C.L. Tang, H.T. Chen and K.L. Wong, "Small Circular Microstrip Antenna with Dual Frequency Operation," Electronic Letters, **33** (13), p1112-1113, 19th June 1997,

[124] S.C. Pan and K.L. Wong, "Dual-Frequency Triangular Microstrip Antenna with a Shorting Pin," IEEE Transactions on Antennas and Propagation, **45** (12), p1889-1891, December 1997

[125] J. George, K. Vasudevan, P. Mohanan and K.G. Nair, "Dual Frequency Miniature Microstrip Antenna," Electron. Letters, **34** (12), p1168-1170, June 1998

[126] R.B. Waterhouse and D.M. Kokotoff, "Novel Technique to Improve the Manufacturing Ease of Shorted Patches," Microwave and Optical Technology Letters, **17** (1), p37-40, January 1998

[127] R.B. Waterhouse, "Design and Performance of Small Printed Antennas," IEEE Transactions on Antennas and Propagation, **46** (11), p1629-1633, November 1998

[128] W.S. Chen, "Single-feed dual-frequency rectangular microstrip antenna with square slot," Elec. Letters, **34** (3), p231-232, 5Feb. 1998

[129] K.L. Wong & K.P. Yang, "Small dual-frequency microstrip antenna with cross slot," Elec. Letters, **33** (33), p1916-1917, Nov. 1997,

[130] K.L. Wong & K.P.Yang, "Compact dual-frequency microstrip antenna with a pair of bent slot," Electron. Letters, **34** (3), p225-226, Feb. 1998

[131] W.S. Chen, C.K. Wu & K.L. Wong, "Novel Compact Circular Polarised Square Microstrip Antenna," IEEE Transactions Ant. & Prop., **49** (3), p340-341, March 2001,

[132] S. Maci, G.B. Gentili, P. Piazzesi & C. Salvador, "Dual-band slot-loaded patch antenna," IEE Proc.-Microw. Antennas Propag., **142** (3), p225-232, June 1995

[133] K.P. Yang and K.L. Wong, "Dual-band Circular Polarised Square Microstrip Antenna," IEEE Transactions on Antennas and Propagation, **49** (3) p377-381, March 2001

[134] K.L. Wong & J.Y. Sze, "Dual-frequency slotted rectangular microstrip antenna," Electron. Letters, **34** (14), p1368-1370, July 1998

[135] J.Y. Sze & K.L. Wong, "Single-Layer Single-Patch Broadband Rectangular Microstrip Antenna," Microwave Opt. Technol. Lett., **22** (4), p234-236, Aug. 1999

[136] J.H. Lu, "Single-feed dual-frequency rectangular microstrip antenna with pair of step-slots," Electron. Lett., **35** (5), p354-355, March 1999

[137] J.H. Lu, "Dual-frequency operation of a single-feed rectangular microstrip antenna with a pair of comb-shaped slots," Microwave Opt. Technol. Lett., **23** (3), p183-186, Nov. 1999

[138] J. Y. Sze & K.L. Wong, "Broadband rectangular microstrip antenna with pair of toothbrush-shaped slots," Electron. Lett., **34** (23), p2186-2187, Nov. 1998

[139] J.Y. Szi & K.L. Wong, "Slotted Rectangular Microstrip Antenna for Bandwidth Enhancement," Electron. Lett., **48** (8), p1149-1152, Aug. 2000

[140] J.H. Lu & K.L. Wong, "Dual-frequency rectangular microstrip antenna with embedded spur-lines and integrated reactive loading," Microwave Opt. Technol. Lett., **21** (4), p272-275, May 1999

[141] J. Chiao et al, "MEMS reconfigurable Vee antenna," IEEE MTT-S International Microwave Symposium Digest, p. 1515-1518, 1999

[142] A.T. Alastalo, ; T. Mattila, ; H. Seppa, "Analysis of a MEMS transmission line," IEEE Transactions on Microwave Theory and Techniques, p1977- 1981, Aug. 2003

[143] T. Okoshi, and Takeuchi.: 'Analysis of planar circuits by segmentation method', Electron. Commun. Japan, **58-B**, p71-80, 1975

[144] R. Chadha, and K.C. Gupta,: 'Segmentation method using impedance

matrices for analysis of planar microwave circuits', IEEE Trans., **MTT-29**, p71-74, 1981

[145] T koshi, and T Miyoshi,: 'The planar circuit – An approach to microwave integrated circuitry', IEEE Trans., **MTT-20**, p245-252, 1972

[146] J.R. James, and P.S. Hall,: 'Handbook of microstrip antennas' Chap. 9, (Peter Peregrinus, 1989),

[147] P.C. Sharma, and K.C. Gupta,: 'Desegmentation method for analysis of two-dimensional microwave circuits' IEEE Trans., **MTT-29**, p1094 – 1098, 1981

[148] P.C. Sharma, and K.C. Gupta,: 'An alternative method for implementing desegmentation method'IEEE Trans., **MTT-32**, p1-4, 1984

[149] MCAD Software, Mathsoft Engineering & Education, Inc., Cambridge, MA, USA

[150] V. Palanisamy and R. Garg, 'Analysis of arbitrary shaped microstrip patch antennas using segmentation technique and cavity model,' IEEE Transactions Antennas and Propagation, **AP-34** (10), Oct. 1986

[151] K.L. Chung & A. Sanagavarapu, "A Systematic Design Method to Obtain Broadband Characteristics for Sngly-Fed Electromagnetically Coupled Patch Antennas for Circular Polarisation," IEEE Transactions and Antennas and Propagation, **51** (12), p3239-3248, December 2003,

[152] P.C. Sharma, K.C. Gupta, "Analysis and optimized design of single feed circular polarised microstrip antenna," IEEE Trans. Antennas Propog., **AP-29**, p949-955, 1983

[153] R. Chadha and K.C. Gupta, 'Green's Functions for Triangular Segments in Planar Microwave Circuits,' IEEE Transactions, **MTT-28**, p1139-1143, 980

[154] W.R. Deal, V. Radisc, Y. Qian and T. Itoh, "Integrated antenna push-pull power amplifiers," IEEE Trans. Microwave Theory and Tech.,**47**, p 1418-1425, Aug. 1999

Appendix A

Substrate Parameters

Substrate Permittivity, ε_r.....2.33

Substrate height, *h*.....1.57mm

Metal thickness, *th*.....35μm

Dielectric loss tangent, tanδ.....0.0012

Metal conductivity, μ_r.....1

Magnetic loss tangent,.....0

Surface roughness, rgh.....0

Appendix 4A

Eigenvalues and Eigenfunctions of Square Patch

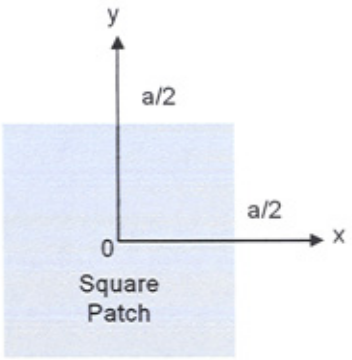

Figure 4A.1: Square patch configuration

With reference to figure 4A.1, the eigenvalue problem consists of the following two dimensional wave equation:

$$\frac{\partial^2\phi}{\partial x^2}+\frac{\partial^2\phi}{\partial y^2}+k^2\phi=0 \qquad \text{inside patch} \qquad (4A.1)$$

subject to the following boundary conditions

$$\frac{\partial\phi}{\partial n}=0 \qquad \text{along patch boundary} \qquad (4A.2)$$

Assuming a trial solution:

$$\phi(x,y)=X(x)Y(y) \qquad (4A.3)$$

Equation (4A.1) becomes:

$$X''Y+Y''X=-k^2XY \qquad (4A.4)$$

where $k^2=kx_m^{\ 2}+ky_n^{\ 2}$

or

$$\frac{X''}{X}+\frac{Y''}{Y}=-k^2 \tag{4A.5}$$

Rearranging yields the following equations:

$$X''+kx_m{}^2X=0 \tag{4A.6}$$

$$Y''+ky_n{}^2Y=0 \tag{4A.7}$$

From equation (4A.4):

$$X(x)=X_m(x)=A\cos(kx_mX)+B\sin(kx_mX) \tag{4A.8}$$

Applying Boundary Conditions along $x=\frac{a}{2}$

$$0=A\cos\left(kx_m\frac{a}{2}\right)+B\sin\left(kx_m\frac{a}{2}\right) \tag{4A.9}$$

Applying Boundary Conditions along $x=-\frac{a}{2}$

$$X_m(x)=A\cos\left(-kx_m\frac{a}{2}\right)+B\sin\left(-kx_m\frac{a}{2}\right)$$

$$X_m(x)=A\cos\left(kx_m\frac{a}{2}\right)-B\sin\left(kx_m\frac{a}{2}\right)$$

$$0=-A\sin\left(kx_m\frac{a}{2}\right)-B\cos\left(kx_m\frac{a}{2}\right) \tag{4A.10}$$

where $kx_m=\frac{m\pi}{a}$ $\qquad m=0,1,2...$

From (4A.9), if m is even:

$$B\cos\left(\frac{m\pi}{2}\right)=0$$

Thus $X_m(x)=\cos\left(\frac{m\pi x}{a}\right)$ (4A.11)

From (4A.10), if m is odd:

$$-A\sin\left(\frac{m\pi}{2}\right)=0$$

Thus $X_m(x)=\sin\left(\frac{m\pi x}{a}\right)$ (4A.12)

Similarly,

$$Y_n(y)=\cos\left(\frac{n\pi y}{a}\right) \qquad \text{if } n \text{ is even} \qquad (4A.13)$$

$$Y_n(y)=\sin\left(\frac{n\pi y}{a}\right) \qquad \text{if } n \text{ is odd} \qquad (4A.14)$$

Therefore:

$$\phi(x,y)=\left\{\begin{matrix}\sin\\ \cos\end{matrix}\right\}\frac{m\pi x}{a}\left\{\begin{matrix}\sin\\ \cos\end{matrix}\right\}\frac{n\pi y}{a} \qquad (4A.15)$$

Appendix 4B: Z Parameters for Multiport Network Model

To develop a multiport network model, Z-parameter expressions for the coupling between the external ports on the patch segment must be developed. There are a number of expressions, with each depending on the position of the ports, together with the orientation of the patch. To this end, this section will develop such expressions for each possible port positions.

Z_{ij} with Both Ports at different points on x axis

With reference to figure 4B.1, below:

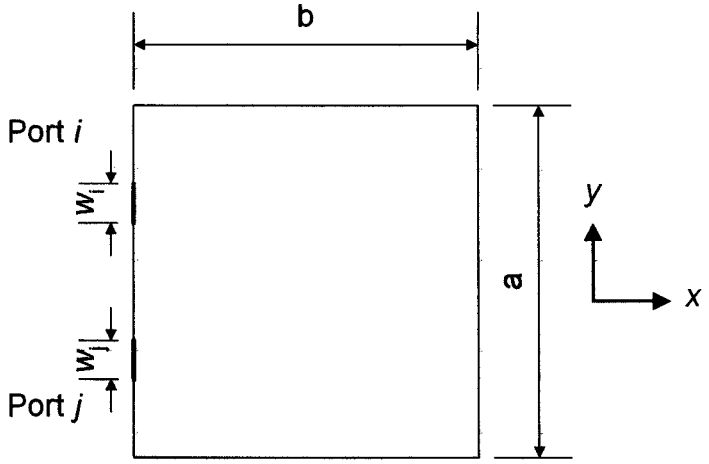

Figure 4B.1: port i and port j at same point on x axis

Port i is located at: $x_i, y_i \pm \frac{W_i}{2}$

Port j is located at: $x_j, y_j \pm \frac{W_j}{2}$

From equation (4.13) in chapter 4::

$$Z_{ij} = \frac{1}{W_i W_j} \int_{Wi} \int_{Wj} G(x_0, y_0; x, y)\ dW_i dW_j \qquad (4B.1)$$

In this case, x_0, y_0 corresponds to the location of port i, and x, y corresponds to port j. The integration is carried out over the port widths, thus:

$$Z_{ij} = \frac{j\omega\mu_0 h}{abW_iW_j} \int_{yi-wi/2}^{yi+wi/2} \int_{yj-wj/2}^{yj+wj/2} \sum_{m=0}^{\infty}\sum_{n=0}^{\infty} \sigma_m\sigma_n \frac{\cos(k_{xm}x_i)\cos(k_{yn}y_i)\cos(k_{xm}x_j)\cos(k_{yn}y_j)\ dW_i dW_j}{k_{xm}^2 + k_{yn}^2 - k^2}$$

(4B.2)

$$Z_{ij} = \frac{j\omega\mu_0 h}{abW_iW_j} \sum_{m=0}^{\infty}\sum_{n=0}^{\infty} \sigma_m\sigma_n \left[\frac{\cos(k_{xm}x_i)\sin(k_{yn}y_i)}{k_{yn}}\right]_{yi-wi/2}^{yi+wi/2} \int_{yj-wj/2}^{yj+wj/2} \sum_{m=0}^{\infty}\sum_{n=0}^{\infty} \frac{\cos(k_{xm}x_j)\cos(k_{yn}y_j)\ dW_j}{k_{xm}^2 + k_{yn}^2 - k^2}$$

(4B.3)

$$Z_{ij} = \frac{j\omega\mu_0 h}{abW_iW_j} \sum_{m=0}^{\infty}\sum_{n=0}^{\infty} \sigma_m\sigma_n \left[\frac{\cos(k_{xm}x_i)\sin(k_{yn}y_i)}{k_{yn}}\right]_{yi-wi/2}^{yi+wi/2} \left[\frac{\cos(k_{xm}x_j)\sin(k_{yn}y_j)}{k_{yn}}\right]_{yj-wj/2}^{yj+wj/2} \left[\frac{1}{k_{xm}^2 + k_{yn}^2 - k^2}\right]$$

(4B.4)

Z_{ij} with Both Ports at same points on x axis

With reference to figure 4B.2, below:

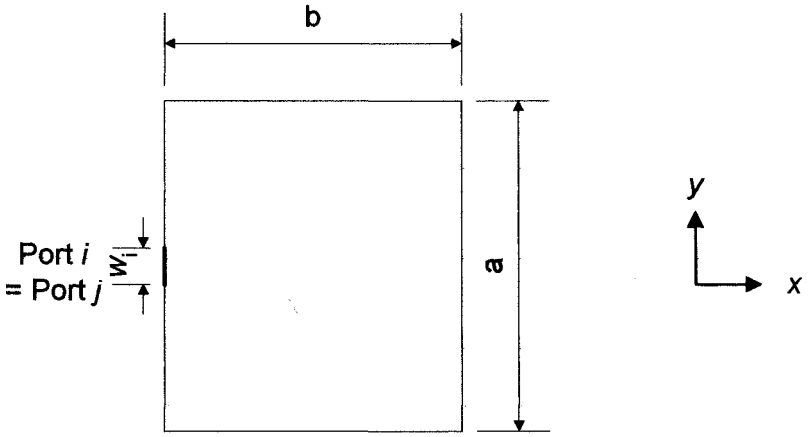

Figure 4B.2: port i and port j at same point on x axis

Considering Z_{ii}, ports i and j are located at the same point, thus

$Z_{ij} = Z_{ji} = Z_{ii} = Z_{jj}$, from (4B.1):

$$Z_{ii} = \frac{j\omega\mu_0 h}{abW_iW_j} \sum_{m=0}^{\infty}\sum_{n=0}^{\infty} \sigma_m\sigma_n \left\{\left[\frac{\cos(k_{xm}x_i)\sin(k_{yn}y_i)}{k_{yn}}\right]_{yi-wi/2}^{yi+wi/2}\right\}^2 \frac{1}{k_{xm}^2 + k_{yn}^2 - k^2} \qquad (4B.5)$$

Z_{ij} with Both Ports at different points at y axis

With reference to figure 4B.3, below:

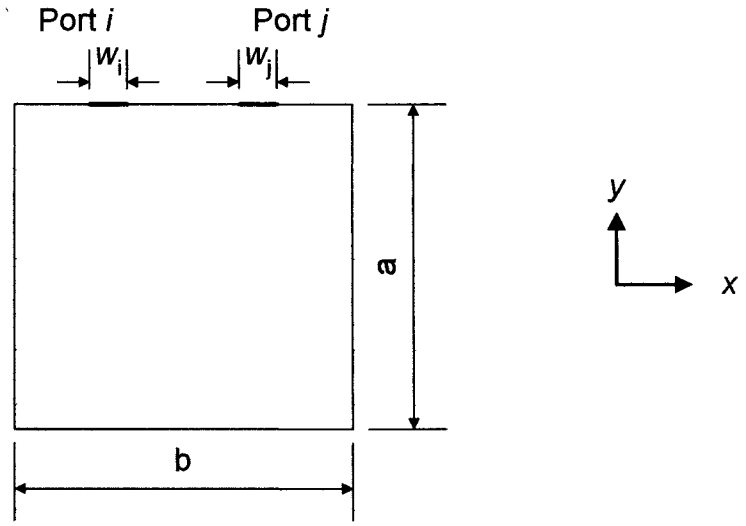

Figure 4B.3: port i and port j at different points on y axis

Port i is located at: $x_i \pm \frac{W_i}{2}, y_i$

Port j is located at: $x_j \pm \frac{W_j}{2}, y_j$

In this case, x_0, y_0 corresponds to the location of port i, and (x, y) corresponds to port j.

$$Z_{ij} = \frac{j\omega\mu_0 h}{abW_iW_j} \int_{xi-wi/2}^{xi+wi/2} \int_{xj-wj/2}^{xj+wj/2} \sum_{m=0}^{\infty}\sum_{n=0}^{\infty} \sigma_m\sigma_n \frac{\cos(k_{xm}x_i)\cos(k_{yn}y_i)\cos(k_{xm}x_j)\cos(k_{yn}y_j)\ dW_i dW_j}{k_{xm}^2 + k_{yn}^2 - k^2}$$

(4B.6)

$$Z_{ij} = \frac{j\omega\mu_0 h}{abW_iW_j} \sum_{m=0}^{\infty}\sum_{n=0}^{\infty} \sigma_m\sigma_n \left[\frac{\sin(k_{xm}x_i)\cos(k_{yn}y_i)}{k_{xm}}\right]_{xi-wi/2}^{xi+wi/2} \int_{xj-wj/2}^{xj+wj/2} \sum_{m=0}^{\infty}\sum_{n=0}^{\infty} \frac{\cos(k_{xm}x_j)\cos(k_{yn}y_j)\ dW_j}{k_{xm}^2 + k_{yn}^2 - k^2}$$

(4B.7)

$$Z_{ij} = \frac{j\omega\mu_0 h}{abW_iW_j}\sum_{m=0}^{\infty}\sum_{n=0}^{\infty}\sigma_m\sigma_n\left[\frac{\sin(k_{xm}x_i)\cos(k_{yn}y_i)}{k_{xm}}\right]_{xi-wi/2}^{xi+wi/2}\left[\frac{\sin(k_{xm}x_j)\cos(k_{yn}y_j)}{k_{xm}}\right]_{xj-wj/2}^{xj+wj/2}\left[\frac{1}{k_{xm}^{\ 2}+k_{yn}^{\ 2}-k^2}\right]$$

(4B.8)

Z_{ij} with Both Ports at same point on y axis

With reference to figure 4B.4, below:

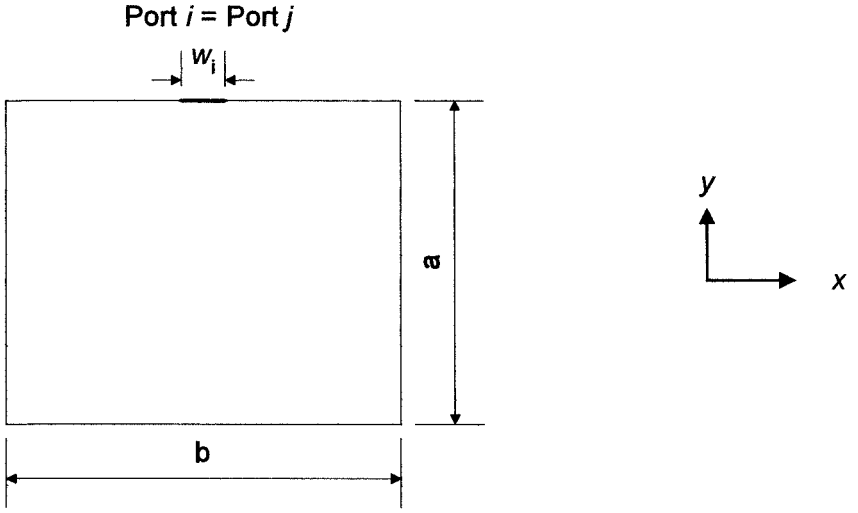

Figure 4B.4: port i and port j at same points on y axis

Considering Z_{ii}, ports i and j are located at the same point, thus

$Z_{ij} = Z_{ji} = Z_{ii} = Z_{jj}$, from (4B.8):

$$Z_{ii} = \frac{j\omega\mu_0 h}{abW_iW_j}\sum_{m=0}^{\infty}\sum_{n=0}^{\infty}\sigma_m\sigma_n\left\{\left[\frac{\sin(k_{xm}x_i)\cos(k_{yn}y_i)}{k_{xm}}\right]_{xi-wi/2}^{xi+wi/2}\right\}^2\frac{1}{k_{xm}^{\ 2}+k_{yn}^{\ 2}-k^2} \qquad (4B.9)$$

Z_{ij} with Ports on opposite y axis

With reference to the following diagram:

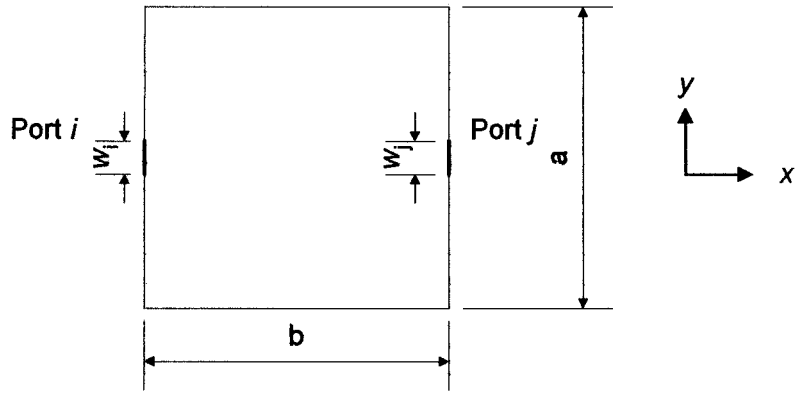

Figure 4B.5: port i and port j on y axis

Port i is located at: $x_i, y_i \pm \frac{W_i}{2}$

Port j is located at: $x_j, y_j \pm \frac{W_j}{2}$

$$Z_{ij} = \frac{j\omega\mu_0 h}{abW_iW_j} \int_{yi-wi/2}^{yi+wi/2} \int_{yj-wj/2}^{yj+wj/2} \sum_{m=0}^{\infty}\sum_{n=0}^{\infty} \sigma_m\sigma_n \frac{\cos(k_{xm}x_i)\cos(k_{yn}y_i)\cos(k_{xm}x_j)\cos(k_{yn}y_j)\ dW_i dW_j}{k_{xm}^2 + k_{yn}^2 - k^2} \tag{4B.10}$$

$$Z_{ij} = \frac{j\omega\mu_0 h}{abW_iW_j} \sum_{m-0}^{\infty}\sum_{n=0}^{\infty} \sigma_m\sigma_n \left[\frac{\cos(k_{xm}x_i)\sin(k_{yn}y_i)}{k_{yn}}\right]_{yi-wi/2}^{yi+wi/2} \int_{yj-wj/2}^{yj+wj/2} \sum_{m=0}^{\infty}\sum_{n=0}^{\infty} \frac{\cos(k_{xm}x_j)\cos(k_{yn}y_j)\ dW_j}{k_{xm}^2 + k_{yn}^2 - k^2} \tag{4B.11}$$

$$Z_{ij} = \frac{j\omega\mu_0 h}{abW_iW_j} \sum_{m-0}^{\infty}\sum_{n=0}^{\infty} \sigma_m\sigma_n \left[\frac{\cos(k_{xm}x_i)\sin(k_{yn}y_i)}{k_{yn}}\right]_{yi-wi/2}^{yi+wi/2} \left[\frac{\cos(k_{xm}x_j)\sin(k_{yn}y_j)}{k_{yn}}\right]_{yj-wj/2}^{yj+wj/2} \left[\frac{1}{k_{xm}^2 + k_{yn}^2 - k^2}\right] \tag{4B.12}$$

Z_{ij} with Ports on opposite x axis

With reference to the following diagram:

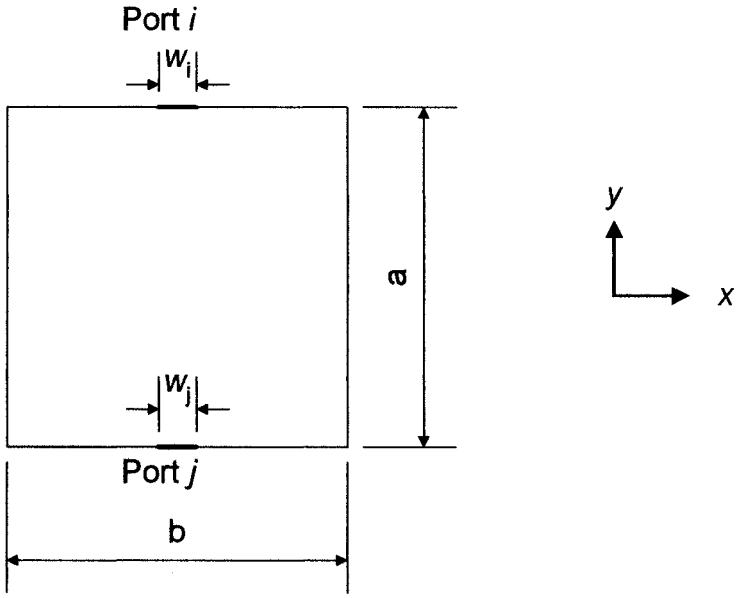

Figure 4B.6: port i and port j on x axis

Port i is located at: $x_i \pm \frac{W_i}{2}, y_i$

Port j is located at: $x_j \pm \frac{W_j}{2}, y_j$

$$Z_{ij} = \frac{j\omega\mu_0 h}{abW_iW_j} \int_{xi-wi/2}^{xi+wi/2} \int_{xj-wj/2}^{xj+wj/2} \sum_{m=0}^{\infty}\sum_{n=0}^{\infty} \sigma_m\sigma_n \frac{\cos(k_{xm}x_i)\cos(k_{yn}y_i)\cos(k_{xm}x_j)\cos(k_{yn}y_j)\ dW_i dW_j}{k_{xm}^2 + k_{yn}^2 - k^2} \tag{4B.13}$$

$$Z_{ij} = \frac{j\omega\mu_0 h}{abW_iW_j} \sum_{m=0}^{\infty}\sum_{n=0}^{\infty} \sigma_m\sigma_n \left[\frac{\sin(k_{xm}x_i)\cos(k_{yn}y_i)}{k_{xm}}\right]_{xi-wi/2}^{xi+wi/2} \int_{xj-wj/2}^{xj+wj/2} \sum_{m=0}^{\infty}\sum_{n=0}^{\infty} \frac{\cos(k_{xm}x_j)\cos(k_{yn}y_j)\ dW_j}{k_{xm}^2 + k_{yn}^2 - k^2} \tag{4B.14}$$

$$Z_{ij} = \frac{j\omega\mu_0 h}{abW_iW_j} \sum_{m=0}^{\infty}\sum_{n=0}^{\infty} \sigma_m\sigma_n \left[\frac{\sin(k_{xm}x_i)\cos(k_{yn}y_i)}{k_{xm}}\right]_{xi-wi/2}^{xi+wi/2} \left[\frac{\sin(k_{xm}x_j)\cos(k_{yn}y_j)}{k_{xm}}\right]_{xj-wj/2}^{xj+wj/2} \left[\frac{1}{k_{xm}^2 + k_{yn}^2 - k^2}\right] \tag{4B.15}$$

Z_{ij} with Port i on y axis, Port j on x axis

With reference to the following diagram:

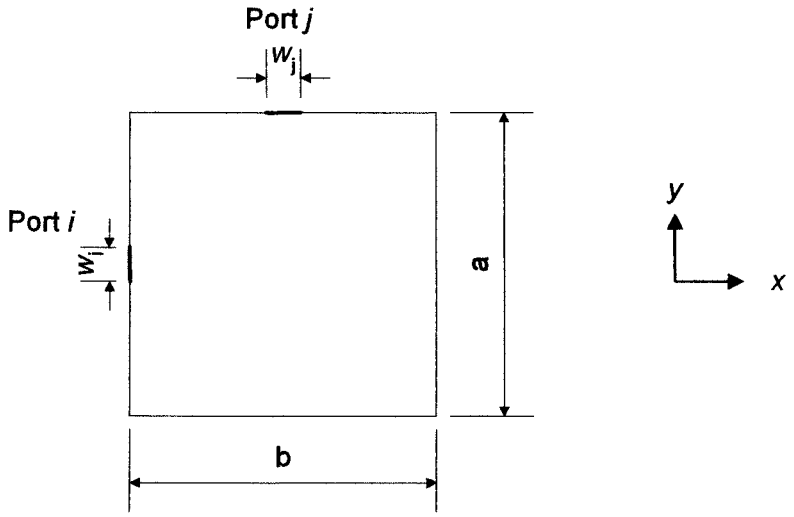

Figure 4B.7: port i on y axis and port j on x axis

Port i is located at: $x_i \pm \frac{W_i}{2}, y_i$

Port j is located at: $x_j, y_j \pm \frac{W_j}{2}$

$$Z_{ij} = \frac{j\omega\mu_0 h}{abW_iW_j} \int_{xi-wi/2}^{xi+wi/2} \int_{yj-wj/2}^{yj+wj/2} \sum_{m=0}^{\infty}\sum_{n=0}^{\infty} \sigma_m\sigma_n \frac{\cos(k_{xm}x_i)\cos(k_{yn}y_i)\cos(k_{xm}x_j)\cos(k_{yn}y_j)\ dW_i dW_j}{k_{xm}^{\ 2} + k_{yn}^{\ 2} - k^2}$$

(4B.16)

$$Z_{ij} = \frac{j\omega\mu_0 h}{abW_iW_j} \sum_{m=0}^{\infty}\sum_{n=0}^{\infty} \sigma_m\sigma_n \left[\frac{\sin(k_{xm}x_i)\cos(k_{yn}y_i)}{k_{xm}}\right]_{xi-wi/2}^{xi+wi/2} \int_{yj-wj/2}^{yj+wj/2} \sum_{m=0}^{\infty}\sum_{n=0}^{\infty} \frac{\cos(k_{xm}x_j)\cos(k_{yn}y_j)\ dW_j}{k_{xm}^{\ 2} + k_{yn}^{\ 2} - k^2}$$

(4B.17)

$$Z_{ij} = \frac{j\omega\mu_0 h}{abW_iW_j} \sum_{m-0}^{\infty}\sum_{n=0}^{\infty} \sigma_m\sigma_n \left[\frac{\sin(k_{xm}x_i)\cos(k_{yn}y_i)}{k_{xm}}\right]_{xi-wi/2}^{xi+wi/2} \left[\frac{\sin(k_{xm}x_j)\cos(k_{yn}y_j)}{k_{xm}}\right]_{yj+wj/2}^{yj-wj/2} \left[\frac{1}{k_{xm}^{\ 2} + k_{yn}^{\ 2} - k^2}\right]$$

(4B.18)